Vol.1, No.4, 241-373 (2010) ABB

TABLE OF CONTENTS

Volume 1, Number 4, October 2010

Advances in Bioscience and Biotechnology (ABB)

Journal Information

SUBSCRIPTIONS

The *Advances in Bioscience and Biotechnology* (Online at Scientific Research Publishing, www.SciRP.org) is published bimonthly by Scientific Research Publishing, Inc., USA.

Subscription rates:

Print: $50 per issue.
To subscribe, please contact Journals Subscriptions Department, E-mail: sub@scirp.org

SERVICES

Advertisements
Advertisement Sales Department, E-mail: service@scirp.org

Reprints (minimum quantity 100 copies)
Reprints Co-ordinator, Scientific Research Publishing, Inc., USA.
E-mail: sub@scirp.org

COPYRIGHT

PRODUCTION INFORMATION

For manuscripts that have been accepted for publication, please contact:
E-mail: abb@scirp.org

Advances in Bioscience and Biotechnology, 2010, 1, 241-262 **ABB**
doi:10.4236/abb.2010.14034 Published Online October 2010 (http://www.SciRP.org/journal/abb/).

Studies on mitochondrial macromolecular syntheses in various organs of aging animals labeled with ^{3}H-precursors as revealed by electron microscopic radioautography

Tetsuji Nagata

Department of Anatomy, Shinshu Institute of Alternative Medicine and Welfare, Nagano and Department of Anatomy and Cell Biology, Shinshu University School of Medicine, Matsumoto, Japan.
Email: nagatas@cnet.ne.jp

Received 8 March 2010; revised 10 April 2010; accepted 8 May 2010.

ABSTRACT

In order to study the aging changes of intramitochondrial macromolecular synthesis in various organs of aging animals during the development and aging, 10 groups of developing and aging mice, each consisting of 3 individuals, total 30, from fetal day 19 to postnatal newborn at day 1, 3, 9, 14 and adult at month 1, 2, 6, 12 to 24 were injected with ^{3}H-thymidine a DNA precurson, another 10 groups consisting of 3 individuals, total 30, were injected with ^{3}H-uridine a RNA precursor, and another 10 groups of 30 individuals were injected with ^{3}H-leucine a protein precursor, total 90 individuals. Then, all the animals were sacrificed 1 hr after the injections and the liver tissues, the lung tissues, the kidney tissues, the testis and ovary tissues, the adrenal tissues were taken out, fixed and processed for electron microscopic radioautography. On electron microscopic radioautograms obtained from each animal, ten photographs in respective groups, numbers of mitochondria per cell profile area, numbers of labeled mitochondria per cell and the mitochondrial labeling index (LI) labeled with ^{3}H-thymidine showing DNA synthesis, LI labeled with ^{3}H-uridine showing RNA synthesis, and LI labeled with ^{3}H-leucine showing protein synthesis, in various organs, were counted and the results in various organs in respective aging groups were compared, respectively. From the results, it was demonstrated that the numbers of mitochondria in hepatocytes as well as in 3 zones of the adrenal cortex, the zona glomerulosa, fasciculata and reticularis of mice at various ages increased from fetal day 19 to postnatal month 1 due to development and aging of animals. On the other hand, the numbers of labeled mitochondria and the labeling indices of intramitochondrial DNA syntheses incorporating ^{3}H-thymidine in hepatocytes and 3 zones of cortical cells increased from fetal day 19 to postnatal month 1 and decreased to month 24. The numbers of labeled mitochondria and the labeling indices of intramitochondrial RNA syntheses incorporating ^{3}H-uridine in hepatocytes and 3 zones of cortical cells increased from fetal day 19 to postnatal month 1 and decreased to month 24. The numbers of labeled mitochondria and the labeling indices of intramitochondrial RNA syntheses incorporating ^{3}H-uridine in hepatocytes and 3 ones of cortical cells increased from fetal day 19 to postnatal month 1 and decreased to month 24. Moreover, some other organs such as the lung and the testis were also review and discussed. From the results, it was shown that the activity of intramitochnodrial DNA synthesis, RNA synthesis, and protein synthesis in hepatocytes, adrenal cortical cells, pulmonary cells and testicular cells in developing and aging mice as well as some other organs increased and decreased due to development and aging.

Keywords: Mitochondrial Macromolecular Syntheses; Aging Animals Labeled; 3H-Precursors; Electron Microscopic Radioautography

1. INTRODUCTION

Intramitochondrial nucleic acid syntheses, both DNA and RNA, in mammalian and avian cells were first demonstrated morphologically by the present author by means of electron microscopic radioautography with accurate localization in primary cultured cells of the livers and kidneys of mice and chickens *in vitro* [1] and then in some other established cell lines such as HeLa cells [2-4] or mitochondrial fractions prepared from in vivo cells [5,6] It was later commonly found in various cells and tissues not only *in vitro* obtained from various

organs in vivo [7-9] but also in vivo cells of various organs such as the salivary glands [10] the liver [11-16] the pancreas [17,18] the trachea [19-21] the kidneys [22] the testis [23,24] the uterus [25,26] the adrenals [27,28] the brains [29] the retina [30-32] of chickens, mice and rats. However, no other literature was available in other laboratory throughout the world. In our laboratory, the relationship between the intramitochondrial DNA synthesis and cell cycle was formerly studied and it was clarified that the intramitochondrial DNA synthesis was performed without nuclear involvement [33]. On the other hand, the relationship between the DNA synthesis and the aging of individual animals has not yet been clarified. This paper deals with the relationship between the DNA synthesis and development in adrenal cortical cells of mice in vivo at various developmental stages from fetal day 19 to postnatal day 14 by means of electron microscopic radioautography as a part of serial studies on special cytochemistry [34] and radioautographology [35].

2. METHODOLOGY

2.1. Animals

The liver, adrenal gland, lung and testis tissues were obtained from 30 groups of normal ddY strain mice, each consisting of 3 litter mates of both sexes, total 90, aged from embryonic day 19 to postnatal day 1, 3, 9 and 14 and month 1, 2, 6, 12 and 24. The embryonic age was based on observation of the vaginal plug of the female mice (vaginal plug = day 0). All the animals were housed under conventional conditions and bred with normal diet (mouse chow Clea EC2, Clea Co., Tokyo, Japan) with access to water ad libitum in our laboratory. They were administered with 3H-thymidine or 3H-uridine or 3H-leucine, DNA, RNA and protein precursors, respectively, and the liver, adrenal and testis tissues were processed for light and electron microscopic radioautography. 34,35) All the procedures used in this study concerning the animal experiments were in accordance with the guidelines of the animal research committee of Shinshu University School of Medicine as well as the principles of laboratory animal care in NIH publication No. 86-23 (revised 1985).

2.2. Technique of Electron Microscopic Radioautography

All the animals were injected intraperitoneally with 3H-thymidine (Amersham, England, specific activity 877 GBq/mM) or 3H-uridine (Amersham, England, specific activity 1.11 TBq/mM) or 3H-4,5-leucine (Amersham, England, specific acitivity 1002 GBq/ mM) in saline, at 9 a.m., one hour before sacrifices. The dosage of injections was 370 KBq/gm body weight. The animals were perfused at 10 a.m., one hour after the injection, via the left ventricles of the hearts with 0.1 m cacodylate-buffered 2.5% glutaraldehyde under Nembutal (Abbott Laboratories, Chicago, ILL, USA) anesthesia. The right medical lobe of the liver, the superior lobe of the right lung, the right adrenal gland and the right testis were taken out, excised and 3 small tissue pieces from the respective organs (1 mm × 1 mm ×1 mm) were immersed in the same fixative at 4˚C for 1 hr., followed by postfixation in 1% osmium tetroxide in the same buffer at 4˚C for 1 hr., dehydrated in graded series of ethanol and acetone, and embedded in epoxy resin Epok 812 (Oken, Tokyo, Japan).

For light and electron microscopic radioautography, thick (2.0 0.2 µm) or semithin (0.2 µm) sections were cut in sequence on a Porter-Blum MT-2B ultramicrotome (Dupont-Sorvall, Newtown, MA, USA) using glass knives. The sections were collected on either collodion coated copper glass slides or grid meshes (VECO, Eerbeek, Netherlands), coated with either Konica NR-M2 (LM) or NR-H2 (EM) radioautographic emulsion (Konica, Tokyo, Japan) by either dipping or wire-loop method [18,35-37] They were stored in dark boxes containing silica gel (desiccant) at 4˚C for exposure. After the exposure for several months, the specimens were processed for development in either SD-X1 developer at 20˚C (LM) or freshly prepared gold latensification solution for 30 sec at 16˚C and then in fresh phenidon developer for 1 min at 16˚C in a water bath, rinsed in distilled water and dried in an oven at 37˚C overnight, stained with either toluidine blue (LM) or lead citrate solution for 3 min and coated with carbon (EM). The electron microscopic radioautograms were examined in a JEOL JEM-4000EX electron microscope (JEOL, Tokyo, Japan) at accelerating voltages of 400 kV for observing thick specimens. 33-35)

2.3. Quantitative Analysis of Electron Micrographs

For quantitative analysis of electron micrographs, twenty EM radioautograms showing cross sections of respective cell types from each group, based on the electron microscopic photographs taken after observation on at least 100 each cell type obtained from each animal, and at least 10 cells were analyzed to calculate the total number of mitochondria in each cell and the number of labeled mitochondria covered with silver grains by visual grain counting.

On the other hand, the number of silver grains in the same area size as a mitochondrion outside cells was also calculated in respective specimens as background fog, which resulted in less than 1 silver grain (0.03/mitochondrial area) almost zero. Therefore, the grain count in

each specimen was not corrected with background fog. From all the data thus obtained, the averages and standard deviations in respective aging groups were computed with a personal computer (Macintosh type 8100/100, Apple Computer, Tokyo, Japan). The data were stochastically analyzed using variance and Student's t-test. The differences were considered to be significant at P value < 0.01.

3. THE LIVER

3.1. Number of Mitochondria of Mouse Hepatocytes

We studied the liver tissues of ddY strain mice at various ages from embryonic day 19 to postnatal 2 years. 15,16) Observing light microscopic microscopic radioautograms labeled with 3H-thymidine, the silver grains were found over the nuclei of some hepatocytes, demonstrating DNA synthesis (**Figure 1**). By electron microscopic radioautography, some nuclei and some mitochondria in hepatocytes in perinatal stages at embryonic day 19 (**Figure 2**), postnatal day 1, 3, 9 and day 14 (**Figure 3**) as well as young adult (**Figure 4**) and senesecent animals (**Figure 5**) were observed. However, those labeled hepatocytes were almost mononucleate cells (**Figures 2-5**) and only a few binucleate cells were found among the mononucleate hepatocytes. 36) In the labeled hepatocytes (**Figures 1, 2, 3, 4, 5**) the silver grains were mainly localized over the euchromatin of the nuclei and only a few or several silver grains were found over the mitochondria of these mononucleate hepatocytes. 37) To the contrary, most hepatocytes were not labeled with any silver grains in their nuclei nor cytoplasm, showing no DNA synthesis even after labeling with 3H-thymidine in aged adult and senescent animals at postnatal month 1 (**Figure 4**), 2, 6, 12 (**Figure 5**) and month 24. On the other hand, labeled binucleate hepatocytes over their nuclei were very rarely found only at the perinatal stages from postnatal day 1, 3 (**Figure 6**), 9 and 14 (**Figure 7**) but not after postnatal month 1 to senescent stages up to month 12 or 24. Among many unlabeled hepatocytes, most mononucleate and binucleate hepatocytes were observed to be labeled with several silver grains over their mitochondria due to the incorporations of 3H-thymidine especially at the perinatal stages from embryonic day 19 to postnatal day 1, 3, 9 and 14 (**Figure 3**). The localizations of silver grains over the mitochondria were mainly on the mitochondrial matrices but some grains over the mitochondrial membranes and cristae when observed by high power magnification (**Figure 3**).

For preliminary quantitative analysis on the number of mitochondria in 10 mononucleate hepatocytes whose

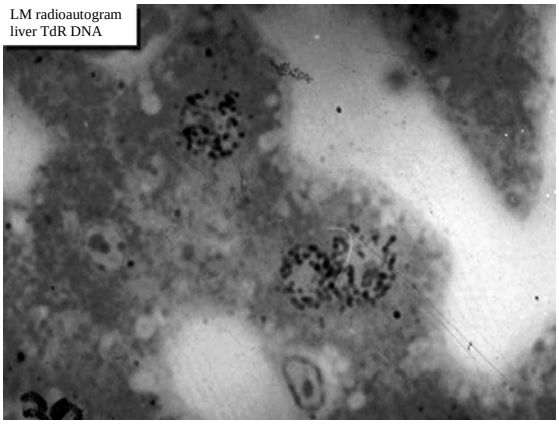

Figure 1. LM radioautogram of the liver of an adlut mouse at postnatal month 1 labeled with 3H-thymidine, demonstrating DNA synthesis in the two nuclei. x 1,000.

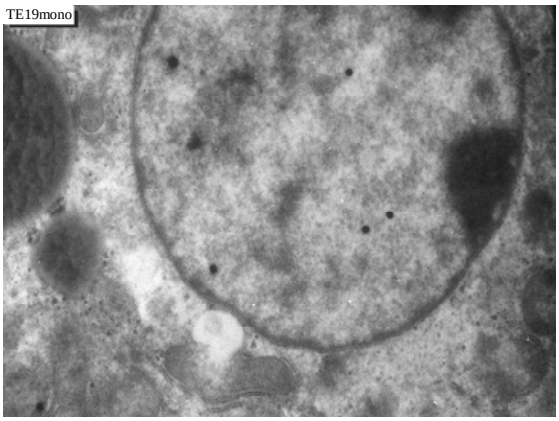

Figure 2. EM radioautogram of a mouse embryo liver aged at fetal day 19, labeled with 3H-thymidine, demonstrating DNA synthesis of a mononucleate hepatocyte. Silver grains are localized over euchromatin of the nucleus as well as over a few mitochondria. x 4,000.

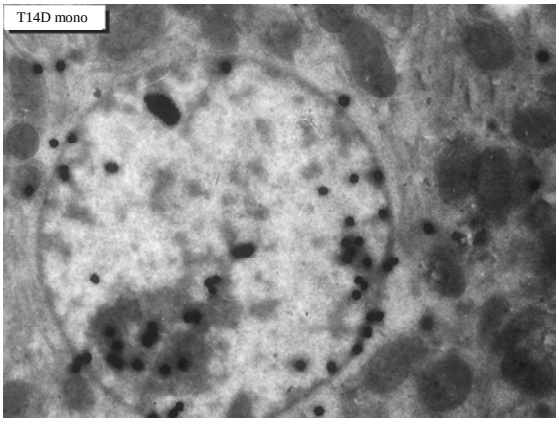

Figure 3. EM radioautogram of a mouse liver aged at postnatal day 14, labeled with 3H-thymidine, demonstrating DNA synthesis of mononucleate hepatocyte. Silver grains are localized over euchromatin of the nucleus as well as over several mitochondria. x 4,000.

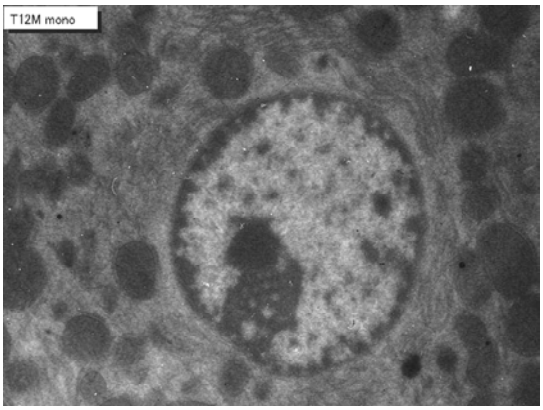

Figure 4. EM radioautogram of a senescent mouse aged at postnatal month 12, labeled with 3H-thymidine, demonstrating DNA synthesis of a mononucleiate hepatocyte. Silver grains are localized not over the nucleus but over a few mitochondria. x 3,000.

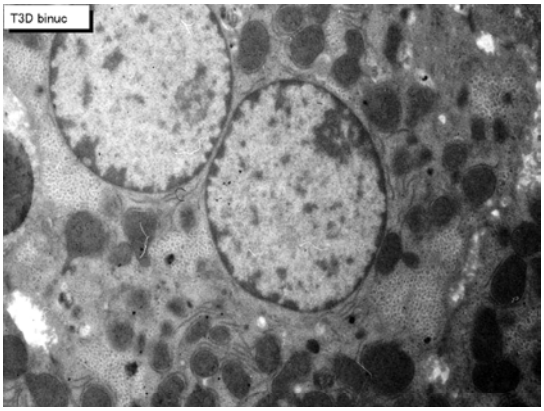

Figure 5. EM radioautogram of a newborn mouse aged at postnatal day 3, labeled with 3H-thymidine, demonstrating DNA synthesis of a binucleiate hepatocyte. Silver grains are localized not over the 2 nuclei but over a few mitochondria. x 3,000.

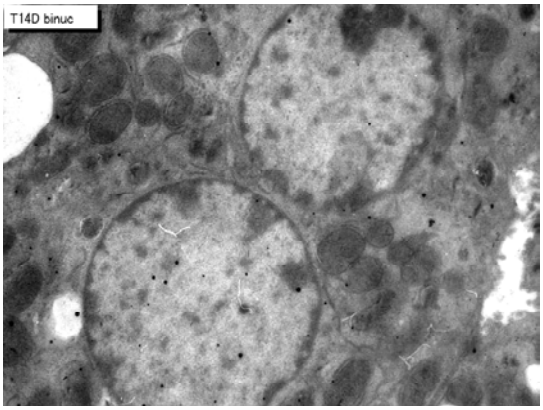

Figure 6. EM radioautogram of juvenile mouse aged at postnatal day 14, labeled with 3H-thymidine, demonstrating DNA synthesis of a binucleiate hepatocyte. Silver grains are localized over one of the 2 nuclei as well as over a few mitochondria. x 3,000.

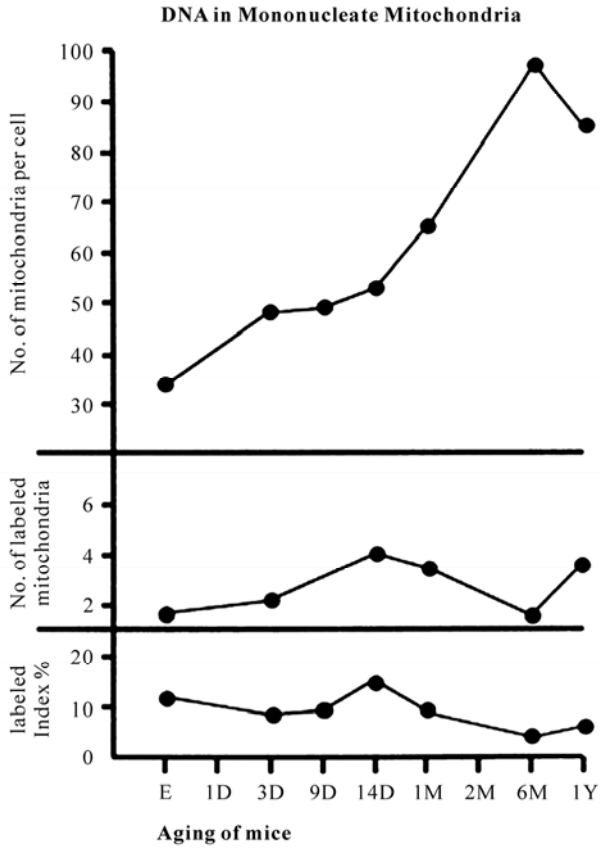

Figure 7. Transitional curves of the number of mitochondria per cell profile area (top), the number of labeled mitochondria per cell (middle) and the labeling index (bottom) of a monucleate hepatocyte in respective aging groups. The numbers and LI increased and decreased due to aging.

nuclei were labeled with silver grains and other 10 mononucleate hepatocytes whose nuclei were not labeled in each aging group injected with either 3H-thymidine revealed that there was no significant difference between the number of mitochondria and the labeling indices in both types of hepatocytes ($P < 0.01$). Thus, the number of mitochondria and the labeling indices were calculated in both types of hepatocytes with labeled or unlabeled nuclei at respective aging stages. The results obtained from the number of mitochondria in mononucleate hepatocytes showed an increase from the prenatal day to postnatal day 14 (26.2-34.5/cell), then to postnatal month 1-6 (89.2-97.1/cell), reaching the maximum, then decreased to year 1-2 (80.4-85.7/cell) as is shown in **Figure 7** (top).

3.2. Mitochondrial DNA Synthesis of Mouse Hepatocytes

The results of visual counts on the number of mitochondria labeled with silver grains obtained from 10 mononucleate hepatocytes of each animal labeled with

3H-thymidine demonstrating DNA synthesis in 7 aging groups at perinatal stages, prenatal embryo day 19, postnatal day 3, 9 and 14, month 1, 6 and 12, are plotted in **Figure 7** (middle). The labeling indices in respective aging stages were calculated from the number of labeled mitochondria (**Figure 7** middle) and the number of total mitochondria per cell (**Figure 7** top) which were plotted in **Figure 7** (bottom), respectively. The results showed that the numbers of labeled mitochondria with 3H-thymidine showing DNA synthesis increased from prenatal embryo day 19 (3.8/cell) to postnatal day 14 (6.2/cell), reaching the maximum, and then decreased to month 6 (3.7/cell) and again increased to year 1 (6.0/cell), while the labeling indices increased from prenatal day 19 (11.8%) to postnatal day 14 (16.9%), reaching the maximum, then decreased to month 6 (4.1%) and year 1 (6.4%) and year 2 (2.3%). The increase of the total number of mitochondria in mononucleate hepatocytes was stochastically significant ($P < 0.01$), while the changes of number of labeled mitochondria and labeling index in mononucleate hepatocytes were not significant ($P < 0.01$).

As for the binucleate hepatocytes, on the other hand, because the appearances of binucleate hepatocytes showing silver grains in their nuclei demonstrating DNA synthesis were not so many in the adult and senescent stages from postnatal month 1 to 24, only binucleate cells at perinatal stages when reasonable numbers of labeled hepatocytes were found in respective groups were analyzed. The number of mitochondria in binucleate hepatocytes at postnatal day 1 to 14 kept around 80 (77-84/cell) which did not show such remarkable changes, neither increase nor decrease, as shown in mononucleate cells. Thus, the number of mitochondria per binucleate cell (**Figure 8** top), the number of labeled mitochondria per binucleate cell (**Figure 8**middle) and the labeling index of binucleat cell (**Figure 8** bottom) in 4 groups from postnatal day 1 to 14 were shown. The number of mitochondria and the number of labeled mitochondria were more in binucleate cells than mononucleate cells.

3.3. Mitochondrial RNA Synthesis of Mouse Hepatocytes

On the other hand, observing light microscopic radioautograms labeled with ^{3}H-uridine, the silver grains were found over both the karyoplasm and cytoplasm of almost all the cells not only at the perinatal stages from embryo day 19 to postnatal day 1, 3, 9, 14, but also at the adult and senescent stages from postnatal month 1 to 2, 6, 12 and 24. By electron microscopic observation, silver grains were observed in most mononucleate hepatocytes in respective aging groups localizing not only over euchromatin and nucleoli in the nuclei but also over many

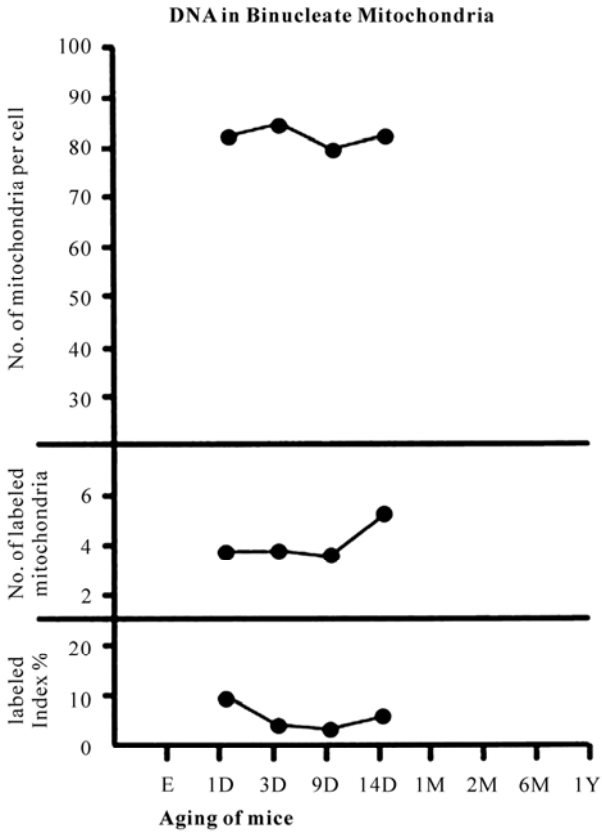

Figure 8. Transitional curves of the number of mitochondria per cell profile area (top), the number of labeled mitochondria per cell (middle) and the labeling index (bottom) of a binucleate hepatocyte in respective aging groups. The numbers and LI did not show any significant changes, but the number was much more than mononucleate cell at the same age.

cell organelles such as endoplasmic reticulum, ribosomes, and mitochondria as well as cytoplasmic matrices from perinatal stage at embryonic day 19 (**Figure 9**), postnatal day 1, 3 (**Figure 10**), 9, 14 (**Figure 11**), to adult and senescent stages at postnatal month 1, 2 (**Figure 12**), 6 (**Figure 13**), 12 and 24. The silver grains were also observed in binucleate hepatocytes at postnatal day 1, 3, 9, 14, month 1, 2, 6 (**Figure 13**), 12 and 24 (**Figure 14**). The localizations of silver grains over the mitochondria were mainly on the mitochondrial matrices but a few over the mitochondrial membranes and cristae when observed by high power magnification (**Figure 11**).

As the results, it was found that almost all the hepatocytes were labeled with silver grains showing RNA synthesis in their nuclei and mitochondria. 38) Preliminary quantitative analysis on the number of mitochondria in 10 mononucleate hepatocytes whose nuclei were intensely labeled with many silver grains (more than 10 per nucleus) and other 10 mononucleate hepatocytes

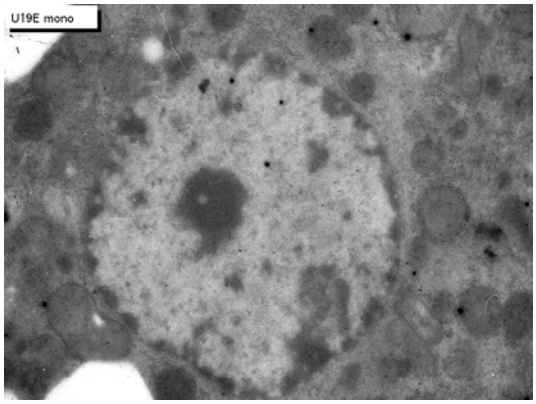

Figure 9. EMRAG of a mouse embryo liver at fetal day 19, labeled with 3H-uridine, demonstrating RNA synthesis of a mononucleate hepatocyte. Several silver grains are localized over euchromatin of the nucleus as well as over several mitochondria. x 4,000.

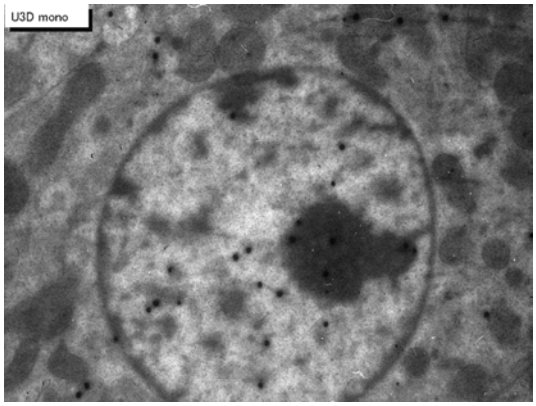

Figure 10. EMRAG of a newborn mouse liver at postnatal day 3, labeled with 3H-uridine, demonstrating RNA synthesis of a mononucleate hepatocyte. Several silver grains are localized over euchromatin and nucleolus of the nucleus and over several mitochondria. x 4,000.

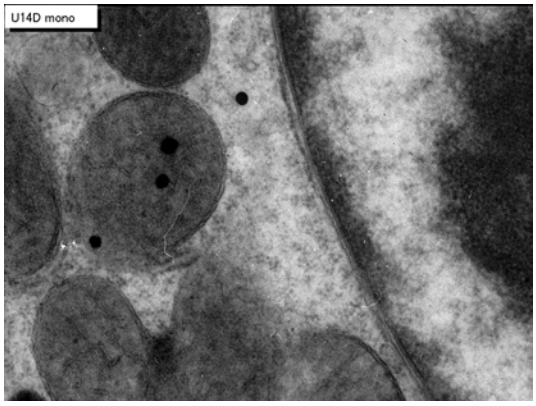

Figure 11. High power magnification EM radioautogram of a juvenile mouse liver at postnatal day 14, labeled with 3H-uridine, demonstrating RNA synthesis. A few silver grains are localized over the mitochondrial matrix and the mitochondrial membrane of the mitochondrion at center. x 15,000.

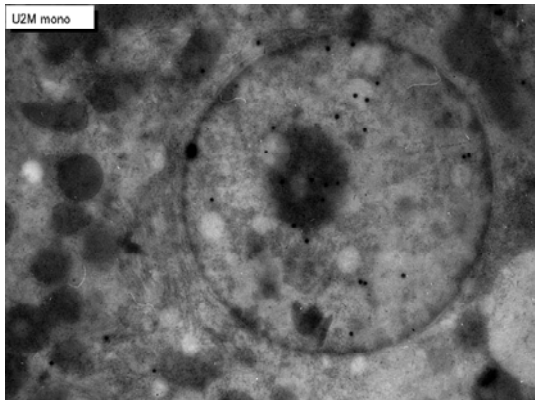

Figure 12. EMRAG of a senescent mouse liver at postnatal month 2, labeled with 3H-uridine, demonstrating RNA synthesis of a mononucleate hepatocyte. Several silver grains are localized over euchromatin and nucleolus of the nucleus as well as over a few mitochondria showing less RNA synthesis than younger animals. x 4,000.

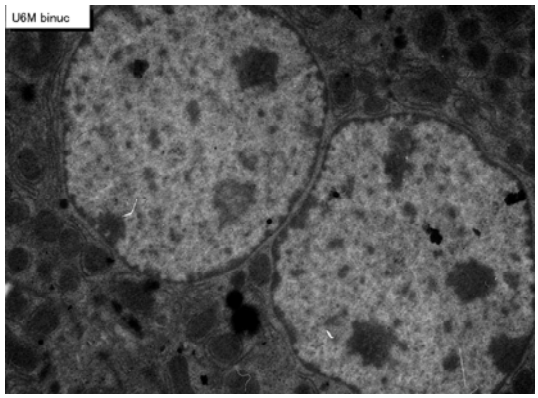

Figure 13. EMRAG of an adult mouse liver at postnatal month 6 labeled with 3H-uridine, demonstrating RNA synthesis of a binucleate hepatocyte. Only a few silver grains are localized over the 2 nuclei and over a few mitochondria. x 4,000.

whose nuclei were not so intensely labeled (number of silver grains less than 9) in each aging group revealed that there was no significant difference between the number of mitochondria, number of labeled mitochondria and the labeling indices in both types of hepatocytes ($P < 0.01$). Thus, the number of mitochondria and the labeling indices were calculated in 10 hepatocytes selected at random in each animal in respective aging stages regardless whether their nuclei were very intensely labeled or not. The results obtained from the number of mitochondria in mononucleate hepatocytes per cellular profile area showed an increase from the prenatal day (mean ± standard deviation 26.2 ± /cell) to postnatal day 1 to day 14 (38.4-51.7/cell), then to postnatal month 1-2 (53.7-89.2/cell), reaching the maximum, then decreased to year 1-2 (83.7-80.4/cell) as is shown in

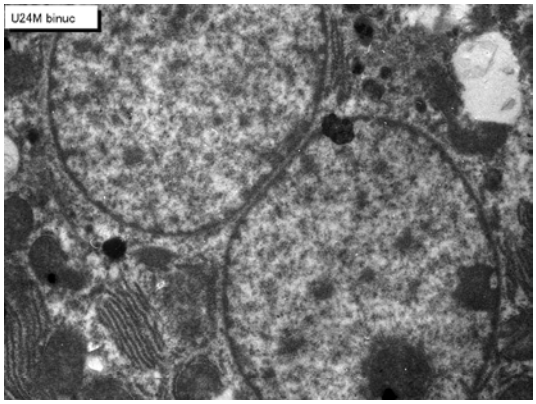

Figure 14. EMRAG of a senescent mouse liver at postnatal month 24, 2 years, labeled with 3H-uridine, demonstrating RNA synthesis of a binucleate hepatocyte. Only a few silver grains are localized over the 2 nuclei and a few silver grains over a few mitochondria. x 4,000.

Figure 15 (top) and the increase was stochastically significant ($P < 0.01$). The results of visual grain counts on the number of mitochondria labeled with silver grains obtained from 10 mononucleate hepatocytes of each animal labeled with 3H-uridine demonstrating RNA synthesis in 10 aging groups at perinatal stages, prenatal embryo day 19, postnatal day 1, 3, 9 and 14, month 1, 6 and year 1 and 2, are plotted in **Figure 15** (middle). The labeling indices in respective aging stages were calculated from the number of labeled mitochondria (**Figure 15**, middle) and the number of total mitochondria per cellular profile area (**Figure 15**, top) which were plotted in **Figure 15** (bottom), respectively. The results showed that the numbers of labeled mitochondria with 3H-uridine showing RNA synthesis increased from prenatal embryo day 19 (3.3/cell) to postnatal month 1 (9.2/cell), reaching the maximum, and then decreased to month 6 (3.5/cell) and again increased to year 1 (4.0/cell) and year 2 (4.3/cell), while the labeling indices increased from prenatal day 19 (12.4%) to postnatal month 1 (16.7%), reaching the maximum, then decreased to year 1 (4.8%) and year 2 (5.3%). Stochastical analysis revealed that the increases and decreases of the number of labeled mitochondria from the perinatal stage to the adult and senescent stage were significant in contrast that the increases and decreases of the labeling indices were not significant ($P < 0.01$). As for the binucleate hepatocytes, on the other hand, because the appearances of binucleate hepatocytes were not so many in the embryonic stage, only several binucleate cells (5-8 at least) at respective stages when enough numbers of binucleate cells available from postnatal day 1 to year 2 were analyzed. The results were shown in **Figure 16**. The results of visual counts on the number of mitochondria labeled with silver grains

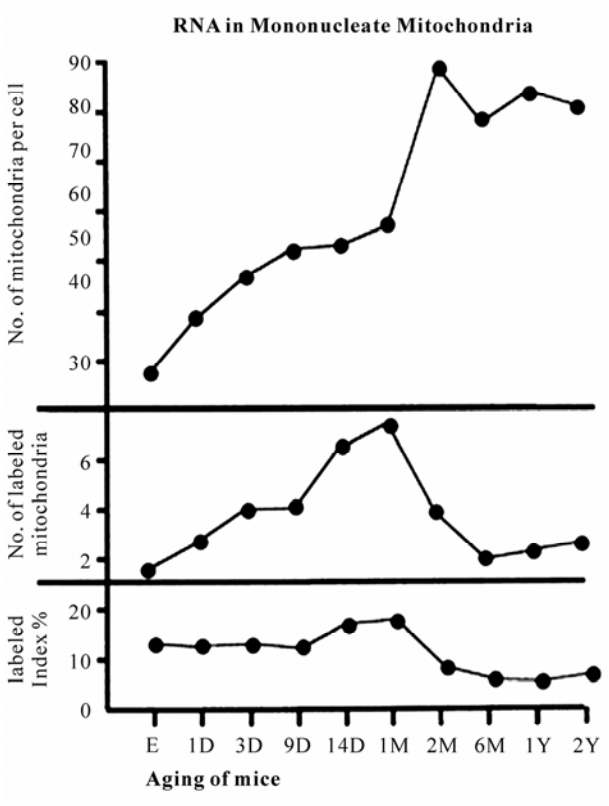

Figure 15. Transitional curves of the aging changes of the number of mitochondria per cell profile area (top), the number of labeled mitochondria per cell (middle) and the labeling index (bottom) of a monucleate hepatocyte in respective aging groups labeled with 3H-uridine showing RNA synthesis. The number of labeled mitochondria and LI peaked at day 14.

obtained from several (5 to 8) binucleate hepatocytes labeled with ^{3}H-uridine demonstrating RNA synthesis in 8 aging groups at perinatal stages, postnatal day 1, 9, 14, and month 1, 2, 6, and year 1 and 2, are plotted in **Figure 16** (middle) and the labeling indices in respective aging stages were calculated from the number of labeled mitochondria (**Figure 16**, middle) and the number of total mitochondria per cellular profile area (**Figure 16**, top) which were plotted in **Figure 16** (bottom), respectively. The results showed that the number of labeled mitochondria increased from postnatal day 1 (2.3/cell) to day 9 (5.2/cell) and remained almost constant around 4-5, but the labeling indices increased from postnatal day 1 (2.1%) to postnatal day 9 (13.6%), remained almost constant around 13% (12.5-13.6%) from postnatal day 9 to month 1, then decreased to month 2 (6.1%) to month 6 (3.9%), and slightly increased to year 1 (6.3%) and 2 (5.3%). The increases and decreases of the number of labeled mitochondria and the labeling indices in binucleate hepatocytes were stochastically not significant ($P < 0.01$).

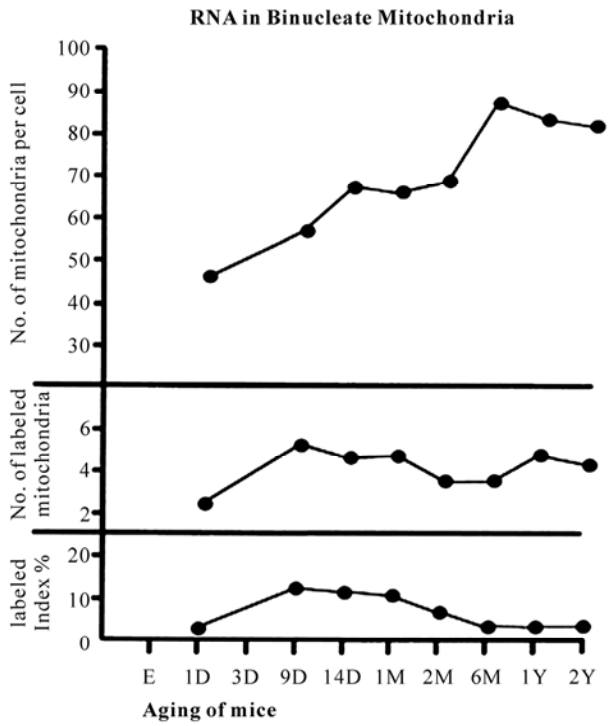

Figure 16. Transitional curves of the aging changes of the number of mitochondria per cell profile area (top), the number of labeled mitochondria per cell (middle) and the labeling index (bottom) of binucleate hepatocyte in respective aging groups labeled with 3H-uridine showing RNA synthesis.

3.4. Protein Synthesis of Mouse Hepatocytes

When the animals were injected with 3H-leucine, it was found that almost all the hepatocytes, from embryonic day 19, postnatal day 1, 3 (**Figure 18**), 9, 14 (**Figure 19**), to adult and senescent stages at postnatal month 1, 2 (**Figure 20**), 12 and 24 (**Figure 21**). The silver grains were also observed in binucleate hepatocytes at postnatal day 1, 3 (**Figure 22**), 9, (**Figure 23**), 14 (**Figure 24**), month 1, 2, 6, 12 (**Figure 25**) and 24. The localizations of silver grains observed over the mitochondria were mainly on the mitochondrial matrices but a few over their nuclei, cytoplasmic matrix, endoplasmic reticulum, ribosomes, Golgi apparatus and mitochondria. 39) In the mitochondria the silver grains were localized over the mitochondrial membranes and cristae when observed by high power magnification (**Figure 19**). Preliminary quantitative analysis on the number of mitochondria in 20 mononucleate hepatocytes whose nuclei were intensely labeled with many silver grains (more than 10 per nucleus) and other 20 mononucleate hepatocytes whose nuclei were not so intensely labeled (number of silver grains less than 9) in each aging group revealed that there was no significant difference between the number of mitochondria, number of labeled mitochondria

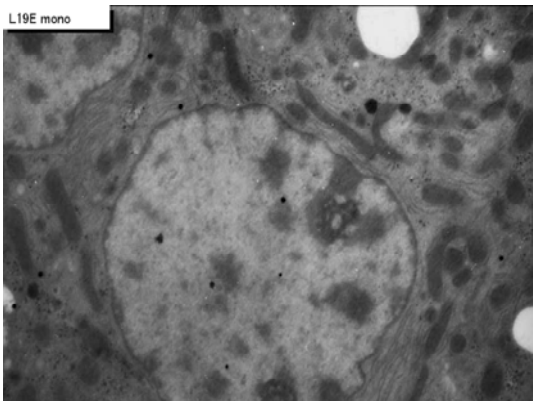

Figure 17. EMRAG of a mouse embryo liver at fetal day 19, labeled with 3H-leucine, demonstrating protein synthesis of a mononucleate hepatocyte. Several silver grains are localized over euchromatin of the nucleus and over several mitochondria. x 4,000.

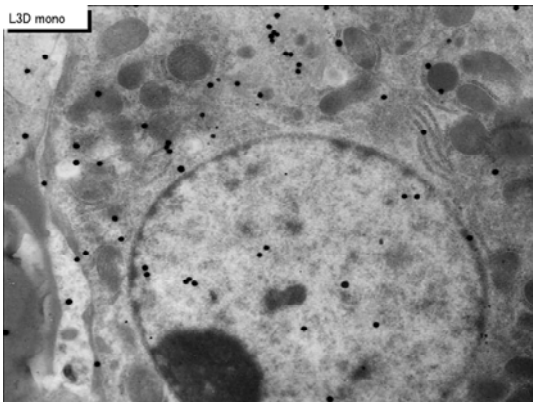

Figure 18. EMRAG of a newborn mouse liver at postnatal day 3, labeled with 3H-leucine, demonstrating protein synthesis of a mononucleate hepatocyte. Several silver grains are localized over euchromatin of the nucleus and over several mitochondria. x 4,000.

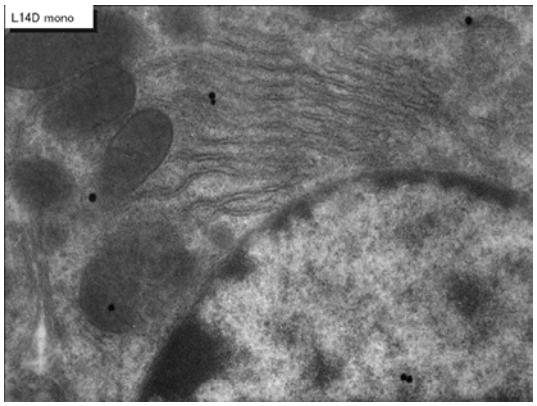

Figure 19. High power magnification radioautogram of a juvenile mouse liver at postnatal day 14, labeled with 3H-leucine, demonstrating protein synthesis. A few silver grains are localized over the mitochondrial matrix of the 2 mitochondria at left. x 8,000.

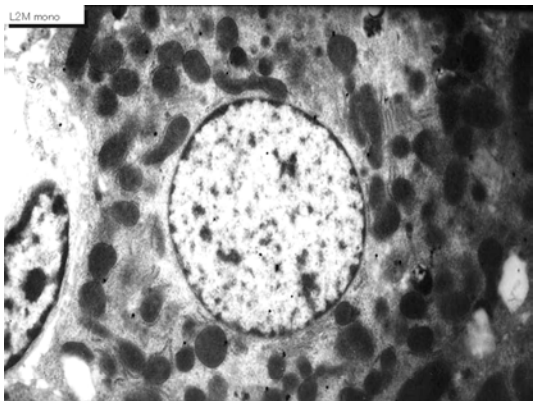

Figure 20. EMRAG of an adult mouse liver at postnatal month 2, labeled with 3H-leucine, demonstrating protein synthesis of a mononucleate hepatocyte. Several silver grains are localized over the nucleus and over several mitochondria. x 3,000.

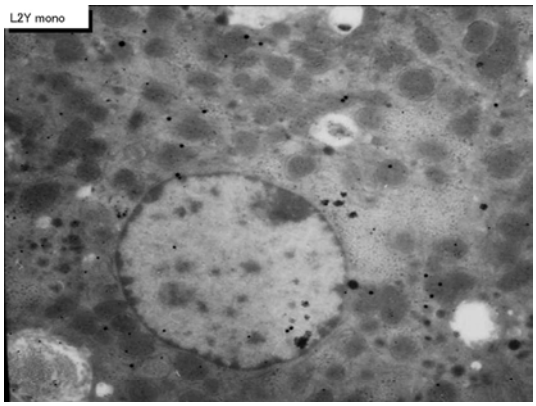

Figure 21. EMRAG of a senescent mouse liver at postnatal month 24, 2 years, labeled with 3H-leucine, demonstrating protein synthesis of a mononucleate hepatocyte. Several silver grains are localized over euchromatin of the nucleus as well as over a few mitochondria showing less protein than younger animals. x 3,000.

and the labeling indices in both types of hepatocytes ($P < 0.01$).

On the other hand, the numbers of mitochondria, the numbers of labeled mitochondria and the labeling indices were calculated in 10 binucleate hepatocytes selected at random in each animal in respective aging stages, regardless whether their nuclei were very intensely labeled or not, except the prenatal stage at embryonic day 19, because no binucleate cell was found at this stage. Thus, the numbers of mitochondria, the numbers of labeled mitochondria and the labeling indices were calculated in 20 hepatocytes selected at random in each animal in respective aging stages regardless whether their nuclei were very intensely labeled or not. The results obtained from the total numbers of mitochondria in mononucleate

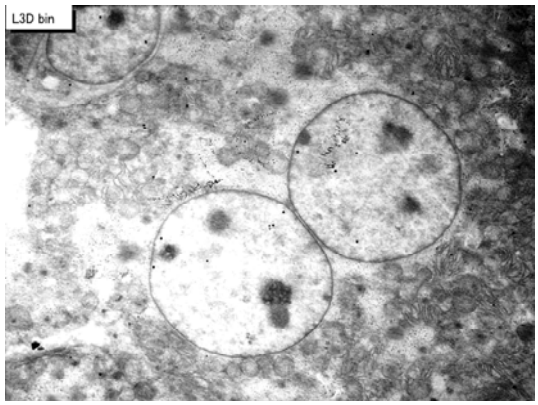

Figure 22. Next slide shows an EMRAG of mouse liver at postnatal day 3, a newborn mouse, labeled with 3H-leucine, demonstrating protein synthesis of a binucleate hepatocyte. Only a few silver grains are localized over the 2 nuclei and over a few mitochondria. x 3,000.

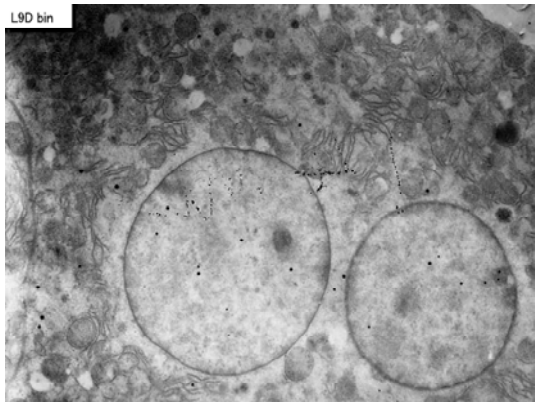

Figure 23. EMRAG of mouse a juvenile mouse liver at postnatal day 9, labeled with 3H-leucine, demonstrating protein synthesis of a binucleate hepatocyte. Only a few silver grains are localized over the 2 nuclei and over a few mitochondria. x 3,000.

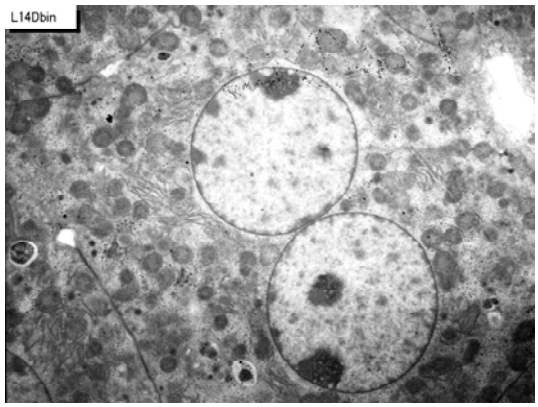

Figure 24. EMRAG of a juvenile mouse liver at postnatal day 14, labeled with 3H-leucine, demonstrating protein synthesis of a binucleate hepatocyte. Only a few silver grains are localized over the 2 nuclei and over a few mitochondria. x 3,000.

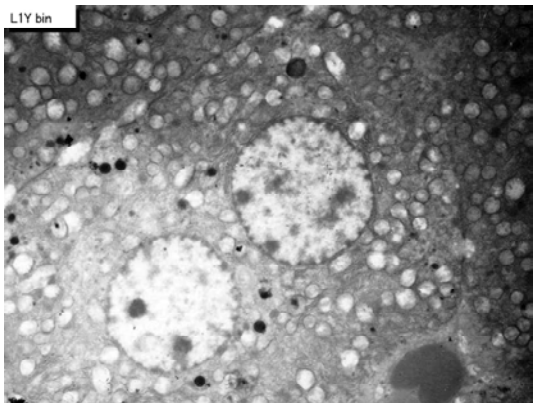

Figure 25. EMRAG of senescent mouse liver at postnatal month 12, year 1, labeled with 3H-leucine, demonstrating protein synthesis of a binucleate hepatocyte. Only a few silver grains are localized over the 2 nuclei and over a few mitochondria. x 3,000.

hepatocytes showed an increase from the prenatal day (34.5/cell) to postnatal days 1 (44.6/cell), 3 (45.8/cell), 9 (43.6/cell), 14 (48.5/cell), to postnatal months 1 (51.5/cell), 2 (52.3/cell), reaching the maximum at month 6 (60.7/cell), then decreased to years 1 (54.2/cell) and 2 (51.2/cell) as shown in **Figure 26** (upper left). The increase and decrease were stochastically significant ($P < 0.01$). The results obtained from visual counting on the numbers of mitochondria labeled with silver grains from 20 mononucleate hepatocytes of each animal labeled with 3H-leucine demonstrating protein synthesis in 10 aging groups at perinatal stages, prenatal embryo day 19, postnatal day 1, 3, 9 and 14, month 1, 2, 6 and year 1 and 2, are plotted in **Figure 26** (lower left). The labeling indices in respective aging stages were calculated from the numbers of labeled mitochondria and the numbers of total mitochondria per cell which were plotted in **Figure 26** (right). The results showed that the numbers of labeled mitochondria with 3H-leucine showing protein synthesis increased from prenatal embryo day 19 (8.3/cell) to postnatal days 1 (9.6/cell), 3 (8.1/cell), 9 (8.9/cell), 14 (9.5/cell), and month 1 (11.2/cell), reaching the maximum, and then decreased to months 2 (9.1/cell), 6 (8.8/cell) to years 1 (6.7/cell) and 2 (2.2/cell), while

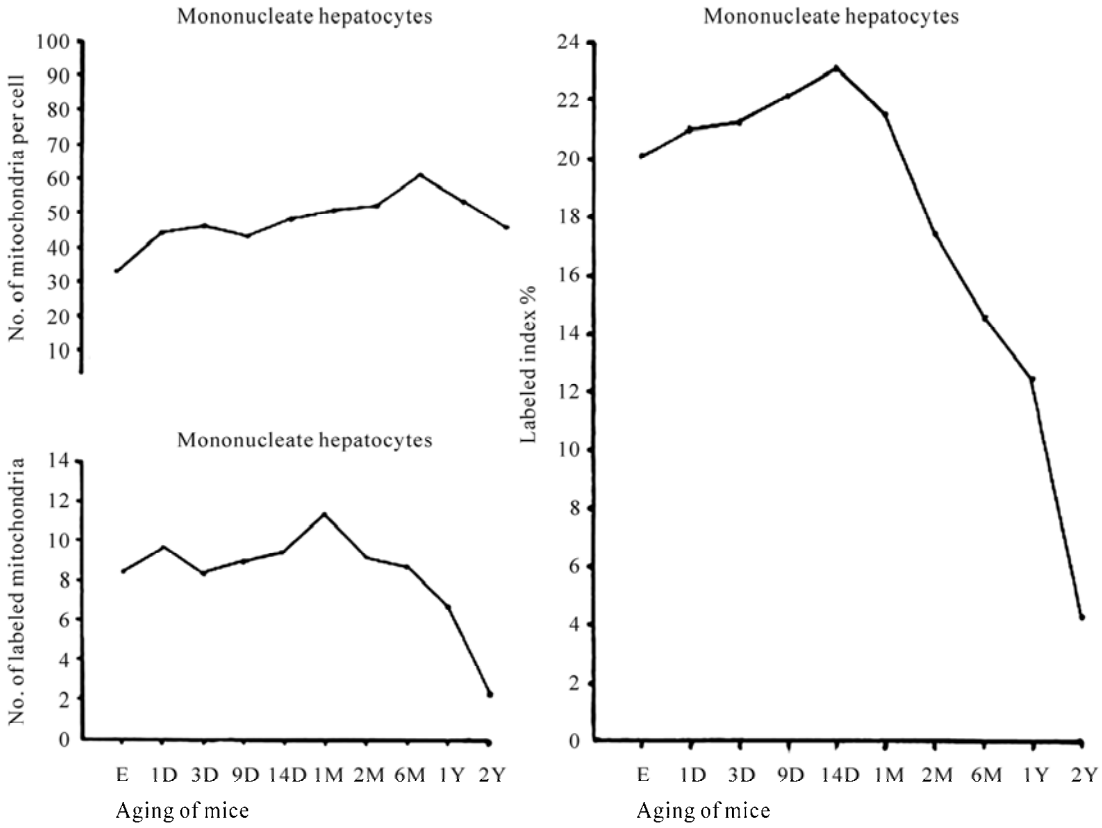

Figure 26. Transitional curves of the aging changes of mononucleate hepatocyte mitochondria labeled with 3H-leucine showing protein synthesis. The upper left curve shows number of mitochondria per cell showing an increase and decrease due to aging, the lower left curve shows number of labeled mitochondria per cell, which showed an increase and decrease, and the right curve shows labeling index which also showed an increase and decrease with aging.

the labeling indices increased from prenatal day 19 (20.1%) to postnatal days 1 (21.2%), 3 (21.6%), 9 (22.2%), 14 (23.1%), reaching the maximum, then decreased to month 1 (21.7%), 2 (17.4%), 6 (14.6%), and years 1 (12.4%) and 2 (4.4%). Stochastical analysis revealed that the increases and decreases of the numbers of labeled mitochondria as well as the labeling indices from the perinatal stage to the adult and senescent stages were significant ($P < 0.01$).

On the other hand, the results obtained from the numbers of mitochondria in binucleate hepatocytes showed an increase from the postnatal days 1 (66.2/cell), to 3 (66.4/cell), 14 (81.8/cell), to postnatal months 1 (89.9/cell), 2 (95.1/cell), and 6 (102.1), reaching the maximum at month 12 (128.0/cell), then decreased to years 2 (93.9/cell) as shown in **Figure 27** (upper left). The increase and decrease were stochastically significant ($P < 0.01$). The results obtained from visual counting on the numbers of mitochondria labeled with silver grains from 10 binucleate hepatocytes of each animal labeled with 3H-leucine demonstrating protein synthesis in 10 aging groups at postnatal day 1, 3, and 14, month 1, 6 and year 1 and 2, are plotted in **Figure 27** (lower left). The labeling indices in respective aging stages were calculated from the numbers of labeled mitochondria and the numbers of total mitochondria per cell which were plotted in **Figure 27** (right). The results showed that the numbers of labeled mitochondria with 3H-leucine showing protein synthesis increased from postnatal day 1 (7.3/cell) to day 3 (6.8/cell), 14 (10.2/cell), and month 1 (15.0/cell), 2 (15.9/cell), reaching the maximum at month 6 (19.6/cell), then decreased to year 1 (8.3/cell) and 2 (5.1/cell), while the labeling indices increased from postnatal day 1 (11.8%) to 3 (10.2%), 14 (12.5%), month 1 (18.3%) and 2 (18.7%), reaching the maximum at month 6 (19.2%), then decreased to year 1 (6.4%) and 2 (5.5%). Stochastical analysis revealed that the increases and decreases of the numbers of labeled mitochondria as well as the labeling indices from the newborn stage to the adult and senescent stages were significant ($P < 0.01$).

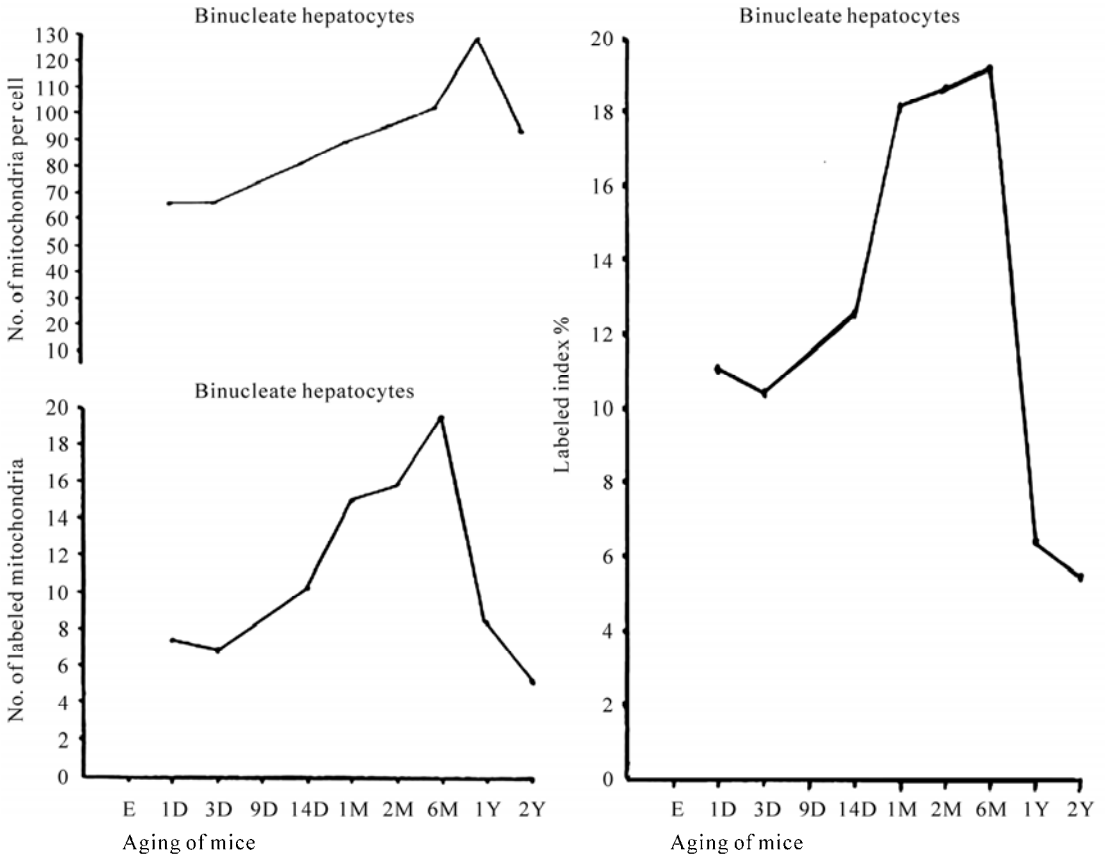

Figure 27. Transitional curves of the aging changes of binucleate hepatocyte mitochondria labeled with 3H-leucine showing protein synthesis. The upper left curve shows number of mitochondria per cell, which had much more mitochondria than mononucleate cell and showed an increase and decrease due to aging, the lower left shows number of labeled mitochondria per cell, which showed an increase and decrease, and the right shows labeling index which also showed an increase and decrease with aging.

4. THE ADRENAL GLAND

4.1. Structure of Mouse Adreno-Cortical Cells

We studied the adrenal tissues at various ages from embryo to postnatal 2 years. 30,31) The adrenal tissues obtained from ddY strain mice at various ages from embryo day 19 to postnatal day 30, consisted of the adrenal cortex and the adrenal medulla. The former consited of 3 layers, zona glomerulosa, zona fasciculata and zona reticularis, developing gradually with aging as observed by light microscopy. At embryonic day 19 and postnatal day 1, the adreno-cortical cells were composed mainly of polygonal cells, while the specific orientation of the 3 layers, zona glomerulosa, zona fasciculata and zona reticularis,was not yet well established. At postnatal day 3, orientation of 3 layers, especially the zona glomerulosa became evident. At postnatal day 9 and 14, the specific structure of 3 layers was completely formed and the arrangements of the cells in respective layer became typical especially at day 14 and month 1 (**Figure 28**). Observing the ultrastructure of the adreno-cortical cells by electron microscopy, cell organelles including mitochondria were not so well developed at perinatal and early postnatal stages from embryonic day 19 to postnatal day 9. However, these cell organelles, mitochondria, endoplasmic reticulum, Golgi apparatus, appeared well developed similarly to the adult stages at postnatal day 14. The zona glomerulosa (**Figures 29, 32, 35, 38**) is the thinnest layer found at the outer zone, covered by the capsule, consisted of closely packed groups of columnar or pyramidal cells forming arcades of cell columns. The cells contained many spherical mitochondria and well developed smooth surfaced endoplasmic reticulum but a compact Golgi apparatus in day 14 animals. The zona fasciculata (**Figures 30, 33, 36, 39**) was the thickest layer, consisted of polygonal cells which were larger than the glomerulosa cells, arranged in long cords disposed radially to the medulla containing many lipid droplets (**Figures 33, 36, 39**). The mitochondria were less numerous and were more variable in size and shape than those of the glomeruloza cells, while the smooth surfaced endoplasmic reticulum were more developed and the Golgi apparatus was larger than the glomerulosa. In the zona reticularis (**Figures 31, 34, 37, 40**), the parallel arrangement of cell cords were anastomosed showing networks continued to the medullar cells. The mitochondria were less numerous and were more variable in size and shape than those of the glomeruloza cells like the fasciculata cells, as well as the smooth surfaced endoplasmic reticulum were developed and the Golgi apparatus was large like the fasciculata cells. However, the structure of the adrenal cortex tissues showed changes due to development and aging at respective developmental stages.

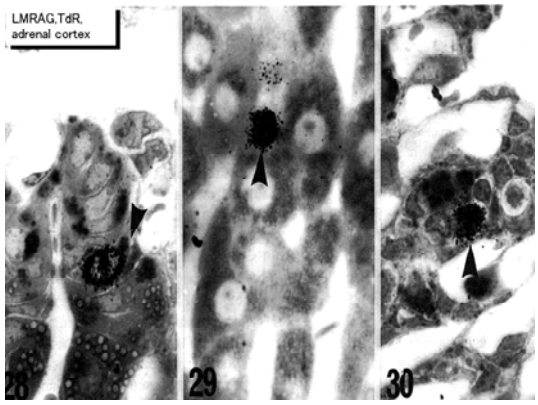

Figure 28. LM radioautograms of a young mouse adrenal cortex, zona glomerulosa (left), fasciculata (center), and reticularis (right), labeled with 3H-thymidine, demonstrating DNA synthesis of adreno-cortical cells. Silver grains are localized over the nuclei in each zone (arrows). x 800.

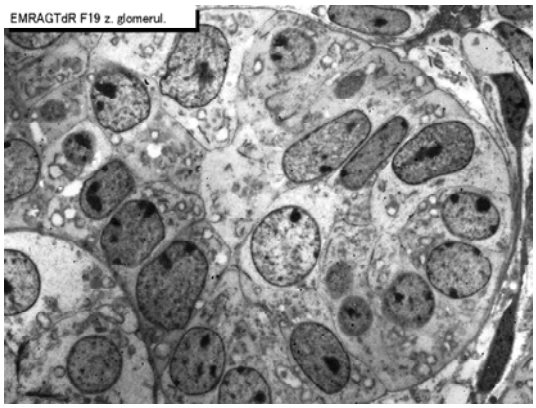

Figure 29. EM radioautogram of a mouse embryo adrenal gland at fetal day 19, labeled with 3H-thymidine, demonstrating DNA synthesis of adreno-cortical cells at zona glomerulosa. Silver grains are localized over euchromatin of the nuclei as well as over a few mitochondria. x 2,000.

4.2. DNA Synthesis in the Adreno-Cortical Cells

Observing EM radioautograms, the silver grains were found over the nuclei of some adreno-cortical cells labeled with 3H-thymidine, demonstrating DNA synthesis mainly in perinatal stages at embryonic day 19 (**Figures 29, 30, 31**), postnatal day 1 (**Figures 32, 33, 34**) and day 3 (**Figures 35, 36**), while less at day 9 (**Figure 37**), and day 14 (**Figures 38, 39, 40**).

However, those labeled cells were found in all the 3 layers, the zona glomerulosa (**Figures 29, 32, 35, 38**), the zona fasciculata (**Figures 30, 33, 36, 39**) and the zona reticularis (**Figures 31, 34, 36, 37, 40**), at respective aging stages. In the labeled adreno-cortical cells in 3

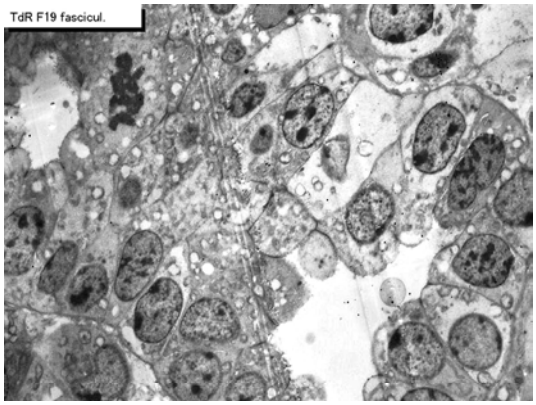

Figure 30. EMRAG of a mouse embryo adrenal gland at fetal day 19, labeled with 3H-thymidine, demonstrating DNA synthesis of adreno-cortical cells at zona fasciculata. Silver grains are localized over euchromatin of the nuclei as well as over a few mitochondria. x 2,000.

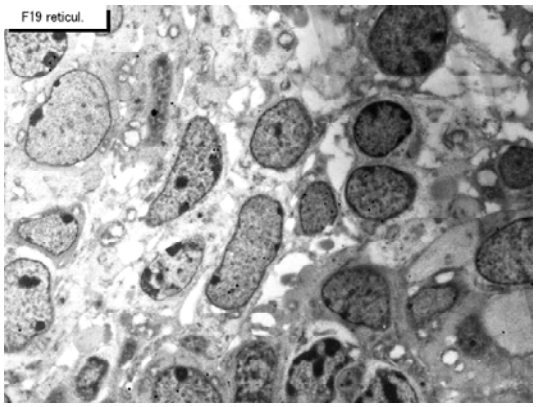

Figure 31. EMRAG of a mouse embryo adrenal gland at fetal day 19, labeled with 3H-thymidine, demonstrating DNA synthesis of adreno-cortical cells at zona reticularis. Silver grains are localized over euchromatin of the nuclei as well as over a few mitochondria. x 2,000.

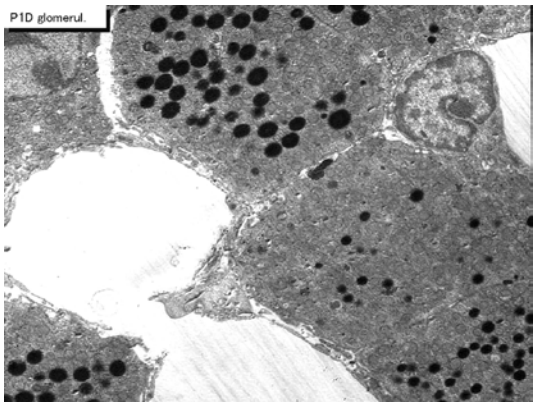

Figure 32. EMRAG of mouse adrenal gland at postnatal day 1, labeled with 3H-thymidine, demonstrating DNA synthesis of adreno-cortical cells at zona glomerulosa. x 3,000.

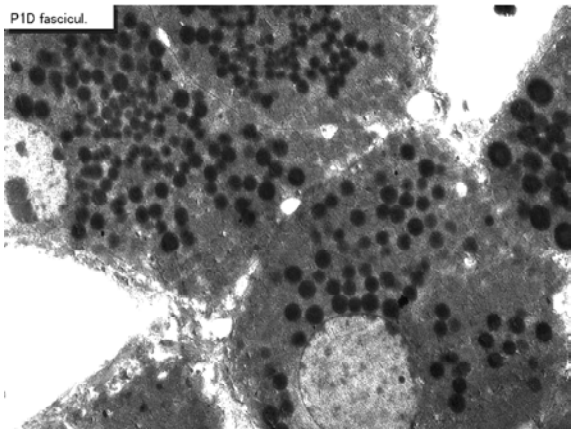

Figure 33. EMRAG of a newborn mouse adrenal gland at postnatal day 1, labeled with 3H-thymidine, demonstrating DNA synthesis of adreno-cortical cells at zona fasciculata. x 3,000.

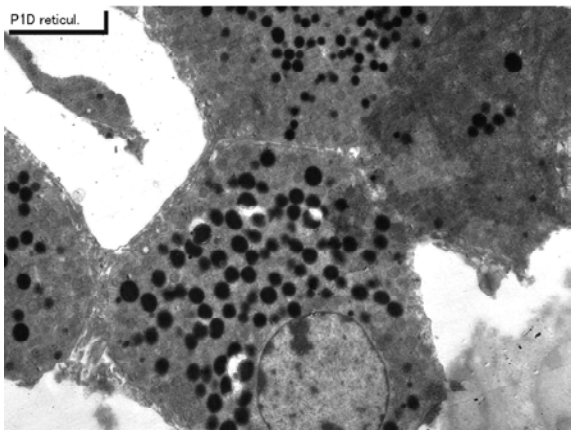

Figure 34. EMRAG of newborn mouse adrenal gland at postnatal day 1, labeled with 3H-thymidine, demonstrating DNA synthesis of adreno-cortical cells at zona reticularis. x 3,000.

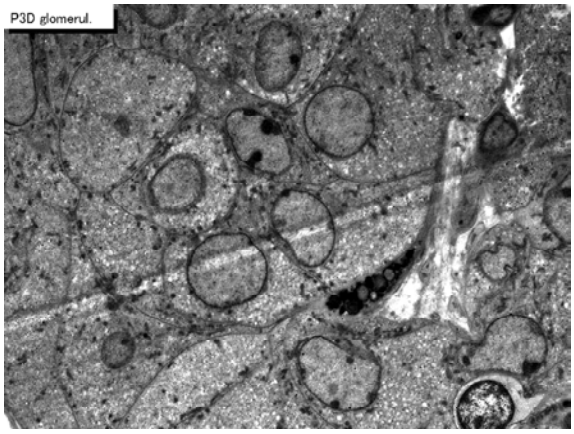

Figure 35. EMRAG of a newborn mouse adrenal gland at postnatal day 3, labeled with 3H-thymidine, demonstrating DNA synthesis of adreno-cortical cells at zona glomerulosa. x 3,000.

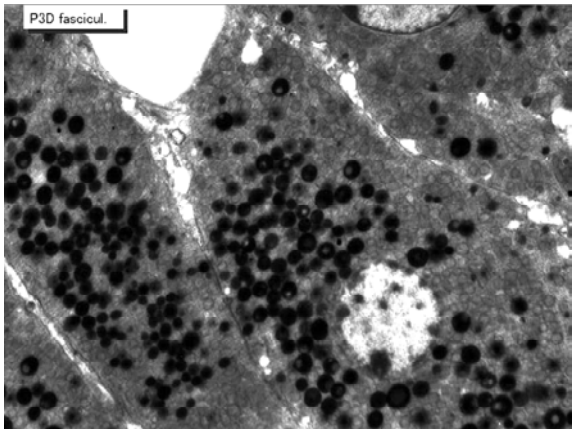

Figure 36. EMRAG of a newborn mouse adrenal gland at postnatal day 3, labeled with 3H-thymidine, demonstrating DNA synthesis of adreno-cortical cells at zona fasciculata. x 3,000.

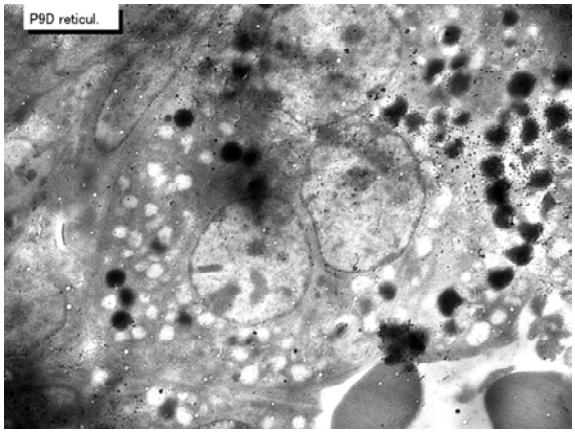

Figure 37. EMRAG of a juvenile mouse adrenal gland at postnatal day 9, labeled with 3H-thymidine, demonstrating DNA synthesis of adreno-cortical cells at zona reticularis. x 3,000.

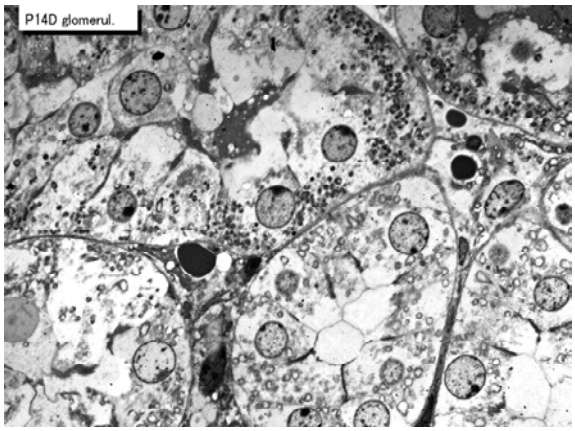

Figure 38. EMRAG of a juvenile mouse adrenal gland at postnatal day 14, labeled with 3H-thymidine, demonstrating DNA synthesis of adreno-cortical cells at zona glomerulosa. x 2,000.

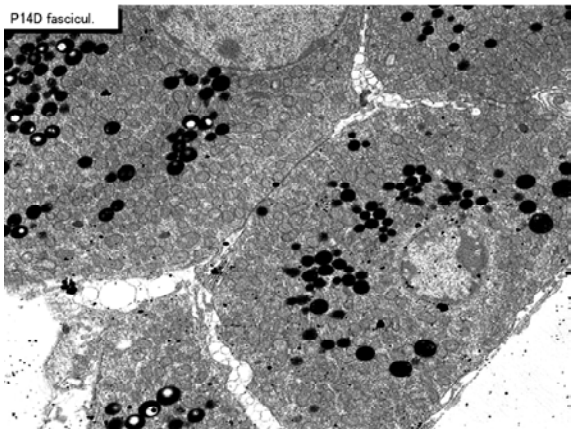

Figure 39. EMRAG of a juvenile mouse adrenal gland at postnatal day 14, labeled with 3H-thymidine, demonstrating DNA synthesis of adreno-cortical cells at zona fasciculata. x 3,000.

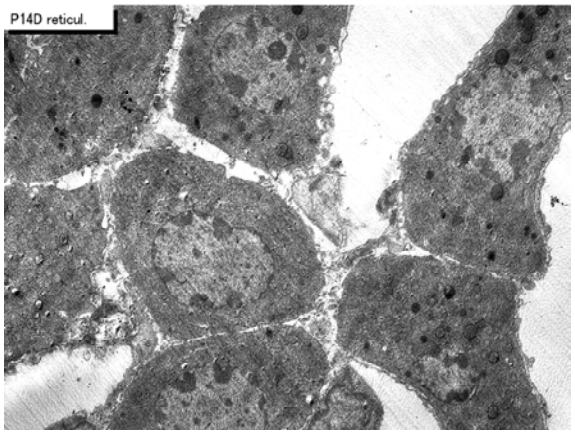

Figure 40. EMRAG of juvenile mouse adrenal gland at postnatal day 14, labeled with 3H-thymidine, demonstrating DNA synthesis of adreno-cortical cells at zona reticularis. x 3,000.

layers the silver grains were mainly localized over the euchromatin of the nuclei and only a few or several silver grains were found over the mitochondria of these cells. To the contrary, most adreno-cortical cells were not labeled with any silver grains in their nuclei nor cytoplasm, showing no DNA synthesis even after labeling with 3H-thymidine. Among many unlabeled adreno-cortical cells, most cells in the 3 layers were observed to be labeled with several silver grains over their mitochondria due to the incorporations of 3H-thymidine especially at the perinatal stages from embryonic day 19 (**Figure 29, 30, 31**) to postnatal day 1 (**Figure 32, 33, 34**), day 3 (**Figure 35, 36**), day 9 (**Figure 37**) and 14 (**Figure 38, 39, 40**). The localizations of silver grains over the mitochondria were mainly on the mitochondrial matrices (**Figure 39**).

4.3. Quantitative Analysis on the Adreno-Cortical Cells

4.3.1. Number of Mitochondria of Adreno-Corticl Cells

Preliminary quantitative analysis on the number of mitochondria in 10 adreno-cortical cells whose nuclei were labeled with silver grains and other 10 cells whose nuclei were not labeled in each aging group revealed that there was no significant difference between the number of mitochondria and the labeling indices ($P < 0.01$). Thus, the number of mitochondria and the labeling indices were calculated regardless whether their nuclei were labeled or not. The results obtained from the number of mitochondria in adreno-cortical cells in the 3 layers of respective animals in 5 aging groups at perinatal stages, prenatal embryo day 19, postnatal day 1, 3, 9 and 14, showed an gradual increase from the prenatal day 19 (glomerulosa 12.5, fasciculata 14.9, reticularis 15/2/cell) to postnatal day 14 (glomerulosa 37.8, fasciculata 37.3, reticularis 40.9/cell), as is shown in **Figure 41**. The increase from embryo day 19 to postnatal day 14 was stochastically significant ($P < 0.01$).

4.3.2. Mitochondrial DNA Synthesis of Mouse Adreno-Cortical Cells

The results of visual grain counts on the number of mitochondria labeled with silver grains obtained from 10 adreno-cortical cells in the 3 layers of each animal labeled with 3H-thymidine demonstrating DNA synthesis in 5 aging groups at perinatal stages, prenatal embryo day 19, postnatal day 1, 3, 9 and 14, are plotted in **Figure 42**. The results demonstrated that the numbers of labeled mitochondria with 3H-thymidine showing DNA synthesis gradually increased from prenatal embryo day 19 (glomerulosa 0.3, fasciculata 0.5, reticularis 0.4/cell) to postnatal day 14 (glomerulosa 1.5, fasciculata 1.5, reticularis 1.6/cell), reaching the maximum.

4.3.3. The Labeling Index of Mouse Adreno-Cortical Mitochondria

On the other hand, the labeling indices in respective aging stages were calculated from the number of labeled mitochondria (**Figure 41**) dividing by the number of total mitochondria per cell (**Figure 42**) which were plotted in **Figure 43**, respectively.

The results showed that the labeling indices gradually increased from prenatal day 19 (glomerulosa 2.4, fasciculata 2.7, reticularis 2.6%) to postnatal day 14 (glomerulosa 4.0, fasciculata 4.1, reticularis 3.9%), reaching the maximum (**Figure 43**).

5. THE LUNG

5.1. Structure of the Lung of Mouse

The pulmonary tissues obtained from ddY strain mice at

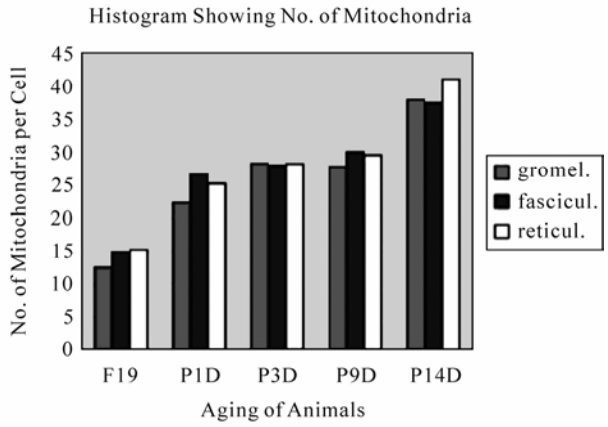

Figure 41. Histogram showing the aging changes of number of mitochondria per cell in 3 zones of glomerulosa, fasciculata and reticularis. It increased from embryo to postnatal day 14.

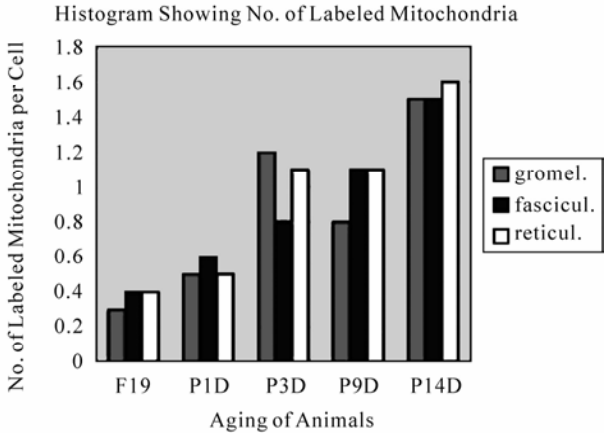

Figure 42. Histogram showing the aging changes of number of labeled mitochondria per cell in 3 zones of glomerulosa, fasciculata and reticularis. It increased from embryo to postnatal day 14.

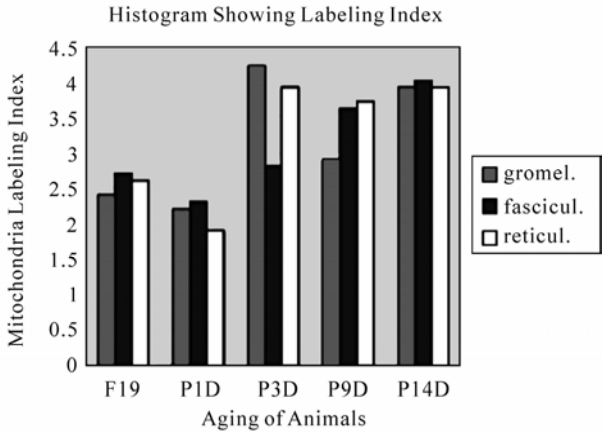

Figure 43. Histogram showing the aging changes of the labeling index of mitochondria in 3 zones of glomerulosa, fasciculata and reticularis. It increased from embryo to postnatal day 14.

embryonic to early postnatal stages consisted of undifferentiated cells (**Figure 44**). However, they differentiated into several types of cells due to aging, the type I epithelial cell (**Figure 45, 51**) or the small alveolar epithelial cell, the type II epithelial cell (**Figure 46, 52**) or the large alveolar epithelial cell, the interstitial cell (**Figure 47, 53**), the endothelial cell and alveolar phagocyte or dust cell as we had formerly observed (Sun 1995, Sun et al. 1994, 1995, 1997). 20,21) At embryonic day 16 and 18, the fetal lung tissues appeared as glandular organizations consisting of many alveoli bordering undifferentiated cuboidal cells and no squamous epithelial cells were seen (**Figure 44**). Mitotic figures were frequently observed in cuboidal epithelial cells. After birth, the structure of the alveoli was characterized by further development of the alveolar-capillary networks from postnatal day 1 to 3 and 7. During the development, the cellular composition of the alveolar epithelium resembled that of the adult lung, with a mixed population of the type I and type II epithelial cells. Up to 1 and 2 weeks after birth, the lung tissues showed complete alveolar structure and single capillary system almost the same as the adult after 1 month (**Figure 51, 52, 53**) to 2 to 6 months, and further to senescent stage over 12 months to 22 months.

5.2. Mitochondrial DNA Synthesis of Mouse Pulmonary Cells

On electron microscopic radioautograms of the pulmonary tissues labeled with 3H-thymidine, silver grains were observed over the nuclei of some pulmonary cells corresponding to the DNA synthesis in S-phase as observed by light microscopic radioautograpy (**Figure 44**). On the other hand, some mitochondria in both S-phase cells and interphase cells which did not show any silver grains over their nuclei were labeled with silver grains showing intramitochondrial DNA synthesis. The intramitochondrial DNA synthesis was observed in all the cell types, the type I epithelial cell (**Figure 45, 51**), the type II epithelial cell (**Figure 46, 52**), the interstitial cell (**Figure 47, 53**) and the endothelial cell. Because enough numbers of electron photographs (more than 5) were not obtained from all the cell types in respective aging groups, only some cell types and some aging groups where enough numbers of electron photographs were available were used for quantitative analysis. The numbers of mitochondria per cell profile area, the numbers of labeled mitochondria per cell and the labeling indices of the type I epithelial cells in only a few aging groups was shown in **Figure 48** (top). Likewise, the similar results from the type II epithelial cells (**Figure 49** top), the interstitial cells (**Figure 50** top) were shown. The labeling indices in respective aging stages were calculated from the number of labeled mitochondria and the number of total mitochondria per cellular profile area which were plotted in **Figures 48, 49, 50** (middle and bottom), respectively. These results demonstrated that the labeling indices in these cell types decreased from perinatal

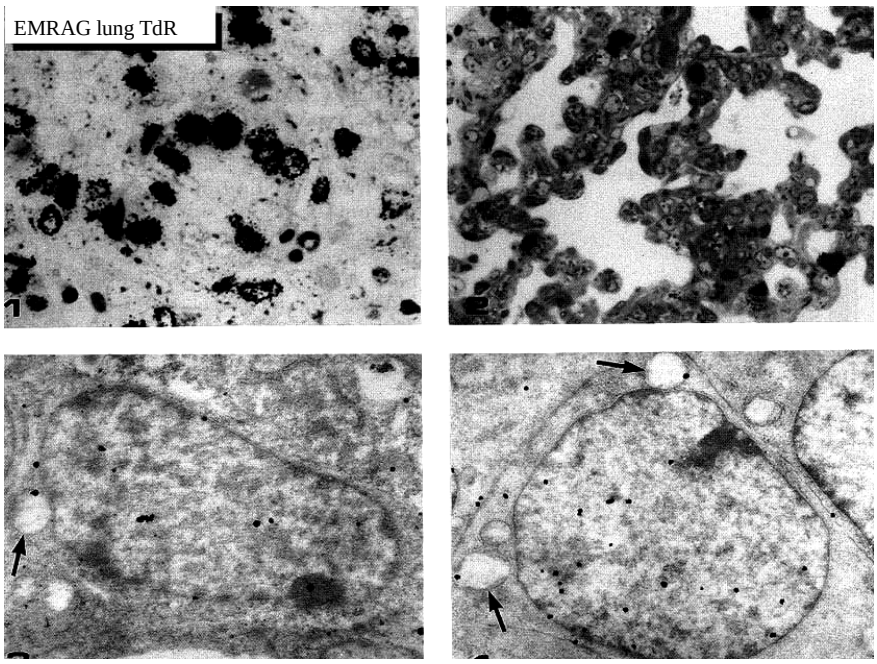

Figure 44. LMRAG of the lung tissues of mice at fetal day 16 (upper left), postnatal day 7 (upper right) x 800, and EMRAG of a mouse cuboidal cell at fetal day 16 (lower left), an interstitial cell (lower right) x 2,000.

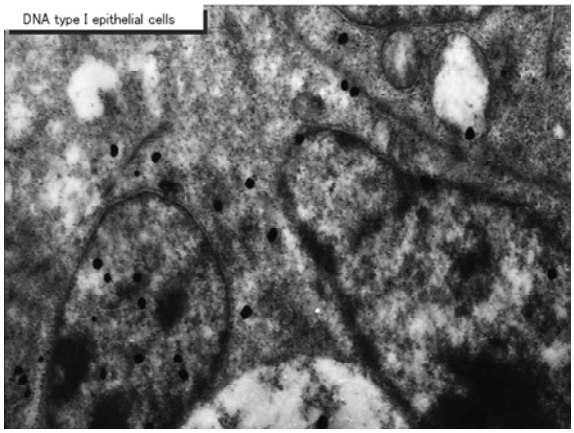

Figure 45. EMRAG of the type I epithelial cell of an aduldt mouse at postnatal month 1, labeled with 3H-thymidine. Silver grains are localized over nuclei and several mitochondria. x 4,000.

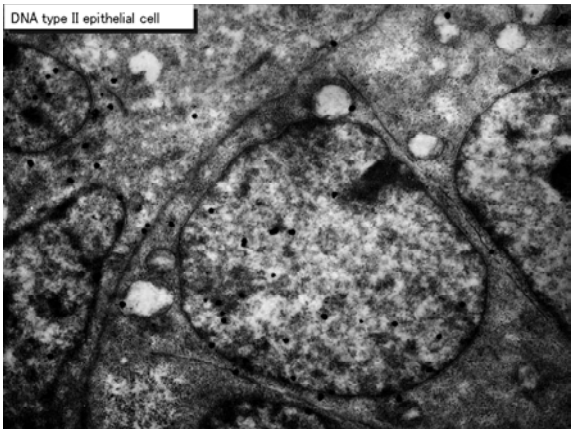

Figure 46. EMRAG of the type II epithelial cell of an adult mouse at postnatal month 1, labeled with 3H-thymidine. Silver grains are localized over nuclei and several mitochondria. x 4,000.

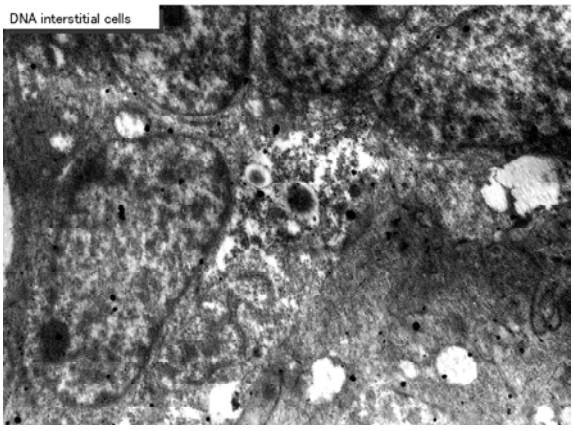

Figure 47. EMRAG of the interstitial cell of an adult mouse at postnatal month 1, labeled with 3H-thymidine. Silver grains are localized over nuclei and several mitochondria. x 4,000.

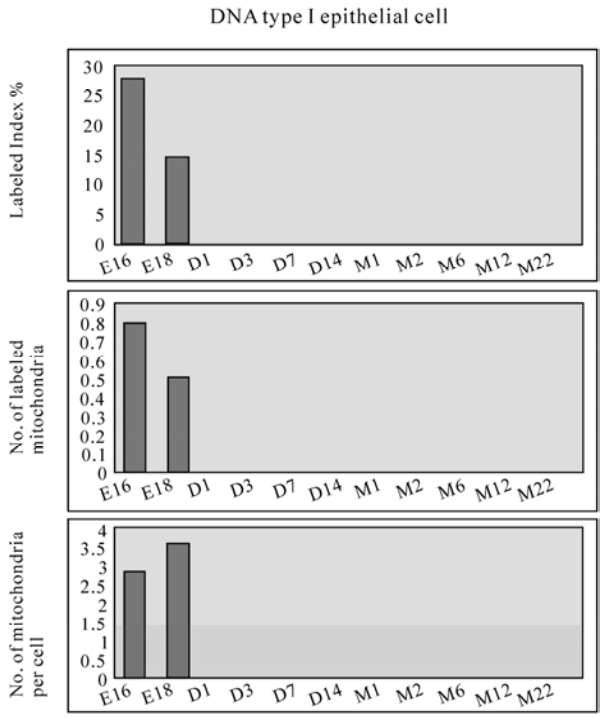

Figure 48. Histograms demonstrating the labeling index (top), number of labeled mitochondria (middle) and number of mitochondria (bottom) of the type I epithelial cells labeled with 3H-thymidine.

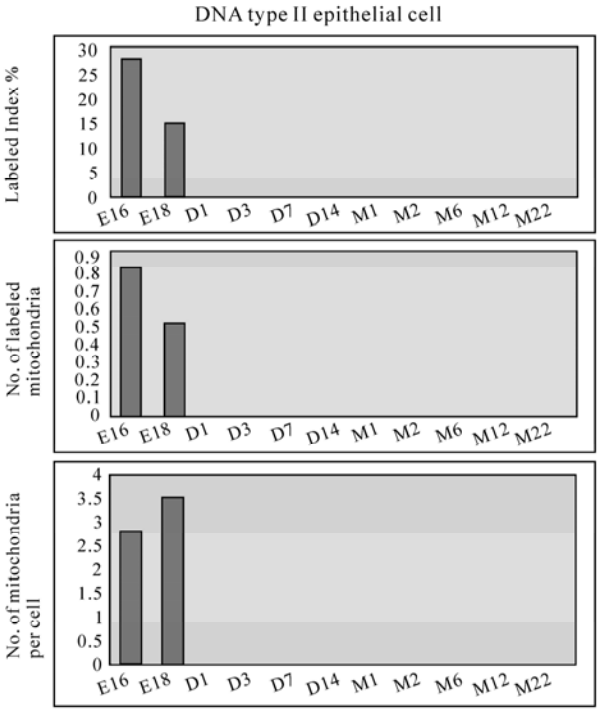

Figure 49. Histograms demonstrating the labeling index (top), number of labeled mitochondria (middle) and number of mitochondria (bottom) of the type II epithelial cells labeled with 3H-thymidine.

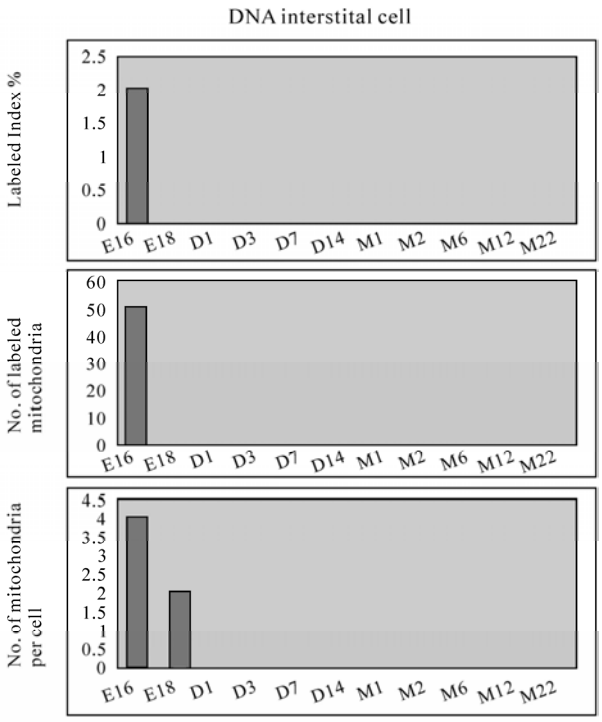

Figure 50. Histograms demonstrating the labeling index (top), number of labeled mitochondria (middle) and number of mitochondria (bottom) of the interstitial cells labeled with 3H-thymidine.

stages to the adult and senescent stage due to aging.

5.3. Mitochondrial RNA Synthesis of Mouse Pulmonary Cells

On electron microscopic radioautograms of pulmonary tissues labeled with 3H-uridine, silver grains were observed over the nuclei of some pulmonary cells corresponding to the RNA synthesis in most cells in respective aging groups as observed by light microscopic radioautograpy. The silver grains were observed to localize not only over euchromatin and nucleoli in the nuclei but also over many cell organelles such as endoplasmic reticulum, ribosomes, and mitochondria as well as cytoplasmic matrices of all the cell types. The intramitochondrial RNA synthesis was observed in all the cell types, the interstitial cell (**Figure 51**) the type I epithelial cell (**Figure 52**), the type II epithelial cell (**Figure 53**), and the endothelial cell. Because enough numbers of electron photographs (more than 5) were not obtained from all the cell types in respective aging groups, only some cell types and some aging groups when enough numbers of electron photographs were available were used for quantitative analysis similarly to DNA synthesis. The numbers of mitochondria per cell profile area, the numbers of labeled mitochondria per cell and the labeling indices of the type I epithelial cells in only a few

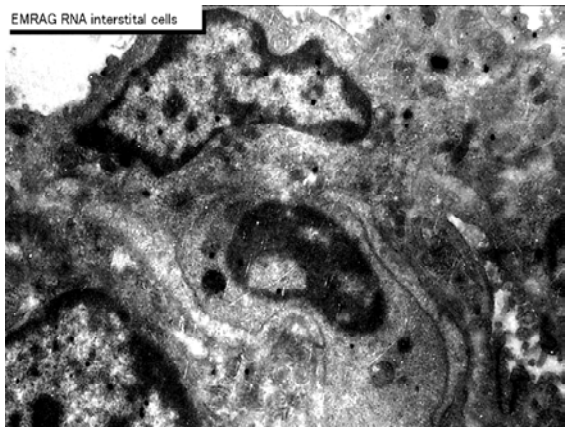

Figure 51. EMRAG of the interstitial cell of an adult mouse at postnatal month 1, labeled with 3H-uridine. Silver grains are localized over nucleus and several mitochondria. x 3,000.

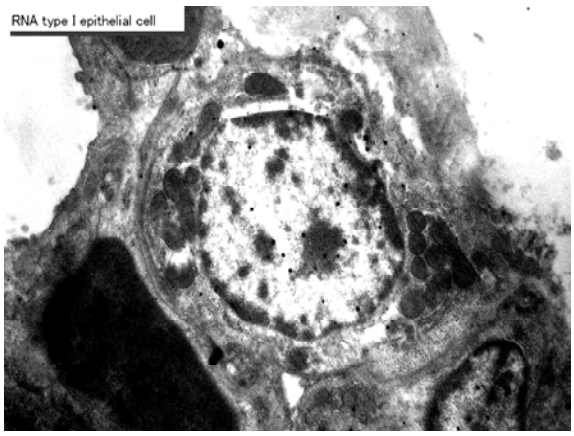

Figure 52. EMRAG of the type I epithelial cell of an adult mouse at postnatal month 1, labeled with 3H-uridine. Silver grains are localized over nucleus and several mitochondria. x 3,000.

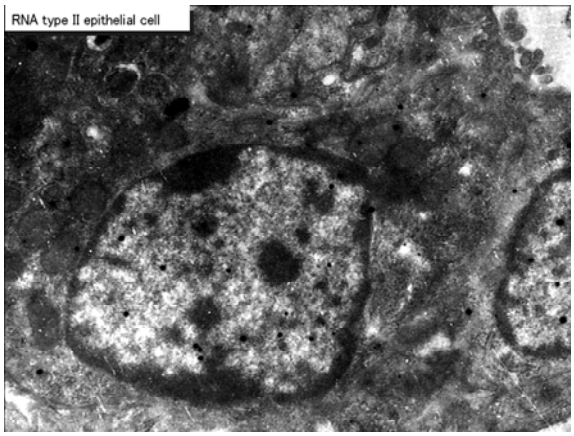

Figure 53. EMRAG of the type II epithelial cell of an adult mouse at postnatal month 1, labeled with 3H-uridine. Silver grains are localized over nucleus and several mitochondria. x 3,000.

aging groups was shown in **Figure 54**. Likewise, the similar results from the type II epithelial cells (**Figure 55** bottom), the interstitial cells (**Figure 56** bottom), and the endothelial cell (**Figure 57** bottom) were shown. The labeling indices in respective aging stages were calculated from the number of labeled mitochondria and the number of total mitochondria per cellular profile area were also shown in **Figures 54-57** (top and middle), respectively. These results demonstrated that the numbers of labeled mitochondria in these cell types increased from perinatal stages to the adult stage, reaching maxima at postnatal month 1, and decreased to the senescent stage due to aging.

6. THE TESTIS

The male reproductive system consists of the testis and its excretory ducts. We studied the macromolecular synthesis in the testis of aging ddY mice at various ages. 22) Gao. By LM and EM radioautography, many spermatogonia and myoid cells were labeled with 3H-thymidine at various ages from embryonic day 19 to postnatal day 1, 4, 7, 14 (**Figure 58**), month 1, 2, 6, 9, 12 and 24. Silver grains are localized over the nucleus and several mitochondria of the spermatogonia showing DNA synthesis. Among of the aging groups, we calculated the numbers of mitochondria per cell profile area, the numbers of labeled mitochondria per cell and the labeling indices of the spermatogonia from 4 aging groups, prenatal embryonic day 19, postnatal day 4, month 1 and 6. The results were listed in Table 1. It is clear that the LI of the spermatogonia increased from embryonic day 19 to postnatal month 1 (day 30), reaching the maximum, then decreased to month 6.

7. CONCLUSIONS

From the results obtained at present in our laboratory, macromolecular synthesis such as nucleic acids, both DNA and RNA, and protein synthesis showing incorporations of 3H-thymidine, 3H-uridine and 3H-leucine, respectively, were demonstrated in the nuclei and mitochondria of some mouse organs, *i. e.*, hepatocytes of the liver, adreno-cortical cells of the adrenal glands, pulmonary cells of the lungs of both sexes and spermatogonia of male mice at various ages from fetal to postnatal newborn, juvenile, young, adult and senescence.

The numbers of mitochondria per cell, the numbers of labeled mitochondria and the labeling indices of hepatocytes, adreno-cortical cells, pulmonary cells and spermatogonia at various ages changed due to aging. The numbers of mitochondria per cell in hepatocytes, adreno-cortical cells, pulmonary cells and spermatogonia increased from fetal to postnatal newborn, juvenile, young and adult animals. However, the numbers of

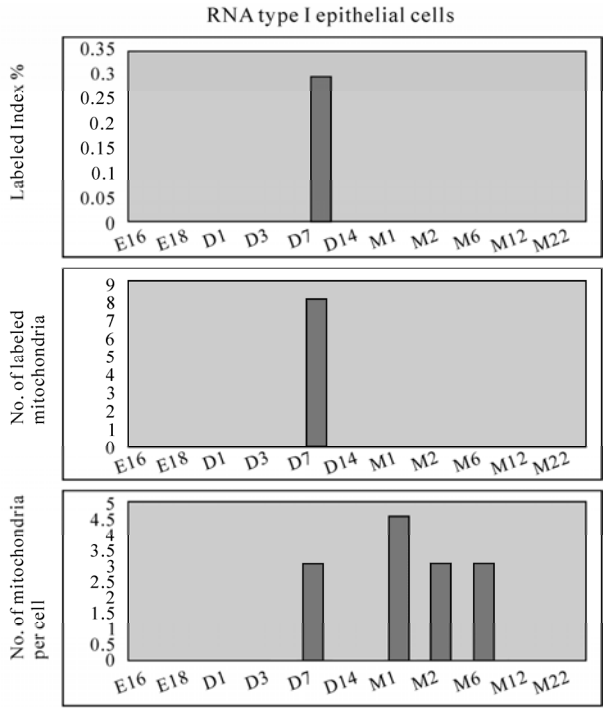

Figure 54. Histograms demonstrating the labeling index (top), number of labeled mitochondria (middle) and number of mitochondria (bottom) of the type I epithelial cell of an adult mouse at postnatal month 1, labeled with 3H-uridine.

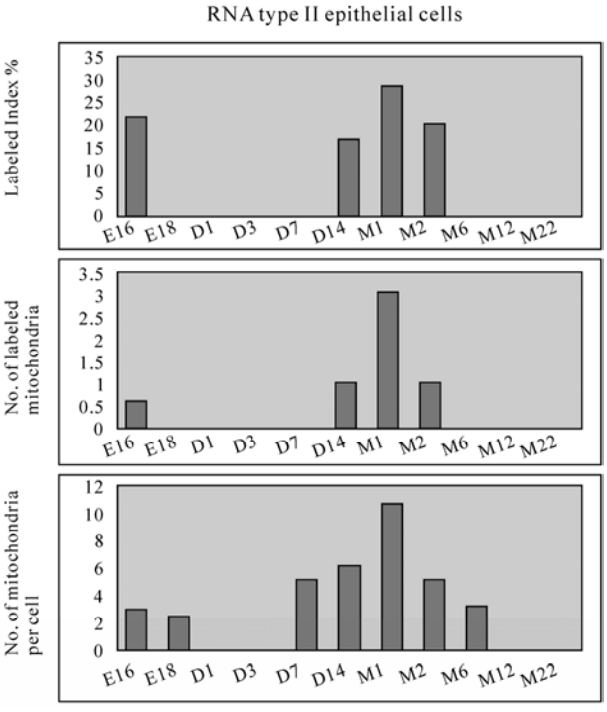

Figure 55. Histograms demonstrating the labeling index (top), number of labeled mitochondria (middle) and number of mitochondria (bottom) of the type II epithelial cells labeled with 3H-uridine.

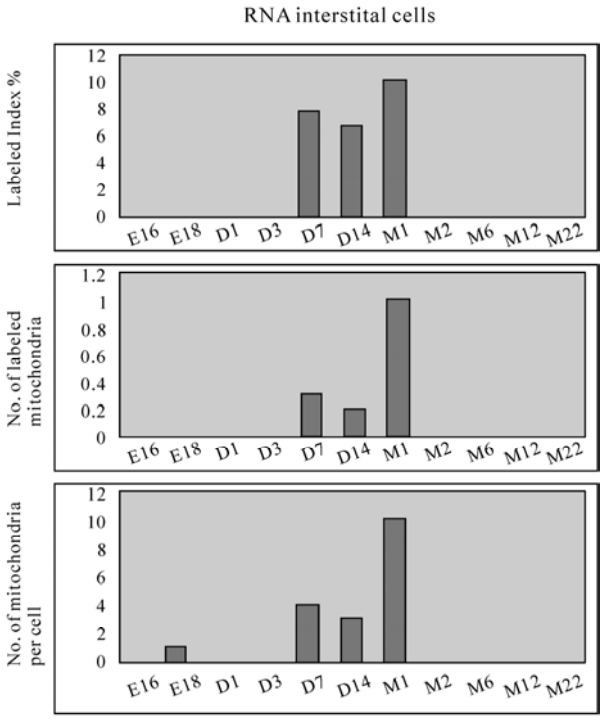

Figure 56. Histograms demonstrating the labeling index (top), number of labeled mitochondria (middle) and number of mitochondria (bottom) of the interstitial cells labeled with 3H-uridine.

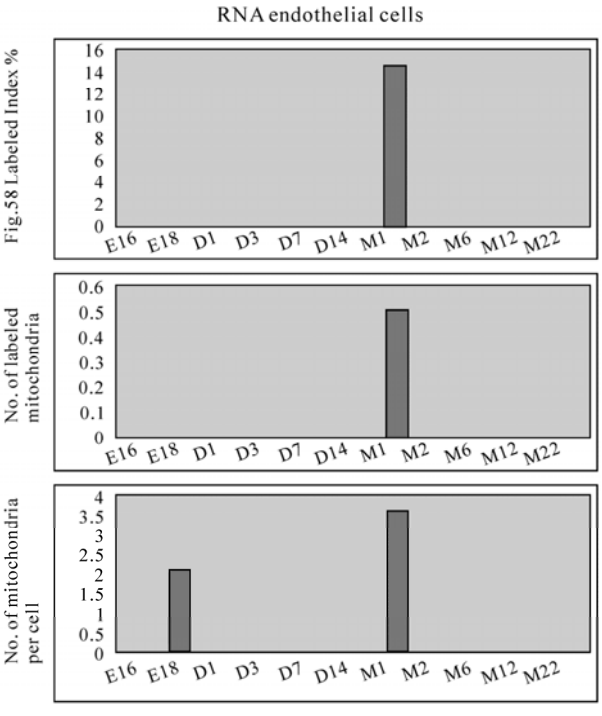

Figure 57. Histograms demonstrating the labeling index (top), number of labeled mitochondria (middle) and number of mitochondria (bottom) of the endothelial cells labeled with 3H-uridine.

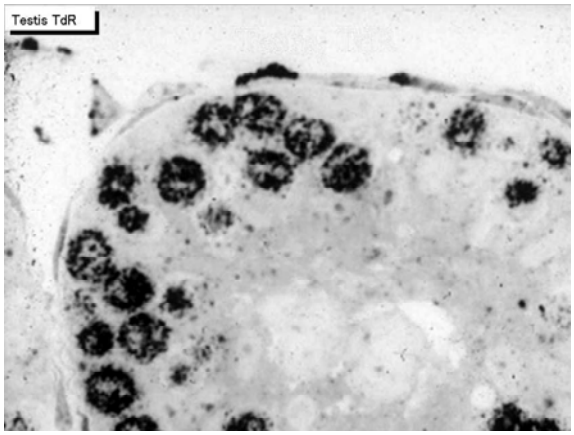

Figure 58. LMRAG of the testis tissue of a mouse at postnatal day month 1. Silver grains are localized over the nucleus as well as over the cytoplasm (mitochondria) of the spermatogonia showing DNA synthesis. x 800.

labeled mitochondria and the labeling indices in these organs increased from fetal to postnatal newborn, juvenile and young adults but decreased from juvenile and young adults to senescence. The maximal timings of respective organs as well as respective macromolecular precursors were different depending upon the organs and precursors. The DNA synthesis in hepatocytes peaked at postnatal day 14, while the RNA synthesis in hepatocytes peaked at postnatal month 1 and the protein synthesis at postnatal month 6. The DNA synthesis in adreno-cortical cells peaked at postnatal month 2. These differences between the organs and the precursors may have reflected the organ specificity.

We have also studied macromolecular synthesis of mitochondria in other cell types in vivo since we had found DNA, RNA and protein syntheses in cultured cells *in vitro* [1]. The results were reviewed in previous review article [35], as well as in several recent monographs [35,43-45].

These results indicate that the mitochondria in respective cell types of these organs synthesize DNA, RNA and proteins by themselves, increase and decrease due to the aging of the individual animals depending upon the organ specificities.

These results form parts of special cytochemistry [34] and special radioautographology [35].

8. ACKNOWLEDGEMENTS

These studies cited from the original articles authored and co-authored by the present author and associates were supported in part by Grant-in-Aids for Scientific Research from the Ministry of Education, Science and Culture of Japan (No. 02454564) while the author worked at Shinshu University School of Medicine as well as Grants for Promotion of Characteristic Research and Education from the Japan Foundation for Promotion of Private Schools (1997, 1998 1999, 2000) while

the author worked at Nagano Women's Jr. College. The author is also grateful to Grant-in-Aids for Scientific Research from the Japan Society for Promotion of Sciences (No. 18924034, No. 19924204 and No. 20929003) while the author has been working at Shinshu Institute of Alternative Medicine and Welfare since 2005 up to the present time. The author thanks Dr. Kiyokazu Kametani, Technical Official, Research Center for Instrumental Analysis, Shinshu University, for his technical assistance in electron microscopy during the course of this study.

REFERENCES

[1] Nagata, T., Shibata, O. and Nawa, T. (1967) Incorporation of tritiated thymidine into mitochondrial DNA of the liver and kidney cells of chickens and mice in tissue culture. *Histochemie*, **10(4),** 305-308.

[2] Nagata, T. (1972) Radioautographic study on intramitochondrial nucleic acid synthesis: Its relationship to the cell cycle in cultivated cells. *Proceedings of the* 4*th International Congress Histochemistry Cytochemistry*, Kyoto, 1972, 223-224.

[3] Nagata, T. (1972) Electron microscopic radioautography of intramitochondrial RNA synthesis of HeLa cells in culture. *Histochemie*, **32(2)**, 163-170.

[4] Nagata, T. (1972) Quantitative electron microscope radioautography of intramitochondrial nucleic acid synthesis. *Acta Histochemica Cytochemica*, **5**, 201-203.

[5] Nagata, T. (1974) Electron microscopic radioautography of intramitochondrial nucleic acid syntheses in mammalian cells *in vitro*. *Proceedings of the* 8*th International Congress of Electron Microscopy*, Canberra, 1974, 346-347.

[6] Nagata, T., Yamada, Y., Iwadare, N. and Murata, F. (1975) Relationship of intramitochondrial nucleic acid synthesis to the nucleoli in cultivated cells as revealed by electron microscopic radioautography. Proceedings of 10th International Congress Anat., Tokyo, 1975, 474-475.

[7] Nagata, T. and Murata, F. (1977) Electron microscopic dry-mounting radioautography for diffusible compounds by means of ultracryotomy. *Histochemistry*, **54(1)**, 75-82.

[8] Nagata, T., Iwadare, N. and Murata, F. (1977) Electron microscopic radioautography of nucleic acid synthesis in cultured cells treated with several carcinogens. *Acta Pharmacologica Toxicologica*, **41**, 64-65.

[9] Nagata, T. (1984) Electron microscopic observation of target cells previously observed by phase-contrast microscopy: Electron microscopic radioautography of laser beam irradiated cultured cells. *Journal of Clinical Electron Microscopy*, **17**, 589-570.

[10] Nagata, T., Ito, M. and Chen, S. (2000) Aging changes of DNA synthesis in the submandibular glands of mice as observed by light and electron microscopic radioautography. *Annals of Microscopy*, **1**, 13-22.

[11] Nagata, T., Ohno, S., Kawahara. I., Yamabayashi, S., Fujii, Y. and Murata, F. (1979) Light and electron microscopic radioautography of nucleic acid synthesis in mitochondria and peroxisomes of rat hepatic cells during and after DEHP administration. *Acta Histochemica Cytochemica*, **16**, 610-611.

[12] Nagata, T., Ohno, S., Yoshida, K. and Murata, F. (1982) Nucleic acid synthesis in proliferating peroxisomes of rat liver as revealed by electron microscopical radioautography. *Histochemica Journal*, **14(2)**, 197-204.

[13] Nagata, T., Fujii, Y. and Usuda, N. (1982) Demonstration of extranuclear nucleic acid synthesis in mammalian cells under experimental conditions by electron microscopic radioautography. *Proceedings of* 10*th International Congress Electron Microscopy*, Hamburg, 1982, 305-306.

[14] Ma, H. and Nagata, T. (1988) Studies on DNA synthesis of aging mice by means of electron microscopic radioautography. *Journal of Clinical Electron Microscopy*, **21**, 335-343.

[15] Ma, H., Gao, F., Sun, L., Jin, C. and Nagata, T. (1994) Electron microscopic radioautographic study on the synthesis of DNA, RNA and protein in the livers of aging mice. *Medical Electron Microscopy*, **27(3-4)**, 349-351.

[16] Nagata, T. and Ma, H. (2005) Electron microscopic radioautographic study of RNA synthesis in hepatocyte mitochondria of aging mouse. *Microscopy Research Technique*, **67(2)**, 55-64.

[17] Nagata, T., Usuda, N. and Ma, H. (1986) Electron microscopic radioautography of nucleic acid synthesis in pancreatic acinar cells of prenatal and postnatal aging mice. *Proceedings of* 11*th International Congress Electron Microscopy*, Kyoto, 1986, 2281-2282.

[18] Nagata, T. (1992) Radiolabeling of soluble and insoluble compounds as demonstrated by light and electron microscopy. In: Wegmann, R.J. and Wegmann, M.A. Eds., *Recent Advances in Cellular and Molecular Biology*, Peters Press, Leuven, 9-21.

[19] Sun, L., Gao, F., Jin, C. and Nagata, T. (1997) DNA synthesis in the trachea of aging mice by light and electron microscopic radioautography. *Acta Histochemica Cytochemica*, **30**, 211-220.

[20] Sun, L., Gao, F. and Nagata T. (1995) Study on the DNA synthesis of pulmonary cells in aging mice by light microscopic radioautography. *Molecular Biology of Cell*. **41(6)**, 851-859.

[21] Sun, L. (1995) Age related changes of RNA synthesis in the lungs of aging mice by light and electron microscopic radioautography. *Molecular Biology of Cell*. **41(8)**, 1061-1072.

[22] Hanai, T. and Nagata, T. (1995) Electron microscopic radioautographic study on nucleic acid synthesis in perinatal mouse kidney tissue. *Medical Electron Microscopy*, **27(3-4)**, 355-357.

[23] Gao, F., Ma, H., Sun, L., Jin, C. and Nagata, T. (1994) Electron microscopic radioautographic study on the nucleic acid and protein synthesis in the aging mouse testis. *Medical Electron Microscopy*, **27(3-4)**, 360-362.

[24] Gao, F., Chen, S., Sun. L., Kang, W., Wang, Z. and Nagata, T. (1995) Radioautographic study of the macromolecular synthesis of Leydig cells in aging mouse testis. *Molecular Biology of Cell*, **41**, 145-150.

[25] Yamada, A.T. and Nagata, T. (1994) Light and electron microscopic radioautography of DNA synthesis in the endometria of pregnant ovariectomized mice during activation of implantation window. *Molecular Biology of Cell*, **38(7)**, 763-774.

[26] Yamada, A.T. and Nagata, T. (1994) Ribonucleic acid and protein synthesis in the uterus of pregnant mouse during activation of implantation window. *Medical Electron*

Microscopy, **27(3-4)**, 363-365.

[27] Ito, M. and Nagata, T. (1996) Electron microscopic radioautographic study on DNA synthesis and the ultrastructure of the adrenal gland in aging mice. *Medical Electron Microscopy*, **29(3-4)**, 145-152.

[28] Liang, Y., Ito, M. and Nagata, T. (1999) Light and electron microscopic radioautographic studies on RNA synthesis in aging mouse adrenal gland. *Acta Anatomica Nipponica*, **74(3)**, 291- 300.

[29] Cui, H., Gao, F., Ma, H. and Nagata, T. (1996) Study on DNA synthesis of cellular elements in the cerebella of aging mice by light and electron microscopic radioautography. *Proceedings of the* 4*th China-Japan Joint Histochemistry and Cytochemistry Symposium*, Chongqing, 1996, 111-112.

[30] Gunarso, W., Gao, F., Cui, H., Ma, H. and Nagata, T. (1996) A light and electron microscopic radioautographic study on RNA synthesis in the retina of chick embryo. *Acta Histochemica*, **98(3)**, 300-322.

[31] Gunarso, W., Gao, F. and Nagata, T. (1997) Development and DNA synthesis in the retina of chick embryo observed by light and electron microscopic radioautography. *Molecular Biology of Cell*, **43(2)**, 189-201.

[32] Kong, Y. and Nagata, T. (1994) Electron microscopic radioautographic study on nucleic acid synthesis of perinatal mouse retina. *Medical Electron Microscopy***, 27(3-4)**, 366-368.

[33] Nagata, T. (1972) Radioautographic study on intramitochondrial nucleic acid synthesis: Its relationship to the cell cycle in cultivated cells. *Proceedings of* 4*th International Congress Histochemica Cytochemica*, Kyoto, 1972, 223-224.

[34] Nagata, T. (2001) Special Cytochemistry in Cell Biology. In: Jeon, K.W. Ed., *International Review of Cytology*, Academic Press, New York, 33-151.

[35] Nagata, T. (2002) Radioautographology General and Special, In: Graumann W. Ed., *Progress in histochemistry and cytochemistry*, Urban & Fischer, Jena, 2002, **37(2)**, 57-226.

[36] Nagata, T. (1997) Techniques and application of microscopic radioautography. *Histology and Histopathology*, **12(4)**, 1091-1124.

[37] Nagata, T. (1996) Techniques and application of electron microscopic radioautography. *The Journal of Electron Microscopy*, **45(4)**, 258-274.

[38] Nagata, T. and Ma, H. (2003) Electron microscopic radioautographic study on nucleic acid synthesis in amitotic hepatocytes of the aging mouse. *Medical Electron Microscopy*, **36(4)**, 263-271.

[39] Nagata, T. and Ma, H. (2005) Electron microscopic radioautographic study on mitochondrial DNA synthesis in hepatocytes of aging mouse. *Annals of Microscopy*, **5**, 4-18.

[40] Nagata, T. and Ma, H. (2005) Electron microscopic radioautographic study on RNA synthesis in hepatocytes of aging mouse. *Microscopy Research and Technique*, **64**, 55-64.

[41] Nagata, T. (2006) Electron microscopic radioautographic study on protein synthesis in hepatocyte mitochondria of developing mice. *Annals Microscopy*, **6**, 43-54, 2006.

[42] Nagata, T. (2007) Macromolecular synthesis in hepatocyte mitochondria of aging mice as revealed by electron microscopic radioautography. I. Nucleic acid synthesis. In: Vilas, A.M. and Alvarez, J.D. Eds., *Modern Research and Educational Topics in Microscopy*, Formatex, Badajoz, Spain, 245-258.

[43] Nagata, T. (2007) Macromolecular synthesis in hepatocyte mitochondria of aging mice as revealed by electron microscopic radioautography. II. Protein synthesis. In: Vilas, A.M. and Alvarez, J.D. Eds., *Modern Research and Educational Topics in Microscopy*. Formatex, Badajoz, Spain, 259-271.

[44] Nagata, T. (2008) Sexual difference between the macromolecular synthesis of hepatocyte mitochondria in male and female mice in aging as revealed by electron microscopic radioautography. In: Benninghouse, H.T. and Rosset, A.G. Eds., *Women and Aging*, Nova Sci. Publishers, USA, 461-487.

[45] Nagata, T. (2009) Protein synthesis in hepatocytes of mice as revealed by electron microscopic radioautography. In: Esterhouse, T.E. and Petrinos, L.B., Eds., *Protein Biosynthesis*, Nova Sci. Publishers, New York, USA, 133-161.

Advances in Bioscience and Biotechnology, 2010, 1, 263-275 **ABB**
doi:10.4236/abb.2010.14035 Published Online October 2010 (http://www.SciRP.org/journal/abb/).

Variations in wood tratis in micro and macro propagated plantation woods of *Populus deltoides* Bartr. ex Marsh

Pramod K. Pande[1], Ramesh C. Dhiman[2]

[1]Wood Anatomy Discipline, Botany Division Forest Research Institute;
[2]WIMCO Ltd. (Wimco Seedlings Division) Bagwala, Udhamsing Nagar, India.
Email: pandep123@rediffmail.com

Received 13 July 2010; revised 18 July 2010; accepted 21 July 2010.

ABSTRACT

The paper presents a comparison between intra-ramet, intra-clonal and inter-clonal variations in girth at breast height (gbh), fiber length, fiber diameter, wall thickness, vessel element length, vessel element diameter and specific gravity in the ramets of L34, G3 and S7C15 clones of *Populus deltoides* at the age of 6 years old produced from planting material grown by macro- and micro-propagation techniques. Variance ratio (F) test indicated that intra-ramet variations were non-significant for all the characters except specific gravity for height in L34 for macro and specific gravity and vessel element diameter for radial locations for micro, and fiber length for G3 (micro) for height, and specific gravity for radial location and fiber length for height for S7C15 clone for both the techniques. The clone L34 showed the significantly higher girth followed by G3 and S7C15. The variations were significant for girth, vessel element length and specific gravity between the wood produced from planting stocks grown by two techniques. Intra-clonal variations were significant for fiber length, fiber diameter and vessel element length. In general wood element's dimensions and specific gravity increased from bottom to top and pith to periphery radial locations. G3 clone was different from the L34 and S7C15 clone for the wood traits. The three different clones of *Populus deltoides* showed variability in wood anatomical properties and specific gravity in the woods grown from macro- and micro-propagated planting stock. So, the plantation raised by two techniques could not produce similar type of wood even from the same clone. G3 clone was the exception as it did not show variation in wood traits for two techniques. Intra-clonal variations in all the three clones of *P. deltoides* indicated that wood traits were not stable within the population of same clone grown by either method.

Keywords: Axial Variation; Radial Variation; Vessel Element's Dimension; Fiber Dimensions; Specific Gravity

1. INTRODUCTION

Populus deltoides is extensively used in plywood, match sticks, sports goods, wood-composites and paper industry. It is grown under different forestry programs as clonal plantations to ensure the genetic superiority for better growth and superior wood quality. Poplar is routinely propagated through shoot cuttings (macro-propagation). But, some plantations were also raised through micro-propagation techniques (tissue culture).

The variability in wood anatomical characteristics has profound influence on the properties of wood [1,2]. Features of interest in this connection include cell size, proportion and arrangements of different elements and specific gravity. The general pattern of variation in wood element dimensions is found not only within a species but also observed within a tree [3-6].

Variations in the dimensions of wood elements and specific gravity both within the ramet and among the clones have come under close scrutiny in recent years. There are reports available on the variation in wood anatomical and other properties in different clones of *Populus* elsewhere [7-10]. It showed that existing literature is only available on the screening of wood quality of poplar clones propagated by macro-propagation technique. No report is available on the comparison of variations on wood properties of macro-propagated with micro-propagated plantation wood.

The growth and wood quality are the two important parameters for the assessment of clones considering their end uses. The parameters *viz.*, wood elements dimensions, specific gravity and growth should be compared for two types of plantation woods *viz*. macro and micro-propagated, so that superior mass propagation technique can be recommended for commercial plantations for its specific end uses.

The present paper deals with the intra-ramet, intra-clonal and inter-clonal variations in wood anatomical parameters and specific gravity in plantation wood of three clones of *P. deltoides* viz., L34, G3. S7C15 which were produced from the planting stock grown by the macro- and micro-propagation techniques. This efforts was made to compare the wood properties of the wood produced thereof and harvested at 6 years age.

2. MATERIALS AND METHOD

2.1. The Experimental Site

Study site was located at Rudrapur (Udhamsing Nagar), Uttarakhand, India. It is situated at around 28˚N latitude; 78˚E longitude and at the altitude of 200 m asl. The annual rainfall was 1200 mm; of which 88% occurs during June-August. The average maximum summer temperature (April-June) was 36.7˚C and average minimum temperature (December-February) was 7.5˚C (2005-06). The soil of the site was sandy loam.

2.2. Planting Material

The micro-propagated plantlets of L34 and G3 clones maintained in containers (root trainers) were procured from Tata Energy Research Institute, New Delhi (India) during February/March 1996, whereas, that of S7C15 clone were procured from the State Forest Department (Haldwani) which they also reportedly procured from the Tata Energy Research Institute, New Delhi (India) during the same period. The plantlets of these three clones were planted along with the standard shoot cuttings (20-22 cm long with 3-4 alive and sound buds) in the nursery beds at the spacing of 80 cm x 50 cm at Research and Development Complex of Wimco Seedlings Ltd., Bagwala (India) during the month of March 1996. The nursery plants were grown through out the year by adopting standard cultural operations followed in growing poplar nurseries. Entire Transplants (ETPs-common name for the planting stock of poplar) of three clones were grown by using micro- and macro-propagation techniques.

The field trial for comparing the performance of the planting stock originally produced by both the techniques was established in Plot No. 6 of Nurpur Block of Parag Agro Farm Ltd. Kichha, Udham Singh Nagar, Uttrakhand in the Randomised Block Design having four replications. Each replicated plot was having 25 plants planted at 7 m × 3 m spacing over an area of 25 m^2. The total experimental area was therefore 12600 m^2 (1.26 ha) having planting stock of three clones grown from micro- and macro-propagated techniques (six treatments) in four replications. The trial was planted in the field on 18th January, 1997. The data on the growth and development of these trees was recorded each year; however the data during the harvesting of the trees at six years is only presented in this paper to indicate the growth variation in the trees during felling. The final survival of the entire trial was 65.7% in which planting stock of micro-propagated origin gave slightly better survival in all the three clones when compared with that of macro-propagated planting stock. The average tree in term of diameter growth was located in each replicated plot and trees from only three replicates were considered for the study. Height and diameter growth of each average tree from each clone in both macro- and micro-propagated categories considered for the present study are given in **Table 1**.

2.3. Sampling

Three ramets, propagated each from micro- and macro-propagated technique for each clone, were consider for this study. In total 18 ramets were felled during January, 2003 for the study. The height and girth of each tree was recorded. Four transverse discs of 10 cm thickness were cut form the trunk; one each at the base and from different three vertical heights at the 2.5 m regular intervals. In total, 72 discs were collected. The discs were referred as D1, D2, D3 and D4 from the base. Each disc was divided into three peripheral direction *i. e.* north, north-east and south-west to cover the peripheral variations. Each direction was divided into three pith to periphery radial locations *viz*. inner, middle and outer. Besides, a central block (pith) from each disc was also considered to see the variation in pith wood. In total 720 sample blocks were considered for anatomical studies like fiber length, fiber diameter, wall thickness, vessel element length, vessel element diameter and specific gravity. Standard laboratory methods were followed for the preparation of macerations. Wooden chips were fragmented into small pieces and put in the test tube. The material was macerated under 50% HNO_3 and a pinch of $KClO_3$. The macerated wood elements were thoroughly mixed and were spread on a glass slide and observations were taken under compound microscope [11]. Measurements for fiber length, fiber diameter, wall thickness, and vessel element length and vessel element diameter were taken from the macerated wood. Twenty

Table 1. Growth data of selected clones.

Clone	Origin	Average Height (m)		Av Diameter (cm)	
		Macro	Micro	Macro	Micro
L. 34	Lalkuan	28.3 ± 0.37	20.1 ± 0.42	27.9 ± 0.49	18.4 ± 0.85
S7C15	USA	23.3 ± 0.32	19.5 ± 0.64	22 ± 0.21	18 ± 0.19
G3	USA	25.1 ± 0.07	15.3 ± 0	22.9 ± 0.32	12.1 ± 0

five unbroken cells were sampled for the measurement of each parameter [12]. Specific gravity was determined by using the following formula [11].

Basic density = Oven dry weight/green volume

The basic density was converted into specific gravity as density of a wood sample relative to the density of water.

2.4. Statistical Analysis

The data obtained were statistically analyzed (using SPSS 10) Multivariate analysis to test the intra-ramet, intra-, inter-clonal variations and variations between the wood produced from planting stock originated by two techniques *i. e*. macro and micro- propagation. The null hypothesis of ANOVA (M) was there were no variations in selected wood anatomical parameters and specific gravity due to the fixed factors viz. radial location, peripheral direction, height, replication, clone and method of propagation. Finally, Variance ratio (F) test was used for the test of significance. The cluster analysis was done using SPSS 10 for wood anatomical properties and specific gravity.

3. RESULTS

Wood element's dimensions and specific gravity of selected clones of *Populus deltoides* propagated by macro- and micro-propagation techniques and the results of Multivariate analysis are given in **Table 2** to **9**.

Table 2. Pith to periphery variations in wood element's dimensions (µm) and specific gravity in micro and macro propagated wood (I = inner, M = middle, O = outer).

Clone	Location	FL	SD	FD(	SD	WT	SD	VL	SD	VD	SD	SG	SD
L34 Macro	I	956.67	76.31	23.67	1.04	3.50	0.15	522.11	32.85	99.3	5.458	0.371	0.030
	M	964.17	98.51	23.64	1.02	3.57	0.23	517.50	28.12	100.2	5.278	0.375	0.023
	O	960.03	63.32	23.89	0.96	3.60	0.37	518.31	35.25	100.9	7.328	0.407	0.049
	Mean	960.29	79.38	23.73	1.01	3.56	0.25	519.31	32.07	100.1	6.021	0.384	0.034
Micro	I	981.50	51.69	21.65	1.38	3.55	0.22	527.75	50.27	89.9	6.349	0.364	0.023
	M	992.39	51.31	21.99	1.43	3.52	0.22	546.36	41.69	91.3	5.469	0.375	0.045
	O	1015.33	94.93	22.10	1.36	3.59	0.25	557.94	43.12	91.6	6.685	0.399	0.041
	Mean	996.41	65.98	21.91	1.39	3.55	0.23	544.02	45.03	90.9	6.168	0.379	0.037
G3 Macro	I	1032.19	78.04	23.31	1.28	3.82	0.43	536.67	45.72	98.1	8.726	0.395	0.031
	M	1086.89	113.45	23.06	1.19	4.54	3.87	544.28	39.20	98.1	9.193	0.420	0.041
	O	1106.33	127.11	23.22	1.20	3.87	0.43	557.17	40.46	101.6	10.327	0.417	0.041
	Mean	1075.14	106.20	23.19	1.23	4.08	1.58	546.04	41.79	99.3	9.415	0.411	0.037
Micro	I	1080.69	134.24	23.72	1.73	3.96	0.47	578.78	32.82	96.2	8.255	0.336	0.025
	M	1083.69	128.52	23.61	1.64	4.03	0.41	577.72	33.31	117.8	136.264	0.334	0.028
	O	1073.11	112.39	23.44	1.78	4.01	0.40	572.75	32.67	95.0	13.624	0.366	0.027
	Mean	1079.17	125.05	23.59	1.72	4.00	0.43	576.42	32.93	103.0	52.714	0.345	0.027
S7C17 Macro	I	1022.03	133.02	22.39	1.25	4.18	0.26	548.92	46.97	90.4	6.005	0.367	0.034
	M	999.17	126.43	22.61	0.99	4.11	0.29	560.56	47.79	92.8	6.193	0.375	0.031
	O	1009.67	129.90	22.64	1.27	4.14	0.35	552.75	47.49	91.9	4.281	0.405	0.032
	Mean	1010.29	129.78	22.55	1.17	4.15	0.30	554.07	47.42	91.7	5.493	0.383	0.032
Micro	I	952.92	46.38	23.44	0.61	3.75	0.14	539.25	17.10	97.3	3.148	0.354	0.024
	M	950.89	46.09	23.42	0.69	3.74	0.13	538.81	24.91	97.3	4.579	0.360	0.030
	O	958.64	50.35	23.47	0.56	3.71	0.13	539.75	15.48	95.8	12.597	0.392	0.038
	Mean	954.15	47.61	23.44	0.62	3.73	0.13	539.27	19.16	96.8	6.775	0.369	0.031

Note: FL = fiber length, FD = fiber diameter, WT = wall thickness, VL = vessel element length, VD = vessel element diameter, SG = specific gravity.

3.1. Variations in Micro vs. Macro Propagated Wood

3.1.1. Variations for All Clones

3.1.1.1. Variation in Growth

Variance ratio (F) test indicated that variation in girth at breast height (gbh) was significant for clone, technique and height. The clone L34 showed the significantly higher girth followed by G3 and S7C15 clone. The girth (cm) was significantly higher in macro-propagated than micro-propagated ramets (**Table 6**). The girth significantly varied from bottom to top. The average girth (cm) of 3 clones at selected height was in D1 (77.39), D2 (61), D3 (55.78) and D4 (46.72).

3.1.1.2. Variation in Wood Anatomical Parameters and Specific Gravity

Variance ratio (F) test indicated that intra-ramet variations were non-significant for all the characters except specific gravity for height in L34 for macro and specific gravity and vessel element diameter for radial locations for micro, and fiber length for G3 (micro) for height, and specific gravity for location and fiber length for height in S7C15 clone for both the techniques (**Table 5**) while inter-clonal variations were significant for fiber length, fiber diameter, wall thickness and vessel element length. The variations were significant for techniques (micro and macro-propagated) for vessel element length and specific gravity. Intra-clonal variations were significant for fiber length, fiber diameter and vessel element length (**Table 6**). In general wood element's dimensions and specific gravity increased from bottom to top and pith to periphery locations (**Table 2** and **3**). The average values of all the clones indicated that wall thickness and specific gravity were higher in macro-propagated wood while fiber length and vessel element length in micro-propagated wood. The range was 954 µm (S7C15, micro)-1079 µm (G3, micro) for fiber length; 21.91 µm (L34, micro) - 23.73 µm (L-34, macro) for fiber diameter; 3.55 µm ((L34, micro) - 4.15 µm (S7C15, macro) for wall thickness; 519 µm (L- (L34, macro) – 575 µm (G3, micro) for vessel element length; 92 µm (S7C15, macro) – 103 µm (G3, micro) and 0.345 (G3, micro) -0.411 (G3, macro) (**Table 5**). The grouping of different clones for fiber length was (S7C15-micro, L34-macro), (L34-micro, L34-macro), (L34-micro, S7C15-macro), (G3-macro, G3-micro); for fiber diameter was (L34-micro), (S7C15-macro), (G3-macro, S7C15-micro, L34-macro) for wall thickness was (L34-micro, L-34 macro, S7C15-micro), (G3-micro, G3-macro, S7C15-macro); for vessel element length was (L34-macro), (G3-macro), (S7C15-micro, L34-micro, G3-macro, S7C15-macro) and for specific gravity was (G3-micro), (S7C15-micro, L34-micro, S7C15-macro), (L34-macro, S7C15-macro, L34-macro) and (G3-micro). The percent co-variance indicated that there was not much difference between variation pattern of micro and macro propagated plantation wood (**Table 4**).

3.1.2. Variations in Individual Clones

3.1.2.1. L-34 Clone

Variations in wood element's dimensions between micro and macro propagated plantation's wood were significant for fiber length, fiber diameter, vessel element length and vessel element diameter; fiber length, fiber diameter, wall thickness and vessel element diameter for replication; vessel element diameter for bottom to top; fiber length for peripheral direction and specific gravity for radial locations. Fiber length and vessel element length were significantly higher in micro-propagated wood while fiber diameter and vessel element diameter were significantly higher in macro-propagated wood (**Table 7**). Bottom to top variation for fiber length ranged between 935 µm (D3) to 985 µm and specific gravity ranged between 0.367 (D1) to 0.392 µm (**Table 3**).

3.1.2.2. G3 Clone

Variations between micro- and macro-propagated plantation's wood were significant for vessel element length and specific gravity; fiber length, fiber diameter and vessel element length for replication; vessel element length and specific gravity for bottom to top and specific gravity for radial locations. Vessel element length was significantly higher for micro-propagated wood while specific gravity for macro- propagated wood (**Table 8**). Bottom to top variation for fiber length ranged between 1053.67 µm (D2)-1122. 41 µm (D1) (**Table 3**).

3.1.2.3. S7 C15 Clone

Fiber length, fiber diameter, wall thickness and vessel element length significantly varied between micro- and macro-propagated plantation's wood; fiber length, wall thickness, vessel element length and specific gravity for replication; fiber length for bottom to top and specific gravity for radial locations. Fiber length, wall thickness and vessel element length was significantly higher in macro-propagated wood whereas fiber diameter in micro propagated wood (**Table 4** and **9**). Bottom to top variation for fiber length ranged between 958 µm (D3) to 1053.37 µm (D1).

3.2 Variations in Macro Propagated Wood

3.2.1 Variations in All Clones

Variations in all wood elements' dimensions were significant for clones; fiber length, fiber diameter, vessel element length and specific gravity for replication; fiber length and specific gravity for bottom to top and for radial

Table 3. Bottom to top variations in wood element's dimensions (µm) and specific gravity (D1 bottom disc and D2, D3, and D4 are 4 successive discs at the 2.5 m intervals).

			Macro						Micro					
Parameter/Clone			FL	FD	WT	VL	VD	SG	FL	FD	WT	VL	VD	SG
L 34	D 1	Mean	973.52	23.56	3.47	514.04	100.56	0.38	981.67	21.56	3.63	531.30	91.15	0.367
		SD	73.26	0.91	0.18	29.83	3.38	0.04	63.82	1.55	0.21	36.03	3.12	0.028
	D2	Mean	946.63	24.11	3.53	517.11	101.74	0.38	1011.44	21.67	3.52	550.67	93.52	0.375
		SD	58.16	1.22	0.22	32.77	4.09	0.03	101.44	1.42	0.29	44.62	7.77	0.030
	D3	Mean	935.37	23.84	3.61	524.37	100.33	0.38	1002.70	22.09	3.53	549.67	88.07	0.383
		SD	49.58	0.58	0.37	30.93	8.78	0.04	56.51	1.50	0.19	65.32	6.76	0.030
	D4	Mean	985.63	23.43	3.61	521.70	97.78	0.39	989.81	22.32	3.53	544.44	91	0.392
		SD	115.94	1.09	0.26	34.93	6.15	0.05	44.67	0.94	0.20	32.94	5.061	0.061
Mean			960.29	23.73	3.56	519.31	100.10	0.38	996.41	21.91	3.55	544.02	90.935	0.379
SD			74.24	0.95	0.25	32.11	5.60	0.04	66.61	1.35	0.22	44.73	5.679	0.037
G3	D1	Mean	1063.89	23.41	3.74	557.93	103.30	0.38	1103.22	23.26	4.14	589.59	101.481	0.326
		SD	107.92	1.45	0.44	39.29	13.07	0.03	156.96	0.86	0.28	31.91	18.404	0.020
	D2	Mean	1053.67	23.22	3.94	552.67	97.89	0.40	1110.37	23.33	4.2	574.78	95.667	0.359
		SD	82.43	1.15	0.19	34.10	6.13	0.04	139.04	1.14	0.29	39.64	5.657	0.025
	D3	Mean	1060.59	22.81	4.76	527.07	96.41	0.43	1056.85	24.04	3.82	572.48	92.481	0.352
		SD	122.33	1.27	4.46	47.39	9.89	0.04	101.23	2.46	0.61	30.20	6.435	0.033
	D4	Mean	1122.41	23.33	3.87	546.48	99.41	0.43	1046.22	23.74	3.85	568.81	122.296	0.345
		SD	121.69	0.92	0.61	43.19	6.15	0.03	78.15	1.87	0.31	25.46	157.546	0.032
Mean			1075.14	23.19	4.08	546.04	99.25	0.41	1079.17	23.59	4.00	576.42	102.981	0.345
SD			108.59	1.20	1.43	40.99	8.81	0.03	118.85	1.58	0.37	31.80	47.011	0.028
S7C15	D1	Mean	1053.37	22.44	4.11	545.33	89.41	0.37	962.67	23.33	3.66	532.59	96.519	0.355
		SD	171.31	1.09	0.37	46.65	6.46	0.04	32.41	0.68	0.12	11.28	4.173	0.031
	D2	Mean	1052.37	22.70	4.16	549.11	91.30	0.39	967.44	23.44	3.71	534.78	97.963	0.366
		SD	159.98	1.35	0.32	59.90	7.16	0.04	49.20	0.51	0.11	23.40	3.436	0.033
	D3	Mean	958.63	22.30	4.09	550.33	92.04	0.38	969.07	23.44	3.76	548.22	99.222	0.380
		SD	65.84	1.27	0.23	33.61	3.09	0.03	52.45	0.75	0.12	21.25	4.003	0.037
	D4	Mean	976.78	22.74	4.21	571.52	93.96	0.39	917.41	23.56	3.80	541.48	93.481	0.374
		SD	37.87	0.94	0.26	43.01	3.92	0.04	33.14	0.51	0.14	16.43	13.891	0.036
Mean			1010.29	22.55	4.15	554.07	91.68	0.38	954.15	23.44	3.73	539.27	96.796	0.369
SD			108.75	1.16	0.30	45.79	5.16	0.04	41.80	0.61	0.123014	18.09	6.376	0.034

Note: FL = fiber length, FD = fiber diameter, WT = wall thickness, VL = vessel element length, VD = vessel element diameter, SG = specific gravity.

Table 4. Mean ± SD for wood element's dimensions (µm) and specific gravity.

Parameter/Clone			FL	FD	WT	VL	VD	SG
L34	Macro	Mean	960	24	3.56	519	100	0.384
		SD	80	1	0.27	32.0	6.1	0.039
		%CV	8	4	8	6	6	10
	Micro	Mean	996	22	3.55	544	91	0.379
		SD	70	1	0.23	46	6	0.040
		%CV	7	6	6	9	7	11
G3	Macro	Mean	1075	23	4.08	546	99	0.411
		SD	112	1	2.27	42	9	0.039
		%CV	10	5	56	8	10	9
	Micro	Mean	1079	24	4.00	576	103	0.345
		SD	124	2	0.42	33	11	0.030
		%CV	12	7	11	6	11	9
S7C15	Macro	Mean	1010	23	4.15	554	92	0.383
		SD	129	1	0.30	47	6	0.036
		%CV	13	5	7	9	6	9
	Micro	Mean	954	23	3.73	539	97	0.369
		SD	47	1	0.13	19	8	0.035
		%CV	5	3	4	4	8	10

Note: FL = fiber length, FD = fiber diameter, WT = wall thickness, VL = vessel element length, VD = vessel element diameter, SG = specific gravity, SD = standard deviation, CV = covariance.

direction (**Table 6**). The range was 960 µm (L34) –1075 µm (G3) for fiber length; 22.55 µm (S7C15) –23.73 (L34) for fiber diameter; 3.56 µm (L34) –4.15 µm (S7C15) for wall thickness; 519 µm (L34) –554 µm (S7C15) for vessel element length; 91.68 µm (S7C15) –100.10 µm (L34) for vessel element diameter and 0.38 (S7C15) –0.41 (G3) for specific gravity. The percent variations were recorded for 8 (L34) –13 (S7C15) for fiber length; 7 (S7C15) –56 (G3) for wall thickness; 6 (L34)-9 (S7c15) for vessel element length and 6 (L34) - 10 (S7C15) for vessel element diameter (**Table 4**). It showed that clones and replicate ramets showed variations in the wood element dimensions and specific gravity.

3.2.2 Variations in Individual Clones

3.2.2.1 L-34 Clone

Variations were significant for fiber length, wall thickness and vessel element length for replication; fiber length for bottom to top and specific gravity for radial locations (**Table 7**). The pith to periphery variations were ranged between 957 µm (pith) – 964 µm (middle) for fiber length; 23.64 µm (middle) – 23.89 µm (outer) for fiber diameter; 3.50 µm (pith) – 3.60 µm (outer) for wall thickness and 0.371 (pith) – 0.407 (outer) for specific gravity.

3.2.2.2 G3 Clone

Variations were significant for fiber length, fiber diameter, vessel element length, vessel element diameter and specific gravity for replication; fiber length and specific gravity from bottom to top and fiber length and specific gravity for radial locations (**Table 8**). The pith to periphery variations were ranged between 1032 µm (pith) – 1106 µm (outer) for fiber length and 0.395 (pith) – 0.42 (middle) for specific gravity (**Table 2**).

3.2.2.3 S7 C15 Clone

Variations were significant for all the characters except vessel element diameter for replication; fiber length for bottom to top and specific gravity for radial locations (**Table 9**). The pith to periphery variations were ranged between 0.367 (pith) – 0.405 for specific gravity (outer) (**Table 2**).

3.3. Variations in Micro Propagated Wood

3.3.1. Variations in All Clones

Fiber length, fiber diameter, wall thickness, vessel element length and specific gravity significantly varied for clones; fiber length, fiber diameter and vessel element length for replication; fiber length and specific gravity for bottom to top; fiber length and specific gravity for peripheral direction and specific gravity for radial locations in micro propagated trees (**Table 6**). The range was 954 µm (S7C15) –1079 µm (G3) for fiber length; 21.91 µm (G3) - 23.59 (G3) for fiber diameter; 3.55 µm (L34) –4.0 µm (G3) for wall thickness; 539 µm (S7C15) –546 µm (G3) for vessel element length; 90.94 µm (L34) – 102.98 µm (G3) for vessel element diameter and 0.35 (G3) –0.379 (L34) for specific gravity. The percent variations were recorded for 5 (S7C15) –12 (G3) for fiber length; 4 (S7C15) –11 (G3) for wall thickness; 4 (S7C15)-9 (L34); 6 (L34)-11 (G3) for vessel element length (Table 4). It shows that variations in wood element dimensions have not much difference among different clones.

3.3.2. Variations in Individual Clones

3.3.2.1. L-34 Clone

Variations were significant for fiber length and vessel element diameter for replication; vessel element diameter for bottom to top; fiber length for peripheral direction and specific gravity for radial locations (**Table 7**). The

Table 5. Intra-ramet variations in different clones.

Wood parameters/Source of variation		MSS					
		FL	FD	WT	VL	VD	SG
L34 (Macro)	df						
Height	3	2164.9	.674	0.023	1359.	49.43	0.019*
Direction	2	70.194	.399	0.026	939.194	22.861	0.0027
Location	2	569.7	0.49	0.011	2531.028	42.52	0.013
Error	28	732.7	.821	0.022	440.7	47.63	0.0011
Micro							
Height	3	20288.102	4.472	0.0037	12200.2	313.963*	0.00073
Direction	2	10802.7	.778	0.0044	5909.361	121.194	0.00028
Location	2	13268.528	1.194	0.017	13022.528	75.444	0.0073*
Error	28	4856.627	1.748	0.056	3297.9	28.835	0.0005
G3 (Macro)							
Height	3	1939.282	1.010	0.01	225.896	15.136	0.004
Direction	2	1073.740	.201	0.036	3052.917	81.419	0.0005
Location	2	2040.307	0.034	0.016	135.816	11.857	0.0045
Error	28	1414.5	.624	0.018	1053.674	16.717	0.0015
Micro							
Height	3	3607.9*	.546	0.026	2924.667	4.963	0.0013
Direction	2	201.083	0.028	0.007	330.333	13.000	0.0016
Location	2	172.583	.361	0.014	193.750	21.000	0.0029
Error	28	364.9	.329	0.021	811.637	10.040	0.00065
S7C15 (Macro)							
Height	3	282340.76*	3.630	.253	2262.7	46.222	0.0027
Direction	2	11651.083	.194	0.019	1954.694	17.028	0.00051
Location	2	6129.250	.778	0.025	3497.861	104.111	0.0066*
Error	28	4930.635	1.312	0.038	2212.048	51.069	0.001
Micro							
Height	3	9797.407*	.324	0.05	1324.917	15.435	0.00085
Direction	2	2315.444	.361	0.0036	839.250	29.694	0.00022
Location	2	920.111	0.028	0.00028	59.250	6.194	0.013*
Error	28	1137.889	.377	0.011	282.393	14.984	0.00010

*P < 0.001. Note: FL = fiber length, FD = fiber diameter, WT = wall thickness, VL = vessel element length, VD = vessel element diameter, SG = specific gravity.

Table 6. ANOVA for wood element's dimensions and specific gravity in macro and micro propagated wood.

Wood parameter/Source of variation		MSS						
		FL	FD	WT	VL	VD	SG	gbh
Macro vs micro	df							
Clone	2	676447.0*	17.2*	14.1*	47203.9*	2890.9	0.0019	3862.3*
Technique	1	4602.7	3.99	4.3	29214.8*	1.8	0.126*	3784.5*
Replication	2	445736.2*	58.5*	0.463	15763.9*	316.9	0.0034	29.2
Height	3	27393.7	1.4	0.565	529.6	674.5*	0.019	2983.8*
Direction	2	12263.9	0.344	1.40	3238.25	950.67	0.0019	
Location	2	14159.8	0.628	0.922	3231.35	1148.6	0.064*	
Error	740	8542.8	1.69	0.93	1488.9	1099.5	0.0012	79.7
Macro								
Clone	2	358140.8*	38.1*	11.23*	35784.3*	2323.6*	0.026*	
Replication	2	251225.5*	22.54*	0.920	37336.0*	230.5	0.012*	
Height	3	35733.2	1.76	2.11	2182.41	30.20	0.012*	
Direction	2	4675.1	0.017	3.047	2089.4	27.0	0.00036	
Location	2	12912.2	0.70	1.79	1340.7	134.45	0.023*	
Error	312	10109.9	1.16	1.76	1448.46	51.53	0.00112	
Micro								
Clone	2	436762.3*	93.77*	5.47*	44139.37*	3919.0	0.032*	
Replication	2	268891.7*	45.75*	0.081	5884.08	635.6	0.006	
Height	3	29046.5*	5.212	0.255	532.2	1178.4	0.0085*	
Direction	2	10308.5	0.753	0.085	4454.5	2138.0	0.0058*	
Location	2	3134.7	0.162	0.012	1916.64	2206.15	0.037*	
Error	312	5651.8	1.44	0.082	1153.64	2140.64	0.00093	

*P < 0.001. Note: FL = fiber length, FD = fiber diameter, WT = wall thickness, VL = vessel element length, VD = vessel element diameter, SG = specific gravity.

pith to periphery variations were ranged between 0.364 (pith) –0.399 for specific gravity (outer) (**Table 2**).

3.3.2.2. G3 Clone

Fiber length, fiber diameter and vessel element length were significantly varied in replication; fiber length, wall thickness and specific gravity from bottom to top and specific gravity in radial locations (**Table 8**). The pith to periphery variations were ranged between 0.336 (pith) –0.366 for specific gravity (outer) (**Table 2**).

3.3.2.3. S7 C15 Clone

Variations were significant only for fiber length for replications; fiber length, wall thickness and vessel element length for bottom to top; vessel length for radial direction and specific gravity for radial location (**Table 9**). The pith to periphery variations were ranged between 0.354 (pith) –0.392 for specific gravity (outer).

3.4. Cluster Analysis

Hierarchical cluster analysis was done using 'Squared Euclidean Distance' for the three clones grown by two techniques. Dendrogram using average linkage (between groups) was made for different clones considering all studied wood traits (**Figure 1**). G3 clone was divergent with other clones. L34 (micro) and S7C15 (macro) was different from L34 (macro) and S7C15 (micro) at 6

Table 7. ANOVA for wood element's dimensions and specific gravity in macro and micro propagated wood of L34 clone.

Wood parameters/Source of variation		MSS					
		FL	FD	WT	VL	VD	SG
Macro vs micro	df						
Technique	1	70452.8*	168.6*	0.00012	32979.4*	4537.5*	0.0012
Replication	2	66248.3*	18.6*	0.883*	4642.3	259.1*	0.00003
Height	3	3161.1	0.89	0.027	2098.1	136.3*	0.003
Direction	2	27175.2*	3.26	0.17	3639.2	94.02	0.001
Location	2	6225.7	2.09	0.094	3137.57	52.78	0.026*
Error	205	4870.94	1.32	0.053	1518.6	33.20	0.0013
Macro							
Replication	2	152521.40*	3.90	1.150*	18649.08*	151.60	0.0021
Height	3	14622.160*	2.50	0.126	575.80	75.12	0.00092
Direction	2	7847.07	1.70	0.186	672.30	16.50	0.00053
Location	2	508.07	0.700	0.083	218.40	24.30	0.014*
Error	98	3256.80	.90*	0.045	700.00	34.04	0.0013
Micro							
Replication	2	8878.0	28.89*	0.183	1638.40	464.06*	0.0017
Height	3	4738.60	3.50	0.075	2143.22	134.20*	0.0030
Direction	2	21377.30*	1.444	0.0212	7611.70	108.60	0.0045
Location	2	10738.30	2.00	0.045	8353.50	29.40	0.012
Error	98	4350.4	1.345	0.050*	1933.01	25.245	0.0013

*P < 0.001. Note: FL = fiber length, FD = fiber diameter, WT = wall thickness, VL = vessel element length, VD = vessel element diameter, SG = specific gravity.

rescaled distance cluster combine. The wood properties of G3 clone were similar in the wood produced by two different techniques, whereas the L34 and S7C15 produced wood by two techniques showed variations in wood properties. It showed that G3 clone was stable whereas L34 and S7C15 showed variations in wood traits between the wood produced by two techniques.

4. DISCUSSION

Variance ratio (F) test indicated that inter-clonal variations were non significant for all studied wood traits except wall thickness and fiber length for central block ($P < 0.001$). Significant inter-clonal variations in wall thickness and vessel element length indicated that these traits had strong inheritance even at the early phase of the tree growth. The pooled data analysis of three clones indicated that fiber length, vessel element length and specific gravity were the wood traits which varied between macro- and micro-propagated wood of *Populus deltoides* clones (**Table 6**). Specific gravity and wall thickness were higher in macro-propagated wood while vessel element length in micro-propagated wood. The trend was more or less similar to individual clones. The grouping of different clones indicated that clones behave differently for different wood traits.

Significant inter-clonal variations were reported for fiber length, fiber diameter, fiber wall thickness, vessel element length and specific gravity. Significant differences among the different clonal ramets of different species in average fiber-length are also reported by many workers [7,9,10,13,14]. Cheng and Bensend [15], Einspahar *et al.* [16], Kennedy [17] and Peszlen [18] reported that fiber length is under genetic control. Clone to clone variations were also reported in *Tectona grandis*

Table 8. ANOVA for wood element's dimensions and specific gravity in macro and micro propagated wood of G3 clone.

Wood parameter/Source of variation		MSS					
		FL	FD	WT	VL	VD	SG
Macro vs micro	df						
Technique	1	876.04	8.560	.308	49837.80*	751.90	0.230*
Replication	2	790333.80*	84.60*	1.315	222478.70*	1959.40	0.0030
Height	3	8201.70*	0.70*	1.9	5529.20	2875.30	0.016*
Direction	2	9263.04	0.50	2.80	28.10	2520.06	0.000093
Location	2	23510.40	0.80	3.24	945.30	2522.70	0.012*
Error	205	6428.21	1.4	2.70	1185.9	3208	0.0009
Macro							
Replication	2	238056.80*	28.90*	4.54	15315.60*	702.90*	0.0072*
Height	3	27301.70*	1.90	5.8	4905.80	237	0.015*
Direction	2	6631.0*	.111	6.80	795.90	72.30	0.00005
Location	2	53196.90*	.60	5.80	3865.8	150.50	0.0066*
Error	63	6712.60	.96	5.09	1401.06	72.40	0.00092
Micro							
Replication	2	601137.7*	61.80*	.50*	9300.25	3811.40	0.00082
Height	3	28220.70*	3.60	1.03*	2246.08	4851.60	0.0056*
Direction	2	8056.08	1.0	.30	490.50	6263.20	0.0004
Location	2	1071.08	0.704	0.039	373.03	5923.40	0.011*
Error	63	3676.60	1.7	.15	865.0	6411.20	0.00059

*P < 0.001. Note: FL = fiber length, FD = fiber diameter, WT = wall thickness, VL = vessel element length, VD = vessel element diameter, SG = specific gravity.

for wood properties [19], in *D. sissoo* by Pande and Singh [20] and in *Populus deltoides* by Chauhan *et al.* [10]. Further, Veenin *et al.* [21] reported significant inter-clonal variation in wood anatomical properties and specific gravity in *Eucalyptus camaldulensis*. In the present study clone to clone variation in specific gravity was observed. Significant inter-clonal variations in specific gravity of *Eucalyptus tereticornis* at the one site was reported by Pande [22]. Significant differences in average specific gravity of different clones in the present study are also in agreement with the earlier findings in *Populus* spp. [7,9], in *Eucalyptus tereticornis*. [14] and in *Dalbergia sissoo* [20,23]. Specific gravity is moderately to strongly inherited trait and is under the influence of additive gene action in case of *Tectona grandis* [24].

Non-significant intra-clonal variations were reported by Pande and Singh [20] in *D. sissoo* and in *E. tereticornis* by Pande [22]. In contrary, present study showed significant intra-clonal variation in fiber length, fiber diameter, wall thickness, vessel element length and specific gravity in macro; fiber length, and fiber diameter and vessel element length in micro propagated plantation wood. It showed that with in clone variability is present among the clonal ramets of *Populus deltoides*. It showed that intra-clonal variations for different wood traits are varied differently for different species and clones.

Axial and horizontal (both peripheral and radial) in pooled data of all the clones were non-significant except specific gravity. But, the individual clone with micro- or macro-propagated method showed somewhat different trend. It showed non-significant variations in most of the cases except few sporadic exceptions. L34 clone showed axial variation for specific gravity in macro-propagated

Table 9. ANOVA for wood element's dimensions and specific gravity in macro and micro propagated wood of S7C15 clone.

Wood parameter/Source of variation		MSS					
		FL	FD	WT	VL	VD	SG
Macro vs micro	df						
Technique	1	170185.04*	43.56*	9.16*	11837.04*	1415.78	0.01
Replication	2	257777.42*	3.81	0.53*	11688.91*	60.67	0.008*
Height	3	54062.63*	1.02	0.14	3332.86	71.67	0.005*
Direction	2	6310.37	1.45	0.0003	21478.1	214.3	0.0001
Location	2	2989.78	0.37	0.03	573.51	36.29	0.02*
Error	205	6448.84	0.85	0.04	1178.12	46.85	0.0008
Macro							
Replication	2	327993.70*	12.30*	1.50*	27288.9*	132.23	0.011*
Height	3	66766.80*	1.22	0.083	3774.0	95.90	0.0027
Direction	2	2463.60	2.01	0.0056	1254.0	2.90	0.00083
Location	2	4714.07	0.70	0.044	1266.50	53.80	0.014*
Error	63	9267.01	1.20	0.064	1711.30	27.40	0.0008
Micro							
Replication	2	41614.80	0.75	0.053	151.70	1.12	0.0006*
Height	3	16398.2*	0.22	0.098*	1348.2*	164.80	0.0031
Direction	2	4518.40	0.36	0.0025	2088.8*	13.62	0.0025
Location	2	581.50	0.027	0.010	8.04	26.60	0.014*
Error	63	989.00	0.40	0.014	324.50	62.40	0.00089

*P < 0.001. Note: FL = fiber length, FD = fiber diameter, WT = wall thickness, VL = vessel element length, VD = vessel element diameter, SG = specific gravity.

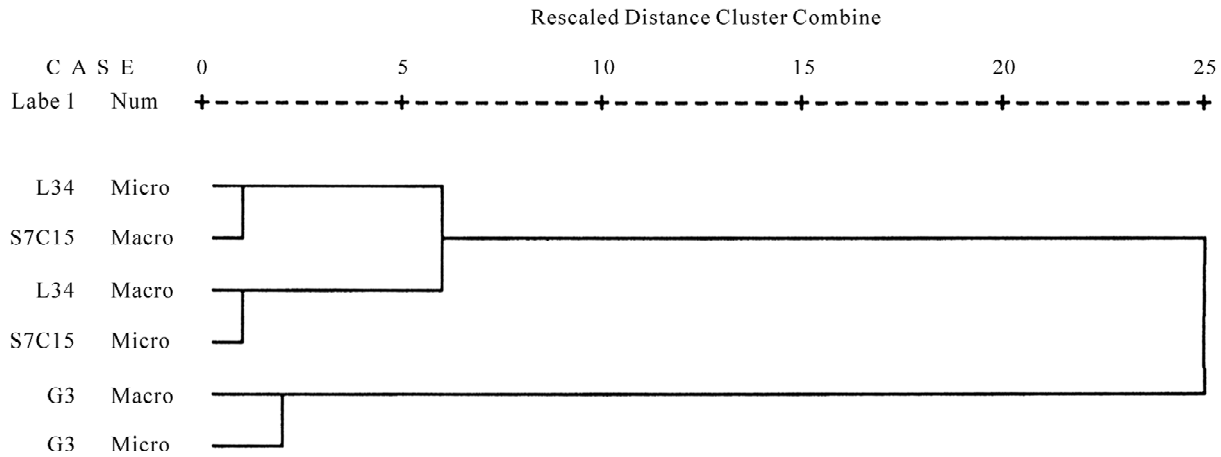

Figure 1. Dendrogram using the wood parameters for three clones with both macro and micro-propagation method.

wood while for micro-propagated wood variations were for vessel element diameter and specific gravity. In G3 and S7C15 clone, axial variations were represented only for fiber length. Radial variation was only for specific gravity for all the clones. It showed that clones of *Populus deltoides* presented different patterns of within tree variations for different wood traits. Even the pattern was not same for individual clone grown by two different techniques. Significant radial variations for fiber length in some poplar clones were also recorded by Kaubaa *et al*. [8]; and in vessel lumen diameter and fiber length by Peszlen, [18]. In general, non-significant variations due to peripheral direction and radial location in wood element dimensions within a ramet and absence of any trend may be related to the early maturity of clone-raised tree. It appears that growing age may not have any impact on the wood element dimensions in clonal ramets of *Populus deltoides* even at the early phase of tree growth. Veenin *et al.* [21] also reported non-significant radial variations in fiber length, vessel element diameter and vessel density in clone raised ramets of *E. camaldulensis.* Such type of results were also reported in clonal plantation of *Populus deltoides* by Chauhan *et al.* [10]; *Dalbergia sissoo* by Pande and Singh [20] and in *Eucalyptus tereticornis* by Pande [22]. However, within tree axial and horizontal variations in wood element's dimension in seed raised trees of different species were reported [6,11,14,25,26]. In general, the increasing trend for specific gravity was observed from bottom to top and pith to periphery. However, radial variations in specific gravity in *E. camaldulensis* are reported by Veenin *et al.* [21]. In *Tectona grandis*, the density increased towards the peripheral direction by 5-6 cm from the pith which stabilizes by the age of 10-12 years [27]. In the case of *Dalbergia sissoo* and other clones of *Populus deltoides*, there was non-significant pith to periphery radial variations and no specific trend was observed for specific gravity [10,20]. Thus, the trends can be different from one species to another.

5. CONCLUSIONS

Populus deltoides clones showed differential pattern of variability for different wood traits. The three different clones of *Populus deltoides* showed variability in wood anatomical properties in the woods of micro- and macro-propagated plantation. So, the plantation raised by two techniques could not produced similar type of wood even from the same clone. G3 clone was the exception as it did not show variations in wood traits for two techniques.

In general, the higher specific gravity and fiber wall thickness can be obtained by growing the plantation of this species by macro-propagation techniques.

Variations are observed in fiber dimensions in macro-propagated wood of all three clones. G3 clone is stable for wood traits as it showed similar type of wood properties in the wood grown by the two techniques. Further, it showed higher fiber dimensions and specific gravity than of the other clones.

Intra-clonal variations in all the three clones of *Populus deltoides* indicated that wood traits were not stable within the population of same clone grown by either method.

Non-significant intra-ramet variation in wood anatomical characteristics in both the techniques indicated narrow juvenile wood zone and may form mature wood even at the early phase of tree growth.

6. ACKNOWLEDGEMENTS

Acknowledgements are also due to Director, Forest Research Institute, Dehradun (India) for providing necessary facilities during the work. Author is also thankful to Mr. G. S. Bisht, Research Assistant, Wood anatomy Discipline, Forest Research Institute, Dehradun for laboratory-assistance and Mr. J N Gandhi of Wimco Ltd. for field work.

REFERENCES

[1] Dadswell, H.E. (1957) Tree growth characteristics and their influence on wood structure and properties. *Proceedings of 7th British Commonwealth Forestry Conference*, CSIRO, Australia, 1957.

[2] Burley, J. and Palmer, R.R. (1979) Pulp and wood densitometric properties of Pinus caribaea from Fiji. *Commonwealth Forestry Institute Occasional Paper*, 66.

[3] Dinwoodie, J.M. (1961) Tracheid and fiber-length in timber. A review of literature. *Forestry*, **34**, 124-144.

[4] Zobel, B. (1965) Inheritance of fiber characteristics and specific gravity in hardwoods-a review. *Proceedings of the Meeting of Section* 41 *Meet*, *IUFRO*, Melbourne, Australia, 1965.

[5] Rao, B.S.S. and Rao, R.V. (1978) Variation in length of vertical elements within one tree of betula pubercens ehrh. *Journal of Indian Academy of Wood science*, **9**(**2**), 105-110.

[6] Pande, P.K., Rao, R.V., Agrawal, S.P. and Singh, M. (1995) Variation in the dimensions of trachied elements of Pinus caribaea var. bahamensis. *Journal of Tropical Forest Products*, **1(2)**, 117-123.

[7] Phelps, J.E., Isebrands, J.G. and Jowett, D. (1982) Raw material quality of short rotation intensively cultured Populus clones. A comparison of stem and branches properties at three species. *IAWA Journal*, **3(3-4)**, 193-200.

[8] Kaubaa, A., Hernandez, A.E., Beaudoin, M. and Poliquin, J. (1998) Interclonal, intra-clonal and within tree variation in fiber-length of Popular hybrid clones. *Wood and Fiber science*, **30(1)**, 1998, 140-147.

[9] Chauhan, L., Raturi, R.D. and Gupta, S. (1999) Studies on anatomical variations in different clones of Populus deltoides. *Indian Forester*, **125**, 526-532.

[10] Chauhan, L., Gupta, L.S., Madhwal, R.C., Pandey, R. and Pal, M. (2001) Interclonal, intraclonal and within tree variation in wood parameters of different clones of Populus deltoids. *Indian Forester*, **127(7)**, 777-784.

[11] Purkayastha, S.K., Agrawal, S.P., Farooqui, P., Tandon, R.D., Chauhan, L. and Misra, N. (1979) Evaluation of wood quality of Eucalyptus plantations in various states, Final Technical Report, (Nov. 1 to Oct. 31, 1979) PL 480 Project no Inn FS-66, 1979-80, 85.

[12] IAWA Committee IAWA (1989) List of microscopic features for hardwood identification. *IAWA Bull*, **10(3)**, 201-232.

[13] Murphey, W.K., Bowersox, T.W. and Blankenhorn, P.R. (1979) Selected wood properties of young Populus hybrid. *Wood Science*, **11(4),** 236-267.

[14] Rao, R.V., Shashikala, S., Sreevani, P., Kothiyal, V., Sharma, C.R. and Lal, P. (2002) Within tree variation in anatomical properties of some clones of Eucalyptus tereticornis Sm. *Wood Science Technology*, **36(3)**, 271-285.

[15] Cheng, W.W. and Bensend, D.W. (1979) Anatomical properties of selected Populus clones grown under intensive culture. *Wood Science*, **11(3)**, 182-187.

[16] Einspahr, D.W., Van Buijtenen, J.P. and Peckham, J.R (1963) Natural variation and heritability in triploid aspen. *Silvae Genetica*, **12(2)**, 51-58.

[17] Kennedy, R.W. (1968) Anatomy and fundamental wood properties of poplar. In: Maini J.S. and Cayford J.S. Eds., *Growth and utilization of poplars in Canada*, Canadian Department for Rural development, Forestry Branch, publication 1025, Canada, 149-168.

[18] Peszlen, I. (1994) Influence of age on selected anatomical properties of Populus clones. *IAWA Journal*, **15(3)**, 311-321.

[19] Rao, R.V. and Shashikala, S. (2003) Assessment of growth rate, basic density and heart wood content in selected teak clones of CSO, Thithimathi in Karnataka state, India. *In International Conference on Quality Timber Products of Teak from Sustainable Forest Management*, 2-5 December 2003, KFRI, Kerala, India (abstracts), 57.

[20] Pande, P.K. and Singh, M. (2005) Intraclonal, inter-clonal and single tree variations of wood anatomical properties and specific gravity of clonal ramets of Dalbergia sissoo Roxb. *Wood Science Technology*, **39(5)**, 351-366.

[21] Veenin, T., Fujita, M., Nobuchi T. and Siripatanandilok, S. (2005) Radial variations of anatomical characters and specific gravity in Eucalyptus camaldulensis clones. *IAWA Journal*, **26**, 353-361.

[22] Pande, P.K. (2005) Assessment of the performance of different clones of Dalbergia sissoo and Eucalyptus tereticornis on the basis of wood quality under different farm forestry programs. FTR submitted to ICFRE, Dehradun, India.

[23] Pande, P.K. and Singh, M. (2003) Variation in Wood Elements Within a ramet of Dalbergia sissoo. *Journal of Timber Development Association India*, **2(3-4)**, 19-22.

[24] Mandal, A.K. and Chawaan, P.H. (2003) Investigations on inheritance of growth and wood properties and their inter-relationship in teak. *In International Conference on Quality timber products of teak from sustainable forest management* (*abstracts*), Kerala, India, 2-5 December 2003, 56.

[25] Tomazello, F. and Variacano, M. (1987) Radial da densidade basica e da estrutura anatomica da Madeira do Eucalyptus globulese, E. pellitae, E. acmenioides. *Inst Pesq. Estud. Florest. Piracicaba*, **(36)**.

[26] Bhat, K.M., Bhat, K.V. and Dhamodaran, T.K. (1990) Wood density and fiber length of Eucalyptus grandis grown in Kerala, India. *Wood Fiber Science*, **22**, 54-61.

[27] Okuyama, T., Yamamoto, H., Wahyudi, I., Hadi, Y.S. and Bhat, K.M. (2003) Some wood quality issues in planted teak. *In International conference on quality timber products of teak from sustainable forest management*, Kerala, India, 2-5 December 2003, 21.

Advances in Bioscience and Biotechnology, 2010, 1, 276-280 **ABB**
doi:10.4236/abb.2010.14036 Published Online October 2010 (http://www.SciRP.org/journal/abb/).

Nickel uptake and intracellular localization in *Cupriavidus pauculus* KPS 201, native to ultramafic ecosystem

Arundhati Pal[1], A. K. Paul[2]

[1]Department of Botany, Serampore College, Serampore, Hooghly, West Bengal, India;
[2]Microbiology Laboratory, Department of Botany, University of Calcutta, 35, Ballygunge Circular Road, Kolkata, West Bengal, India.
Email: arundhatipalcu@gmail.com, akpbot@caluniv.ac.in

Received 14 July 2010; revised 21 July 2010; accepted 25 July 2010.

ABSTRACT

The nickel-resistant bacterium, *Cupriavidus pauculus* KPS 201 was isolated from the rhizosphere of *Rinorea bengalensis* (Wall.) O. K. endemic to metal-percolated ultramafic ecosystem of Andaman, India. This study investigates nature of Ni resistance, growth associated uptake and localization of Ni in cellular compartments of KPS 201. Growth kinetics of *C. pauculus* KPS 201 exhibited a typical inducible Ni resistance in Ni-supplemented (1.0-10.0 mM) Tris-minimal medium. The Ni-induced cells showed a high degree of Ni resistance and accumulated a maximum of 29.3 µM Ni/g protein after 48 h of growth in 5 mM Ni. The accumulated Ni was preferentially retained (90.6%) in the periplasm and was associated with the expression of two periplasmic proteins (74 and 66 kDa) under Ni-induced condition. Inducible nickel resistance in *C. pauculus* KPS 201 may possibly be due to extracytoplasmic binding and accumulation coupled with expression of specific periplasmic proteins. These findings will provide an insight in understanding metal-microbe interaction in geogenous environments and their exploitation in bioremediation of heavy metal pollutants.

Keywords: *Cupriavidus pauculus*; Inducible Ni Resistance; Intracellular Uptake; Periplasmic Proteins; Ultramafic Soil

1. INTRODUCTION

Ultramafic ecosystem comprises nutritionally poor, metal enriched soils characterized by high concentrations of nickel in addition to chromium and cobalt [1]. Majority of the endemic metallophytes inhabiting such ecosystem are Ni-hyperaccumulators which provide a niche for Ni-resistant bacteria in their rhizosphere [2]. These Ni-resistant microorganisms bear strong homologies with those isolated from anthropogenically Ni-polluted ecosystems [3]. Although Ni is an essential micronutrient, high levels of Ni along with Cr and Co favor inhibition of microbial population, growth and activity. However, the indigenous Ni-metallophiles from such Ni-percolated habitat has adopted diverse strategies to overcome Ni toxicity. Ni detoxification in bacteria takes place either by avoiding entry of metal into the cell or via intracellular sequestration and compartmentalization of Ni in different cell sectors. Resistance to Ni in *Cupriavidus metallidurans* CH 34 (formerly *Ralstonia metallidurans*, *Alcaligenes eutrophus*) isolated from a zinc-decantation tank in Belgium, is inducible and due to energy dependent efflux driven by chemiosmotic proton-antiporter system [4]. Bioaccumulation of Ni by growing or resting cells was found linked to cellular metabolism. Pre-induced cells of *Burkholderia* 32W-2, native to serpentines of New Caledonia, showed nickel accumulation during growth [3]. Nickel transport across the cell membrane occurs in *Escherichia coli* [5] and *Pseudomonas aeruginosa* [6] under Ni induction and was found to encode a periplasmic Ni-binding protein.

We have screened Ni resistance in microorganisms underneath Ni-hyperaccumulators, *Rinorea bengalensis* and *Dichapetelum gelonioides* ssp. a*ndamanicum*, endemic to Indian ultramafics located in Andaman Islands. One of the 123 microbial isolates, the bacterium *Cupriavidus pauculus* KPS 201 (MTCC 6280) showed high resistance to Ni (MIC 29 mM Ni in nutrient broth) and resting cells pre-grown in nutrient broth accumulated 224 µM Ni/g protein in 60 min from aqueous Ni(II) solution in HEPES buffer [7]. Our present study investigates the nature of Ni resistance, growth associated uptake and possible localization of accumulated Ni in *C. pauculus* KPS 201 cells.

2. MATERIALS AND METHODS

2.1. Organism and Culture Conditions

Cupriavidus pauculus KPS 201 (MTCC 6280), used throughout the present study was maintained on slopes of Tris gluconate minimal medium [2] supplemented with 1.0 mM Ni(II) as chloride salt and grown at 28ºC for 24 h.

2.2. Growth and Nickel Uptake

Ni uptake by KPS 201 cells was conducted in Tris-minimal medium (50 ml per 250 ml Erlenmeyer flask) supplemented with Ni. The medium was inoculated with 18 h old inoculum, grown either in absence (non-induced cells) or in presence of 0.25 mM Ni (induced cells) and agitated on a rotary shaker (120 rpm) at 28ºC. Growth was monitored by recording optical density changes at 540 nm (UV-Vis-spectrophotometer, Jenway 6505) and measuring total protein content per ml of the culture. For nickel estimation, growing cells were harvested by centrifugation in a Hermle Z36HK cold centrifuge (10,000 x g at 4ºC) and the cell pellet was digested with 6 M HNO_3 at 80ºC for 2 h. Protein and nickel content of biomass were estimated following the methods as described below.

2.3. Cell Fractionation

Ni-loaded cells were harvested, washed and fractionated following the modified procedure of Bernhard *et al.* [8]. Periplasmic fraction was obtained by osmotic shock method using sucrose and lysozyme. Sphaeroplasts obtained were lysed by sonication (Hielscher ultrasonic processor, UP 100H) and centrifuged at 10,000 x g (10 min at 4ºC) to remove cell debris. The supernatant was further centrifuged at 90,000 x g for 45 min at 4ºC (Beckman Coulter Ultracentrifuge LE-80K) to separate membrane (pellet) and cytoplasmic (soup) fractions. Protein from each fraction was precipitated with 10% (w/v) cold trichloroacetic acid, washed and dissolved in 10 mM Tris-Cl (pH 8.0).

2.4. Protein Estimation and Gel Electrophoresis

Total protein of biomass was extracted with 1% (w/v) SDS and precipitated with 25% cold trichloroacetic acid. Protein content was estimated by folin-phenol reagent using bovine serum albumin as standard [9]. Proteins in the isolated cell fractions were resolved in 10% (w/v) SDS-PAGE [10] and stained with silver nitrate [11].

2.5. Estimation of Nickel

Nickel content (μM Ni/g protein) of the digested biomass and cellular fractions was quantified using Atomic Absorption Spectrometer (Varian SpectrAA20 Plus) operating at 232 nm, 0.2 mm slit width and air-acetylene flame.

3. RESULTS

3.1. Nickel Resistance in *Cupriavidus pauculus* KPS 201

Growth kinetics of *C. pauculus* KPS 201 in Ni-supplemented (1.0-10.0 mM) Tris-minimal medium exhibited a typical metal-induced response for Ni resistance. Non-induced cells of KPS 201 when grown in presence of Ni showed a characteristic prolonged lag which increases with increasing metal concentration showing a maximum (22 h) in 10 mM Ni (**Figure 1(a)**). Under identical conditions, cells induced with 0.25 mM Ni grew exponentially without any distinguishable lag (**Figure 1(b)**).

The induced cells also showed high Ni resistance

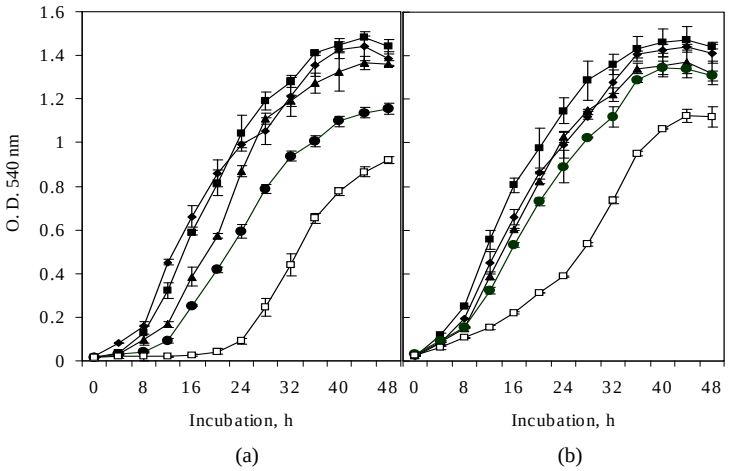

Figure 1. Growth of non-induced (a) and Ni-induced (b) cells of *Cupriavidus pauculus* KPS 201 in absence (-◆-) and presence of 1.0 mM (–■–), 2.0 mM (–▲–), 5.0 mM (–●–) and 10.0 mM (–□–) Ni.

(MIC 21.3 mM) contrary to non-induced cells (15 mM Ni) (**Figure 2**).

3.2. Nickel Uptake during Growth

In view of enhanced growth performance in Ni and high degree of metal resistance, nickel uptake studies were conducted using Ni-induced (pre-grown in 0.25 mM Ni) KPS 201 cells. During growth in presence of non-toxic concentrations of Ni (1.0 – 10.0 mM), KPS 201 cells accumulated metal and attained equilibrium at late exponential to early stationary phase. The extent of Ni uptake in the biomass increased with increasing Ni concentration in the growth medium, attaining maxima (29.3 µM Ni/g protein) after 48 h of incubation in 5 mM Ni (**Figure 3**).

3.3. Cellular Compartmentalization of Nickel

Metal-loaded cells of KPS 201 (29.3 µM Ni/g protein) were disrupted and separated into periplasmic, membrane and cytosolic fractions [8] and their purity was confirmed by the assay of marker enzymes like alkaline phosphatase [12], gluconate dehydrogenase [13] and

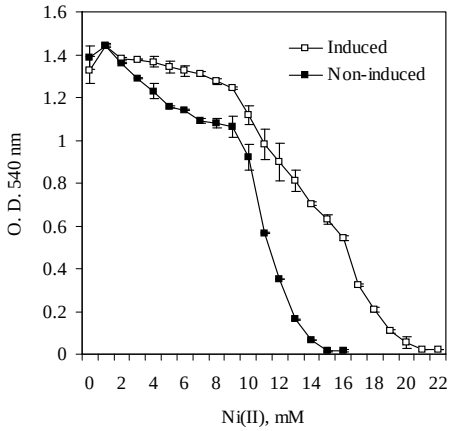

Figure 2. Ni resistance in *Cupriavidus pauculus* KPS 201 cells grown in Tris-minimal medium. The medium was inoculated with 18 h grown culture prepared in the same medium either without Ni (non-induced) or supplemented with 0.25 µM Ni (induced). The flasks were incubated on a rotary shaker (120 rpm) at 30ºC for 24 h and growth was monitored by recording optical density changes at 540 nm.

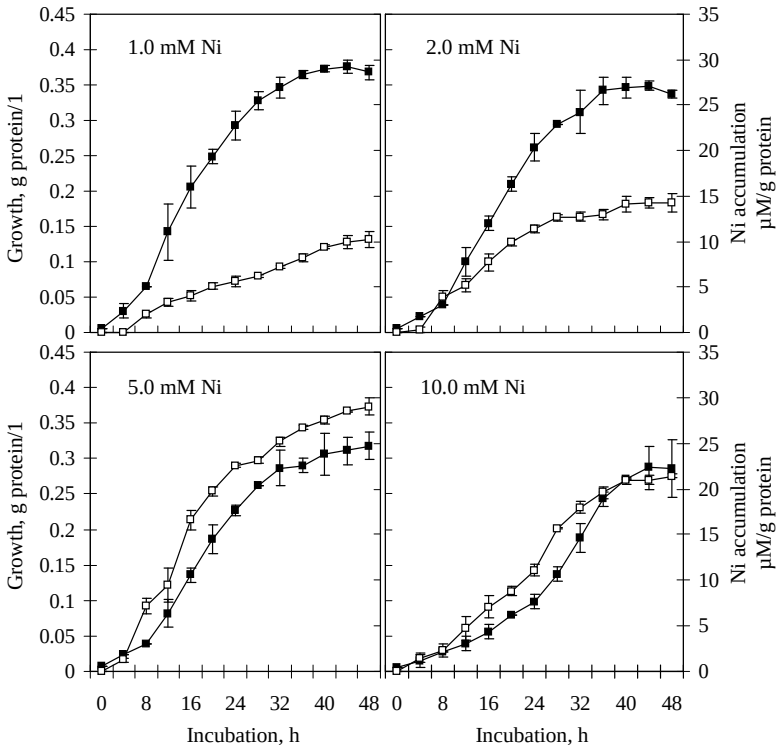

Figure 3. Growth (–■–) associated Ni accumulation (–□–) in *Cupriavidus pauculus* KPS 201. Cells previously induced in 0.25 mM Ni were grown in Tris-minimal medium supplemented with 1–10 mM Ni. Total protein (g/l) of biomass was estimated along with amount of accumulated Ni (µM/g protein) following folin phenol assay and Atomic Absorption Spectrometry respectively.

PHA depolymerase [14] respectively. A major part (90.62%) of the accumulated metal was retained in the periplasm (26.58 µM Ni/g protein), while only 0.51% Ni (0.15 µM Ni/g protein) was bound to the cell membrane. Cytoplasmic fraction contained 8.83 % of the total Ni accumulated by intact cells (**Table 1**).

3.4. Protein Profile

Protein profiles of periplasmic, membrane and cytoplasmic fractions of Ni-induced KPS 201 cells were compared with those of the non-induced control following SDS-PAGE. Periplasmic protein fractions (**Figure 4**) of Ni-induced cells grown in presence of 1 to 10 mM Ni (Lane 3-6) showed two distinct bands of approximately 74 and 66 kDa, but similar protein bands were missing in cells not exposed to nickel (Lane 2). Cytosolic and membrane protein profiles of Ni-grown and control cells, however, have failed to show any visible variation in their banding patterns (data not shown).

Table 1. Cellular compartmentalization of Ni in metal-loaded *Cupriavidus pauculus* KPS 201 grown in nickel supplemented medium *

Fraction	Ni(II) accumulation, µM Ni/g protein	Percentage
Whole cell	29.33 ± 0.99	100.0
Periplasmic fraction	26.58 ± 0.35	90.62
Cytoplasmic fraction	2.59 ± 0.11	8.83
Membrane fraction	0.15 ± 0.08	0.51

*Nickel-induced cells were grown in Tris minimal medium supplemented with 5 mM Ni for 48h at 28ºC. Inoculum was developed by growing the cells in Tris minimal medium supplemented with 0.25 mM Ni at 28ºC for 18 h.

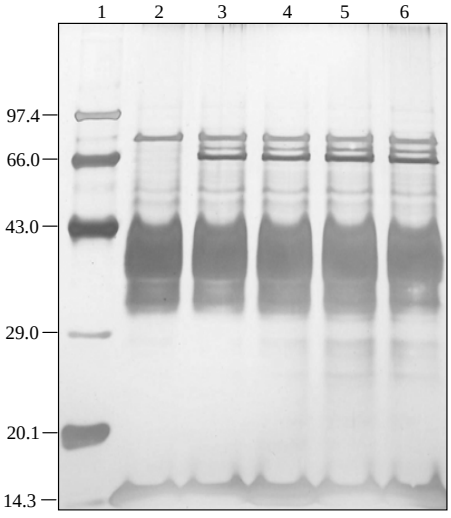

Figure 4. Electrophoretic analysis of periplasmic proteins of Ni-induced *Cupriavidus pauculus* KPS 201 cells grown in presence of 1–10 mM Ni. Lane 1: Marker proteins (kDa), Lane 2: Non-induced control, Lane 3: 1.0 mM Ni, Lane 4: 2.0 mM Ni, Lane 5: 5.0 mM Ni, Lane 6: 10.0 mM Ni.

4. DISCUSSION

Nickel resistance in bacteria from nickel-polluted ecosystem is reported to be inducible [4,15]. Similar induction of Ni resistance system in *Burkholderia* 32W-2, native to New Caledonian ultramafics was evident at 1.0 mM Ni [3]. On the contrary, induction of Ni resistance in *Cupriavidus pauculus* KPS 201 (**Figure 1**) was achieved at a much lower concentration of Ni (0.25 mM). Under such induced state the MIC in Tris minimal medium (21.3 mM Ni, **Figure 2**) was much lower compared to that of non-induced cells grown in enriched medium [7]. Such a variation could be attributed to complexation of Ni with organic constituents of the enriched medium [16].

Although uptake of Ni (29.33 µM Ni/g protein) by induced KPS 201 cells during growth was dependent on initial metal concentration up to 5 mM Ni, it declined at higher concentration (**Figure 3**). Such a decline could be attributed to induction of KPS 201 cells with low Ni concentration as well as toxicity imparted at high metal concentration leading to inhibition of RNA and protein synthesis [17]. It was further evident that in *C. pauculus* preferential accumulation (90.62 %) of Ni in the periplasm (**Table 1**) was coupled with the expression of two periplasmic proteins of molecular weights 74 and 66 kDa under Ni induced condition (**Figure 4**). Similar low molecular weight periplasmic proteins involved in Ni resistance have also been demonstrated in *E. coli* K-12 (56 kDa) [5]; *P. putida* (18 kDa) [6] and *C. necator* H16 (33.1 kDa) [18]. Further research is needed to establish the Ni-sequestering property of these periplasmic proteins in *C. pauculus* KPS 201.

5. ACKNOWLEDGEMENTS

Financial support to A. Pal from Department of Science and Technology, New Delhi, India (DST Fast Track Young Scientist Scheme; SR/FT/L-125/2005 dated 12.07.06) is duly acknowledged.

REFERENCES

[1] Brooks, R.R. (1987) Serpentine and its vegetation, a multidisciplinary approach. Croom Helm, London.

[2] Schlegel, H.G., Cosson, J.P. and Baker, A.J.M. (1991) Nickel hyperaccumulating plants provide a niche for nickel resistant bacteria. *Botanica Acta*, **104**, 18-25.

[3] Stoppel, R.D. and Schlegel, H.G. (1995) Nickel resistant bacteria from anthropogenically nickel polluted and naturally nickel percolated ecosystems. *Applied and En-*

vironmental Microbiology, **61(6)**, 2276-2285.

[4] Nies, D.H. and Silver, S. (1989) Plasmid determined inducible efflux is responsible for resistance to cadmium, zinc and cobalt in *Alcaligenes eutrophus*. *Journal of Bacteriology*, **171(2)**, 896-900.

[5] De Pina, K., Navarro, C., Mcwalter, L., Boxer, D.H., Price, N.C., Kelly, S.M., Mandrand-Berthelot, M. and Wu, L. (1995) Purification and characterization of nickel-binding protein NikA of *Escherichia coli* K 12. *European Journal of Biochemistry*; **227(3)**, 857-865.

[6] Tripathi, V.N. and Srivastava, S. (2006) Extracytoplasmic storage as the nickel resistance mechanism in a natural isolate of *Pseudomonas putida* S4. *Canadian Journal of Microbiology*, **52(4)**, 287-292.

[7] Pal, A., Wauters, G. and Paul, A.K. (2007) Nickel tolerance and accumulation by bacteria from rhizosphere of nickel hyperaccumulators from serpentine soil of Andaman, India. *Plant and Soil*; **293(1-2)**, 37-48.

[8] Bernhard, M., Friedrich, B.R. and Siddiqui, R.A. (2000) *Ralstonia eutropha* TF93 is blocked in Tat-mediated protein export. *Journal of Bacteriology*, **182(3)**, 581-588.

[9] Lowry, O.H., Rosebrough, N.J. and Farr, A.L. (1951) Protein measurement with the folin-phenol reagent. *Journal of Biological Chemistry*, **193(1)**, 265-275.

[10] Laemmli, U.K. (1970) Cleavage of structural proteins during the assembly of the head of bacteriophage T4. *Nature*, **227(5259)**, 680-685.

[11] Shevchenko, A., Wilm, M., Vorm, O. and Mann, M. (1996) Mass spectrometric sequencing of proteins from silver stained polyacrylamide gels. *Analitycal Chemistry*, **68(5)**, 850-858.

[12] McAlister, T.J., Costertan, J.W., Thompson, L., Thompson, J. and Ingram, J.N. (1972) Distribution of alkaline phosphatatse within the periplasmic space of Gram-negative bacteria. *Journal of Bacteriology*, **111(3)**, 827-832.

[13] Matsushita, K., Shinagawa, E., Adichi, O. and Ameyama, M. (1979) Membrane-bound D-gluconate dehydrogenase from *Pseudomonas aeruginosa*: purification and structure of cytochrome binding form. *Journal of Biochemistry*, **85(5)**, 1173-1181.

[14] Kobayashi, T., Nishikoriand, K. and Saito, T. (2004) Properties of an intracellular poly (3-hydroxybutyrate) depolymerase (PhaZ1) from *Rhodobacter sphaeroides*. *Current Microbiology*, **49(3)**,199-202.

[15] Rubikas, J., Matulis, D., Leipus, A. and Urbaitiene, D. (1997) Nickel resistance in *Escherichia coli* V38 is dependent on the concentration used for induction. *FEMS Microbiology Letters*, **155(2)**, 193-198.

[16] Angle, J.S. and Chaney, R.L. (1989) Cadmium resistance screening in nitrilotriacetate-buffered minimal media. *Applied and Environmental Microbiology*, **55(8)**, 2101-2104.

[17] Mulrooney, S.B. and Hausinger, R.P. (2003) Nickel uptake and utilization by microorganisms. *FEMS Microbiology Reviews*, **27(2-3)**, 239-261.

[18] Wolfram, L., Friedrich, B. and Eitinger, T. (1995) The *Alcaligenes eutrophus* protein HoxN mediates nickel transport in *Escherichia coli*. *Journal of Bacteriology*, **177(7)**, 1840-1843.

Advances in Bioscience and Biotechnology, 2010, 1, 281-291 **ABB**
doi:10.4236/abb.2010.14037 Published Online October 2010 (http://www.SciRP.org/journal/abb/).

Molecular markers and their applications in fisheries and aquaculture

Tanya Chauhan[1], Kumar Rajiv[2]

[1]National Institute of Criminology and Forensic Science, Rohini, New Delhi, Delhi, India;
[2]Department of Chemistry, (SC), University of Delhi, Delhi, India.
Email: tanyachauhan@yahoo.com; chemistry_rajiv@hotmail.com

Received 10 June 2010, revised 20 June 2010, accepted 25 June 2010.

ABSTRACT

Genetic variation in a species enhances the capability of organism to adapt to changing environment and is necessary for survival of the species. Genetic variation arises between individuals leading to differentiation at the level of population, species and higher order taxonomic groups. The genetic diversity data has varied application in research on evolution, conservation and management of natural resources and genetic improvement programmes, etc. Development of Molecular genetic markers has powerful ability to detect genetic studies of individuals, populations or species. These molecular markers combined with new statistical developments have revolutionized the analytical power, necessary to explore the genetic diversity. Molecular markers and their statistical analysis revolutionized the analytical power, necessary to explore the genetic diversity. Various molecular markers, protein or DNA (mt-DNA or nuclear DNA such as microsatellites, SNP or RAPD) are now being used in fisheries and aquaculture. These markers provide various scientific observations which have importance in aquaculture practice recently such as: 1) Species Identification 2) Genetic variation and population structure study in natural populations 3) Comparison between wild and hatchery populations 4) Assessment of demographic bottleneck in natural population 5) Propagation assisted rehabilitation programmes. In this review article, we have concentrated on the basics of molecular genetics, overview of commonly used markers and their application along with their limitations (major classes of markers) in fisheries and aquaculture studies.

Keywords: Genetic Diversity; Molecular Markers; Microsatellite; Aquaculture

1. INTRODUCTION

All organisms are subject to mutations because of normal cellular operations or interactions with the environment, leading to genetic variation (polymorphism). Genetic variation in a species enhances the capability of organism to adapt to changing environment and is necessary for survival of the species [1]. In conjunction with other evolutionary forces like selection and genetic drift, genetic variation arises between individuals leading to differentiation at the level of population, species and higher order taxonomic groups. Molecular genetic markers are powerful tools to detect genetic uniqueness of individuals, populations or species [2,3]. These markers have revolutionized the analytical power, necessary to explore the genetic diversity [4]. The conclusion from genetic diversity data has varied application in research on evolution, conservation and management of natural resources and genetic improvement programmes, etc [5-10]

In addition to protein markers, application of DNA markers is finding wide acceptance in population genetics. With DNA markers, it is theoretically possible to observe and exploit genetic variation in the entire genome. Both genomic and mitochondrial DNA is used for varied applications. The commonly used technique are allozyme analysis, types of restriction fragment length polymorphism (RFLP), randomly amplified polymorphic DNA (RAPD), amplified fragment length polymorphism (AFLP), microsatellite typing, single nucleotide polymorphism (SNP), and expressed sequence tag (EST) markers, etc.

Molecular markers can be classified into type I and type II markers. Type I markers are associated with genes of known function, while type II markers are associated with anonymous genomic regions [11]. Under this classification, allozyme markers are type I markers because the protein they encode has known function. RAPD markers are type II markers because RAPD bands

are amplified from anonymous genomic regions via the polymerase chain reaction (PCR). Microsatellite markers are also type II markers unless they are associated with genes of known function. The significance of type I markers is becoming extremely important for aquaculture genetics. Type I markers serve as a bridge for comparison and transfer of genomic information from a map-rich species into a relatively map-poor species. In general, type II markers such as RAPDs, microsatellites, and AFLPs are considered non-coding and therefore selectively neutral. Such markers have found widespread use in population genetic studies to characterize genetic divergence within and among the populations or species [12]

2. ALLOZYME MARKERS

Analysis of allozyme loci remained one of the most popular approaches in examining population genetics and stock structure questions in fishes [13]. The technique is rapid, relatively inexpensive and provides an independent estimate of level of variation within a population without an extensive morphological and quantitative survey [14]**.** Isohyets are structurally different molecular forms of an enzyme system with qualitatively the same catalytic function encoded by one or more loci [15]. Isohyets, which are encoded by different alleles of the same gene locus, are designated as "allozymes" or "alloenzymes" [16]. Amino acid differences in the polypeptide chain of the different allelic forms of an enzyme reflect changes in the underlying DNA sequence. Depending on the nature of the amino acid changes, the resulting protein products may migrate at different rates (due to charge and size differences) when run through a gel subjected to an electrical field. Differences in the relative frequencies of alleles are used to quantify genetic variation and distinguish among genetic units at the levels of populations, species, and higher taxonomic designations. Disadvantages associated with allozymes include occasional heterozygote deficiencies due to null (enzymatically inactive) alleles and sensitive to the amount as well as quality of tissue samples. In addition, some changes in DNA sequence are masked at the protein level, reducing the level of detectable variation. Some changes in nucleotide sequence do not change the encoded polypeptide (silent substitutions), and some polypeptide changes do not alter the mobility of the protein in an electrophoretic gel (synonymous substitutions). At present 75 isozyme systems representing several hundred genetic loci are known [17]. With the strength as codominant marker, ease of use, and low cost, the allozyme markers are popular in population structure and phylogenetic studies, though has limited role in aquaculture genetics.

3. MITOCHONDRIAL DNA MARKERS

Mitochondrial DNA (mtDNA) analysis is being increasingly used in recent population and phylogenetic surveys of organisms. Studies of vertebrate species generally have shown that sequence divergence accumulates more rapidly in mitochondrial than in nuclear DNA [18]. This has been attributed to a faster mutation rate in mtDNA that may result from a lack of repair mechanisms during replication [19] and smaller effective population size due to the strict maternal inheritance of the haploid mitochondrial genome [20]. Due to its rapid rate of evolution, mtDNA analysis has proven useful in clarifying relationships among closely related species. Different parts of the mitochondrial genome are known to evolve at different rates [21]. Almost the entire mtDNA molecule is transcribed except for the approximately 1-kb control region (D-loop), where replication and transcription of the molecule is initiated. In general, non-coding segments like the D-loop exhibit elevated levels of variation relative to coding sequences such as the cytochrome b gene [22], presumably due to reduced functional constraints and relaxed selection pressure. The 16S rRNA gene in the mitochondrial genome is one of the slowest evolving genes [21] whereas rapidly evolving regions are control regions [23,24]. Due to non-Mendelian mode of inheritance, the mtDNA molecule is considered as a single locus [2]. In addition, because mtDNA is maternally inherited, the phylogenies and population structures derived from mtDNA data may not reflect complete picture of the nuclear genome if gender-biased migration or selection [20] or introgression [25] exists.

Analyses of mtDNA markers have been used extensively to investigate stock structure in a variety of vertebrates including fishes [26-30], birds [31-34], mammals [35] and reptiles [36-39].

4. RANDOM AMPLIFIED POLYMORPHIC DNA (RAPD) MARKERS

RAPD markers are the amplified products of less functional part of the genome that do not strongly respond to selection on the phenotypic level. Such DNA regions may accumulate more nucleotide mutations with potential to assess inter-population genetic differentiation [40]. The amplification of genomic DNA by PCR with arbitrary nucleotide sequence primers, RAPD can detect high levels of DNA polymorphisms [41,42]. The technique detects coding as well as non-coding DNA sequences, and many of the most informative polymorphic sequences are those derived from repetitive (non-coding) DNA sequences in the genome [43]. Because 90% of the vertebrate nuclear genome is non-coding, it is presumed

that most of the amplified loci will be selectively neutral. RAPD loci are inherited as Mendelian markers in a dominant fashion and scored as present/absent. RAPDs have all the advantages of a PCR-based marker, with the added benefit that primers are commercially available and do not require prior knowledge of the target DNA sequence or genome organization. Other advantages of RAPDs include the ease with which a large number of loci and individuals can be screened simultaneously. Shortcomings of this type of marker include the difficulty of demonstrating Mendelian inheritance of the loci and the inability to distinguish between homozygotes and heterozygotes. Analysis follows the assumption that populations under study follow Hardy-Weinberg expectations. In addition, the presence of paralogous PCR product (different DNA regions which have the same lengths and thus appear to be a single locus), low reproducibility due to the low annealing temperature used in the PCR amplification, have limited the application of this marker in fisheries science [44].

5. SINGLE NUCLEOTIDE POLYMORPHISM (SNP)

Single nucleotide polymorphism (SNP) describes polymorphisms caused by point mutations that give rise to different alleles containing alternative bases at a given nucleotide position within a locus. SNPs are becoming a focal point in molecular marker development since they represent the most abundant polymorphism in any organism's genome (coding and non-coding regions), adaptable to automation, and reveal hidden polymorphism not detected with other markers and methods [9, 10]. Theoretically, a SNP within a locus can produce as many as two alleles, each containing one of two possible base pairs at the SNP site. Therefore, SNPs have been regarded as bi-allelic. SNP markers are inherited as co-dominant markers. Several approaches have been used for SNP discovery including SSCP analysis [45], heteroduplex analysis, and direct DNA sequencing. DNA sequencing has been the most accurate and most used approach for SNP discovery. SNPs are not without their limitations, however, might provide marginal additional, or even less, utility in some applications (e.g. relatedness) [9].

6. MICROSATELLITE MARKERS

Microsatellites consist of multiple copies of tandemly arranged simple sequence repeats (SSRs) that range in size from 1 to 6 base pairs [e.g., ACA or GATA; 46,47]. Abundant in all species studied to date, microsatellite motifs have been estimated to occur as often as once every 10 kb in fishes [48]. Microsatellites tend to be evenly distributed in the genome on all chromosomes and all regions of the chromosome. However, data from whole genome sequencing has somewhat contradicted this statement. They have been found inside gene coding regions [49], introns, and in the non-gene sequences. Most microsatellite loci are relatively small, ranging from a few to a few hundred repeats. Regardless of specific mechanisms, changes in numbers of repeat units can result in a large number of alleles at each microsatellite locus in a population. Microsatellites have been inherited in a Mendelian fashion as codominant markers. Microsatellites were found to be informative in several species, which showed almost no variation at other markers [50]. However, use of microsatellite markers involves a large amount of up-front investment and effort. Each microsatellite locus has to be identified and its flanking region sequenced to design of PCR primers. Due to polymerase slippage during replication, small size differences between alleles of a given microsatellite locus (as little as 2 bp in a locus comprised of di-nucleotide repeats) are possible. Microsatellites recently have become an extremely popular marker type in a wide variety of genetic investigations.

7. NEW DEVELOPING MARKERS IN FISHERIES AND AQUACULTURE

Various type of DNA markers have been developed, including Allozymes, microsatellites, RAPDs, mt-DNA and SNPs. These markers in fish populations have revealed high levels of genetic variation distributed throughout the fish genome. A recent initiative has been made to accelerate efforts of DNA marker development, genome mapping and species identification. Major progress has been made toward Expressed Sequence Tags (EST) and DNA barcode development in several aquaculture species.

8. EXPRESSED SEQUENCE TAGS (ESTs)

Expressed sequence tags (ESTs) are single-pass sequences generated from random sequencing of cDNA clones [51]. The EST is use to identify genes and analyze their expression by means of expression profiling. It helps for rapid and valuable analysis of genes expressed in specific tissue types, under specific physiological conditions, or during specific developmental stages. ESTs offer the development of cDNA microarrays that allow analysis of differentially expressed genes to be determined in a systematic way [52], in addition to their great value in genome mapping [53]. For genome mapping, ESTs are most useful for linkage mapping and physical mapping in animal genomics such as those of cattle and swine, where radiation hybrid panels are available for mapping non-polymorphic DNA markers [54]. A radiation panel is composed of lines of hybrid

cells, with each hybrid cell containing small fragments of irradiated chromosomes of the species of interest. Typically, the cells from species of interest are radiated to break chromosomes into small fragments. The radiated cells are unable to survive by themselves. However, the radiated cells can be fused with recipient cells to form hybrid cells retaining a short segment of the radiated chromosome. Characterization of the chromosomal break points within many hybrid cell lines would allow linkage and physical mapping of markers and genes. In spite of its popularity in mammalian genome mapping [55, 56], radiation hybrid panels are not yet available for any aquaculture species. Development of radiation hybrid panels from aquaculture species is not expected in the near future, given the fact that physical mapping using BAC libraries can provide even higher resolution and the fact that BAC libraries are already available from several aquaculture species. Therefore, ESTs are useful for mapping in aquaculture species only if polymorphic ESTs are identified [57]. The value of EST resources and applications of bioinformatics in aquaculture genetics/genomics is inevitable, and it is expected that various EST databases will serve as rich sources of genomic information not only for aquaculture geneticists, but also for aquaculture physiologists, immunologists and biotechnologists.

9. DNA BARCODING

The principle of conservation biology is the preservation and management of biodiversity. The two major problems to such an endeavor are the difficulty of developing an assessment of this diversity for prioritization of hotspots of species richness [58] and the identification of lineages particularly worthy, or in need, of preservation [59-64]. Understudied taxa are greatly susceptible to extinction [65], suggesting there is a conservation penalty for our ignorance. Even there are millions of unidentified and unknown species [66]. DNA barcodes, segments of approximately 600 base pairs of the mitochondrial gene cytochrome oxidase I (COI), have been proposed as a fast, efficient, and inexpensive technique to catalogue all biodiversity [67-70]. Barcoding is the use of universal polymerase chain reaction (PCR) primers to amplify and sequence an approximately 600-base-pair fragment of the COI gene. That portion of sequence is then compared using distance-based algorithms with an existing database of "known" sequences from specimens previously identified by taxonomists. DNA barcodes from a small portion of the mitochondrial genome might seem like an effective and rapid way to assess at least some, perhaps minimal, level of biodiversity. And for groups that are already relatively well known, especially birds and mammals, molecular studies based on barcode sized sequences have revealed cryptic DNA lineages and may be helpful [70].

10. APPLICATION OF MOLECULAR MARKERS SPECIES IDENTIFICATION

The inter-specific genetic divergence established through species specific diagnostic molecular markers provides precise knowledge on phylogenetic relationships and also resolve taxonomic ambiguities [71-74]. These markers can be used to detect hybrid and introgressed or backcrossed individuals [75], distinguish early life history stage of morphologically close species [76] both in hatchery and in natural populations.

Species-specific allozyme markers have been identified in many fishes [Tilapia: 72,77,78; Sciaenid: 73; *Anguilla* sp: 79; Mugilidae: 80] Specific diagnostic allozyme loci were used for different species: apache trout (*Oncorhynchus apache*), cutthroat (*Oncorhynchus clarki*) and rainbow trout (*Oncorhynchus mykiss*) [81] and *Gambusia affinis* and *G. holbrooki* [82]. Allozyme markers have also been used for individual classification in cyprinid species *Zacco pachycephalus and Z. platypus* [83], in cyprinodontid species *V. letourneuxi* and *V. hispanica* [84], in mullets *Mullus barbatus and M. surmuletus* [85] and hake species *Merluccius australis* and *M. hubbsi* [86].

Species-specific diagnostic RAPD fingerprints were generated in several fish species and their taxonomic relationship has been analyzed. The RAPD-PCR technique was employed to identify three endemic morphologically similar Spanish species of *Barbus*: *Barbus bocagei, B. graellsii* and *B. sclateri* that have similar morphologies [87]. RAPD markers were characterized to identify five species of family Cyprinidae: *Chondrostoma lemmingii, Leuciscus pyrenaicus, Barbus bocagei, Barbus comizo*, all endemic in the Iberian Peninsula, and introduced *Alburnus alburnus* [88], for studying genetic relationship and diversities in four species of Indian Major carps (family Cyprinidae): rohu (*Labeo rohita*), kalbasu (*L. calbasu*), catla (*Catla catla*) and mrigal (*Cirrhinus mrigala*) [89], for identification of three eel species, *A. japonica, A. australis* and *A. bicolor* [90] and to estimate the population structure and phylogenetic relationships among the eight species of the genus *Barbus* [88].

Large variation in mtDNA sequences among species can be utilized to produce species-specific markers. Since the structures of mitochondrial RNA genes (tRNA and rRNA) and the functional molecule of the 16S rRNA are highly conserved among the animal taxa that are related even distantly [21], change of even few nucleotides in such a gene between closely related taxa might

indicate a substantial degree of genetic divergence [2]. Mt-DNA sequences have been used as useful marker for species-specific identification in many fishes [Tuna: 91; Billfish: 92 Snappers: 29, 93; Myctophidae: 94; Grey mullets: 95]. Comparable levels of divergence based on 12S rRNA and 16S rRNA sequences have been reported for several recently diverged fish species [genus *Sternoptyx*: 96; *Cyclothone* sp: 97]. Sequence variation in the control region (D-loop) of the mitochondrial DNA (mtDNA) was examined to assess the genetic distinctiveness of the short-jaw cisco, *Coregonus zenithicus* [98] and revealed high similarity of *C. zenithicus* and the related species *C. artedi*, *C. hoyi*, *C. kiyi*, and *C. clupeaformis*

Identification of *Astyanax altiparanae* (Teleostei, Characidae) in the Iguacu River, Brazil, was done on the basis of mitochondrial DNA and RAPD markers [99]. Two species, *Acipenser baeri*, and *A. stellatus*, was studied using mitochondrial DNA (D-loop, cytochrome b (cyt-b) and ND5/6 genes) sequencing to determine whether traditionally defined subspecies correspond to taxonomic entities and conservation management units [100].

11. GENETIC VARIATION AND POPULATION STRUCTURE STUDY IN NATURAL POPULATIONS

Molecular markers provide direct assessment of pattern and distribution of genetic variation [5] thus helping in answering, "if the population is single unit or composed of subunits". Several evolutionary forces affect the amount and distribution of genetic variation among populations and thereby population differentiation [101]. Geographic distance and physical barriers enhance reproductive isolation by limiting the migration and increase genetic differentiation between populations [102]. Impact of migration and gene flow on genetic differentiation also depends upon effective size of receiving population and number of migrants. Increased computational power and mathematical models have enhanced the scope of conclusions that can be drawn out of genotype data generated through molecular markers. Some of the possibilities are assignment of migrants [103], determination of genetic bottlenecks [104], effective breeding population estimates [105] besides genetic variation and differentiation estimations [106-108]. These markers have been extensively employed across various taxonomic groups [mosquito: 109**;** turtle: 39; amphibians: 7; panda: 110; five vertebrate classes including fish, amphibian, reptiles, birds and mammals: 6]. Experiments on fish populations have significantly contributed towards development of science of population genetics, models and analytical softwares.

Population genetic structure has been investigated using allozyme markers in many fish species [*Oncorhynchus gorbuscha*: 111; *Tenualosa ilisha*: 112 and Lal *et al*., 113; *Pagrus auratus:* 114].

Fifteen random primers were used to analyze the genome DNA of Jian carp (*Cyprinus carpio* var jian) by the RAPD technique [115]. Study on cold tolerant traits for common carp *Cyprinus carpio* was conducted by Chang *et al*. [116] and nine RAPD-PCR markers associated with cold tolerance of common carp were identified. The genetic diversity has been studied using RAPD markers in *Carassius auratus* [117], *Epinephelus merra* population [118] and *Solea solea* [119].

Genetic variation have been assessed with Allozyme and RAPD markers on *Mullus surmuletus* L., [120] and three species of Pimelodidae catfish [121].

Population structure has been examined using microsatellite markers of sockeye salmon [122], Chinook salmon [123] and Arctic charr populations [124]. Genetic variation have been assessed using microsatellite genetic markers to identify the population structure of brook charr, *Salvelinus fontinalis* [125] and 14 populations of northern pike (*Esox lucius*) in the North Central United States and in six populations from Quebec, Alaska, Siberia, and Finland [126].

Based on five microsatellite loci, the genetic structure of endangered fish species *Anaecypris hispanica* was studied in eight distinct populations in the Portuguese Guadiana drainage to determine levels of genetic variation within and among populations and suggested implications for conservation of the species [127].

Combination of allozyme and microsatellites was used to investigate genetic divergence in *Salmo trutta* [128] and *Salmo salar* [129].

Alarcon *et al*. [130] represents population genetic analysis of gilthead sea bream (*Sparus aurata*) and Kanda [131], Kanda and Allendorf [132] examine population genetic structure of bull trout *Salvelinus confluentus* using a combination of allozyme, microsatellite and mtDNA variation.

Genetic variability of *Salmo trutta* [133] and Sparus aurata [130] was evaluated on the basis of Allozyme, Microsatellites and RAPD markers.

Patterns of population subdivision and the relationship between gene flow and geographical distance in the tropical estuarine fish *Lates calcarifer* (Centropomidae) were investigated using mtDNA control region sequences [134].

Allozymes and mtDNA sequences were assessed to evaluate the genetic variability in small marine fish *Pomatoschistus microps* [135], brown trout [136] and *Macquaria novemaculeata* [137].

12. COMPARISON OF GENETIC VARIATION BETWEEN WILD AND HATCHERY POPULATIONS

Molecular markers also find application in aquaculture to assess loss of genetic variation in hatcheries through, comparison of variation estimates between hatchery stocks and wild counterparts. The information is useful obtained in monitoring farmed stocks against inbreeding loss and to plan genetic up gradation programmes. A major aspect such studies address is concerned with the assessment of farm escapes into the natural population and introgression of wild genome.

Brook trout *Salvelinus fontinalis* from ustocked waters, naturalized lakes, and hatcheries in New York and Pennsylvania were analyzed electrophoretically for allozyme expression [138]. All wild-unstocked samples were highly differentiated populations and significantly different from each other and from hatchery samples.

Genetic diversity was investigated using microsatellites between farmed and wild populations of Atlantic salmon [139]. Farmed salmon showed less genetic variability than natural source population in terms of allelic diversity.

Variation in allozymes and three microsatellite loci was assessed in populations of wild and cultured stocks of *Sparus aurata* [140] and *Sparius auratus* [130]. The microsatellite heterozygosity values were high in wild, but lower in the cultured samples.

13. ASSESSMENT OF DEMOGRAPHIC BOTTLENECK IN NATURAL POPULATION

Demographic bottlenecks occur when populations experience severe, temporary reduction in size. Because bottlenecks may influence the distribution of genetic variation within and among populations, the genetic effects of reductions in population size have been studied extensively by evolutionary biologist [141,142].

It may often be necessary to perform genetic analyses of temporal replicates to estimate the significance of spatial variation independently from that of temporal variation in order to ensure the reliability of estimates of a defined population structure. Such estimates provide understanding about changes in genetic variation, effective population size and other historical bottlenecks and can be extrapolated to define evolutionary trends of species. Today various models are available that can resolve bottlenecks or effective population size changes through use of heterozygosity excess, linkage disequilibrium etc. However, estimates through temporal changes are considered more accurate. Analysis of temporal changes is limited due to lack of historical data as well as samples. Therefore, such studies are limited and mostly use archived samples, wherever available. In vertebrates, a limited number of studies have specifically assessed the temporal changes in genetic variation for more than one generation.

Microsatellite DNA markers have been used to assess bottlenecks in many fish species. A microsatellite analysis of DNA was performed, from archived scales to compare the population structure among four sympatric landlocked populations of Atlantic salmon [143], Atlantic salmon [144], European hake [145] and steelhead from [146].

Larson *et al*. [147] recommended close monitoring of negative effects on sea otter population based on the conclusion from mtDNA, D-loop, microsatellite variability comparison between prefur trade and present population. Prefur trade DNA samples were obtained from excavated bones.

14. PROPOGATION ASSISTED REHABILITATION PROGRAMMES

Habitat alterations and over harvesting have contributed to the decline or disappearance of numerous natural populations. In addition, reinforcement programs of wild populations based on releases of hatchery reared fish of non-native origin compromise the conservation of remnant native trout resources. Effect of these programmes through releases in natural populations has been studies in many fishes through molecular markers.

Beaudou *et al*. [148] found through allozyme polymorphism that brown trout (*Salmo trutta* L.) in the Abatesco river basin on the eastern coast of Corsica restoration was mainly due to the populations of the tributaries, which had been less disturbed by the spate. This study has shown that the wild population was primarily restored by the surviving individuals, particularly those from the tributaries that escaped the spate.

To assess the levels of gene introgression from cultured to wild brown trout populations, four officially stocked locations and four non-stocked locations were sampled for one to three consecutive years and compared to the hatchery strain used for stocking. Allozyme analysis for 25 loci included providing allelic markers distinguishing hatchery stocks and native populations [133]. Different levels of hybridization and introgression with hatchery individuals were detected in stocked drainages as well as in protected locations.

The foregoing review incorporates the wide spectrum of information that the molecular markers provide. The literature indicates that different markers have been employed depending upon the question to be answered. The importance of the research on molecular markers improved due to enhanced computational power, large data

available that has enabled researchers to derive various mathematical estimators. Such innovations provide insight concerning the population bottleneck, migration patterns besides the genetic structure in natural populations.

REFERENCES

[1] Fisher, R.A. (1930) The Genetical Theory of Natural Selection. Oxford University Press, UK.

[2] Avise, J.C. (1994) Molecular Markers, Natural History and Evolution. Chapman and Hall, New York, London.

[3] Linda, K.P. and Paul, M. (1995) Developments in molecular genetic techniques in fisheries. In: G.R. Carvalho and T.J. Pitcher, Eds., *Molecular Genetics in Fisheries*, Chapman and hall, London, 1-28.

[4] Hillis, D.M., Mable, B.K. and Moritz, C. (1996) Applications of molecular systematics: The state of the field and a look to the future. In: Hillis, D.M., Moritz, C. and Mable, B.K. Eds., *Molecular systematics*, Sinauer Associates, Massachusetts, 515-543.

[5] Ferguson, A., Taggart, J.B., Prodohl, P.A., McMeel, O., Thompson, C., Stone, C., McGinnity, P. and Hynes, R.A. (1995) The application of molecular markers to the study and conservation of fish populations with special reference to *Salmo*. *Journal of Fish Biology*, **47(A)**, 103-126.

[6] Neff, B.D. and Gross, M.R. (2001) Microsatellite evolution in vertebrates: Inference from AC dinucleotide repeats. *Evolution*, **55(9)**, 1717-1733.

[7] Jehle, R. and Arntzen, J.W. (2002) Microsatellite markers in amphibian conservation genetics. *Herpetological Jour nal*, **12**, 1-9.

[8] Wasko, A.P., Martins, C., Oliveira, C. and Foresti, F. (2003) Non-destructive genetic sampling in fish. An improved method for DNA extraction from fish fins and scales. *Hereditas*, **138(3)**, 161-165.

[9] Morin, P.A., Luikart, G., Wayne, R.K. and the SNP working group, SNPs in ecology, evolution and conservation. *Trends in Ecology and Evolution*, **19(4)**, 208-216.

[10] Liu, Z.J. and Cordes, J.F. (2004) DNA marker technologies and their applications in aquaculture genetics. *Aquaculture*, **238**, 1-37.

[11] O'Brien, S.J. (1991) Molecular genome mapping: lessons and prospects. *Current Opinion in Genetic Development*, **1(1)**, 105-111.

[12] Brown, B. and Epifanio, J. (2003) Nuclear DNA. In: Hallermann, E.M. Ed., *Population Genetics: Principles and Applications for Fisheries Scientists*, American Fisheries Society, Bethesda, 458-472.

[13] Suneetha, B.K. (2000) Interspecific and inter specific genetic variation in selected mesopelagic fishes with emphasis on microgeographic variation and species characterization. Dr. Scient. Dissertation, Department of Fisheries and Marine Biology, University of Bergen, Bergen, Norway.

[14] Menezes, M.R., Naik, S. and Martins, M. (1993) Genetic characterization in four sciaenid species from the Arabian Sea. *Journal of Fish Biology*, **43(1)**, 61-67.

[15] Markert, C.L. and Moller, F. (1959) Multiple forms of enzymes: Tissue, ontogenetic and species-specific patterns. *Proceedings of the Naionall Academy of Science* (*USA*), **45(5)**, 753-763.

[16] Starck, M.G. (1998) Isozymes in Molecular tools for screening biodiversity. In: Angela, K., Peter, G.I. and. David, S.I. Eds., Chapmann and Hall, London, 75-80.

[17] Murphy, R.W., Sites, J.J.W. Buth, D.G. and Haufler, C.H. (1996) Proteins I: Isozyme electrophoresis. In: Hillis, D.M., Moritz, C. and Mable, B.K. Eds., *Molecular Systematics*, Sinauer Associates, Sunderland, 51-132.

[18] Brown, W.M. (1985) The mitochondrial genome of animals. In: MacIntyre, R.J. Ed., *Molecular Evolutionary Genetics*, Plenum, New York, 95-130.

[19] Wilson, A.C., Cann, R.L., Carr, S.M., George, M., Gyllensten, U.B., Helm-Bychowski, K.M., Higuchi, R.G., Palumbi, S.R. and Prager, E.M. (1985) Mitochondrial DNA and two perspectives on evolutionary genetics. *Biological Journal of Linnean Society*, **26(4)**, 375-400.

[20] Birky, C.W., Fuerst, P. and Maruyama, T. (1989) Organelle gene diversity under migration, mutation, and drift: equilibrium expectations, approach to equilibrium, effect of heteroplasmic cells, and comparison to nuclear genes. *Genetics*, **121(3)**, 613-627.

[21] Meyer, A. (1993) Evolution of mitochondrial DNA in fishes. In: Mochachka, P.W. and Mommsen, T.P. Eds., Biochemistry and molecular biology of fishes. Elsevier Press Amsterdam, New York, 1-38.

[22] Brown, J.R., Bechenbach, A.T. and Smith, M.J. (1993) Intraspecific DNA sequence variation of the mitochondrial control region of white sturgeon (*Acipenser transmontanus*). *Molecular Biology Evolution*, **10(2)**, 326-341.

[23] Chow, S., Okamoto, H., Uozumi, Y., Takeuchi, Y. and Takeyama, H. (1997) Genetic stock structure of the swordfish (*Xiphias gladius*) inferred by PCR-RFLP analysis of the mitochondrial DNA control region. *Marine Biology*, **127(3)**, 359-367.

[24] Gold, J.R. Sun, F. and Richardson, L.R. (1997) Population structure of red snapper from the Gulf of Mexico as inferred from analysis of mitochondrial DNA. *Transaction of American Fisheries Society*, **126(3)**, 386-396.

[25] Chow, S. and Kishino, H. (1995) Phylogenetic relationships between tuna species of the genus *Thunnus* (Scombriidae: Teleosrei): Inconsistent implications from morphology, nuclear and mitochondrial genomes. *Journal of Molecular Evolution*, **41**, 741-748.

[26] Avise, J.C., Helfman, G.S., Saunders, N.C. and Hales, L.S. (1986) Mitochondrial DNA differentiation in North Atlantic eels: Population genetic consequences of an unusual life history pattern. *Proceeding of the National Academy Science* (*USA*), **83(12)**, 4350-4354.

[27] Graves, J.E., McDowell, J.R. and Jones, M.L. (1992) A genetic analysis of weakfish *Cynoscion regalis* stock structure along the mid-Atlantic coast. *Fisheries Bulletin*, **90**, 469-475.

[28] Gold, J.R., Richardson, L.R., Furman, C. and King, T.L. (1993) Mitochondrial DNA differentiation and population structure in red drum (*Sciaenops ocellatus*) from the Gulf of Mexico and Atlantic Ocean. *Marine Biology*, **116(2)**, 175-185.

[29] Chow, S., Clarke, M.E. and Walsh, P.J. (1993) PCR-RFLP analysis of thirteen western Atlantic snappers (subfamily Lutjaninae): A simple method for species and stock identification. *Fisheries Bulletin* (*US*), **91**, 619-627.

[30] Heist, E.J. and Gold, J.R. (1999) Microsatellite DNA variation in sandbar sharks (*Carcharhinus plumbeus*) from the Gulf of Mexico and mid-Atlantic bight. *Copeia*, **1**, 182-186.

[31] Baker, A.J. and Marshall, H.D. (1997) Molecular evolution of the mitochondrial genome. In: Mindell, D.P. Ed., *Avian Molecular Evolution and Systematics*, Academic Press, San Diego, 51-82.

[32] Greenberg, R., Cordero, P.J., Droege, S. and Fleischer, R.C. (1998) Morphological adaptation with no mitochondrial DNA differentiation in the coastal plain swamp sparrow. *Journal of American Ornithologists' Union*, **115(3)**, 706-712.

[33] Mila, B., Girman, D.J., Kimura, M. and Smith, T.B. (2000) Genetic evidence for the effect of a postglacial population expansion on the phylogeography of a North American songbird. *Proceedings of the Royal Society London Series B*, **267(1447)**, 1033-1040

[34] Zink, R.M., Barrowclough, G.F., Atwood, J.L. and Blackwell-Rago, R.C. (2000) Genetics, taxonomy, and conservation of the threatened California gnatcatcher. *Conservation Biology*, **14(5)**, 1394-1405.

[35] Menotti-Raymond, M. and O'Brien, S.J. (1993) Dating the genetic bottleneck of the African cheetah. *Proceedings of the National Academy of Science* (*USA*.), **90(8)**, 3172-3176.

[36] Avise, J.C., Walker, D. and Johns, G.C. (1998) Speciation durations and Pleistocene effects on vertebrate phylogeography. *Proceedings of the Royal Society of London Series B*, **265(1407)**, 1707-1712.

[37] Serb, J.M., Phillips, C.A. and Iverson, J.B. (2001) Molecular phylogeny and biogeography of *Kinosternon flavenscens* based on complete mitochondrial control region sequences. *Molecular Phylogenetics and Evolution*, **18(1)**, 149-162.

[38] Riberon, A., Sotiriou, E., Miaud, C., Andreone, F. and Taberlet, P. (2002) Lack of genetic diversity in *Salamandra lanzai* revealed by cytochrome b gene sequences. *Copeia*, **2002**, 229-232.

[39] Shanker, K., Ramadevi, J., Choudhaury, B.C., Singh, L. and Aggarawal, R.K. (2004) Phylogeny of olive ridley turtles (*Lepidochelys olivacea*) on the east coast of India: implications for conservation theory. *Moelcular Ecology*, **13(7)**, 1899-1909.

[40] Mamuris, Z., Sfougaris, A.I., Stamatis, C. and Suchentrunk, F. (2002) Assessment of genetic structure of Greek Brown Hare (*Lepus europeaus*) populations based on variation in Random Amplified Polymorphic DNA (RAPD). *Biochemical Genetics*, **40(9-10)**, 323-338.

[41] Williams, J.G.K., Kubelik, A.R., Livak, K.J., Rafalski, J.A. and Tingey, S.V. (1990) DNA polymorphisms amplified by arbitrary primers are useful as genetic markers. *Nucleic Acids Research*, **18(22)**, 6531-6535.

[42] Welsh, J. and McClelland, M. (1990) Fingerprinting genomes using PCR with arbitrary primers. *Nucleic Acids Research*, **18(24)**, 7213-7218.

[43] Haymer, D.S. (1994) Random amplified polymorphic DNAs and microsatellites: what are they, and can they tell us anything we don't already know? *Annals of Entomological Society of American*, **87**, 717-722.

[44] Wirgin, I.I. and Waldman, J.R. (1994) What DNA can do for you? *Fisheries*, **19**, 16-27.

[45] Hecker, K.H., Taylor, P.D. and Gjerde, D.T. (1999) Mutation detection by denaturing DNA chromatography using fluorescently labeled polymerase chain reaction products. *Analytical Biochemistry*, **272(2)**, 156-164.

[46] Tautz, D. (1989) Hypervariability of simple sequences as a general source for polymorphic DNA markers. *Nucleic Acids Research*, **17(16)**, 6463-6471.

[47] Litt, M. and Luty, J.A. (1989) A hypervariable microsatellite revealed by *in-vitro* amplification of dinucleotide repeat within the cardiac muscle actin gene. *American of Journal of Human Genetics*, **44(3)**, 397-401.

[48] Wright, J.M. (1993) DNA fingerprinting in fishes. In: W. Hochachka, P. and Mommsen, T. Eds., *Biochemistry and Molecular Biology of Fishes*, Elsevier, Amsterdam, 58-91.

[49] Liu, Z.J., Li, P., Kocabas, A., Ju, Z., Karsi, A., Cao, D. and Patterson, A. (2001) Microsatellite-containing genes from the channel catfish brain: evidence of trinucleotide repeat expansion in the coding region of nucleotide excision repair gene RAD23B. *Biochemical Biophysical Research Communication*, **289(2)**, 317-324.

[50] Taylor, A.C., Sherwin, W.B. and Wayne, R.K. (1994) Genetic variation of microsatellite loci in a bottlenecked species: The northern hairy-nosed wombat *Lasiorhinus krefftii*. *Molecular Ecology*, **3(4),** 277-290.

[51] Adams, M.D., Kelley, J.M., Gocayne, J.D., Dubnick, M., Polymeropoulos, M.H., Xiao, H., Merril, C.R., Wu, A., Olde, B., Moreno, R.F., Kerlavage, A.R., McCombie, W.R. and Venter, J.C. (1991) Complementary DNA sequencing: Expressed sequence tags and human genome project. *Science*, **252(5013)**, 1651-1656.

[52] Wang, K., Gan, L., Jeffry, E., Gayle, M., Gown, A.M., Skelly, M., Nelson, P.S., Ng, W.V., Schummer, M., Hood, L. and Mulligan, J. (1999) Monotoring gene expression profile changes in ovarian carcinomas using cDNA microarray. *Gene*, **229(1-2)**, 101-108.

[53] Boguski, M.S.and Schuler, G.D. (1995) Establishing a human transcript map. *Nature Genetics*, **10(4)**, 369-371.

[54] Cox, D.R., Burmeister, M., Price, E., Kim, S. and Myers, R.M. (1990) Radiation hybrid mapping: a somatic cell genetic method for constructing high-resolution map of mammalian chromosomes. *Science*, **250(4978)**, 245-250.

[55] Korwin-Kossakowska, A., Reed, K.M., Pelak, C., Krause, E., Morrison, L. and Alexander, L.J. (2002) Radiation hybrid mapping of 118 new porcine microsatellites. *Animal Genetics*, **33(3)**, 224-227.

[56] McCoard, S.A., Fahrenkrug, S.C., Alexander, L.J., Freking, B.A., Rohrer, G.A., Wise, T.H. and Ford, J.J. (2002) An integrated comparative map of the porcine X chromosome. *Animal Genetics*, **33(3)**, 178-185.

[57] Liu, Z.J., Karsi, A. and Dunham, R.A. (1999) Development of polymorphic EST markers suitable for geneticlinkage mapping of catfish. *Marine Biotechnology*, **1(5)**, 437-447.

[58] Dobson, A.P., Rodriguez, J.P., Roberts, W.M. and Wilcove, D.S. (1997) Geographic distribution of endangered species in the United States. *Science*, **275(5299)**, 550-555.

[59] Daugherty, C.H., Cree, A., Hay, J.M. and Thompson, M.B. (1990) Neglected taxonomy and continuing extinctions of tuatara (*Sphenodon*). *Nature*, **347(6289)**, 177-

179.
[60] Faith, D.P. (1994) Genetic diversity and taxonomic priorities for conservation. *Biological Conservation*, **68(1)**, 69-74.
[61] Crozier, R.H. (1997) Preserving the information content of species: genetic diversity, phylogeny, and conservation worth. *Annual Review of Ecology and Systematics*, **28(1)**, 243-268.
[62] Haig, S.M. (1998) Molecular contributions to conservation. *Ecology*, **79(2)**, 413-425.
[63] Soltis, P.S. and Gitzendanner, M.A. (1999) Molecular systematics and the conservation of rare species. *Conservation Biology*, **13(3)**, 471-483.
[64] Moritz, C. (2002) Strategies to protect diversity and the evolutionary processes that sustain it. *Systematic Biology*, **51(2)**, pp. 238-254.
[65] McKinney, M.L. (1999) High rates of extinction and threat in poorly studied taxa. *Conservation Biology*, **13(6)**, 1273-1281.
[66] Novotny, V., Basset, Y., Miller, S.E., Weiblen, G.D., Bremer, B., Cizek, L. and Drozd, P. (2002) Low host specificity of herbivorous insects in a tropical forest. *Nature*, **416**, 841-844.
[67] Hebert, P.D.N., Ratnasingham, S. and deWaard, J.R. (2003) Barcoding animal life: cytochrome c oxidase subunit 1 divergences among closely related species. *Royal Society London*, **270 (Suppl 1)**, S96-S99.
[68] Stoeckle, M. (2003) Taxonomy, DNA, and the bar code of life. *BioScience*, **53(9)**, 2-3.
[69] Stoeckle, M., Janzen, D., Hallwachs, W., Hanken, J. and Baker, J. (2003) Taxonomy, DNA, and the barcode of life," Draft conference report. *Rubinoff DNA Barcodes and Conservation Barcode Conference*, The Rockefeller University, New York, http://phe.rockefeller.edu/BarcodeConference/docs/B2summary.doc
[70] Hebert, P.D.N., Stoeckle, M.Y., Zemlak, T.S. and Francis, C.M., (2004) Identification of birds through DNA barcodes. *PLoS Biology*, **2(10)**, 312-316.
[71] Rocha-Olivares, A., Moser, H.G. and Stannard, J. (2000) Molecular identification and description of pelagic young of the rockfishes *Sebastes constellatus* and *Sebastes ensifer*. *Fisheries Bulletin*, **98**, 353-363.
[72] Backer, J., Bentzen, P. and Moran, P. (2002) Molecular markers distinguish coastal cutthroat trout from coastal rainbow trout/steelhead and their hybrids. *Transaction of American Fisheries Society*, **131(3)**, 404-417.
[73] Asensio, L., Gonzalez, I., Fernandez, A., Rodriguez, M.A., Lobo, E., Hernandez, P.E., Garcia, T. and Martin, R. (2002) Application of random amplified polymorphic DNA (RAPD) analysis for identification of grouper (*Epinephelus guaza*), wreckfish (*Polyprion americanus*), and nile perch (*Lates niloticus*) fillets. *Journal of Food Product*, **65(2)**, 432-435.
[74] Rasmussen, C., Ostberg, C.O., Clifton, D.R., Holloway, J.L. and Rodriguez, R.J. (2003) Identification of a genetic marker that discriminates ocean-type and stream-type Chinook salmon in the Columbia River Basin. *Transaction American Fisheries Society*, **132(1)**, 131-142.
[75] Compton, D. and Utter, F.M. (1985) Natural hybridization between steelhead trout (*Salmo gairdneri*) and coastal cutthroat trout (*Salmo clarki clarki*) in two Puget sound streams. *Canadian Journal of Fisheries and Aquatic Science*, **42**, 110-119.
[76] Olivar, M.P., Moser, H.G. and Beckley, L.E. (1999) Lantern fish larvae from the Agulhas current (SW Indian Ocean). *Science of Marine*, **63**, 101-120.
[77] McAndrew, B.J. and Majumdar, K.C. (1983) Tilapia stock identification using electrophoretic markers. *Aquaculture*, **30(1-4)**, 249-261.
[78] Bartly, D.M. and Gall, G.A.E. (1991) Genetic identification of native cutthroat trout (*Onchorynchus clarki*) and introgressive hybridization with introduced rainbow trout (*O. mykiss*) in streams associated with the Alvord basin, Oregon and Nevada. *Copeia*, **3**, 854-859.
[79] Lee, S.C., Tosi, S.C.M., Cheng, H.L. and Chang, J.T. (1997) Identification of *Anguilla Japonica* and *A. marmorata* elvers by allozyme electrophoresis. *Journal of Fish Biology*, **51(1)**, 208-210.
[80] Rossi, A.R., Capula, M., Crosetti, D., Sola, L. and Campton, D.E. (1998) Allozyme variation in global populations of striped mullet, *Mugil cephalus* (Pisces: Mugilidae). *Marine Biololgy*, **131(2)**, 203-212.
[81] Carmichael, G.J., Hanson, J.N., Schmidt, M.E. and Morizot, D.C. (1993) Introgression among apache, cutthroat and rainbow trout in Ariozona. *Transaction of American Fisheries Society*, **122**, 121-130
[82] Wooten, M.C. and Lydeard, C. (1990) Allozyme variation in a natural contact zone between G*ambusia affinis* and *Gambusia holbrooki*. *Biochemical Systematics and Ecology*, **18(2-3)**, 169-173.
[83] Wang-Hurng, Y., Lee, S.C. and Yu, M.J. (1997) Genetic evidence to clarify the systematic status of the genra *Zacco* and *Candidia* (Cypriniformes: Cprinidae). *Zoological Studies*, **36(3)**, 170-177.
[84] Perdices, A., McChordom, A. and Doadrio, I. (1996) Allozyme variation and relationships of the endangered cyprinodontid genus *Valencia* and its implications for conservation. *Journal of Fish Biology*, **49(6)**, 1112-1127.
[85] Mamuris, Z., Apostolidis, A.P. and Triantaphyllidis, C. (1998) Genetic protein variation in red mullet (*Mullus barbatus*) and striped red mullet (*M. surmuletus*) populations from the Mediterranean sea. *Marine Biology*, **130(3)**, 353-360.
[86] Roldán, M.I. and Pla, C. (2001) Species identification of two sympatric hakes by allozyme markers. *Science of Marine*, **65**, 81-84.
[87] Callejas, C. and Ochando, M.D. (1998) Identification of Spanish barbel species using the RAPD technique. *Journal of Fish Biology*, **53(1)**, 208-215.
[88] Callejas, C. and Ochando, M.D. (2002) Phylogenetic relationships among Spanish Barbus species (Pisces, Cyprinidae) shown by RAPD markers. *Heredity*, **89(1)**, 36-43.
[89] Barman, H.K., Barat, A., Yadav, B.M., Banerjee, S., Meher, P.K., Reddy, P.V.G.K. and Jana, R.K. (2003) Genetic variation between four species of Indian major carps as revealed by random amplified polymorphic DNA assay. *Aquaculture*, **217(1-4)**, 115-123.
[90] Takagi, M. and Taniguchi, N. (1995) Random amplified polymorphic DNA (RAPD) for identification of three species of *Anguilla*, *A. japonica*, *A. australis* and *A. bicor*. *Fisheries Science*, **61**, 884-885.
[91] Chow, S. and Inoue, S. (1993) Intra-and interspecific

restriction fragment length polymorphism in mitochondrial genes of Thunnus tuna species. *Bulletin of National Research Institute of Far Seas Fisheries*, **30**, 229-248.

[92] Finnerty, J.R. and Block, B.A. (1992) Direct sequencing of mitochondrial DNA detects highly divergent haplotypes in blue marlin (*Makaira nigricans*). *Molecular Marine Biology and Biotechnology*, **1(3)**, 206-214.

[93] Hare, J.A., Crown, R.K., Zehr, J.P., Juanes, F. and Day, K.H. (1998) A correction to: biological and oceanographic insights from larval labrid (Pisces: Labridae) identification using mtDNA sequences. *Marine Biology*, **130(4)**, 589-592.

[94] Suneetha, B.K. and Dahle, G. (2000) Analysis of mitochondrial DNA sequences from *Benthosema glaciale* and two other myctophids (Pisces: Myctophiformes): Intra- and interspecific genetic variation. *In: Interspecific and inter specific genetic variation in selected mesopelagic fishes with emphasis on microgeographic variation and species characterization*, Dr. Scient. Dissertation, Departement of Fisheries and Marin Biology, University of Bergen, Bergen, Norway.

[95] Murgia, R., Tola, G., Archer, S.N., Vallerga, S. and Hirano, J. (2002) Genetic identification of grey mullet species (Mugilidae) by analysis of mitochondrial DNA sequence: application to identify the origin of processed ovary products (bottarga). *Marine Biotechnology*, **4(2)**, 119-126.

[96] Miya, M. and Nishida, M. (1998) Molecular phylogeny and evolution of the deep-sea fish genus *Sternoptyx*. *Molecular Phylogenetics and Evolution*, **10(1)**, 11-22.

[97] Miya, M.and Nishida, M. (1996) Molecular phylogenetic perspective on the evolution of the deep-sea fish genus *Cyclothone* (Stomiiformes: Gonostomatidae). *Ichthyolgical Research*, **43(4)**, 375-398.

[98] Reed, K.M., Dorschner, M.O., Todd, T.N. and Phillips, R.B. (1998) Sequence analysis of the mitochondrial DNA control region of ciscoes (genus *Coregonus*): Taxonomic implications for the Great Lake species flock. *Molecular Ecology*, **7(9)**, 1091-1096.

[99] Prioli, S.M.A.P., Prioli, A.J. and Julio, H.F.J. (2002) Identification of *Astyanax altiparanae* (Teleostei, Characidae) in the Iguacu River, Brazil, based on mitochondrial DNA and RAPD markers. *Genetics and Molecular Biology*, **25(4)**, 421-430.

[100] Doukakis, P., Birstein, V.J., Ruban, G.I. and Desalle, R. (1999) Molecular genetic analysis among subspecies of two Eurasian sturgeon species, *Acipenser baerii* and *A. stellatus*. *Molecular Ecology*, **8(12 Suppl 1)**, 117-127.

[101] Felsenstein, J. (1985) Confidence limits on phylogenies: An approach using the bootstrap. *Evolution*, **39**, 783-791.

[102] Ryman, N., (2002) Population genetic structure. *NOAA Technical Memoranda*, Northwest Fisheries Science Centre Publication Page, http://www.nwfsc.noaa.gov/ publications/techmemos/index.cfm

[103] Piry, S., Alapetite, A., Cornuet, J.M., Paetkau, D., Baudoiin, L. and Estoup, A. (2004) Geneclass2: A software for genetic assignment and first generation migrant detection. *Journal of Heredity*, **95(6)**, 536-539.

[104] Luikart, G. and Cornuet, J.M. (1998) Empirical evaluation of a test for identifying recently bottlenecked populations from allele frequency data. *Conservation Biology*, **12(1)**, 228-237.

[105] Luikart, G. and Cornuet, J.M. (1999) Estimating the effective number of breeders from heterozygote excess in progeny. *Genetics*, **151(3)**, 1211-1216.

[106] Weir, B.S. and Cockerham, C.C. (1984) Estimating F-statistics for the analysis of population structure. *Evolution*, **38(6)**, 1358-1370.

[107] Nei, M. (1983) Genetic Polymorphism and the role of mutation in evolution. In: Nei, M. and Kohen, R.K. Eds., *Evolution of Gene and Proteins*, Sinaver Associates, Sunderlans, 165-190.

[108] Raymond, M. and Rouseet, F. (1995) An exact test for population differentiation. *Evolution*, **49**, 1280-1283.

[109] Fonseca, D.M., Dennis, A., Pointe, L. and Fleischer, C. (2000) Bottlenecks and multiple introductions: Population genetics of the vector of avian malaria in Hawaii. *Molecular Ecology*, **9(11)**, 1803-1814.

[110] Zhang, Y.P., Wang, X.X., Ryder, O.A., Li, M.P., Zhang, Y. Yong, H.M. and Wang, P.Y. (2002) Genetic diversity and conservation of endangered animal species. *Pure Applied Chemestry*, **74(4)**, 575-584.

[111] Efremov, V.V., (2002) Allozyme Variation in Pink Salmon *Oncorhynchus gorbuscha* from Sakhalin Island. *Journal of Ichthyology*, **42**, 339-347.

[112] Salini, J.P., Milton, D.A., Rahaman, M.J. and Hussein, M.G. (2004) Allozyme and morphological variation throughout the geographic range of the tropical shad, hilsa *Tenualosa ilisha*. *Fisheries Research*, **66(1)**, 53-69.

[113] Lal, K.K., Kumar, D., Srivastava, S.K., Mukherjee, A., Mohindra, V., Prakash, S., Sinha, M. and Ponniah, A.G. (2004) Genetic variation in Hilsa shad (*Tenualosa ilisha*) population in River Ganges. *Indian Journal of Fisheries*, **51**, 33-42.

[114] Meggs, L.B., Austin, C.M. and Coutin, P.C. (2003) Low allozyme variation in snapper, *Pagrus auratus*, in Victoria, Australia. *Fisheries Management and Ecology*, **10(3)**, 155-162.

[115] Dong, Z., Zhu, J., Yuan, X. and Wang, J. (2002) RAPD analysis of the genome DNA of Jian carp. *Journal of Zhanjiang Ocean University*, **22**, 3-6.

[116] Chang, Y., Sun, Y. and Liang, A. (2003) Study on cold tolerant traits for common carp *Cyprinus carpio*. *Journal of Shanghi Fisheries University*, **12**, 102-105.

[117] Feng, J., Zhang, X., Zhou, X., Chen, J. and Wang, L. (2003) RAPD markers and genetic diversity of *Carassius auratus* in the Qihe River. *Transaction of Oceanology and Limnology*, **4**, 90-94.

[118] Zheng, L. and Liu, C. (2002) Studies on random amplified polymorphic DNA (RAPD) of *Epinephelus merra* Bloch. *Journal of Zhanjiang Ocean University*, **22**, 14-18.

[119] Exadactylos, A., Geffen, A.J., Panagiotaki, P. and Thorpe, J.P. (2003) Population structure of Dover sole *Solea solea*: RAPD and allozyme data indicate divergence in European stocks. *Marine Ecollogy Progress Series*, **246**, 253-264.

[120] Mamuris, Z., Stamatis, C. and Triantaphyllidis, C. (1999) Intraspecific genetic variation of striped red mullet (*Mullus surmuletus* L.) in the Mediterranean Sea assessed by allozyme and random amplified polymorphic DNA (RAPD) analysis. *Heredity*, **83(pt1)**, 30-38.

[121] Almeida, F.S., Fungaro, M.H.P. and Sodré, L.M.K. RAPD and isoenzyme analysis of genetic variability in

three allied species of catfishes (Siluriformes: Pimelodidae) from the Tibagi river, Brazil. *Journal of Zoology*, **253**, 113-120.

[122] Nelson, R.J., Wood, C.C., Cooper, G., Smith, C. and Koop, B. (2003) Population structure of sockeye salmon of the central coast of British Columbia: Implications for recovery planning. *North American Journal of Fisheries Management*, **23**, 703-720.

[123] Beacham, T.D., Supernault, K.J., Wetklo, M., Deagle, B., Labaree, K., Irvine, J.R., Candy, J.R., Miller, K.M., Nelson, R.J. and Withler, R.E. (2003) The geographic basis for population structure in Fraser River chinook salmon (*Oncorhynchus tshawytscha*). *Fisheries Bulletin*, **101**, 229-242.

[124] Brunner, P.C., Douglas, M.R. and Bernatchez, L. (1998) Microsatellite and mitochondrial DNA assessment of population structure and stocking effects in Arctic charr *Salvelinus alpinus* (Teleostei: Salmonidae) from central Alpine lakes. *Molecular Ecology*, **7**, 209-223.

[125] Adams, B.K. and Hutchings, J.A. (2003) Microgeographic population structure of brook charr: A comparison of microsatellite and mark-recapture. *Journal of Fish Biology*, **62(3)**, 517-533.

[126] Senanan, W. and Kapuscinski, A.R. (2000) Genetic relationships among populations of northern pike (*Esox lucius*). *Canadian Journal Fisheries Aquatic Science*, **57**, 391-404.

[127] Salgueiro, P., Carvalho, G., Collares-Pereira, M.J. and Coelho, M.M. (2003) Microsatellite analysis of genetic population structure of the endangered cyprinid *Anaecypris hispanica* in Portugal: implications for conservation. *Biological Conservation*, **109(1)**, 47-56.

[128] Palm, S., Dannewitz, J., Jaervi, T., Petersson, E., Prestegaard, T. and Ryman, N. (2003) Lack of molecular genetic divergence between sea-ranched and wild sea trout (*Salmo trutta*). *Molecular Ecology*, **12(8)**, 2057-2071.

[129] Elliott, N.G. and Reilly, A. (2003) Likelihood of bottleneck event in the history of the Australian population of Atlantic salmon (*Salmo salar* L.). *Aquaculture*, **215(1-4)**, 31-44.

[130] Alarcon, J.A., Magoulas, A., Georgakopoulos, T., Zouros, E. and Alvarez, M.C. (2004) Genetic comparison of wild and cultivated European populations of the Gilthead Sea bream (*Sparus aurata*). *Aquaculture*, **230(1-4)**, 65-80.

[131] Kanda, N. (1998) Genetics and conservation of Bull trout: Comparison of population genetic structure among different genetic markers and hybridization with brook trout. *Dissertation Abstracts International Part B: Science and Engineering*, University of Montana, Missoula.

[132] Kanda, N. and Allendorf, F.W. (2001) Genetic population structure of Bull trout from the Flathead River basin as shown by microsatellite and mitochondrial DNA marker. *Transaction of American Fisheries Society*, **130**, 92-106.

[133] Cagigas, M.E., Vazquez, E., Blanco, G. and Sanchez, J.A. (1999) Genetic effects of introduced hatchery stocks on indigenous brown trout (*Salmo trutta* L.) populations in Spain. *Ecological of Freshwater Fish*, **8(3)**, 141-150.

[134] Chenoweth, S.F., Hughes, J.M., Keenan, C.P. and Shane, L. (1998) Concordance between dispersal and mitochondrial gene flow: Isolation by distance in a tropical teleost, *Lates calcarifer* (Australian barramundi). *Heredity*, **80**, 1897-1907.

[135] Gysels, E.S., Hellemans, B., Pampoulie, C. and Volckaert, F.A. (2004) Phylogeography of the common goby, *Pomatoschistus microps*, with particular emphasis on the colonization of the Mediterranean and the North Sea. *Molecular Ecololgy*, **13(2)**, 403-417.

[136] Marzano, F.N., Corradi, N., Papa, R., Tagliavini, J. and Gandolfi, G. (2003) Molecular evidence for introgression and loss of genetic variability in *Salmo* (*trutta*) *macrostigma* as a result of massive restocking of Apennine populations (Northern and Central Italy). *Environmental Biology of Fishes*, **68(4)**, 349-356.

[137] Jerry, D.R. (1997) Population genetic structure of the catadromous Australian bass from through out its range. *Journal of Fish Biology*, **51(5)**, 909-920.

[138] Perkins, D.L. and Krueger, C.C. (1993) Heritage brook trout in northeastern USA: Genetic variability within and among populations. *Transaction of American Fisheries Society*, **122**, 1515-1532.

[139] Norris, A.T., Bradley, D.G. and Cunningham, E.P. (1999) Microsatellite genetic variation between and within farmed and wild Atlantic salmon (*Salmo salar*) populations. *Aquaculture*, **180(3-4)**, 247-264.

[140] Palma, J., Alarcon, J.A., Alvarez, C., Zouros, E., Magoulas, A. and Andrade, J.P. (2001) Developmental stability and genetic heterozygosity in wild and cultured stocks of gilthead sea bream. *Journal of Marine Biological Association of United Kingdom*, **81(2)**, 283-288.

[141] Wright, S. (1931) Evolution in Mendelian populations. *Genetics*, **16(2)**, 97-159.

[142] Nei, M., Maruyama, T. and Chakraborty, R. (1975) The bottleneck effect and genetic variability in populations. *Evolution*, **29(1)**, 1-10.

[143] Tessier, N. and Bernatchez, L. (1999) Stability of population structure and genetic diversity across generations assessed by microsatellites among sympatric populations of landlocked Atlantic salmon (*Salmo salar* L.). *Molecular Ecology*, **8**, 169-179.

[144] Nielsen, E.E., Hansen, M.M. and Loeschcke, V. (1999) Genetic variation in time and space: Microsatellite analysis of extinct and extant populations of Atlantic salmon. *Evolution*, **53**, 261-268.

[145] Lundy, J.C., Rico, C. and Hewitt, M.G. (2000) Temporal and spatial genetic variation in spawning grounds of European hake (*Merluccius merluccius*) in the Bay of Biscay. *Molecular Ecology*, **9(12)**, 2067-2079.

[146] Heath, D.D., Bryden, C.A., Shrimpton, J.M., Iwama, G.K., Kelly, J. and Heath, J.W. (2002) Relationships between heterozygosity, allelic distance (d^2), and reproductive traits in Chinook salmon, *Oncorhynchus tshawytscha*. *Canadian Journal of Fisheries and Aquatic Science*, **59**, 77-84.

[147] Larson, S., Jameson, R., Etnier, M., Flemings, M. and Bentzen, P. (2002) Loss of genetic diversity in sea otters (*Enhydra lutris*) associated with the fur trade of the 18th and 19th centuries. *Molecular Ecology*, **11(10)**, 1899-1903.

[148] Beaudou, D., Baril, D., Roche, Â.B. and Le. Baron, M. (1995) Recolonization in a devastated Corsican river: Respective contribution of wild and domestic brown trout. *Bulletin Francais de la Peche et de la Pisciculture*, **337**, 259-266.

Advances in Bioscience and Biotechnology, 2010, 1, 292-299 **ABB**
doi:10.4236/abb.2010.14038 Published Online October 2010 (http://www.SciRP.org/journal/abb/).

In vitro activity of neem oil [*Azadirachta indica* A. Juss (*Meliaceae*)] on *Aspergillus flavus* growth, sporulation, viability of spores, morphology and Aflatoxins B_1 and B_2 production

Christiane L. da Costa[1], Marcia R. F. Geraldo[2], Carla C. Arrotéia[1], Carlos Kemmelmeier[1]

[1]Department of Biochemistry, Universidade Estadual de Maringá. Avenida Colombo, Maringá. PR Brazil;
[2]Universidade Tecnológica Federal do Paraná, Campo Mourão, Brazil.
Email: christiane@ffalm.br; mperdoncini@ibest.com.br; ccarroteia@uem.br; ckemmelmeier@uem.br

Received 29 June2010; revised 15 July2010; accepted 25 July 2010.

ABSTRACT

The effectiveness of neem (*Azadiracta indica*) oil on the growth, morphology, sporulation, viability of spores, aflatoxin B_1 and B_2 production by *A. flavus* on Yeast Extract-Sucrose medium was determined. Neem oil inhibited the fungal growth (*i.e.* mycelia dry weight, diameter of colony and growth rate) on solid media at concentrations from 0.5 to 5.0% v/v, although it significantly increased sporulation in the same conditions. Spores obtained from cultures grown without neem oil reduced germination when incubated in a neem-oil supplemented medium. Colonies grown on solid media and in submerged cultures in the presence of neem oil exhibited morphological alterations, including granular cytoplasm, atypical hyphae branching pattern, abnormal and undifferentiated conidiophores. High Performance Liquid Chromatography was used to measure aflatoxins. In submerged cultures, neem oil at concentrations from 0.5 to 4.0% v/v caused approximately 95% inhibition in Aflatoxin B_1 and B_2. On other hand, these conditions failed to suppress fungal growth. Current research emphasized that neem oil was not fungistatic or fungicidal, but exhibited anti-aflatoxigenic activity.

Keywords: *Azadirachta indica*; *Aspergillus flavus*; Neem oil; Aflatoxins

1. INTRODUCTION

Aflatoxins are polyketide secondary metabolites produced by toxigenic strains of *Aspergillus* section Flavi group: *Aspergillus flavus*, *A. parasiticus*, *A. nomius*, *A. tamarii* and *A. bombysis*. *A. flavus* is the main source of aflatoxins, the most important mycotoxins in the world's food supplies, due to its mutagenic, carcinogenic and teratogenic properties. Aflatoxin B_1 (AFB_1) and B_2 (AFB_2) are the most important among 18 different types. World-wide occurrence of *Aspergillus flavus* and aflatoxins in a great variety of food crops has triggered much research with regard to its causes, progress and prevention [1,2].

There has recently been an extensive search for alternatives to fungicides that would provide satisfactory aflatoxin control with low impact on the environment and on human health [3]. Previous studies have shown that biosynthesis of aflatoxins may be inhibited by neem extracts. *Azadirachta indica* (*Meliaceae*), commonly know as neem, is an evergreen tree, cultivated in arid regions of Africa and the Asian subcontinent. Every part of the neem tree has been used in traditional folk medicine in India as a household remedy against various human ailments and also as a pesticide. Several active substances from different parts of the tree have an unusual effectiveness on a wide spectrum of pests, including fungi. Due to its efficacy, biodegradability and minimum side effects, azadirachtin, a tetranortriterpenoid obtained from neem seeds, has emerged as a natural biopesticide [4,5].

Previous studies have shown that biosynthesis of aflatoxins may be inhibited by neem extracts. Bhatnagar and co-workers have demonstrated that blended neem leaf extracts inhibited aflatoxin production by *A. parasiticus* and *A. flavus*, but they failed to affect fungal growth [6,7]. Further, neem leaves contain specific volatile compounds with fungicidal properties. This complex mixture of volatiles affected both fungal growth and aflatoxin production in *A. parasiticus* [8]. Other studies on *A. parasiticus* have shown that aflatoxin inhibition by

neem leaf extract is associated with changes in the activities of cytosolic enzymes [9] and also with morphological alterations in the mycelia [10].

Data on fungal growth and mycotoxin production in the presence of neem extracts, besides those on aflatoxins, are scanty, but *in vitro* studies with neem extracts showed inhibition of the polyketide mycotoxins, namely, patulin [11,12], citrinin [13], sterigmatocystin [14], but no inhibitory effect on penicillic acid [14], fumonisin [15] and ochratoxin A production [16].

The main chemical fractions of neem oil with antifungal activities are a mixture of triterpenoidal and tetranortriterpenoid compounds. Azadirachtin, 6-deacetylnimbin, azadiradione, nimbin, salannim and epoxyazadiradione were the major compounds obtained from chemical fractions of neem oil. Although when tested alone they did not have any appreciable activity, they showed antifungal activity when mixed and indicated possible additive/synergistic effects [17].

There is scanty information available in the literature on the effect of neem oil on growth, sporulation level and aflatoxins production by *A. flavus* in submerged cultures. Thus, current study determines the effectiveness of neem oil on the growth, morphology, sporulation, viability of spores and AFB_1 and AFB_2 production by *A. flavus* on a semi-synthetic medium.

2. MATERIALS AND METHODS

2.1. Microorganism

The aflatoxigenic strain *Aspergillus flavus* 42 was isolated from peanut seeds and identified by physiological and morphological tests [1] at the Laboratory of Chemistry and Physiology of Microorganisms (Biochemistry Department, State University of Maringá, Maringá. PR Brazil). The isolate was stored in silica [18] and cultured on Potato Dextrose Agar (PDA) for seven days, at 25°C, in the dark [19], for the production of conidia. The conidia suspension used as inoculum was prepared by washing the cultures in sterile Tween 80 (0.01%) solution and placed in a Neubauer chamber for conidia counting.

2.2. Neem Seed Oil (NO)

Oil from neem seeds (NO) used in organic agriculture (Bioneem® Co., Brazil) was obtained by cold pressing, which is the best method to obtain quality neem oil.

2.3. Culture Conditions for Aflatoxin Production in Submerged Cultures

The semi-synthetic YES (Yeast Extract Sucrose) medium, conventionally employed for testing aflatoxin production [20], was used as culture medium. Flasks containing 50 mL of autoclaved YES liquid medium, in the absence (control) and presence of NO (treatments) were inoculated with 1.0 mL of conidia suspension (10^6 conidia mL^{-1}) and incubated in a static condition for 7 days, in the dark, at 25˚C. Emulsified NO was evaluated at 0.25, 0.5, 1.0 and 4.0% (v/v). Neem oil is frequently used at 0.5% in aqueous solutions to control pests on crops. Flasks in each treatment were prepared in five replicates. Two replicates were used in the analysis of aflatoxins and the remaining three processed for morphological studies, as described in the "Morphological studies" section.

2.4. Extraction and Quantification of Aflatoxins

After cultures have been filtered at the end of the growth period, an aliquot from the culture (20 mL) was extracted twice, with chloroform (30 mL), at each period. The combined chloroform extract was filtered by anhydrous sodium sulfate to remove residual water, evaporated till dryness and then re-suspended in 1 mL chloroform [21]. Fresh mycelia obtained from each flask were washed in water, dried at 85˚C for 24 hrs and weighed. Dry weight of the fungus was determined as an index of fungal growth [6]. Aflatoxins were quantitatively determined by HPLC, following the methodology proposed by Passone *et al*. [22]. The limit of detection of the analytical method was 1ng/g. and the recovery coefficient was 85.5%. Aflatoxins are expressed in terms of ppm (μg aflatoxin/g mycelial growth weight). Analyses were performed by LAMIC (Laboratório de Análises Micotoxicológicas, Santa Maria, RS Brazil) and results extracted from the 01/2008 analysis.

2.5. Mycelial Growth and Sporulation Measurement

The effect of NO on the growth and sporulation of *A. flavus* in solid media was determined by growing the fungus on a YES agar in the absence (control) and presence (treatments) of different concentrations of NO: 0.25, 0.5, 1.0, 2.0, 3.0, 4.0 and 5.0 % (v/v). The solid media were prepared by adding 2% of agar in liquid media, autoclaved, transferred to 95mm-Petri dishes, solidified and inoculated with a single culture at the center of the plate. To this purpose, fungi had been previously cultured in PDA in Petri dishes, according to the streaking technique [1] for producing isolated colonies. *A. flavus* was subsequently incubated at 25˚C for 7 days, in the dark. All plates of each treatment were prepared in six replicates. Whereas three plates were used to determine the growth, the other plates were used for sporulation measurement. Growth was recorded in terms of diameter of colony and dry weight. The advantage of the first method was that sequential records might be obtained from each colony, although only lateral but not aerial

growth was measured [23]. The diameter of fungal colonies was measured daily in two directions at 90° from each other to obtain the mean diameter for each colony [24]. Each plate's diameter increase was plotted as a function of incubation time whereas radial growth rate was obtained from the slope by regression of the linear growth phase [25]. So that the mycelium dry weight after the growth period could be evaluated, each Petri plate was placed in a microwave oven during 20s to melt the medium. The mycelium was then separated from the medium by filtration and washed in distilled water, at an approximate temperature of 60˚C. This preparation was placed in an oven at 85˚C until weight constant [26].

Procedures for sporulation measurement followed Gusmán-de-Peña and Ruiz-Herrera [27] with modifications. A solid medium has been used in this study since the fungus sporulation is inconsistent in liquid media [28]. Three agar discs (8 mm diameter) were aseptically removed from central, intermediate and peripheral zones of each replicate plate using a cork borer, transferred to flasks containing a sterile 0.1% Tween 80 solution (10 mL) and stirred for two minutes with a vortex to release the spores. After mycelium sedimentation, the supernatant containing the spores was recovered and estimated by a Neubauer counting chamber. The sporulation data were recorded in spores/cm^2 of colony.

2.6. Germination

Two experiments were performed to evaluate the effects of NO on viability of spores:

Experiment 1: *Viability of spores grown in the presence NO in a NO-less medium.*

Suspensions prepared as in the previous section were diluted to obtain approximately 600 spores/mL. 1 mL of each suspension was inoculated on sterile strips of dialysis membrane (1 cm × 1 cm) placed on the surface of Petri plates containing YES agar without NO and incubated at 25˚C for 10 hrs. The membranes were placed on a slide, stained with lacto-phenol cotton blue and examined under the microscope. A germinated spore was considered as such when its germ tube was longer than half the diameter of the spore. Further, 300 spores were randomly counted on each slide, giving a total of 900 spores per treatment. Germination was reported as a percentage of spore population and compared with the corresponding control. Three slides were sampled per treatment. The analysis of germ-tube morphology in each slide was performed for observation by biological optic photomicroscope [29].

Experiment 2: *Viability of spores grown in the absence of NO in a NO-supplemented medium.* Spore suspension obtained from cultures grown on the agar YES without NO were prepared and inoculated in Petri plates containing YES agar with different concentrations of NO (0.25; 0.5; 1.0; 2.0; 3.0; 4.0 and 5.0 v/v), incubated and analyzed, following the methodology previously described.

2.7. Morphological Studies

The same plates used in the sporulation test were employed in the morphological studies. Samples of mycelial growth were taken at the central, intermediate, peripheral zones of the colonies. They were then stained with lactophenol cotton blue or lactofuchsin, and examined under the Zeiss Axiophot light microscope. Slides from germination test were analyzed to evaluate the polarity of germ tubes, although no quantitative tests were performed to assess this parameter.

3. RESULTS

3.1. Effect of NO on *A. flavus* Growth, Sporulation and Viability of Spores in Solid Media

Data in **Table 1** showed that diameter, dry weight, growth rate, were suppressed by NO and that this reduction effect was more efficient in concentrations above 0.5%. However, it significantly increased the sporulation in the same concentrations.

Results of experiments to find the effect of NO on viability of spores showed a 1.0% decrease in the germination percentage of spores produced by colonies in the presence of NO. Furthermore, germination was significantly reduced when spores from control cultures were incubated in a NO-supplemented medium at concentrations above 0.5% (**Table 1**).

3.2. Effect of NO on morphology of *A. flavus*

Besides inhibited growth, colonies grown on solid media in the presence of NO at all concentrations exhibited morphological alterations when compared to control (**Figure 1(a)** and **1(c)**). Analysis showed that treated hyphae (**Figure 1(b)**) present granular cytoplasm containing large number of vesicular structures. This feature was detected in all segments from the center to the peripheral zones. Furthermore, the hyphae presented variation in the typical branching pattern (**Figure 1(d)**), with more than two tips per branching point. Hyphae diameter increased too, although specific measures were not undertaken. Treated hyphae obtained from submerged cultures also showed granular cytoplasm and the same branching pattern. Morphological alterations have not varied in the presence of different concentrations employed in this study. Although spores normally produced a single germ-tube (**Figure 1(e)**), some spores revealed bipolar germination in NO-supplemented media (**Figure 1(f)**). In spite of the fact that control hyphae showed typical

Table 1. Effect of NO on *A. flavus* growth, sporulation and viability of spores in solid media.

NO (% v/v)	Mycelial dry weight (g)	Diameter (cm)	Growth rate (cm/h)	Sporulation (10^6 spores/cm^2)	Germination Experiment 1 (%)*	Germination *Experiment* 2 (%)**
0 **(Control)**	0.44^{a} (0.02)	7.90^{a} (0,1)	0.044^{a} (3.0×10^{-4})	1.41^{c} (0.15)	95.76 ^{ab} (1.01)	95.76^{a} (1.01)
0.25	0.32^{b} (0.04)	7.20^{b} (0,1)	0.043^{b} (8.6×10^{-5})	4.24^{c} (0.26)	98.31^{a} (1.11)	89.08^{a} (0.80)
0.5	0.42^{a} (0.02)	7.93^{a} (0,057)	0.045^{a} (1.5×10^{-4})	24.32^{b} (2.02)	96.25^{ab} (0.52)	85.42^{b} (3.85)
1.0	0.17^{c} (0.02)	3.30^{c} (0,1)	0.018^{c} (3.4×10^{-4})	42.46^{a} (3.98)	91.04^{c} (2.91)	87.21^{b} (2.15)
2.0	0.16^{c} (0.03)	3.00^{d} (0,1)	0.017^{d} (5.6×10^{-4})	41.57^{a} (4.26)	94.04^{bc} (1.51)	85.55^{b} (3.37)
3.0	0.14^{c} (0.01)	2.73^{e} (0,05)	0.016^{e} (2.5×10^{-4})	49.53^{a} (3.86)	95.94^{ab} (0.78)	86.49^{b} (2.52)
4.0	0.14^{c} (0.02)	2.83^{de} (0,05)	0.015^{f} (3.2×10^{-4})	46.44^{a} (3.71)	95.94^{ab} (0.40)	81.82^{b} (2.99)
5.0	0.17^{c} (0.01)	2.80^{de} (0,00)	0.018^{c} (2.5×10^{-4})	49.89^{a} (5.36)	93.52^{bc} (1.38)	84.27^{b} (3.31)

Note. Values (mean from three replicates) in the same column followed by a similar letter are not significantly different, according to Tukey HSD test ($p < 0.05$). Values between parentheses are standard deviation of replicates. *Viability of spores grown in the presence of Neem oil in a medium without this compound. **Viability of spores grown in the absence of Neem oil in a medium supplemented with this compound.

conidiophores (**Figure 1(g)**), dichotomous branching and homogenous cytoplasm, vesicles were detected in the apical regions. The above morphological characteristics were consistent with those described in literature [1,30]. Abnormal conidiophores were recorded in colonies on solid media in the presence of NO at concentrations above 1.0%. Secondary conidiophores (**Figure 1(h)**) formed from globose vesicles and undifferentiated conidiophores were detected (**Figure 1(i)** and **1(j)**).

3.3. Effect of NO on Aflatoxins Production by *A. flavus* in Submerged Cultures

As shown in **Table 2**, the production of AFB_1 and AFB_2 was inhibited by NO, which, at concentrations above 0.5%, caused approximately 95% inhibition in AFB_1 and AFB_2 production. Presence of NO 4.0% in the fungal growth medium was sufficient to obtain total inhibition of AFB_2 production. Results (**Table 2**) demonstrate that NO does not depress fungal growth in submerged culture.

4. DISCUSSION

Several authors have described the inhibitory effect of neem extracts on aflatoxin production. Bankole [31] showed that the NO at 1000 ppm was able to block the AFB_1 synthesis by *Aspergillus flavus* inoculated in maize grain. Similar results were found by Zeringue and Bhatnagar [7], where the application of aqueous extract from neem leaves in cotton balls infected with *Aspergillus flavus*, was able to inhibit up to 98% the AFB_1 production, without reducing the mycelial growth. The addition of the aqueous neem leaf extract in submerged cultures of *Aspergillus parasiticus* over 5.0% concentrations caused inhibition of over 90% in AFB_1 production, but did not affect mycelial growth [6,32]. The above authors have suggested that the inhibitory components in these extracts are non-volatile and influence the regulation of secondary metabolic pathway involved in aflatoxin biosynthesis. The results of present study corroborates this previous finding, show inhibition of approximately 95% in the AFB_1 and AFB_2 production when 0.5, 1.0 and 4.0% of NO were added in submerged cultures of *Aspergillus flavus*. However, there was an increase in mycelial growth. The difference in the efficacy of anti-aflatoxigenic activity of neem extracts may be attributed to their composition and to different fungus metabolism. Although different commercial formulations of NO are available, the recommended aspersion of aqueous solution 5.0 % in crops seems to be promising as a protector during storage [3]. It is not yet known which substance has anti-aflatoxigenic activity. Azadirachtin, a tetranortriterpenoid, is the most important active component in the neem tree and its highest concentration is found in seeds. When the neem tree was screened for antioxidant property, it was found that azadirachtin has a strong antioxidant activity [33]. A common feature of

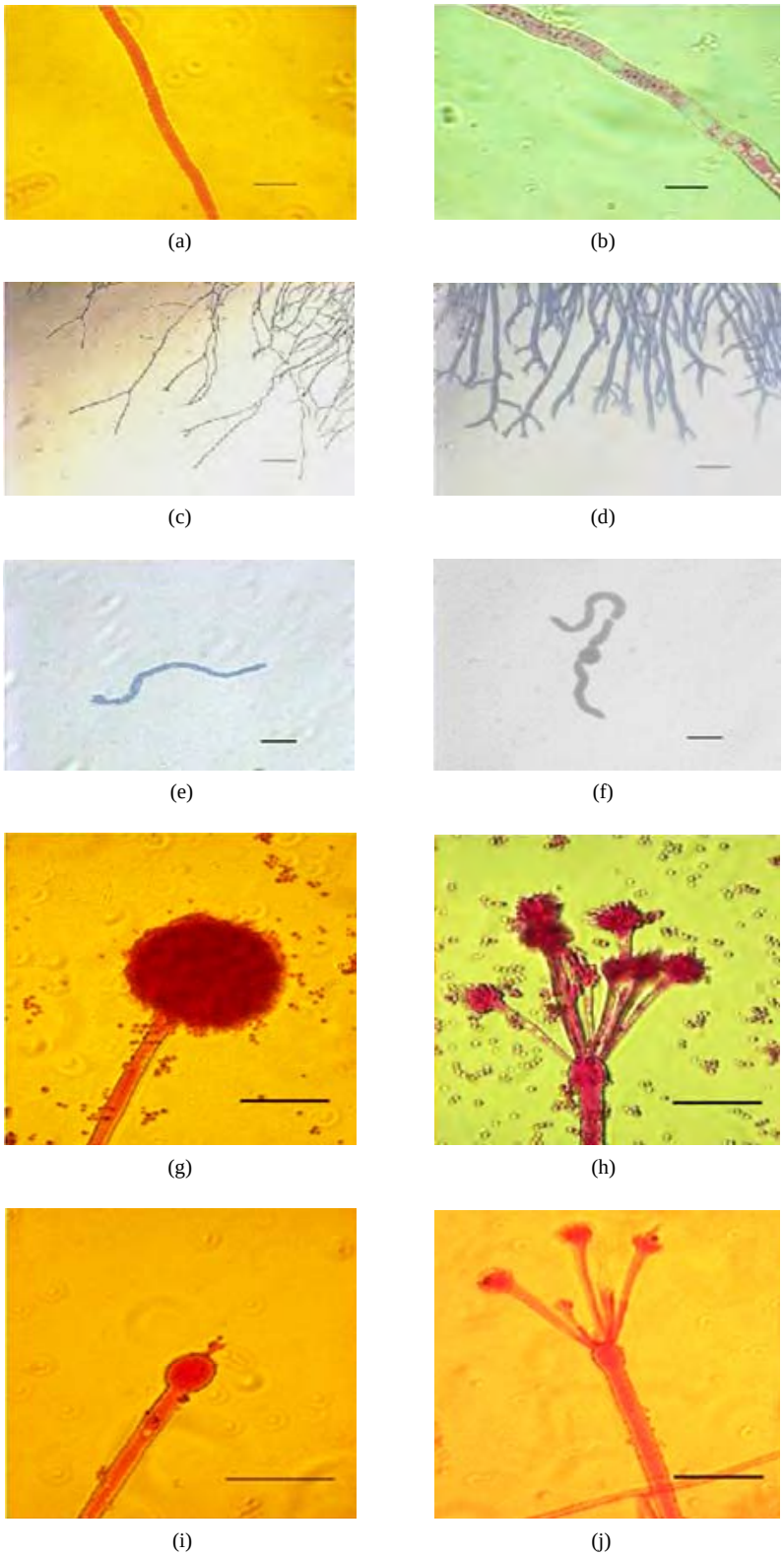

Figure 1. Effects of NO on the morphology of *A. flavus* in solid media: (a) Control hyphae; (b) and in the presence of 5% NO. Scale bars represent 10 µm. (c) Control mycelia, (d) and in the presence of 5% NO. (e) Spore obtained from control culture grown in the absence of NO, (f) and in the presence of 5% NO after 10 hrs of incubation at 25°C. (g) Control and treated conidiophores (h, i, j) grown in the presence of 5, 3 and 2% NO, respectively. Scale bars represent 40 µm.

Table 2. Effects of NO on growth and aflatoxins production by *A. flavus* in submerged culture.

NO (% v/v)	Mycelial dry weight (g/50 mL)	AFB_1 (µg/g dry weight)	% of AFB_1 inhibition	AFB_2 (µg/g dry weight)	% of AFB_2 inhibition
0 **(Control)**	0.80^b (0.04)	12195.43^a (1299.43)	0	891.60^a (156.77)	0
0.25	0.83^b (0.02)	4888.13^b (527.80)	59.92	104.20^b (29.00)	88.34
0.5	0.94^b (0.05)	581.96^c (129.84)	95.23	31.50^b (21.30)	94.17
1.0	0.94^b (0.04)	622.90^c (137.69)	94.90	48.90^b (10.17)	94.96
4.0	1.13^a (0.14)	523.36^c (35.67)	95.71	ND*	–

Note. Values (mean from three replicates) in the same column followed by a similar letter are not significantly different, according to Tukey HSD test ($p < 0.05$). Values between parentheses are standard deviation of replicates. * Not detected.

many aflatoxin inhibitors is their antioxidant activity [3], although the modes of action of most inhibitors, including neem, are still poorly understood. In spite of the fact that we have not investigated the complex area on the mode of neem's function on the *Aspergillus flavus* metabolism, earlier reports from our laboratory have demonstrate an inhibitory effect on *in vitro* polyketide mycotoxins production, such as sterigmatocystin (second-to-last intermediate item in aflatoxin pathway), patulin and citrinin by *Aspergillus nidulans*, *Penicillium expansum* and *P. citrinum* [11-14], respectively. Thus, neem activity may be extant in the biosynthetic polyketide pathway, including oxidation reactions. In solid media, NO in concentrations above 0.5% had inhibitory effect on diameter, dry weight and growth rate, but the spore count (*i.e.* sporulation) in all the treated groups remained high. Gowda and co-workers [34] showed a similar result when they isolated *A. parasiticus* in solid media. The presence of oil in the solid media caused inhibition in spore germination. Similarly, Suberu [35] reported inhibition of spore germination in *A. flavus* by lichen extracts. On other hand, the viability of spores obtained from cultures in the presence of NO in a NO-less medium is not affected (**Table 2**), except at concentration 1.0%.

According to Razzaghi-Abyaneh *et al.* [10], the suppressive effects of neem leaf and seed extract on aflatoxin biosynthesis are associated with morphological alterations in the mycelium, such as vacuolation of cytoplasm and attenuation of cell wall. This fact suggests that probably the integrity of the cell barriers, particularly that of the cell wall, is crucial in the regulation of aflatoxin production and excretion. Our investigations show that treated hyphae, obtained from solid media and submerged cultures, present granular cytoplasm with many vesicular structures and variation in the typical branching pattern. The atypical branching pattern and the spores that showed bipolar germination suggest that NO probably affected hyphal polarity maintenance (the continued deposition of wall material at the extending tip). Abnormal and undifferentiated conidiophores were recorded in colonies on solid media in the presence of NO at concentrations above 1.0%. The ketone β-ionone is an antiaflatoxigenic agent and presented similar effects on the morphology of the asexual reproductive structures of *A. flavus*. Aflatoxin synthesis may be positively correlated with the asexual reproductive process [36]. In addition, other authors demonstrated that the loss of aflatoxigenic capacity in the *Aspergillus* mutant form is correlated with the aberrant morphology of conidiophores [37]. The present study emphasized that NO was not fungistatic or fungicidal, but exhibited anti-aflatoxigenic activity.

Neem aqueous and oily extracts, in a similar range of concentrations such as those used in the present study, showed inhibitory effects when tested against some polyketide mycotoxins [11-14], albeit ineffective to penicillic acid [14], and ochratoxin A [16]. Thus, the above data and those obtained in current research reinforce the fact that the use of NO could be implemented as part of a sustainable integrated pest management strategy for mycotoxin control and plant diseases.

5. ACKNOWLEDGEMENTS

We would like to thank Dr. Thomas Bonnici for the grammatical review of the manuscript and to the National Council of Scientific and Technological Development–CNPq for its support in this research.

REFERENCES

[1] Pitt, J.I. and Hocking, A.D. (1977) Fungi and Food Spoilage. 2nd Edition, Blackie Academic & Professional,

London, United Kingdom.
[2] Hedayati, M.T, Pasqualotto, A.C, Warn, P.A, Bowyer, P. and Denning, D.W. (2007) *Aspergillus flavus*: human pathogen, allergen and mycotoxin producer. *Microbiology*, **153**, 1677-1692.
[3] Holmes, R.A., Boston, R.S. and Payne, G.A. (2008) Diverse inhibitors of aflatoxin biosynthesis. *Applied Microbiology and Biotechnology*, **78(4)**, 559-572.
[4] Martinez, S.S. (2002) O Nim-Azadirachta indica. Natureza, Usos Múltiplos, Produção. Martinez, S.S. Ed., IAPAR, Londrina, PR, Brazil.
[5] Locke, J.C. (1995) Fungi. In Schmutterer, H. Ed., *The Neem Tree*. VHC. Weinheim, Germany, 118-126.
[6] Bhatnagar, D. and McCormick, S.P. (1988) The inhibitory effect of neem (*Azadirachta indica*) leaf Extracts on aflatoxin synthesis in *Aspergillus parasiticus*. *Journal of American Oil Chemical Society*, **65**(7), 1166-1168.
[7] Zeringue, H.J. and Bhatnagar, D. (1994) Effects of neem leaf volatiles on submerged cultures of aflatoxigenic *Aspergillus parasiticus*. *Applied and Environmental Microbiology*, **60(10)**, 3543-3547.
[8] Zeringue, H.J. and Bhatnagar, D. (1990) Inhibition of aflatoxin production in *Aspergillus flavus* infected cotton bolls after treatment with neem (*Azadirachta indica*) leaf extracts. *Journal of American Oil Chemical Society*, **67(4)**, 215-216.
[9] Allameh, A., Razzaghi-Abyaneh, M., Shams-Gahahfarokhi, M., Rezzar, M.B. and Jaimand, K. (2001) Effects of neem leaf extract on production of aflatoxins and activities of fatty acid synthetase, isocitrate dehydrogenase and glutathione S-transferase in *Aspergillus parasiticus*. *Mycopathologia*, **154(2)**, 79-84.
[10] Razzaghi-Abyaneh, M., Allameh, A., Tiraihi, T., Shams-Ghahfarokhi, M. and Ghorbanian, M. (2005) Morphological alterations in toxigenic *Aspergillus parasiticus* exposed to neem (*Azadirachta indica*) leaf and seed aqueous extracts. *Mycopathologia*, **159(4)**, 565-570.
[11] Mossini, S.A.G., de Oliveira, K.P. and Kemmelmeier, C. (2004) Inhibition of patulin production by *Penicillium expansum* cultured with neem (*Azadirachta indica*) leaf extracts. *Journal of Basic Microbiology*, **44(2)**, 106-113.
[12] Arrotéia, C.C., Kemmelmeier, C. and Machisnki, Jr., M. (2007) Effect of aqueous and oily extracts of Neem [*Azadirachta indica* A. Juss (Meliaceae)] on patulin production in apples contaminated with *Penicillium expansum*. *Ciência Rural*, **37**, 1518-1523.
[13] Mossini, S.A.G. and Kemmelmeier, C. (2008) Inhibition of citrinin production in *Penicillium citrinum* cultures by neem [*Azadirachta indica* A. Juss (Meliaceae)]. *International Journal of Molecular Science*, **9(9)**, 1676-1684.
[14] Costa, C.L. and Kemmelmeier, C. (2008) Effect of aqueous and oily extracts from Neem [*Azadirachta indica* A. Juss (Meliaceae)] on the production of mycotoxins by the polyketide pathway (penicillic acid and sterigmatocystin). *Current topics in Biotechnology*, **4**, 35-40.
[15] Fandohan, P., Gbenou, J.D., Gnonlonfin, B., Hell, K., Marasas, W.F.O. and Wingfield, M.J. (2004) Effect of essential oils on the growth of *Fusarium verticillioides* and fumonisin contamination in corn. *Journal of Agricultural and Food Chemistry*, **52(22)**, 6824-6829.
[16] Mossini, S.A.G., Arrotéia, C.C. and Kemmelmeier, C. (2009) Effect of Neem Leaf extract and Neem oil on *Penicillium* growth, sporulation, morphology and ochratoxin a production. *Toxins*, **1**, 2-13.
[17] Govindachari, T.R., Suresh, G., Gopalakrishnan, G., Banumathy, B. and Masilamani, S. (1998) Identification of antifungal compounds from the seed oil of *Azadirachta indica*. *Phytoparasitica*, **26(2)**, 109-116.
[18] Smith, D. and Onions, A.H.S. (1983) The preservation and maintenance of living fungi. Commonwealth Mycological Institute, Page Bros Ltd., Great Britain.
[19] Betina, V. (1984) Prodution, Isolation, Separation and Purification. In: Betina, V. Ed., *Mycotoxins*. Elsevier Science Publishers BV, Amsterdam, Netherlands, 183-215.
[20] Davis, N.D., Diener, U.L. and Eldridge, D.W. (1966) Production of aflatoxin B1 and G1 by a *Aspergillus flavus* in a semi-synthetic medium. *Applied Microbiology*, **14(3)**, 378-380.
[21] Farag, R.S., Daw, S.Y. and Abo-Raya, S.H. (1989) Influence of some spice essential oils on *Aspergillus parasiticus* growth and production of aflatoxins in a synthetic medium. *Journal of Food Science*, **54**, 74-76.
[22] Passone, M.A., Resnik, S.L. and Etcheverry, M.G. (2005) *In vitro* effect of phenolic antioxidants on germination, growth and aflatoxin B1 accumulation by peanut *Aspergillus* section Flavi. *Journal of Applied Microbiology*, **99(3)**, 682-691.
[23] Sutton L.M. and Starzyk, M.J. (1972) Procedure and analysis of a useful method in determining mycelial dry weights from agar plates. *Applied Microbiology*, **24(6)**, 1011-1012.
[24] Bluma, R.V, Etcheverry, M.G. (2008) Application of essential oils in maize grain: Impact on *Aspergillus* section Flavi growth parameters and aflatoxin accumulation. *Food Microbiology*, **25(2)**, 324-334.
[25] López-Malo, A., Alzamora, S.M. and Argaiz, A. (1995) Effect of natural vanilin on germination time and radial growth of moulds in fruit-based agar systems. *Food Microbiology*, **12**, 213-219.
[26] Vargas-Isla, R. and Ishikawa, N.K. (2008) Optimal conditions of in vitro mycelial growth of *Lentinus strigosus*, an edible mushroom isolated in the Brazilian Amazon. *Mycoscience*, **49(3)**, 215-219.
[27] Gusmán-De-Peña, D. and Ruiz-Herrera, J. (1997) Relationship between Aflatoxin Biosynthesis and Sporulation in *Aspergillus parasiticus. Fungal Genetics and Biology*, **21(2)**, 198-205.
[28] Bischoff, T.W. and Garraway, M.O. (1985) Ammonium production by races and mating types of *Bipolaris maydis* and its relationship to mycelium dry weight, sporulation and pH of the culture medium. *Ohio Journal of Science*, **85**, 155-158.
[29] Marques, R.P., Monteiro, A.C. and Pereira, G.T. (2004) Crescimento, esporulação e viabilidade de fungos entomopatogênicos em meios contendo diferentes concentrações do óleo de Nim (*Azadirachta indica*). *Ciência Rural*, **34**, 1675-1680.
[30] Deacon, J.W. (2006) Fungal Biology, 4th edition. Blackwell Publishing, Oxford, UK.
[31] Bankole, S.A. (1997) Effect of essential oils from two Nigerian medicinal plants (*Azadirachta indica* and *Morinda lucida*) on growth and aflatoxin B1 production in maize grain by a toxigenic *Aspergillus flavus*. *Letters*

in Applied Microbiology, **24(3)**, 190-192.

[32] Ghorbanian, M., Razzaghi-Abyaneh, M., Allameh, A., Shams-Ghafarokhi, M. and Qorbani, M. (2008) Study on the effect of neem (*Azadirachta indica* A. juss) leaf extract on the growth of *Aspergillus parasiticus* and production of aflatoxin by it at different incubation times. *Mycoses*, **51(1)**, 35-39.

[33] Sithisarn, P., Supabphol, R. and Gritsanapan, W. (2005) Antioxidant activity of Siamese neem tree (VP1209). *Journal of Ethnopharmacology*, **99(1)**, 109-112.

[34] Gowda, N.K.S., Malathi, V. and Suganthi, R.U. (2004) Effect of some chemical and herbal compounds on growth of *Aspergillus parasiticus* and aflatoxin production. *Animal Feed Science and Technology*, **116**, 281-291.

[35] Suberu, H. (2004) Preliminary studies of inhibitions in *Aspergillus flavus* with extracts of two lichens and Bentex-T fungicide. *African Journal of Biotechnology*, **3(9)**, 468-472.

[36] Wilson, D.M., Gueldner, R.C., McKinney, J.K., Lievsay, R.H., Evans, B.D. and Hill, R.A. (1981) Effect of β-ionone on *Aspergillus flavus* and *Aspergillus parasiticus* growth, sporulation, morphology and aflatoxin production. *Journal of the American Oil Chemists' Society*, **58**, A959-A961.

[37] Kale, S.P., Cary J.W., Bhatnagar, D. and Bennet J.W. (1996) Characterization of experimentally induced, non-aflatoxigenic variant strains of *Aspergillus parasiticus*. *Applied and Environmental Microbiology*, **62(9)**, 3075-3092.

Advances in Bioscience and Biotechnology, 2010, 1, 300-304 **ABB**
doi:10.4236/abb.2010.14039 Published Online October 2010 (http://www.SciRP.org/journal/abb/).

Cellular effects of an aqueous solution of Losartan® on the survival of *Escherichia coli* AB1157 in the presence and absence of SnCl2, and on the physiological property (osmotic fragility) of the erytrocyte

Thais Lima Zaidan[1], Wevelin Santos de Matos[1], Éric Guimarães Machado[1], Thais Nery Figorelle Junqueira[1], Solange Campos Vicentini[1], Giuseppe Antonio Presta[1], Sebastião David Santos-Filho[1,2]

[1]Centro de Ciências da Saúde, Faculdade de Medicina, Departamento de Biofísica e Fisiologia, Universidade Severino Sombra, Vassouras, RJ, Brasil;
[2]Departamento de Biofísica e Biometria, Instituto de Biologia Roberto Alcantara Gomes, Universidade do Estado do Rio de Janeiro, Rio de Janeiro, RJ, Brasil.
Email: thais.zaidan@gmail.com

Received 12 July 2010; revised 19 July 2010; accepted 25 July 2010.

ABSTRACT

The angiotensin receptors type 1 (AT1) have affinity by Losartan®, low affinity to non-peptides antagonists and similar effect as Angiotensin-convert-enzyme inhibitors. It have been reported that natural and synthetic products might reduce the genotoxic and cytotoxic effects related to stannous chloride (SnCl2). SnCl2 is used in nuclear medicine as a reducing agent to obtain technetium-99 m-radiopharmaceuticals. The aim of this work was to evaluate the cellular effects produced by a solution of Losartan® (25 mg/ml) on the survival of *Escherichia coli* AB1157 in the presence and absence of SnCl2, and on the osmotic fragility of erythrocytes of the blood of *Wistar* rats. Briefly, blood sample was withdrawn by *Wistar* rats with heparinized syringe and incubated with Losartan® solution. Saline (NaCL 0.9%) was used as a control. The samples were gently mixed with hypotonic solutions of NaCl. After that it was centrifuged and the supernadant isolated for optical determination of the hemoglobin present. *E. coli* AB1157 cultures (exponential growth phase) were collected by centrifugation, washed and resuspended in 0.9%NaCl. Samples were incubated in water bath shaker with: (a) SnCl2 (25 µg/ml), (b) Losartan® (25 mg/ml) and (c) SnCl2 (25 µg/ml) + Losartan® (25 mg/ml). Incubation with 0.9% NaCl was also carried out (control). At 60 min intervals, aliquots were withdrawn, diluted, spread onto Petri dishes with solid LB medium and incubated overnight. The colonies formed were counted and the survival fractions calculated. Statistical analysis was performed. The results showed that there was a significantly increase ($P < 0.05$) in the osmotic fragility of the blood cells treated with Losartan®. Moreover, Losartan® was also able to protect the *E. coli* cultures against the lesive action of SnCl2. Although, in erythrocyte the osmotic fragility was increased by the presence of Losartan® that could 1) alter the physical properties of this cell, or 2) had a direct or indirect effect on the intracellular sodium concentration or 3) had acted on the cardiovascular system. It suggested that the Losartan® did interfere strongly with cellular metabolism and did alter the survival fractions of *E. coli* AB1157.

Keywords: Losartan®; Surveillance; *Escherichia Coli* AB1157; Osmotic fragility; Erythrocyte

1. INTRODUCTION

Losartan® is an angiotensin II receptor antagonist drug used mainly to treat high blood pressure due to cardiovascular diseases. As with all angiotensin II type 1 receptor (AT_1) antagonists, Losartan® is indicated for the treatment of hypertension [1]. Losartan® may also delay progression of diabetic nephropathy and is also utilized for the reduction of renal disease progression in patients with type-2 diabetes or hypertension or microalbuminuria or proteinuria [2]. Losartan® has been found to downregulate the expression of transforming growth factor beta (TGF-β) types I and II receptors in the kidney of diabetic rats, which may partially account for its

nephroprotective effects [3]. Alterations on TGF-β expression may also account for its potential efficacy in Marfan syndrome and Duchenne muscular dystrophy (DMD)–Losartan® has been shown to prevent aortic aneurysm and certain pulmonary complications in a mouse model of the disease [4].

Blood contains many types of cells with very different functions, ranging from the transport of oxygen to the production of antibodies. The sodium-potassium pump has a direct role in regulating red blood cell (RBC) volume: It controls the solute concentration inside the cell, thereby regulating the osmotic forces that can make a cell swell or shrink [5]. The capability of RBC to resist hemolysis characterizes what is called the osmotic fragility (OF) of the membrane. The OF is classically used as a general screening procedure [6]. The "fragility curve" reflects the structural and geometrical changes in RBC. Hemolytic results from a structural perturbation of the RBC and its cytoskeleton caused by its high partition in the membrane [7,13].

Some deleterious effects of stannous chloride (SnCl2) have been described in humans, it has been reported that it is highly irritant to the mucous membrane and skin, although it presents low systemic toxicity [8]. In animals, it can produce stimulation or depression of the central nervous system [8]. As for bacterial assays, as experiments with *Escherichia coli* survival, SnCl2 appears to be capable of inducing and/or producing injuries in deoxyribonucleic acid (DNA), being considered as a potential genotoxic agent. These effects may be, at least in part, attributed to free radicals (FR), generated during SnCl2 treatment [9-12].

The aim of this work was to evaluate the cellular effects produced by a solution of Losartan® (25 mg/ml) on the survival of *Escherichia coli* AB1157 in the presence and absence of SnCl2, and on osmotic fragility of erythrocytes of the blood withdrawn from *Wistar* rats.

2. MATERIAL AND METHODS

2.1. Losartan® Preparation

The solution of Losartan® was prepared by a dilution of 250 mg of Losartan® dust in 10 ml of saline. The final concentration of Losartan® was considered 25 mg/ml.

2.2. Osmotic Fragility

Blood was withdrawn from rat *Wistar* (2.5 ml) with a heparinized syringe. The osmotic fragility evaluations of the RBC were performed (once) with from rat *Wistar* (2.5 ml) blood samples incubated with Losartan® (0.5 ml; 25 mg/ml) or with 0.15 M NaCl as a control, for 60 minutes at room temperature. The blood samples (100 µl) after treatment were gently mixed with 5ml of hypotonic NaCl solutions with concentrations from 0.02 to 0.12 M. After 30 min, these tubes were centrifuged at 3500 rpm/ 5 min and the supernatants were isolated to determine the optical density (OD) of the hemoglobin in a spectrophotometer (540 nm). It was performed 9 (triplicate) experiments total [13]. The results were compared with the control samples and statistical analysis was performed by independent t-test [13].

2.3. Bacterial Cultures

E. coli AB1157, a wild-type strain, proficient to repair damage in the DNA, was used in this work. From stock (in glycerol 50% v/v), a sample (50 µl) of the culture was grown on liquid LB medium (5 ml, Luria and Burrous, 1957) at 37°C overnight on a shaking water bath (reciprocal water bath shaker (*Quimis Equipamentos Industriais Ltda*, *model* 215.1, *São Paulo, BR*) up to the stationary growth phase.

2.4. Bacteria Inactivation

A sample (200 µl) was taken from this culture and further incubated (20 ml; liquid LB medium) under the same conditions to exponential growth (10^8 cells/ml). The cells were collected by centrifugation, washed twice in 10 ml of saline and suspended again in the same solution until they reached 10^8 cells/ml. Samples (1.0 ml) of these washed cultures (10^8 cells/ml) were incubated on the shaking water bath with 1) 0.5 ml of SnCl2 (75 µg/ml) and 0.1 ml of saline, or 2) 0.1 ml of Losartan® solution (25 mg/ml) and 0.5ml of saline, or 3) 0.1 ml of Losartan® solution (25 mg/ml) and 0.5ml of SnCl2 (75 µg/ml), or 4) 0.6 ml of saline as a control, on initial time and after 60 min, at 37°C. During the assay, at 0 and 60 min, aliquots (100 µl) were diluted with saline and spread onto Petri dishes containing solidified LB medium (1.5% agar). Colonies units formed, after overnight incubation at 37°C, were determined. The survival fraction was calculated dividing the number of viable cells obtained per ml in each time of the treatment (N) by the number of viable cells obtained per ml in zero time (N0).

2.5. Statistical Analysis

The ANOVA test following by Boferroni test was performed and the significance is accepted if $P < 0.05$. This statistical test was realized according the methodology showed by Cavalcanti *et al.*, 2003 for the osmotic fragility test.

3. RESULTS

Figure 1 shows the osmotic fragility of the rats erythrocyte incubated with Losartan® solution when reacted with different NaCl hypotonic solutions. The curve tendency shows that in small concentrations of the salt, the hemolysis increased.

The results showed that there is a significantly increase

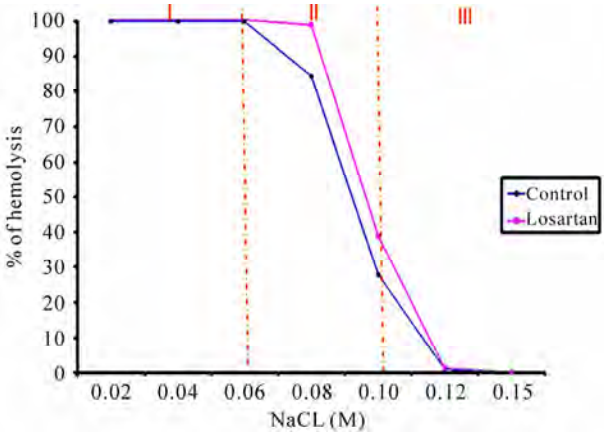

Figure 1. Osmotic fragility tendency of red blood cell, treated with Losartan®. A blood sample was withdrawn *Wistar* rats (2, 5 mL), rats with heparinized syringe and incubated with Losartan® (0.5 mL; 25 mg/mL) or with solution of sodium chloride (NaCl 0.15 M) a control, for 60 minutes at room temperature. Blood sample (25 mL), treated or not were gently mixed with 5 mL of hypotonic NaCl solutions with concentrations from 0.02 to 0.12 M after treatment or not, were gently mixed with hipotonic of NaCl (from 0.02 to 0.15 M), were centrifuged 3500 rpm/5 min and the supernatants were isolated to determine the optical density (OD) of the hemoglobin in a spectrophotometer (540 nm).

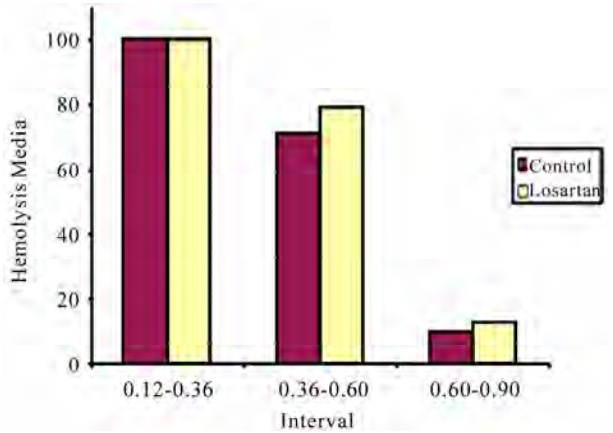

Figure 2. The osmotic fragility of red blood cells treated with Losartan®. The ANOVA test following by Boferroni test was performed and the significance is accepted if $P < 0.05$. This statistical test was realized according the methodology showed by Cavalcanti *et al.*, 2003 for the osmotic fragility test.

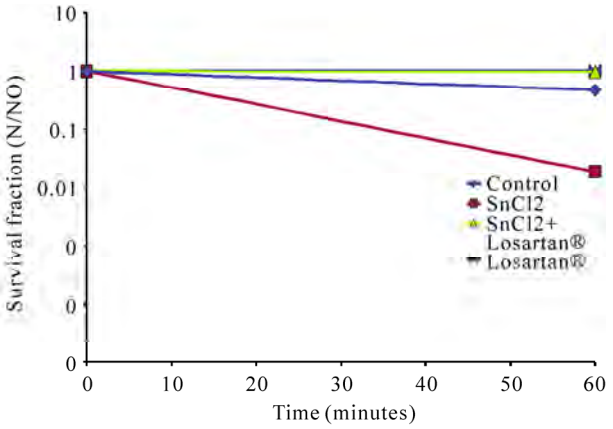

Figure 3. Losartan®'s solution effect on the survival of *E.coli* AB1157 culture treated or not with SnCl2. Samples of E. coli cultures with 108 cells/ml were incubated on the shaking water bath with 1) SnCl2 and saline, or 2) Losartan® and saline, or 3) Losartan® and SnCl2, or 4) saline as a control, on initial time and after 60 min, at 37 °C. During the assay, at 0 and 60 min, aliquots (100 µl) were diluted with saline and spread onto Petri dishes containing solidified LB medium. The survival fraction was calculated dividing the number of viable cells obtained in each time of the treatment (N) by the number of viable cells obtained in zero time (N0).

($p < 0.05$) in the osmotic fragility of the Losartan® treated cells on the curve interval between the 0.06 and 0.10 M concentrations of NaCl, that is a hypotonic interval of the osmotic curve. The isotonic interval between 0.10 and 0.15 M of NaCl, the osmotic fragility also increased significantly ($p < 0.05$) in the presence of Losartan®.

Figure 2 shows the mean of the osmotic fragility after analysis of the three NaCl concentrations intervals obtained of the osmotic curve of the **Figure 1**. The analysis of the results showed a significant statistical increase ($p < 0.05$) on osmotic fragility of erythrocyte incubated with Losartan® solution in the intervals 2 (0.06 until 0.10 M) and 3 (0.10 until 0.15 M).

Figure 3 shows that Losartan® was able to protect the *E. coli* cultures against the lesive action of SnCl2. The Losartan® also did not interfere with the survival of the cultures. It suggested that the Losartan® did interfere strongly with cellular metabolism and did alter the survival fractions of *E. coli* AB1157

4. DISCUSSION

A large number of drugs that cause alterations on the shape and physiology of the red cells have been cited by some authors [14-17].

The results obtained with the quality comparison of the shape of the RBC (non treated and treated with natural extracts) under optical microscopy could justify the modifications in the uptake of 99 mTc for the red blood cells in the presence of *Mentha crispa* extract, similar to that observed with the extract of *Maytenus iliciofolia* [18-22].

In the present study we have found that the RBC osmotic fragility was changed by presence of the Losartan® solution in the studied concentration. **Figure 1** shows the osmotic fragility of the rats erythrocyte incubated with Losartan® solution when reacted with different NaCl hypotonic solutions. The curve tendency

shows that in small concentrations of the salt, the hemolysis increased. The results reported that there is a significantly increase ($p < 0.05$) in the osmotic fragility of the Losartan® treated cells on the curve interval between the 0.06 and 0.10 M concentrations of NaCl, that is a hypotonic interval of the osmotic curve. The isotonic interval between 0.10 and 0.15 M of NaCl, the osmotic fragility also increased significantly ($p < 0.05$) in the presence of Losartan®.

Figure 2 presents the mean of the osmotic fragility after analyses of the three NaCl concentrations intervals obtained of the osmotic curve of the **Figure 1**. The analysis of the results showed a significant statistical increase ($p < 0.05$) on osmotic fragility of erythrocyte incubated with Losartan® solution in the intervals 2 (0.06 until 0.10 M) and 3 (0.10 until 0.15 M).

The findings presented in **Figure 3** reveal that the studied Losartan® solution in the concentration did not presented a cytotoxic effect on the metabolism of *E.coli* AB1157. Although several cytotoxic properties have been related to SnCl2, humans may be exposed to stannous ions in several situations [23-24]. The results in **Figure 3** reinforce the fact that SnCl2 exerted a lesive action on the survival of the culture of *E. coli* AB1157 in accordance with what had been previously reported by other authors [25-30].

Moreover, when treated simultaneously with SnCl2 and Losartan®, the *E. coli* cultures were protected against the effects of the reducing agent (SnCl2). Although, in other reports Losartan® can induce damage to bacterial culture [31] based in the protect effect studied in this work, we could hypothesized the evaluation the collateral effects of the Losartan® on the cardiovascular system, as well as, bacterial endocarditis and bacterial pericarditis.

5. CONCLUSIONS

Probably, components present in Losartan® solution could be altering 1) the erythrocyte membrane morphology, 2) the erythrocyte membrane ions transport or 3) the osmotic transport balance. The different alterations could be inducing the stronger osmotic fragility in isotonic concentrations of NaCl, causing hemolytic alterations as anemia, jaundice. The substance present in Losartan® solution could also has a protective action on the surveillance of *E. coli* AB1157 against the effects produced for the SnCl2 presence. Although, this work had been done with animals or bacterial culture, we suggest paying attention with cardiovascular diagnosis in patients who are undergoing Losartan®.

6. ACKNOWLEDGEMENTS

This work was supported by FUSVE, USS and UERJ.

REFERENCES

[1] Dahlöf , B., Devereux, R.B., Kjeldsen, S.E., Julius, S., Beevers, G., de Faire, U., Fyhrquist, F., Ibsen, H., Kristiansson, K., Lederballe-Pedersen, O., Lindholm, L.H., Nieminen, M.S., Omvik, P., Oparil, S. and Wedel, H. (2002) Cardiovascular morbidity and mortality in the Losartan Intervention for Endpoint reduction in hypertension study (LIFE): a randomised trial against atenolol. *Lancet*, **359(9311)**, 995-1003.

[2] Rossi, S. (2006) Australian Medicines Handbook. *Adelaide: Australian Medicines Handbook.*

[3] Guo, Z.X. and Qiu, M.C. (2003) Losartan® downregulates the expression of transforming growth factor beta type I and type II receptors in kidney of diabetic rat. *Zhonghua Nei Ke Za Zhi*, **42(6)**, 403-408.

[4] Habashi, J.P., Judge, D.P., Holm, T.M., Cohn, R.D., Loeys, B.L., Cooper, T.K. *et al*. (2006) Losartan®, an AT1 antagonist, prevents aortic aneurysm in a mouse model of Marfan syndrome, and preserves muscle tissue architecture in DMD mouse models. *Science*, **312(5770)**, 117-121.

[5] Alberts, B., Johnson, A., Lewis, A., Raff, J., Roberts, M. and Walter, P. (2002) Molecular biology of the cell. Garland Science, New York.

[6] Wang, X., Wei, I., Ouyang, J.P., Muller, S., Gentils, M., Cauchois, G. and Stoltz, J.F. (2001) Effects of an angelica extract on human erythrocyte aggregation, deformation and osmotic fragility. *Clinical Hemorheology and Microcirculation*, **24(3)**, p. 201.

[7] Didelon, J., Mazeron, P., Muller, S. and Stoltz, J.F. (2000) Osmotic fragility of the erythrocyte membrane: characterization by modeling of the transmittance curve as a function of the NaCl concentration. *Biorheol*, **37(5-6)**, 409-416.

[8] Silva, C.R., Oliveira, M.B., Melo, S.F., Dantas, F.J., de Mattos, J.C., Bezerra, R.J., Caldeira-de-Araujo, A., Duatti, A. and Bernardo-Filho, M. (2002) Biological effects of stannous chloride, a substance that can produce stimulation or depression of the central nervous system. *Brain Research Bulletin*, **59(3)**, 213-216.

[9] Bernardo-Filho, M., Gutfilen, B. and Maciel, O.S. (1994) Effect of different anticoagulants on the labelling of red blood cells and plasma proteins with Tc-99m. *Nuclear Medicine Communications*, **15**, 730-734.

[10] Dantas, F.J.S., Moraes, M.O., Mattos, J.C.P., Bezerra, R.J.A.C., Carvalho, E.F., Bernardo-Filho, M., *et al*. (1999) Stannous chloride mediates single strand breaks in plasmid DNA through reactive oxygen species formation. *Toxicology Letters*, **110(3)**, 129-136.

[11] Mattos, D.M.M., Gomes, M.L., Freitas, R.S., Rodrigues, P.C., Nascimento, V.D., Boasquevisque, E.M., Paula, E.F. and Bernardo-Filho, M. (2000) Assessment of the vincristine on the biodistribution of 99mTc-labelled glucoheptonic acid in female Balb/c mice. *Nuclear Medicine Communications*, **21**, 117-121

[12] Assis, M.L., De Mattos, J.C., Caceres, M.R., Dantas, F.J., Asad, L.M., Asad, N.R., Bezerra, R.J., Caldeira de Araujo, A. and Bernardo-Filho, M. (2002) Adaptative response to H(2)O(2) protects against SnCl (2) damage:

the oxyr system involvement. *Biochimie*, **84(4)**, 291-294.

[13] Cavalcanti, T.C., Gregorini, C.G., Guimarães, F., Rettori, O. and Vieira-Matos, A.N. (2003) Changes in red blood cell osmotic fragility induced by total plasma and plasma fractions obtained from rats bearing progressive and regressive variants of the Walker 256 tumor. *Brazilian Journal of Medical and Biological Research*, **36(7)**, 887-895.

[14] Ammus, S. and Yunis, A.A. (1989) Drug-induced red cell dyscrasias. *Blood Review*, **3(2)**, 71-82.

[15] Braga, A.C.S., Oliveira, M.B.N., Feliciano, G.D., Reininger, I.W., Oliveira, J.F., Silva, C.R. and Bernardo-Filho, M. (2000) Mecanismo de ação e efeito de um derivado tiazolidinônico na radiomarcação de elementos sanguíneos com Tc-99m. *Current Pharmaceutical Design*, **6**, 1179-1191.

[16] Santos-Filho, S.D., Ribeiro, C.K., Diré, G.F., Lima, E. and Bernardo-Filho, M. (2002) Technetium, Rhenium and other Metals in Chemistry an Nuclear Medicine. In: Nicolini, M. and Mazzi, U. Eds., *Padova, SGE editoriali*, **6**, 503-505.

[17] Nicolini, M. and Mazzi, U. (2002) Technetium, Rhenium and other Metals in Chemistry a Nuclear Medicine. *Padova, SGE editoriali*, **6**, 503-505, 2002.

[18] Oliveira, J.F., Braga, A.C.S., Ávila, A.S.R., Araújo, A.C., Cardoso, V.N., Bezerra, R.J.A.C. and Bernardo-Filho, M. Assessment of the effect of Maytenus ilicifolia (espinheira santa) extract on the labeling of red blood cells and plasma proteins with technetium-99m. *Journal of Ethnopharmacology*, **72(1-2)**, 179-184.

[19] Santos-Filho, *et al*. Erythrocyte osmotic fragility is the resistance of RBC hemolysis to osmotic changes that is used to evaluate RBC friability. *Journal Biological Sciences*, **4(3)**, 266-270.

[20] Wu, S.G., Jeng, F.R., Wei, S.Y., Su, C.Z. Chung, T.C., Chang, W.J.,and Chang, H.W. (1998) Red blood cell osmotic fragility in chronically hemodialyzed patients. *Nephron*, **78(1)**, 28-32

[21] Maiworm, A.I., Presta, G.A., Santos-Filho, S.D. *et al*. (2008) Osmotic and morphological effects on red blood cell membrane: action of an aqueous extract of Lantana camara. *Revista Brasileira de Farmacognosia ou Brazilian Journal of Pharmacognosy*, **18(1)**, 42-46

[22] Gian, T.S., de Paoli, S., Presta, G.A. *et al*. (2007) Assessment of effects of a formula used in the traditional Chinese medicine (Buzhong Yi Qi Wan) on the morphologic and osmotic fragility of red. *Revista Brasileira de Farmacognosia ou Brazilian Journal of Pharmacognosy*, **17(4)**, 2007, 501-507

[23] Howard-Flanders, P., Simsom, E. and Therlot, L. (1964) A locus that controls filament formation and sensitivity to radiation in Escherichia coli K-12. *Genetics*, **49(2)**, 237-246

[24] De Mattos, J.C., Dantas, F.J., Bezerra, R.J.,. Bernardo-Filho, M., Cabral-Neto, J.B., Lage, C., Leitão, A.C. and Caldeira de Araujo, A. (2000) Damage induced by stannous chloride in plasmid DNA. *Toxicology Letters*, **116(1-2)**, 159-163

[25] Caldeira de Araujo, A. (2002) Genotoxic effects of stannous chloride (SnCl2) in K562 cell line. *Food and Chemical Toxicology*, **40(10)**, 1493-1498

[26] Dantas, F.J., Moraes, M.O., Carvalho, E.F., Valsa, J.O., Bernardo-Filho, M. and Caldeira de Araujo, A. (1996) Lethality induced by stannous chloride on Escherichia coli AB1157: participation of reactive oxygen species. *Food and Chemical Toxicology*, **34(10)**, 959-962.

[27] Reiniger, W., Silva, C.R., Feizenszwalb, I., Mattos, J.C.P., Oliveira, F.F., Dantas, F.I.S., Bezerra, A.A.C. and Bernardo-Filho, M. (1999) Boldine action against the stannous chloride effect. *Journla of Ethnopharmacology*, **68(1-3)**, pp. 345.

[28] Melo, S.F., Soares, S.F., Costa, R.F., Silva, C.R., Oliveira, M.B.N., Bezerra, R.J.A.C. *et al*., (2001) Effect of the Cymbopogon citratus, Maytenus ilicifolia and Baccharis genistelloides extracts against the stannous chloride oxidative damage in Escherichia coli. *Mutation Research*, **496(1-2)**, 33-38.

[29] Bernardo-Filho, M. (2002) Effect of eggplant (Solanum melongena) extract on the *in vitro* labeling of blood elements with technetium-99m and on the biodistribution of sodium pertechnetate in rats. *Molecular Biology of the Cell* (*Noisy-le- grand*), **48(7)**, 771-776.

[30] Soares, S.F., Brito, L.C., Souza, D.E., Almeida, M.C., Bernardo, L.C. and Bernardo-Filho, M. (2004) Citotoxic effects of stannous salts and the action of Maytenus ilicifolia, Baccharis genistelloides and Cymbopogon citratus aqueous extracts. *Brazilian Journal of Biomedical Engineering*, **20**, 2004; pp. 73-79.

[31] Tadros, T., Traber, D.L. and Herndon, D.N. (2000) Trauma and sepsis-induced hepatic ischemia and reperfusion injury: role of angiotensin II. *Archives of Surgery*, **135(7)**, 766-772.

Advances in Bioscience and Biotechnology, 2010, 1, 305-314 **ABB**
doi:10.4236/abb.2010.14040 Published Online October 2010 (http://www.SciRP.org/journal/abb/).

Subtle differences in receptor binding specificity and gene sequences of the 2009 pandemic H1N1 influenza virus

Wei Hu

Department of Computer Science Houghton College Houghton, NY, USA.
Email: wei.hu@houghton.edu

Received 4 June 2010; revised 20 June 2010; accepted 25 June 2010.

ABSTRACT

A recent phylogenetic inference indicated that the 2009 pandemic H1N1 strains circulating from March 2009 to September 2009 could be divided into two closely related but distinct clusters. Cluster one contained most strains from Mexico, Texas, and California, and cluster two had most strains from New York, both of which were reported to co-circulate in all continents. The same study further revealed nine nucleotide changes in six gene segments of the new virus specific for the two clusters. In the current study, the informational spectrum method (ISM), a bioinformatics technique, was employed to study the receptor binding patterns of the two clusters. It discovered that while both groups shared the same primary human binding affinity, their secondary binding preferences were different. Cluster one favored swine binding as its secondary binding pattern, whereas cluster two mostly exhibited the binding specificity of A/South Carolina/1/18 (H1N1) (one of the 1918 flu pandemic strains) as its secondary binding pattern. Besides all the nine nucleotide changes found in the previous study, Random Forests were applied to uncover several new nucleotide polymorphisms in 10 genes of the strains between the two clusters, and several amino acid changes in the HA protein that might be accountable for the discrepancy of the secondary receptor binding patterns of the two clusters. Finally, entropy analysis was conducted to present a global view of gene sequence variations between the two clusters, which illustrated that cluster one had much higher genetic divergence than cluster two. Furthermore, it suggested a significant overall correspondence between the nucleotide positions of high importance in differentiating the two clusters and nucleotide positions of high entropy in cluster one.

Keywords: 2009 Pandemic H1N1; Influenza; Informational Spectrum Method; Mutation; Random Forests

1. INTRODUCTION

The 2009 pandemic H1N1 influenza virus has brought great challenges and opportunities to flu research. Extensive studies to date on different genes of 2009 pandemic H1N1 have offered valuable insight into the nature of this novel virus. A brief summary of the recent findings on the 2009 pandemic H1N1 virus can be found in [1]. One of the key issues in the study of this new virus is to discover its molecular characteristics. However, many of the molecular indicators of adaptation to human hosts or to the generation of a pandemic virus are found to be lacking in 2009 pandemic H1N1, implying that other previously unrecognized molecular determinants are accountable for its capacity to infect humans [2]. Therefore, it is important to uncover new molecular features of 2009 pandemic H1N1. In [1] Random Forests were employed to identify specific amino acids as novel host markers in 10 proteins of the 2009 pandemic H1N1 virus, and to determine specific nucleotides as host markers in 10 genes of the avian, human, 2009 pandemic H1N1, and swine influenza viruses in a follow-up study [3].

In [4,5] the informational spectrum method (ISM) [6] was applied to probe the interaction between HA and its receptors, and to find one single highly conserved domain in HA of various subtypes of influenza viruses that was responsible for each binding pattern. The study in [7] located multiple such domains in the HAs of 2009 pandemic H1N1 and avian H5N1, thus expanding the known repertoire of key regions in HA associated with receptor binding affinity. These conserved domains in HA might be served to identify new therapeutic targets for drug development.

The analysis of amino acid sequence and the three-dimensional structure of HA indicated the antigenic similarity between the viruses of the pandemics of 1918 and 2009, and demonstrated that both are susceptible to neutralization by the same antibodies [8-10]. HA is not only a primary target of host immune responses,

but also is a major player in host cell receptor binding. Uncovering the receptor binding affinity of 2009 pandemic H1N1 is essential for the understanding of this new virus. In one study [11], two 2009 pandemic H1N1 viruses, A/California/4/2009 and A/Hamburg/5/2009, exhibited dual receptor specificity (human and avian), whereas another virus (A/Darwin/2001/2009) revealed a strict preference for human receptors in a subsequent report [12], which implied that the binding preference of one strain might be different from other strains.

HA mutations have an impact on the host cell receptor specificity. The ISM was employed to identify mutations in the influenza viruses within or between hosts, and to quantify the contribution from each mutation to receptor binding switch. It reported that the strains of 2009 pandemic H1N1 tended to favor human receptor binding as a group, demonstrating that this bioinformatics approach offered a valuable alternative in the study of receptor binding that could process many strains in one analysis. Additionally, the ISM was also applied to quantify the effects of several well-known mutations on binding preference shifts, including E190D/G225D in H1N1 and Q192R/ S223L/ Q226L/ G228S in H5N1 [13]. A recent report [14] revealed that the HAs of human H1N1 followed two different evolutionary paths at positions 190 and 225. The antigenic drift of 1918 pandemic has occurred at position 225, and that of epidemic HAs happened at position 190. Surprisingly, the HAs of 2009 pandemic H1N1 took a different path, i.e., they were highly conserved at both positions 190 and 225.

In [4,5] it was found that the consensus informational spectrum (CIS) of HA of influenza strains have the following characteristic dominant peaks at different IS frequencies as presented in **Table 1**. In this study, F(0.295) will be termed as 2009 pandemic H1N1 receptor interaction frequency, F(0.055) as swine receptor interaction frequency, and F(0.258) as 1918 pandemic H1N1 receptor interaction frequency. In addition to the dominant peak at IS frequencies in each subtype, there are secondary peaks at various IS frequencies [4,5,13].

Elucidation of the genetic evolution of the 2009 pandemic H1N1 influenza virus is an important undertaking. Current research suggested that the 2009 pandemic H1N1 strains have already diversified into distinct viral lineages with defined spatial patterns. One study reported that the strains circulating from April 2009 to July 2009 could be divided into seven phylogenetically distinct viral clades [15], and another analysis indicated that the strains circulating from March 2009 to September 2009 could be divided into two distinct clusters [16]. Cluster one contained most strains from Mexico, Texas, and California, and cluster two had most strains from New York. Strains of cluster one occurred about two weeks earlier than those of cluster two. Both clusters were reported to co-circulate in all continents. Nine nucleotide changes were uncovered in six gene segments (HA, NA, M, NP, NS, PB2) of the strains between the two clusters. A subsequent report [17] revealed that the 2009 pandemic H1N1 virus has evolved worldwide, shifting from an initial mixed clade patterns to one predominant clade (clade 7 in [15] or cluster 2 in [16]), and cluster 2 virus has been under strong purifying selection pressure.

Table 1. Characteristic IS frequencies of HA proteins in 2009 pandemic H1N1, swine H1N1/H1N2, and 1918 pandemic H1N1.

Subtype	2009 Pandemic H1N1	Swine H1N2/H1N1	A/South Carolina/1/18 (H1N1)
Frequency	F(0.295)	F(0.055)	F(0.258)

It is of interest to determine the differences in the biological functions of the 2009 pandemic H1N1 strains in the two clusters identified in [16]. The purpose of this study is three fold. One is to explore the HA receptor binding preferences of the two clusters using ISM. The second is to investigate new nucleotide polymorphisms that can characterize the differences between the two clusters with the feature selection capability of Random Forests. The third is to calculate the entropy of 10 genes in the two clusters to achieve a global revelation of the sequence variations of these two clusters.

2. MATERIALS AND METHODS

2.1. Sequence Data

All the protein and nucleotide sequences were retrieved from the Influenza Virus Resource (http://www.ncbi/nlm.nih.giv/genomes/FLU/FLU.html) of the National Center for Biotechnology Information (NCBI). We utilized 96 isolates that had all six gene segments belonging to cluster one, and 155 isolates that had all six gene segments belonging to cluster two [16]. All the sequences used in the study were aligned with MAFFT [18].

2.2. Entropy

In information theory [19], entropy is a measure of disorder or randomness associated with a random variable. Let x be a discrete random variable that has a set of possible values $\{a_1, a_2, a_3, \ldots a_n\}$ with probabilities $\{p_1, p_2, p_3, \ldots p_n\}$ where $P(x = a_i) = p_i$. The entropy H of x is

$$H(x) = -\sum_i p_i \log p_i$$

In the current study, each of the n columns in a multiple sequence alignment of a set of sequences of N symbols

is considered as a discrete random variable x_i $(1 \le i \le N)$ that takes on one of the 20 amino acid types or 4 nucleotide types with some probability. $H(x_i)$ has its minimum value 0 if all the symbols at position *i* are the same, and achieves its maximum if all the 20 amino acid types or all the 4 nucleotide types appear with equal probability at position i, which can be verified by the Lagrange multiplier technique. A position of high entropy means that the sequences are often varied at this position. $H(x_i)$ measures the genetic diversity at position *i* in our current study.

2.3. Random Forests

Random Forest, proposed by Leo Breiman in 1999 [20], is an ensemble classifier based on many decision trees. Each tree is built on a bootstrap sample from the original training set and is unpruned to obtain low-bias trees. The variables used for splitting the tree nodes are a random subset of the whole variable set. The classification decision of a new instance is made by majority voting over all trees. About one-third of the instances are left of the bootstrap sample and not used in the construction of the tree. These instances in the training set are called "out-of-bag" instances and are used to evaluate the performance of the classifier, which can achieve both low bias and low variance with bagging and randomization.

2.4. Feature Selection Using Random Forests

Random Forest calculates several measures of variable importance. The mean decrease in accuracy measure was employed in [21] to rank the importance of the features in prediction. This measure is based on the decrease of classification accuracy when values of a variable in a node of a tree are permuted randomly. In this study, two packages of R, randomForest and varSelRF [21], were utilized to compute the importance of the amino acids in a given sequence dataset. The effectiveness and robustness of this technique as a feature selection method has been demonstrated in various studies [22-27].

Random Forests produce non-deterministic outcomes. To compensate this bias, the Random Forests algorithm was run multiple times and then the average of the results was taken. The importance of each residue or nucleotide in the sequences was based on the averaged calculations by using the function randomVarImpsRF in varSelRF repeated 20 times.

3. RESULTS

3.1. Receptor Binding Patterns of the Strains in the Two Clusters

As demonstrated in [11,13], the HAs of 2009 pandemic H1N1 largely favored human receptor binding, although some of them exhibited dual binding preference. It was intriguing to explore the receptor binding differences of the two clusters identified in [16]. The ISM confirmed that the primary binding specificity of both clusters was human receptor types at IS frequency F(0.295). After setting the S/N ratio to zero at the primary frequency F(0.295), the secondary peaks of IS of the two clusters were different (**Figure 1**). Cluster one revealed a peak at frequency F(0.055) (swine binding) but cluster two showed a peak at frequency F(0.258) (1918 pandemic binding) according to the definition given in [4,5].

While all the stains in the two clusters had the same primary binding frequency F(0.295), the secondary binding frequencies varied between the two clusters. To sharpen the search of the true amino acids causing this discrepancy of the secondary binding preferences, two new sub-clusters were constructed by selecting the strains from cluster one that had the primary frequency F(0.295) and the secondary frequency F(0.055) (n = 83), and the strains from cluster two that had the primary frequency F(0.295) and the secondary frequency F(0.258) (n = 148). Random Forests produced the top important amino acid positions in the HA protein and the top nucleotide positions in the HA gene (**Figure 2**) that could separate the two new sub-clusters, having homogenous primary and secondary binding patterns within each sub-cluster.

Although the amino acids in HA were mainly accountable for the receptor binding affinity, the codon positions in HA were also displayed in **Figure 2** to provide finer details of these positions that could differentiate these two sub-clusters. Because there were only a few residue positions of non-zero importance in the HA protein, all these positions were present in the left plot of **Figure 2**. Seven residue positions 49, 100, 214, 220, 239, 240, and 293 in the left plot of **Figure 2** were located in HA1, one of the two domains of HA that is directly involved in the binding of HA to its receptors. It was of note that several codon positions in the right plot of **Figure 2** were not present in the left plot of **Figure 2**, since some nucleotide changes might not be detected at the protein level as a consequence of synonymous mutations. In one case, the consensus HA protein sequence of cluster one had an S (triple-letter codon: tca) at residue 220 and that of cluster two had a T (triple-letter codon: aca) at the same position. In another case, the consensus HA protein sequence of cluster one had a L (triple-letter codon: cta) at residue 470 and that of cluster two had a L (triple-letter codon: tta) at the same position. For this reason, both plots in **Figure 2** had position 220 but only the right plot contained position 470.

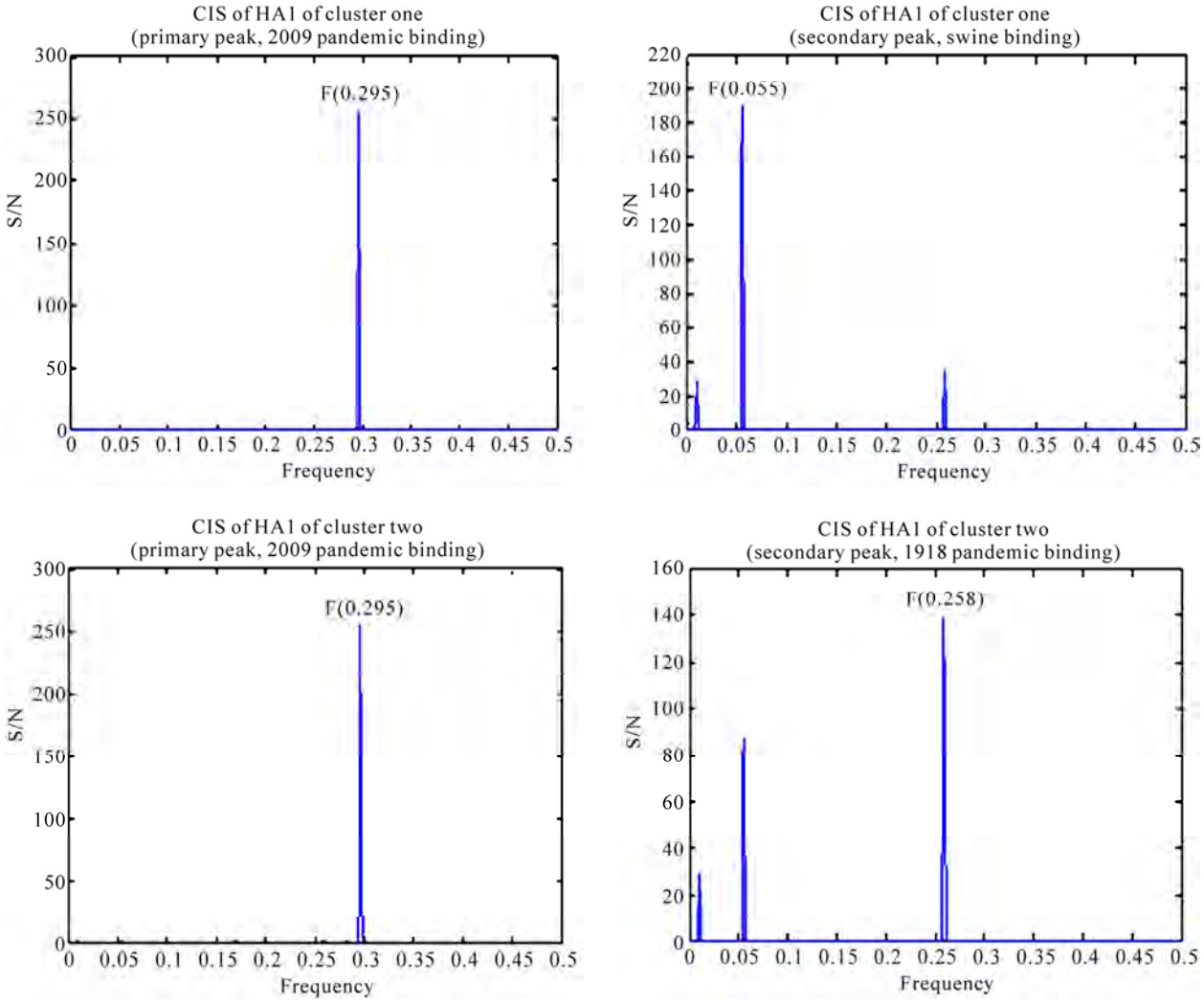

Figure 1. CIS (primary peaks and secondary peaks) of consensus HA1 sequences of the two clusters discovered in [16].

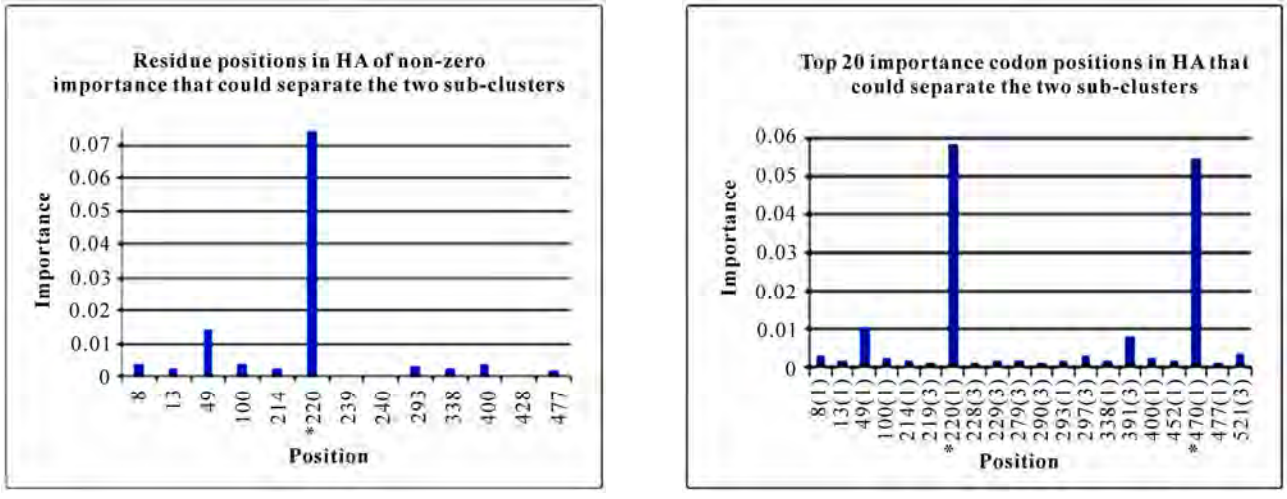

Figure 2. Important positions in the HA of 2009 pandemic H1N1 that could separate the two sub-clusters. The positions with an asterisk are those that were identified in [16]. The number in parenthesis is the position within the codon that was selected by Random Forests.

3.2. Significant Codon Positions That Could Distinguish the Two Clusters

In addition to locating all the nine nucleotide changes found in [16], Random Forests were also able to report two new nucleotide mutations that were as significant as these nine mutations, including codon 106(1) in NA and codon 416(3) in NP (**Figure 3**). Sequence inspection indicated that the consensus NA sequence of cluster one had a V (triple-letter codon: gta) at residue position 106 and that of cluster two had an I (triple-letter codon: ata) at the same position, with a nucleotide difference in the first position within codon 106. Moreover, the consensus NP sequence of cluster one had an R (triple-letter codon: cgg) at residue position 416 and that of cluster two had an R (triple-letter codon: cga) at the same position, with a nucleotide difference in the third position within codon 416. Even though their importance was not as high as those nine mutations, two significant codon positions, 353(2) in PB1 and 581(1) in PA, were revealed by Random Forests. All the other codon positions in **Figure 3** were subtle in the differentiation of the two clusters.

3.3. Entropy of Ten Genes of the Strains in the Two Clusters

To gain an overall perspective of sequence variations, the entropy of 10 genes of the strains in the two clusters was computed (**Figure 4**). The observed pattern of entropy suggested that cluster one had more sequence divergence than cluster two, highlighting the evolutionary trends of this novel virus. The top 10 entropy positions in each of the 10 genes were listed in **Table 2**, where many of the high entropy positions in cluster one were also important positions that could discriminate the two clusters (**Figure 3**). It appeared that the high entropy positions in cluster one, not those in cluster two, could influence the separation of the two clusters. This tendency was more apparent among NP, PA, PB1, and PB2, the genes that are critically involved in the replication of the influenza viruses. As expected, the M2 gene in both clusters exhibited the least sequence variation having only five non-zero entropy positions (**Table 2**). There were two nucleotide positions 279(3) in HA and 65(3) in M2 that displayed high entropy in both clusters, and

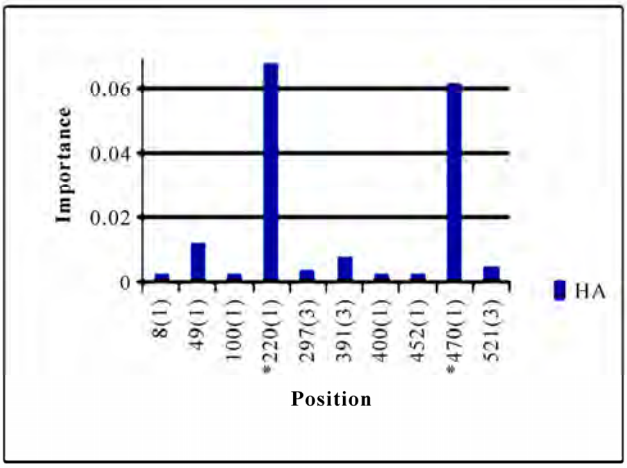

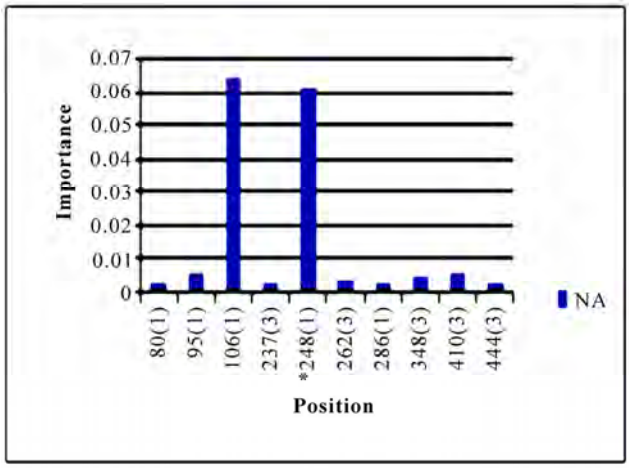

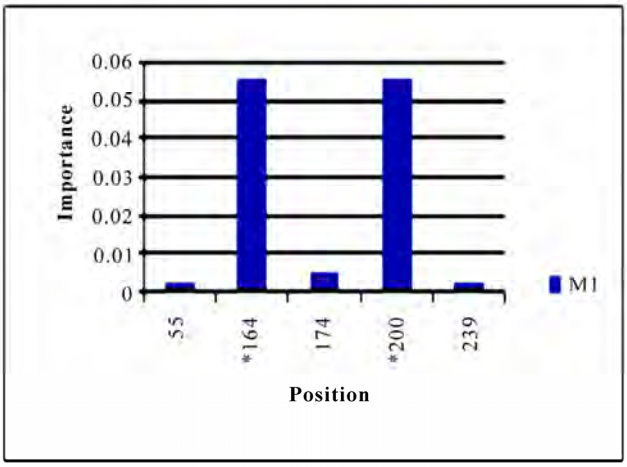

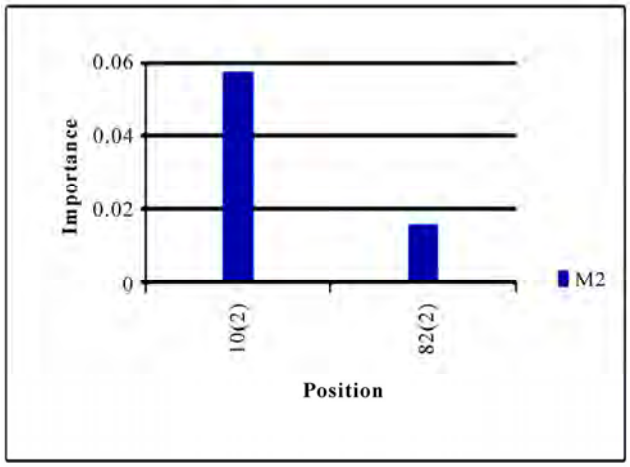

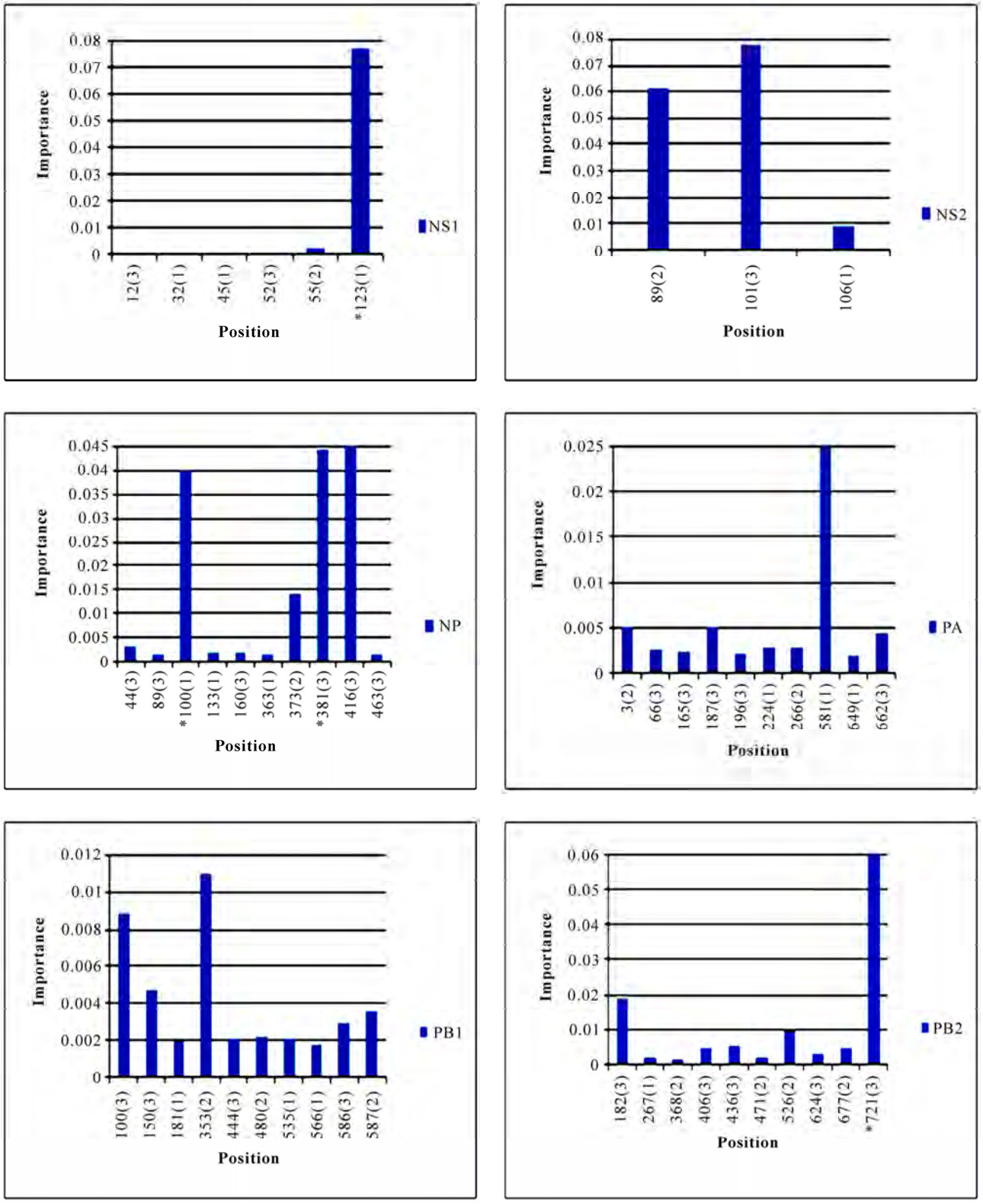

Figure 3. Top 10 important codon positions in 10 genes of 2009 pandemic H1N1 that could differentiate the two clusters. If a gene had less than 10 positions of nonzero importance, then all the nonzero positions in that gene were plotted. The positions with an asterisk are those that were identified in [16]. The number in parenthesis is the position within the codon that was selected by Random Forests.

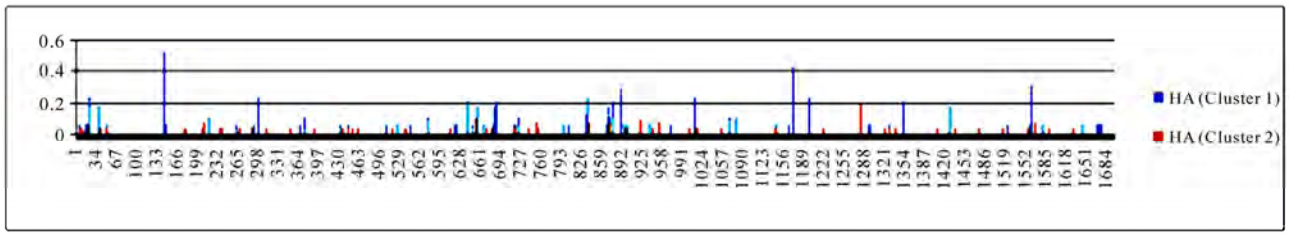

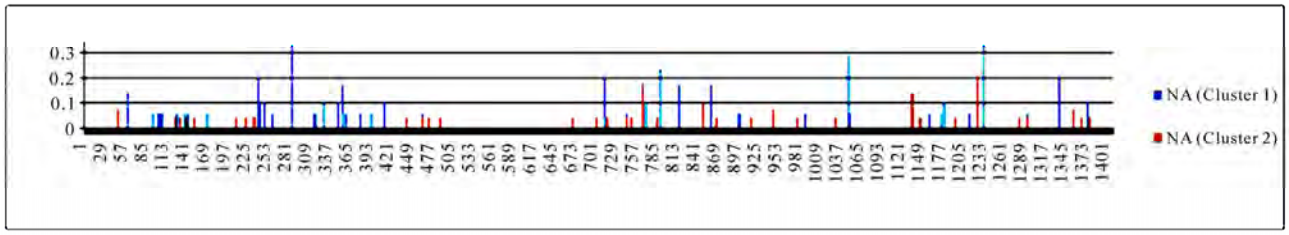

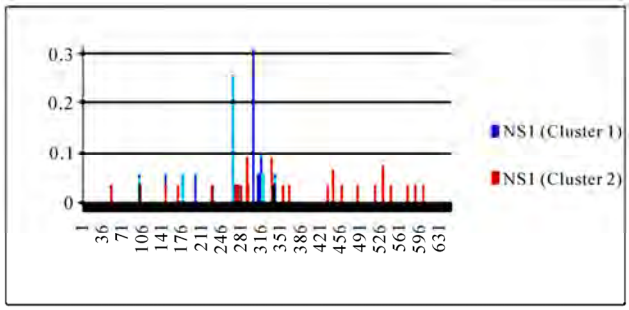

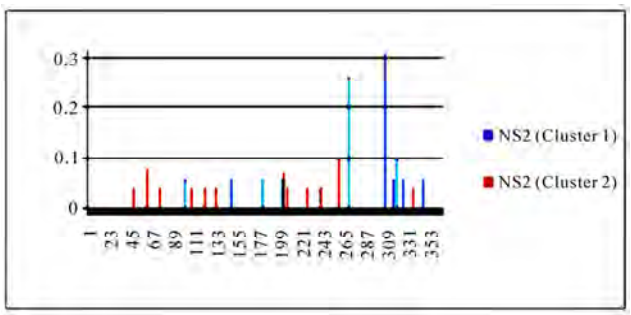

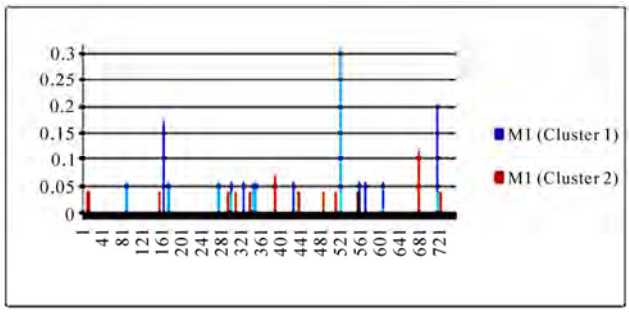

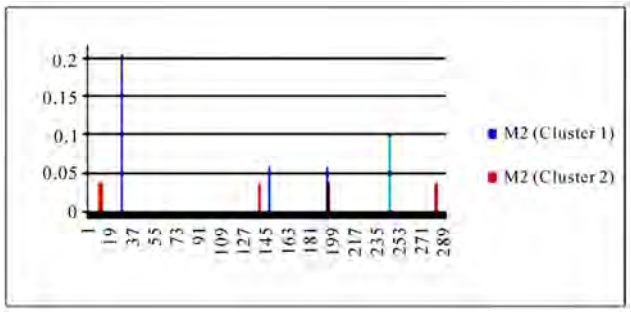

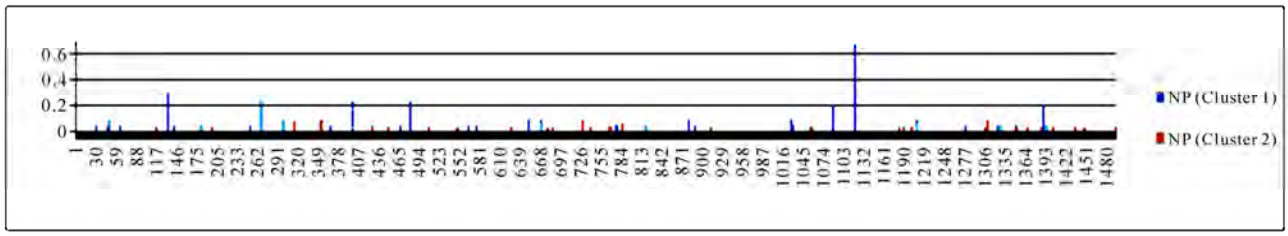

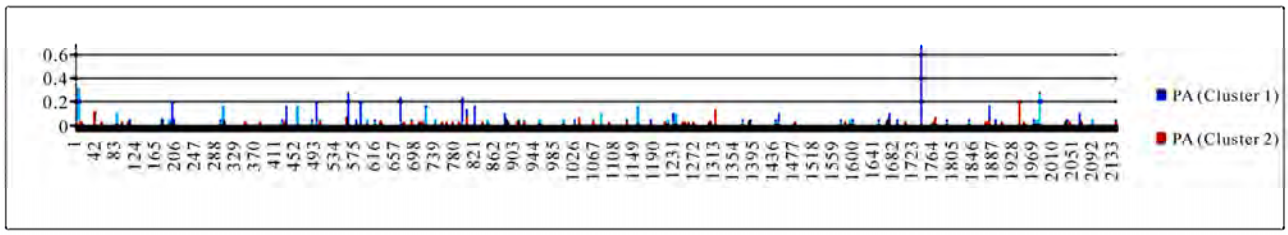

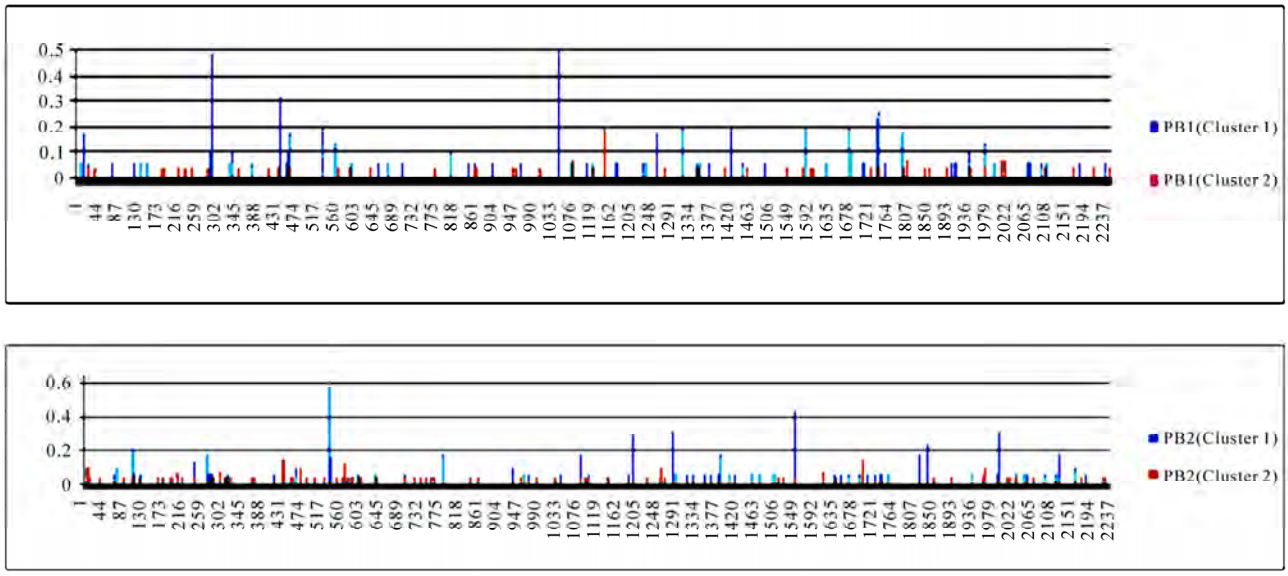

Figure 4. Entropy of 10 genes of the strains in the two clusters. In each plot, the x-axis represents the nucleotide positions in a gene and the y-axis represents the entropy.

Table 2. Top 10 entropy codon positions, ordered by their decreasing entropy values from left to right in each row, in 10 genes of the strains in the two clusters. The positions with an asterisk are those that were identified as important positions in **Figure 3**. The number in parenthesis is the position within the codon where the corresponding nucleotides had high entropy. The M2 gene of the strains in both clusters had only five non-zero entropy positions.

HA (Cluster 1)	*49(1)	391(3)	521(3)	*297(3)	*8(1)	*100(1)	279(3)	338(1)	*400(1)	241(1)
HA (Cluster 2)	428(1)	427(3)	218(3)	307(3)	70(2)	251(1)	279(3)	291(1)	318(3)	522(3)
NA (Cluster 1)	*95(1)	*410(3)	*348(3)	*262(3)	*80(1)	*237(3)	*444(3)	118(3)	271(3)	*286(1)
NA (Cluster 2)	407(3)	254(3)	377(3)	282(3)	16(1)	314(3)	451(2)	15(3)	42(1)	44(2)
M1 (Cluster 1)	*174(3)	*239(3)	*55(3)	30(2)	58(3)	92(3)	100(3)	108(3)	115(1)	117(1)
M1 (Cluster 2)	227(1)	129(3)	3(3)	4(3)	52(1)	98(1)	103(3)	113(2)	146(1)	162(3)
M2 (Cluster 1)	*10(2)	*82(2)	49(3)	65(2)	65(3)	-	-	-	-	-
M2 (Cluster 2)	3(3)	4(3)	47(1)	65(3)	95(1)	-	-	-	-	-
NS1 (Cluster 1)	*55(2)	*12(3)	*32(1)	*45(1)	*52(3)	18(3)	25(1)	43(1)	51(3)	52(1)
NS1 (Cluster 2)	97(3)	112(3)	178(1)	148(3)	17(1)	34(3)	49(3)	57(1)	77(3)	91(1)
NS2 (Cluster 1)	*101(3)	*89(2)	*106(1)	34(1)	49(3)	60(2)	67(1)	104(3)	105(1)	108(2)
NS2 (Cluster 2)	86(2)	20(3)	67(3)	16(3)	25(3)	36(1)	40(3)	44(3)	68(3)	75(3)
NP (Cluster 1)	*373(2)	*44(3)	*89(3)	*133(1)	*160(3)	*363(1)	*463(3)	16(2)	*100(1)	217(1)
NP (Cluster 2)	118(2)	242(3)	436(3)	105(1)	261(3)	16(1)	39(3)	65(3)	142(3)	149(3)
PA (Cluster 1)	*581(1)	*3(2)	*187(3)	*662(3)	*224(1)	*266(2)	*66(3)	*165(3)	*196(3)	*649(1)
PA (Cluster 2)	648(3)	439(3)	14(1)	186(3)	269(2)	346(1)	591(3)	3(2)	4(3)	17(3)
PB1 (Cluster 1)	*353(2)	*100(3)	*150(3)	*587(2)	*586(3)	*181(1)	*444(3)	*480(2)	*535(1)	*566(1)
PB1 (Cluster 2)	387(3)	363(3)	608(3)	678(2)	680(3)	263(3)	10(1)	14(1)	63(3)	65(3)
PB2 (Cluster 1)	*182(3)	*526(2)	*436(3)	*677(2)	*406(3)	*624(3)	37(2)	91(3)	*267(1)	*368(2)
PB2 (Cluster 2)	147(3)	576(3)	194(1)	2(2)	2(3)	3(1)	3(2)	3(3)	160(3)	427(3)

three codon positions 65 in M2, 67 in NS1, and 16 in NP that showed high entropy in both clusters.

4. CONCLUSIONS

Although the strains in the two clusters defined in [16] shared the same primary binding specificity (2009 pandemic binding), their secondary bindings were different. Cluster one liked swine binding, on the other hand cluster two favored 1918 pandemic binding. Residue positions 49, 100, 214, 220, 239, 240, and 293 in the HA1 domain of HA were reported by Random Forests to be responsible for this discrepancy of secondary bindings. Random Forests also found several new nucleotide polymorphisms including codon 106(1) in NA, codon 416(3) in NP, codon 353(2) in PB1, and codon 581(1) in PA, thus expanding the known nucleotide changes that could distinguish the two clusters. Finally, entropy analysis illustrated that the strains in cluster one exhibited an increased genetic variation compared with cluster two. It also highlighted a remarkable overall association between the nucleotide positions of high importance in differentiating the two clusters and nucleotide positions of high entropy in cluster one.

5. ACKNOWLEDGEMENTS

We thank Houghton College for its financial support.

REFERENCES

[1] Hu, W. (2010) Novel host markers in the 2009 pandemic H1N1 influenza a virus. *Journal of Biomedical Science and Engineering*, **3(6)**, 584-601

[2] Garten, R.J., Davis, C,T,, Russell, C.A., Shu, B., Lindstrom, S., Balish, A., Sessions, W.M., Xu, X., *at el*. (2009) Antigenic and genetic characteristics of swine-origin 2009 A(H1N1) influenza viruses circulating in humans, *Science*, **325 (5937)**, 197-201.

[3] Hu, W. (2010) Nucleotide host markers in the influenza a viruses. *Journal of Biomedical Science and Engineering*, **3**, 684-699.

[4] Veljkovic, V., Niman, H.L., Glisic, S., Veljkovic, N., Perovic, V. and Muller, C.P. (2009) Identification of hemagglutinin structural domain and polymorphisms which may modulate swine H1N1 interactions with human receptor, *BMC Structural Biology*, **9**, 62.

[5] Veljkovic, V., Veljkovic, N., Muller, C.P., Müller, S., Glisic, S., Perovic, V., Köhler, H., (2009) Characterization of conserved properties of hemagglutinin of H5N1 and human influenza viruses: possible consequences for therapy and infection control. *BMC Structural Biology*, 7, 9-21.

[6] Cosic, I. (1997) The resonant recognition model of macromolecular bioreactivity, theory and application. Birkhauser Verlag, Berlin.

[7] Hu, W. (2010) Identification of highly conserved domains in hemagglutinin associated with the receptor binding specificity of influenza viruses: 2009 H1N1, avian H5N1, and swine H1N2. *Journal of Biomedical Science and Engineering*, **3**, 114-123.

[8] Wei, C.J., Boyington, J.C., Dai, K., Houser, K.V., Pearce, M.B., Kong, W.P., Yang, Z.Y., Tumpey, T.M. and Nabel, G.J. (2010) Cross-neutralization of 1918 and 2009 influenza viruses: Role of glycans in viral evolution and vaccine design. *Science Translational Medicine*, **2**, 24ra21.

[9] Xu, R., Damian, C., Ekiert, J.C.K., Rong, H., James, E., Crowe, J., Ian, A.W. (2010) Structural basis of preexisting immunity to the 2009 H1N1 pandemic influenza virus. *Science*, **328(5976)**, 357-360

[10] Igarashi, M., Ito, K., Yoshida, R., Tomabechi, D., Kida, H. and Takada, A. (2010) Predicting the antigenic structure of the pandemic (H1N1) 2009 influenza virus hemagglutinin, *PLoS One*. **5(1)**, e8553.

[11] Childs, R.A., Palma, A.S., Wharton, S., Matrosovich, T., Liu, Y., Chai, W., Campanero-Rhodes, M.A., Zhang, Y., Eickmann, M., Kiso, M., Hay, A., Matrosovich, M. and Feizi, T. (2009) Receptor-binding specificity of pandemic influenza A (H1N1) 2009 virus determined by carbohydrate microarray. *Nat Biotechnol*. **27(9)**, 797-799.

[12] Yang, H., Carney, P. and James, S. (2010) Structure and receptor binding properties of a pandemic H1N1 virus hemagglutinin. *PLoS Curr Influenza*. **22**, RRN1152.

[13] Hu, W. (2010) Quantifying the effects of mutations on receptor binding specificity of influenza viruses. *Journal of Biomedical Science and Engineering*, **3**, 227-240.

[14] Shen, J., Ma, J., Wang, Q. (2009) evolutionary trends of a (H1N1) influenza virus hemagglutinin since 1918. *PLoS One*, **4(11)**, e7789.

[15] Nelson, M., Spiro, D., Wentworth, D., Beck, E., Jiang, F. *et al*. (2009) The early diversification of influenza A/H1N1pdm. *PLoS Curr Influenza*, **3**, RRN1126.

[16] Fereidouni, S.R., Beer, M., Vahlenkamp, T. and Starick, E. (2009) Differentiation of two distinct clusters among currently circulating influenza A (H1N1) viruses. *Euro Surveill*, **14(46)**.

[17] Valli, M.B., Meschi, S., Selleri, M., Zaccaro, P., Ippolito, G., Capobianchi, M.R. and Menzo, S. (2010) Evolutionary pattern of pandemic influenza (H1N1) 2009 virus in the late phases of the 2009 pandemic, *PLoS Currents Influenza*, **3**, RRN1149.

[18] Katoh, K., Kuma, K., Toh, H. and Miyata, T. (2005) MAFFT version 5: improvement in accuracy of multiple sequence alignment. *Nucleic Acids Research*, **33(2)**, 511-518.

[19] MacKay, D. (2003) Information theory, inference, and learning algorithms. Cambridge University Press, UK.

[20] Breiman, L. (2001) Random forests. *Machine Learning*, **45(1)**, 5–32.

[21] Díaz-Uriarte, R. and Alvarez de Andrés, S. (2006) Gene selection and classification of microarray data using random forest. *BMC Bioinformatics*, 7, 3.

[22] Kellie, J.A. and Ryan V.K. (2008) Empirical characterization of random forest variable importance measures, *Computational Statistics and Data Analysis*, **52**(4), 2249-2260.

[23] Reif, D.M.M., Alison, A.M., Brett, A.C., James, E.M., Jason, H. (2006) Feature selection using a random forests classifier for the integrated analysis of multiple data types, *Proceedings of* 2006 *IEEE Symposium on Compu-*

tational Intelligence and Bioinformatics and Computational Biology, *CIBCB* '06, Toronto, 2006, 1-8.

[24] Pablo, M.G., Cesare, F., Franco, B. and Flavia, G. (2006) Recursive feature elimination with random forest for PTR-MS analysis of agroindustrial products. *Chemometrics and Intelligent Laboratory Systems*, **83(2)**, 83-90.

[25] Bjoern, H.M., Kelm, B.M., Masuch, R., Himmelreich, U., Bachert, P., Petrich, W. and Hamprecht, F.A. (2009) A comparison of random forest and its Gini importance with standard chemometric methods for the feature selection and classification of spectral data. *BMC Bioinformatics*, **10**, 213.

[26] Gao, D., Zhang, Y.X. and Zhao, Y.H. (2009) Random forest algorithm for classification of multi-wavelength data. *Research in Astronomy and Astrophysics*, **9(2)**, 220-226.

[27] Hu, W. (2009) Identifying predictive markers of chemosensitivity of breast cancer with random forests. J*ournal of Biomedical Science and Engineering*, **3(1)**, 59-64.

Advances in Bioscience and Biotechnology, 2010, 1, 315-321 **ABB**
doi:10.4236/abb.2010.14041 Published Online October 2010 (http://www.SciRP.org/journal/abb/).

The embryonic blood–CSF barrier has molecular elements for specific glucose transport and for the general transport of molecules via transcellular routes

Maryam Parvas, David Bueno

Departament de Genètica, Facultat de Biologia, Universitat de Barcelona, Barcelona, Catalonia, Spain.
Email: dbueno@ub.edu; parvas_maryam@yahoo.com

Received 21 June 2010; revised 12 July 2010; accepted 15 July 2010.

ABSTRACT

In vertebrates, early brain development takes place at the expanded anterior end of the neural tube, which is filled with embryonic cerebrospinal fluid (E-CSF). We have recently identified a transient blood–CSF barrier that forms between embryonic days E3 and E4 in chick embryos and that is responsible for the transport of proteins and control of E-CSF homeostasis, including osmolarity. Here we examined the presence of glucose transporter GLUT-1 as well the presence of caveolae-structural protein Caveolin1 (CAV-1) in the embryonic blood-CSF barrier which may be involved in the transport of glucose and of proteins, water and ions respectively across the neuroectoderm. In this paper we demonstrate the presence of GLUT-1 and CAV-1 in endothelial cells of blood vessels as well as in adjacent neuroectodermal cells, located in the embryonic blood–CSF barrier. In blood vessels, these proteins were detected as early as E4 in chick embryos and E12.7 in rat embryos, *i.e.* the point at which the embryonic blood–CSF barrier acquires this function. In the neuroectoderm of the embryonic blood-CSF barrier, GLUT-1 was also detected at E4 and E12.7 respectively, and CAV-1 was detected shortly thereafter in both experimental models. These experiments contribute to delineating the extent to which the blood–CSF embryonic barrier controls E-CSF composition and homeostasis during early stages of brain development in avians and mammals. Our results suggest the regulation of glucose transport to the E-CSF by means of GLUT-1 and also suggest a mechanism by which proteins are transported via transcellular routes across the neuroectoderm, thus reinforcing the crucial role of E-CSF in brain development.

Keywords: Embryonic Cerebrospinal Fluid; GLUT-1; CAV-1; Blood-CSF Barrier; CNS Development

1. INTRODUCTION

The microenvironment of the Central Nervous System (CNS) is decisive for neuronal development and function. After closure of the anterior neuropore, brain walls form a large and physiologically sealed cavity that encloses embryonic cerebrospinal fluid (E-CSF), a complex and protein-rich fluid involved in several crucial roles in brain anlagen growth and development [1-8]. Chick and rat E-CSF proteomes analysed at E4 or HH23 (following Hamburger and Hamilton, 1951) [9] and at E12.7, respectively, include molecules whose roles explain the general functions reported for this fluid [10-13], most of which is transported from the embryonic serum to the E-CSF [14]. Recently, we identified a transient blood–CSF barrier located in the brain stem lateral to the ventral midline, at the mesencephalon and prosencephalon level, between embryonic days E3 and E5 in chick embryos and 12.7–13.7 days post-coitum in rats [15,16].

This embryonic blood–CSF barrier transports proteins in a selective manner via transcellular routes [15] as well as water and ions via specific transporters, identified by the presence of aquaporins 1 and 4 (AQP1 and AQP4) and the inwardly rectifying K+ channel (Kir4.1) [16]. Anatomically, this barrier is formed by specific blood vessels and the adjacent neuroectoderm, and, functionally, it controls E-CSF composition and homeostasis during this early stage of brain development, before the formation of functional choroid plexuses [15,16]. However, several questions regarding the embryonic blood–CSF barrier deserve further investigation, such as whether it also controls the transport of energetic molecules for the developing CNS, namely glucose, and the mechanism by which protein, water and ions are transported across the neuroectoderm. In this regard, AQP1,

AQP4 and Kir4.1 have been identified solely in the blood vessels of the embryonic blood–CSF barrier, but not in the adjacent neuroectoderm [15], and proteins following transcellular routes have been visualized within the neuroectoderm [16].

Therefore, the analysis of the anatomical location of the glucose transporter GLUT-1 and the caveolae-structural protein Caveolin1 (CAV-1), both present in the adult blood-brain barrier (BBB) [17-19], for transcellular protein, water and ion transport, may provide new data on the embryonic blood-CSF barrier. CAV-1 (21–24 kDa), a member of the caveolin family of proteins, is the main structural component of caveolae, which are 50- to 100-nm vesicular invaginations of the plasma membrane that are involved in transcellular molecular transport, as well as in cell adhesion and signal transduction. Endothelial cells show the highest expression of CAV-1 [20], which is also found in the human BBB-provided vessels [21].

GLUT-1, an isoform of the glucose transporter (42–55 kDa), is highly expressed by BBB microvessels and is localized in the endothelial plasma membrane but absent from circumventricular organs, which lack BBB properties [22-24]. Since glucose supports most cerebral functions, the glucose requirements of the brain are high [22]. Thus, GLUT-1 plays a major role in brain metabolism since it is responsible for more than 90% of the glucose transport through the BBB. Thus, GLUT-1 immunoreactivity has been detected in the neuroectoderm of developing brains of mice and rats from E9; however, it has been described that this expression progressively reduces as development proceeds, being finally restricted to intraneural capillaries [25-27]. Thus, according to Harik *et al*. [26], GLUT-1 immunoreactivity in rat neuroectoderm is no longer detected at E16, and according to Bauer *et al*. [27] this transporter is not detected in this tissue from E11 onwards in mice. These observations may reflect interspecific differences.

Here we addressed these two BBB-specific markers to further analyse some of the molecular features of the embryonic blood–CSF barrier in avian (chick) and mammal (rat) in more detail, *i.e*. the existence of other known transporters as GLUT-1 and of caveolae vesicles. We demonstrate the presence of glucose transporter (GLUT-1) within the same blood vessels that exhibit barrier properties for proteins, water and ions, as visualized by AQP1 co-detection, as well as in the transporting neuroectoderm adjacent to them. We also show that CAV-1 is also present in both the neuroectodermal and the endothelial cells that fulfil this barrier function, as shown by AQP1 co-detection. Our results contribute to delineating the extent to which the embryonic blood–CSF barrier controls E-CSF composition and homeostasis and also elucidate the mechanism by which molecules are transported across the neuroectoderm. The findings reported here reinforce the crucial role of E-CSF in brain development.

2. MATERIAL AND METHODS

2.1. Obtaining Chick and Rat Embryos

Fertile chicken eggs (*Gallus gallus*; White-Leghorn strain) were incubated at 38°C in a humidified atmosphere to obtain embryos at the desired developmental stage, *i.e*. at E3 (HH20), E4 (HH23) and E5 (HH26) (E is for embryonic day from the beginning of incubation; HH is for Hamburger and Hamilton developmental stages [9], as described in [24]. Rats (*Rattus norvegicus*; Wistar strain) were mated naturally. The morning of the appearance of a vaginal plug was designated as embryonic day 0.5 (E0.5). Embryos at stages E12.7 and E13.7 were dissected out from rats previously killed by CO_2 asphyxia. Local animal welfare regulations were followed.

2.2. SDS-Polyacrylamide Gel Electrophoresis and Western Blot Analysis

SDS-polyacrylamide gel electrophoresis (SDS-PAGE) was performed under denaturing conditions following the method described by Laemmli (1979) [28], with a Miniprotean II electrophoresis system (BioRad). Samples were obtained by homogenisation of brain stem tissues from dissected chick embryos obtained at E5, and from dissected rat embryos obtained at E13.7. Protein extracts from the dorsal mesencephalon were used as negative controls. At least five embryos were pooled for each stage, and the experiment was performed four times from separate protein collections.

Molecular mass standards of high and low range (Bio-Rad) were also used. SDS-PAGE was performed in a discontinuous buffer system for 40 min at 100 volts. Proteins were then electrotransferred (Trans-Blot Transfer System, BioRad) from the SDS-PAGE to activated nitrocellulose membrane (Hybond-N) for 1 hr at 100 volts, using a basic transfer buffer and following standard protocols. Proteins were immunodetected as described in [15]. Welfare regulations were followed.

2.3. PCR

PCR analysis was performed on brain stems from chick embryos at E5 and rat embryos at E13.7 dissected under a dissecting microscope, and also on dorsal mesencephalon as the negative control. The total mRNA was purified by the RNeasy Mini Kit for RNA extraction (Qiagen). The primers used are shown in **Table 1**. A regime consisting of 94°C for 2 min (1 cycle), then 35 cycles of 94°C for 1 min, 48°C for 30 s, and 72°C for 45 s, followed by a single terminal extension step (72°C for

Table 1. Primers used for PCR analysis.

Gene	F/R	Sequence (5' to 3')	bp
		Chick	
GLUT-1	F	CACTGTTGTTTCGCTCTTCG	316
	R	AATGTACTGGAAGCCCATGC	
CAV-1	F	GCCCAATAACAAGATGATGGC	410
	R	GGATGCTGCACACCTTGC	
B-Actin	F	CTACAATGAGCTGCGTGTGGC	275
	R	CAGGTCCAGACGCAGGATGGC	
		Rat	
GLUT-1	F	GCCTGAGACTTGAAAGAAC	248
	R	CTGCTTAGGTAAAGTTACAGGAG	
CAV-1	F	GACTTTGAAGATGTGATTGC	273
	R	AGATGGAATAGACACGGCTG	
B-Actin	F	CTACAATGAGCTGCGTGTGGC	275
	R	CAGGTCCAGACGCAGGATGGC	

5 min) on an Eppendorf Mastercycler was used for all primer sets. Actin was used as a positive control. Each PCR experiment was performed with four separate RNA-cDNA collections from five specimens for each stage. 100bp standards were used (Quimigen). Welfare regulations were followed.

2.4. Immunohistochemistry

To detect CAV-1 and GLUT-1 expression, chick embryos at E3 (HH20), E4 (HH23) and E5 (HH26) and rat embryos at E12.7 and E13.7 were processed as described in [1]. These embryos were incubated with the corresponding primary antibodies: rabbit anti-GLUT1 (Millipore, AB1340) at 1/500; and rabbit anti-CAV1 (Beckton, C13630) at 1/500. Anti-rabbit conjugated to Alexa-488 at 1/500 (Molecular Probes) was used as the secondary antibody. To simultaneously detect the area of GLUT-1 and CAV-1 expression with respect to the previously described blood vessels involved in the blood-CSF, several sections were immunostained with rabbit anti-CAV1 or rabbit anti-GLUT1 and rabbit anti-AQP1 (Alpha Diagnostic), and the antibodies were then sequentially detected with goat anti-rabbit conjugated to Alexa-488 at 1/500 (Molecular Probes) for anti-AQP1 and goat anti-rabbit conjugated to Alexa-568 at 1/500 (Molecular Probes) for anti-GLUT1 and anti-CAV1. Half-mount embryos cut sagittally were also stained for GLUT-1 and CAV-1 expression.

Immunostained sections were counterstained with phalloidin-TRITC at 1/2000 (Sigma, P1951) and/or with TOTO-3 at 1/1000 (Molecular Probes, T3604) in the presence of 1% Rnase (Sigma, R6513) as described in [15]. Photomicrographs were taken using a confocal microscope (Olympus) or with a dissecting microscope equipped with epifluorescence (Leica MZ16F), and were assembled with Photoshop software.

3. RESULTS

Immunochemical methods were used to determine the localisation of the caveolae-structural protein CAV-1 and the glucose transporter protein GLUT-1 in the head region of chick and rat embryos at early developmental stages. Examination of the head region included the area from the brachial arches level (*i.e.* approximately from the 5th somite) to all cephalic vesicles, thus comprising the entire brain primordium neuroectoderm as well as all surrounding tissues, *i.e.* the mesenchyma including the blood vessels within it, and the ectoderm. This area was selected on the basis of previous studies, in which blood vessels located in the brain stem lateral to the ventral midline, at the mesencephalon and prosencephalon level, were reported to form a blood–CSF barrier for proteins, water and ions.

Chick embryos were examined from E3 (HH18) to E5 (HH25), that is to say, just after closure of the anterior neuropore and before the initiation of neuroectodermal cavitation. Neither CAV-1 nor GLUT-1 was detected in E3 embryos (data not shown). In contrast, at E4, both CAV-1 and GLUT-1 immunostaining was detected in the endothelial cells of some blood vessels immersed in the mesenchyma in the brain stem, lateral to the ventral midline, at the mesencephalon and prosencephalon level, and close to the neuroectoderm. GLUT-1 was also expressed in the neuroectoderm close to these blood vessels at both E4 and E5. However, CAV-1 expression in the neuroectoderm was not detected at E4 but shortly thereafter. The number of CAV-1 and GLUT-1 immunoreactive blood vessels and the intensity in the adjacent neuroectoderm increased in this region from E4 to E5, as development proceeded (**Figure 1(a), (b)**), and they were not clearly detected in other neuroectodermal areas of the head region. At these two stages, neither CAV-1 nor GLUT-1 expression were detected in any other blood vessel or vascular sprout of the head region (**Figure 1(b)**).

To check whether blood vessels expressing CAV-1 and GLUT-1 were the same as those involved in the previously reported embryonic blood-CSF barrier, double immunostaining with anti-CAV1 or alternatively anti-GLUT1 and with anti-AQP1 was performed (**Figure 1(c)**). AQP1 was chosen as it had previously been reported to

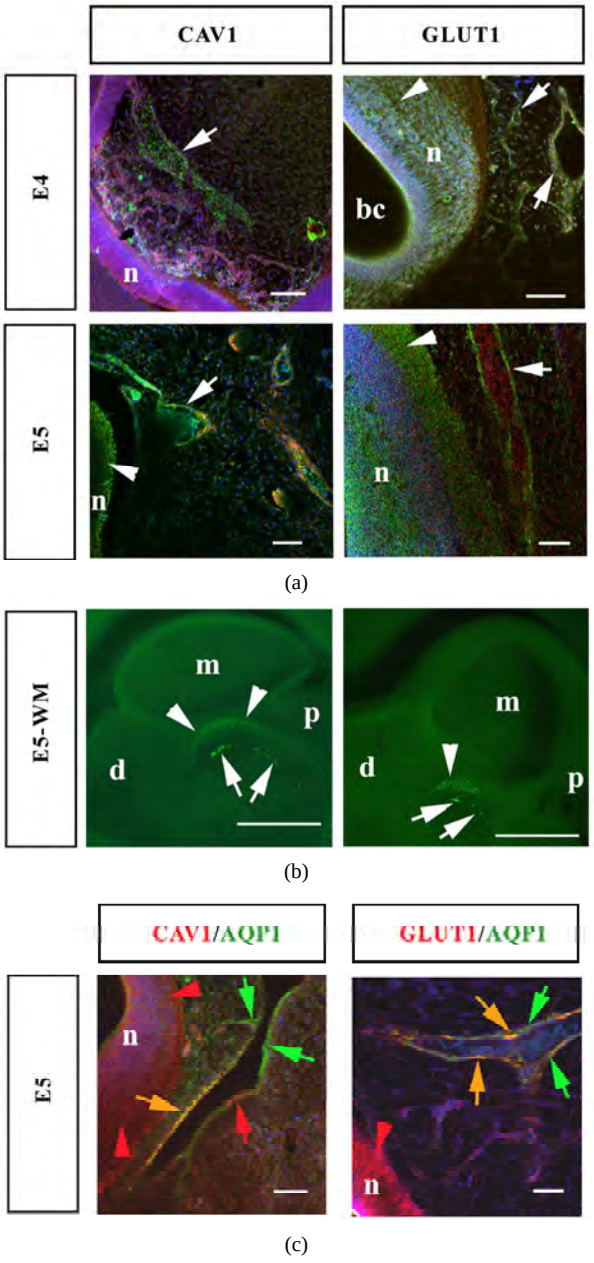

Figure 1. Immunohistochemical localisation of CAV-1 and GLUT-1 in the head process of chick embryos at E4 and E5. A and C are merged confocal images (50 µm thick) of 200 µm vibratome sections. B is half-mount heads seen under a dissecting microscope. Note the immunoreactive blood vessels and vascular sprouts immersed within the parenchyma (arrows) and the staining within the neuroectoderm (arrowheads). In C), green arrows are for AQP1 green immunostaining; red arrows and arrowheads are for CAV-1 or GLUT-1 red immunostaining; and orange arrows are for areas simultaneously immunostained for AQP1 and CAV-1 or GLUT-1, which are seen in orange after merging. Nuclear counterstaining is shown in blue and cellular counterstaining in red (except in B). Scale bars: A: 0.1 mm; B: 1 mm; C: 0.25 mm. Abbreviations: bc, brain cavity; d, diencephalon; m, mesencephalon; n, neuroectoderm; p, prosencephalon.

be expressed in the same blood vessels fulfilling the blood-CSF function for proteins, and because its expression coincides with other molecular markers of this barrier, namely AQP4 and Kir4.1. Embryos, which were examined at E5, showed the presence of CAV-1 and AQP1 or GLUT-1 and AQP1 in the same blood vessels. Certain areas of these blood vessels expressed both molecules (CAV-1/AQP1 or GLUT-1/AQP1) simultaneously while others expressed only one of them. However, these molecules were always located in the brain stem, lateral to the ventral midline, at the mesencephalon and prosencephalon level.

To extrapolate the avian data to a mammalian system, we also examined the localisation of CAV-1 and GLUT-1 in rat embryos from E12.7 to E13.7, as these developmental stages are equivalent to those examined in chick embryos with respect to brain development. Thus, these stages correspond to the period between the closure of the anterior neuropore and the initiation of neuroectodermal cavitation, coincide with the starting period of maximum anterior CNS neurogenesis, and occur before the functional embryonic choroid plexus is formed. This strategy enabled us to determine whether mammals have a similar area with blood–CSF barrier functions.

In rat embryos, CAV-1 and GLUT-1 were expressed at both E12.7 and E13.7 in the endothelial cells of some blood vessels located within the mesenchyma in the brain stem, lateral to the ventral midline, at the mesencephalon and prosencephalon level, as well as in some vascular sprouts penetrating the neuroectoderm. With respect to neuroectodermal cells close to these blood vessels, GLUT-1 was detected at both E12.7 and E13.7. However, as in chick embryos CAV-1 expression was not detected at E12.7 but shortly thereafter (**Figure 2**). Again, at these two stages, CAV-1 and GLUT-1 expression was not detected in any other blood vessel or vascular sprout of the head and immunostaining within the neuroecftoderm was not clearly detected in other neuroectodermal areas of the head region.

Finally, to check the specificity of the immunodetection of CAV-1 and GLUT-1 in the brain stem of chick and rat embryos, we performed Western blot and PCR analysis on brain stem protein and RNA extracts respectively, obtained from E5 chick and E13.7 rat embryos, as well as on extracts from the dorsal mesencephalon, as a negative control. The corresponding proteins and RNAs were detected in rat and chick brain stem extracts at the expected molecular mass and nucleotide length respectively (**Figure 3**).

4. DISCUSSION

In adults, CSF composition and homeostasis is controlled

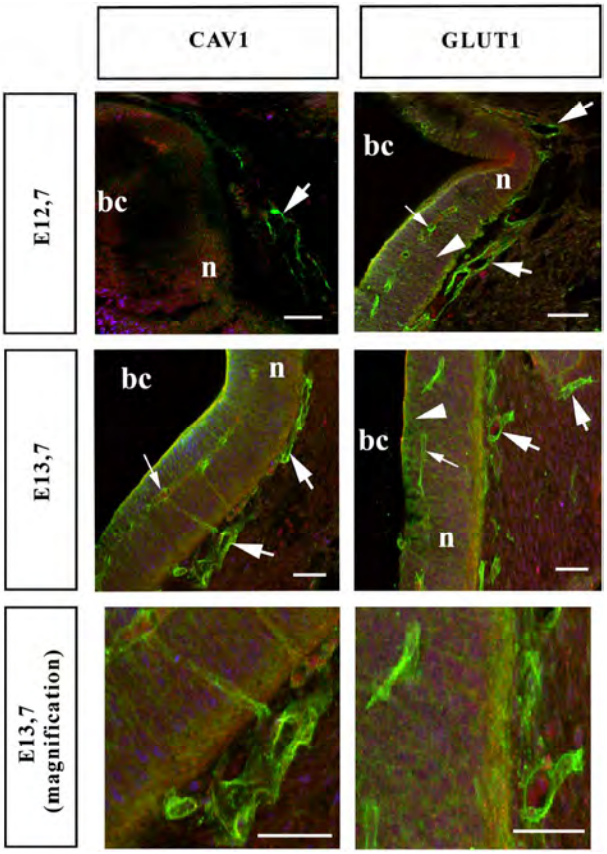

Figure 2. Immunohistochemical localization of CAV-1 and GLUT-1 in the head process of rat embryos at E12.7 and E13.7. Merged confocal image (50 µm thick) of 200 µm vibratome sections. Note the immunoreactive blood vessels immersed within the parenchyma (thick arrows), the immunoreactive vascular sprouts within the neuroectoderm (thin arrows) and the staining within the neuroectoderm (arrowheads), in green. Nuclear counterstaining is shown in blue and cellular counterstaining in red. Last column shows a magnified area from the images of the middle column. Scale bars: 0.1 mm. Abbreviations: bc, brain cavity; n, neuroectoderm.

by the choroid plexus and, to some extent, by BBB-provided vessels within the brain. The relevance of blood-to-brain and blood-to-CSF barriers for CNS development is beginning to be elucidated, although little is known about early embryos. Recently, we demonstrated the presence of blood-barrier-forming vessels in chick and rat embryos, located in the brain stem, lateral to the ventral midline, at the mesencephalon and prosencephalon level. The barrier properties develop between E3 (HH18) and E4 (HH24) in chick embryos and at E12.7 in rat embryos, the equivalent developmental stage in terms of brain vesicle formation. The blood vessels exhibiting these properties, in conjunction with the neuroectoderm adjacent to them, provide an effective blood–CSF barrier for proteins as early as E4 in chick embryos [15], *i.e.* just after the closure of the neuropores,

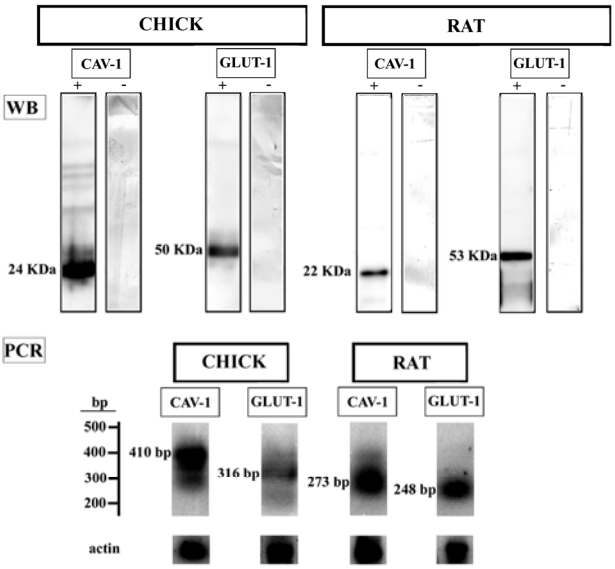

Figure 3. Western blot and PCR analysis of CAV-1 and GLUT-1 in the brain stem (+) of chick and rat embryos at E5 and E13.7 respectively. Negative controls (-) for Western blot were made from the homogenized dorsal mesencephalon of chick and rat embryos at E5 and E13.7 respectively. Actin controls for PCR are also shown.

at a developmental stage at which the neural progenitor cells forming the brain wall exhibit both intense proliferation and the initiation of a period characterized by a high rate of neurogenesis.

Moreover, we also showed that channels for water (AQP1 and AQP4) and ion transport (inwardly rectifying K+ channel Kir4.1) were present in the same blood vessels that carry out barrier functions for blood–CSF protein transport. This observation thus supports the hypothesis that these blood vessels, together with the adjacent neuroectoderm, regulate E-CSF composition and homeostasis [16]. Interestingly, this area does not coincide with the zones from which the adult choroid plexuses form in a subsequent developmental stage [24]. Later in development, during foetal stages, as well as in adults, choroid plexuses and BBB-provided vessels express a wide variety of specific transporters for a broad spectrum of molecules, ranging from proteins to glucose, amino acids, water and ions.

Our findings show that GLUT-1, a glucose transporter, and CAV-1, which is present in caveolae transcellular transport in the adult BBB, are also in blood vessels located in the embryonic blood–CSF barrier in chick and rat embryos at early stages of brain development. That is to say, they are present in blood vessels located in the brain stem, lateral to the ventral midline, at the mesencephalon and prosencephalon level, where protein transport from embryonic serum to the E-CSF and *vice versa* has been described [13]. Moreover, the presence of

blood vessels expressing water and ion channel proteins (*i.e.* AQP1, AQP4 and Kir4.1) has been reported. Thus, double immunostained sections of chick embryos have shown that GLUT-1 and CAV-1 are expressed in the same blood vessels expressing AQP1, which in turn are those that express CAV-4 and Kir4.1, as previously reported [16]. On the basis of our results and those from previous papers, we propose that in mammals these molecules may also be expressed in the same blood vessels, namely those involved in the blood-CSF barrier.

Moreover, GLUT-1 was also detected in the neuroectoderm involved in the embryonic blood–CSF barrier, thereby suggesting that glucose destined for developing brain cells is transported from the blood to the E-CSF by this glucose transporter. Of note, GLUT-1 was not detected in any other location of the brain stem, thus indicating the relevance of this barrier area for E-CSF composition control and homeostasis. Previous reports on GLUT-1 expression [25-27] indicate that this glucose transporter is expressed in mammals (mice in rat) from very early stages of brain development throughout the entire brain neuroectoderm, but that its expression decreases as development proceeds, becoming finally undetectable. In this regard, Dermietzel *et al.* [25] showed that the gradual decrease in GLUT-1 expression is not homogeneous in the neuroectoderm, and that this glucose transporter becomes progressively restricted to some brain areas, including that involved in the blood-CSF barrier, as reported in this paper.

Conversely, AQP1 and AQP4 for water transport, and Kir4.i for ion transport are present solely in these blood vessels [16], but not in the adjacent neuroectoderm. These observations therefore raise questions regarding the mechanisms by which they are transported through this tissue to reach the E-CSF. In this regard, protein transport has been reported to be transcellular [15], but no transcellular transporting structures have been described. Our results demonstrate that CAV-1 is present in the blood vessels and the neuroectoderm forming the embryonic blood–CSF barrier. As caveolae are involved in transcellular transport, we propose that these are the structures by which proteins are transported from blood to E-CSF and *vice versa*. In addition, as caveolae may also transport water and ions alongside proteins, and neither water nor ion transporters have been identified in the embryonic blood–CSF barrier neuroectoderm, it is possible that these molecules, when outside the blood vessels, are transported by the caveolae to the E-CSF, along with transported proteins. However, the lack of functional data do not allow us to support this hypothesis. Finally, CAV-1 was not detected in any other location of the brain stem. This observation also indicates the relevance of this barrier area for E-CSF composition control and homeostasis. It is also important to note that GLUT-1 and CAV-1 were detected at the same time as the development of protein barrier properties in chick embryos at E4, as previously reported [15].

5. CONCLUSIONS

Our results suggest that 1) glucose destined for the developing brain cells is transported from the blood to the E-CSF across endothelial and neuroectodermal cells that form the embryonic blood–CSF barrier via the GLUT-1 glucose transporter; 2) proteins are transported across these embryonic tissues by CAV-1 caveolae–transcellular transport; and 3) water and ions, following transport out of the blood vessels by specific transporters, are taken by CAV-1 caveolae to be transported to the E-CSF along with proteins. Taken together, our results reinforce the hypothesis of an embryonic blood–CSF barrier in both avians and mammals that controls E-CSF composition and homeostasis, *i.e.* protein, water, ion and glucose transport, and acts before the formation of the choroid plexuses, thus contributing to the roles ascribed to the E-CSF in early brain development.

6. ACKNOWLEDGEMENTS

This work was supported by a grant from the "Ministerio de Educación y Ciencia" (BFU2007-62361-FEDER) to DB. MP has a Fellowship grant from the Catalan Government (Generalitat de Catalunya–FI)

REFERENCES

[1] Alonso, M.I., Gato, A., Moro, J.A., Martin, P. and Barbosa, E. (1999) Involvement of sulfated proteoglycans in embryonic brain expansion at earliest stages of development in rat embryos. *Cells Tissues Organs* **165(1)**, 1-9.

[2] Alonso, M.I., Gato, A., Moro, J.A. and Barbosa, E. (1998) Disruption of proteoglycans in neural tube fluid by D-xyloside alters brain enlargement in chick embryos. *The Anatomical Record Part A*, **252(4)**, 499-508.

[3] Desmond, M.E. and Jacobson, A.G. (1977) Embryonic brain enlargement requires cerebrospinal fluid pressure. *Developmental Biology*, **57(1)**, 118-198.

[4] Jelinek, R. and Pexieder, T. (1970) Pressure of the CNS in chick embryo. *Folia morphologica*, **2**, 102-110.

[5] Miyan, J.A., Nabiyouni, M. and Zendah, M. (2003) Development of the brain: A vital role for cerebrospinal fluid. *Canadian Journal of Physiology and Pharmacology*, **81(4)**, 317-328.

[6] Gato, A. and Desmond, M.E. (2009) Why the embryo still matters: CSF and the neuroepithelium as interdependent regulators of embryonic brain growth, morphogenesis and histiogenesis. *Development Biology*, **327(2)**, 263- 272.

[7] Gato, A., Moro, J.A., Alonso, M.I., Bueno, D., De La Mano, A. and Martin. C. (2005) Embryonic cerebrospinal fluid regulates neuroepithelial survival, proliferation, and neurogenesis in chick embryo. *The Anatomical Record*

Part A, **284(1)**, 475- 484.

[8] Parada, C., Martín, C., Alonso, M.I., Moro, J.A., Bueno, D. and Gato, A. (2005) Embryonic cerebrospinal fluid collaborates with the isthmic organizer to regulate mesencephalic gene expression. *Journal of Neuroscience Research*, **82(3)**, 333-345.

[9] Hamburger, V. and Hamilton, H.L. (1951) A series of normal stages in the development of the chick embryo. *Journal of Morphology*, **88**, 49-92.

[10] Parada, C., Gato, A. and Bueno, D. (2005) Mammalian embryonic cerebrospinal fluid proteome has greater apolipoprotein and enzyme pattern complexity than the avian proteome. *Journal of Proteome Research*, **4(6)**, 2420- 2428.

[11] Parada, C., Gato, A., Aparicio, M. and Bueno, D. (2006) Proteome analysis of chick embryonic cerebro-spinal fluid. *Proteomics*, **6(1)**, 1-34.

[12] Zappaterra, M.D., Lisgo, S.N., Lindsay, S., Gygi, S.P., Walsh, C.A. and Ballif, B.A. (2007) A comparative proteomic analysis of human and rat embryonic cerebrospinal fluid. *Journal of Proteomic Research*, **6(9)**, 3537-3548.

[13] Parada, C., Parvas, M. and Bueno, D. (2007) Cerebrospinal fluid proteomes: from neural development to neurodegenerative diseases. *Current Proteomics*, **4**, 89-106.

[14] Parvas, M., Rius, M. and Bueno, D. (2008) Most of the abundant protein fractions of embryonic cerebrospinal fluid are produced out of the brain anlagen. *The Open Proteomics Journal*, **1**, 1-4.

[15] Parvas, M., Parada, C. and Bueno, D. (2008) A blood–CSF barrier function controls embryonic CSF protein composition and homeostasis during early CNS development. *Developmental Biology*, **321(1)**, 51-63.

[16] Parvas, M. and Bueno, D. (2010) The embryonic blood-CSF barrier controls E-CSF osmolarity during early CNS development. *The Journal of Neuroscience Research*, **88(6)**, 1205-1212.

[17] Rubin, L.L. and Staddon, J.M. (1999) The cell biology of the blood brain barrier. *The Annual Review of Neuroscience*, **22**, 11-28.

[18] Frank, P.G., Woodman, S.E., Park, D.S. and Lisanti, M.P. (2003) Caveolin, caveolae, and endothelial cell function. *Arteriosclerosis, Thrombosis, and Vascular Biology*, **23**, 1161-1168.

[19] Virgintino, D., Robertson, D., Errede, M., Benagiano, V., Taure, U., Roncali, L. and Bertossi, M. (2002) Expression of caveolin-1 in human brain microvessels. *Neuroscience*, **115(1)**, 145-152.

[20] Dermeitzel, R. and Krause, D. (1991) Molecular anatomy of the blood brain barrier as defined by immunocytochemistry. In: Jeon, K.W. and Friedlander, M. Eds., *International review of cytology.* Academic Press, New York, 57-109.

[21] Laterra, J. and Goldstein, G.W. (1993) Brain microvessels and microvascular cells *in vitro*. In: Pardridge, W.M. Eds., *The blood-brain barrier*, Raven Press, New York, 1-24.

[22] Pardridge, W.M. and Boado, R.J. (1993) Molecular cloning and regulation of gene expression of blood-brain barrier glucose transporter. In: Pardridge, W.M. Eds., *The blood-brain barrier*, Raven Press, New York, 395-440.

[23] Rahner-Welsch, S., Vogel, J. and Kuschinsky, W. (1995) Regional congruence and divergence of glucose transporters (GLUT1) and capillaries in rat brains. *Journal of Cerebral Blood Flow & Metabolism*, **15**, 681-686.

[24] Bellairs, R. and Osmond, M. (2005) Atlas of Chick Development. Elsevier Academy Press, London.

[25] Dermietzel, R., Krause, D., Kremes, M., Wang, C. and Stevenson, B. (1992) Pattern of glucose transporter (Glut1) expression in embryonic brains is related to maturation of blood-brain barrier tightness. *Developmental Dynamics*, **193**, 152-163.

[26] Harik, S.I., Hall, A.K., Richey, P., Andersson, L., Lundahl, P. and Perry, G. (1993) Ontogeny of the erythroid/HepG2-type glucose transporter (GLUT-1) in the rat nervous system. *Developmental Brain Research*, **72**, 41-49.

[27] Bauer, H., Sonnleitner, U., Lametschwandter, A., Steiner, M., Adam, H. and Bauer, H.C. (1995) Ontogenic expression of the erythroid-type glucose transporter (Glut1) in the telencephalon of the mouse: correlation to the tightening of the blood-brain barrier. *Developmental Brain Research*, **86(1-2)**, 317-325.

[28] Laemmli, U.K, (1970) Cleavage of structural proteins during the assembly of the head of bacteriophage T4. *Nature*, **227**, 680-685.

Advances in Bioscience and Biotechnology, 2010, 1, 322-329 **ABB**
doi:10.4236/abb.2010.14042 Published Online October 2010 (http://www.SciRP.org/journal/abb/).

Gold Nanoparticles for Colorimetric detection of hydrolysis of antibiotics by penicillin G acylase

Neha R. Tiwari[1], Ambrish Rathore[2], Asmita Prabhune[2], Sulabha K. Kulkarni[3]

[1]DST unit on nanoscience and nanotechnology, Dept. of Physics, University of Pune, Pune, India;
[2]Biochemical Sciences Divisions, National Chemical Laboratory, Pune, India;
[3]Indian Institute of Science Education and Research, Pune, India.
Email: rt.neha@gmail.com

Received 23 June 2010; revised 12 July 2010; accepted 24 July 2010.

ABSTRACT

A simple inexpensive method of monitoring hydrolysis of an antibiotic penicillin G (pen G) and subsequent enzyme detection using gold nanoparticles is presented. Gold nanoparticles capped with Cetyl trimethyl ammonium bromide (CTAB) are synthesized using chemical route. The particles could be used for detection of Penicillin G acylase (PGA) enzyme by incorporating hydrolysis reaction with pen G. This hydrolysis reaction leads to a shift in the surface plasmon band of gold nanoparticles from 527 nm to 545 nm accompanied by a visual colorimetric change in the solution from red to blue. The process is attributed to aggregation of nanoparticles caused due to displacement of CTAB bilayer by byproducts of the hydrolysis reaction. It is proposed that the presence of 0.007 mg/ml of PGA can be detected by a color change of gold nanoparticles solution without requiring any complicated instrument or highly trained operator to conduct the test. The method could also identify the presence of different penicillins by showing different spectral shifts. Thus the work presented here would be useful not only for the detection of the pharmaceutically important drug Pen G, but also represents a general methodology for the detection of enzymes, eg PGA.

Keywords: Gold Nanoparticles, Penicillin G Acylase, Aggregation, Colorimetric Detection, Surface Plasmon Resonance

1. INTRODUCTION

Metal nanoparticles based enzymatic assays [1-5] are increasingly becoming popular due to their increased sensitivity as well as rapidness when compared to the conventional methods [6-9]. The potential of gold nanoparticles in this field stems from the phenomenon of surface plasmon resonance (SPR), which is the collective oscillation of free electrons in metal nanoparticles when electromagnetic radiation is incident on them [10]. Based on metal nanoparticles, there are various sensing mechanisms [11-19] which lead to the detection of biomolecules by monitoring changes in the localized surface plasmon resonance (LSPR) extinction. The sensing mechanisms include local refractive index changes, nanoparticle aggregation, charge-transfer interactions at nanoparticle surfaces, resonant Rayleigh scattering from nanoparticles, surface enhanced Raman scattering and plasmon enhanced molecular florescence.

Enzyme biosensing has been achieved using gold nanoparticles [20], pH responsive hydrogels and supramolecular assemblies [21]. Fischer *et al.* [22] used anionically functionalized monolayer protected gold nanoclusters for inhibition of chymotrypsin. Apart from these examples, detection of enzymes such as proteases has been achieved by binding nanoparticles with peptides [1,2]. These peptides lead to assembly of nanoparticles due to their cross linking by long chain molecules. Enzymes specific for these peptides are then introduced which cleave the peptide bond leading to dispersion of nanoparticles. This aggregation–dispersion process leads to the colorimetric changes in the nanoparticle solution. Aggregation of gold nanoparticles leads to red shift in the plasmon band due to the electric dipole-dipole interaction leading to a coupling between the plasmon oscillations of different particles [23]. The color of gold nanoparticle solution turns from red to blue/purple due to red shift in the plasmon band. Here the red shift refers to the shift in the plasmon band towards longer wavelength *i.e* red region of the electromagnetic spectrum. This color change has been used to detect the presence of analytes that induce selective aggregation of gold nanoparticles. The position and intensity of plasmon band is used to monitor this aggregation process.

The results presented in this paper describe detection

of enzyme Penicillin G acylase. Acylases are a group of enzymes that catalyze the cleavage of carbon–nitrogen bonds in amides. Penicillin acylases are members of the N-terminal nucleophile (Ntn) hydrolase superfamily, which share a common fold around the active site and a catalytic residue in the N-terminal position [24,25]. These enzymes are used mainly in the pharmaceutical industry for the production of 6-Aminopenicillinic acid (6-APA), a key intermediate in the production of semi synthetic penicillins and cephalosporins, which are now far the most widely used antibiotics. In addition, these enzymes are very useful as biocatalysts in some important reactions like peptide synthesis [26,27], and also in the resolution of clinically active compounds [28,29]. Penicillin acylases specifically catalyse hydrolysis of Penicillins. For each type of penicillin, there exists an enzyme which performs this hydrolysis reaction. Penicillin G acylase (PGA) is a specific enzyme for an important drug, Penicillin G (Pen G).The hydrolysis reaction of penicillins by penicillin acylases leads to breaking of its molecules into different byproducts, thereby leading to consumption of penicillins. All the enzymatic assays quantify consumption of the respective penicillins or detect the formation of byproducts over time. Enzymatic activity, which is the measure of amount of active enzymes in the solution, is then determined using such different kinds of assays. The earliest procedures to assay penicillin acylase activity are tedious and time consuming [7,30-33]. Some of these include paper chromatography [6], gas chromatography [34], assays using 6-nitro-3-(phenylacetamido) benzoic acid (NIPAB) [35], titrimetric determination using pH stat [8] etc. Methods stated above either require expert operators or expensive instruments or reagents e.g. NIPAB.

Our method consists of detecting 6-Aminopenicillin acid, which is a byproduct in hydrolysis of pen G, and in turn assaying PGA without any chromogenic reagent. There is a distinct color change observable in the gold nanoparticle solution with naked eyes from initial red to final blue, when the pen G hydrolysis reaction is performed by PGA in the presence of gold nanoparticles. Although various enzymes have also been detected by using nanoparticles as probes, there are no reports of detection of Penicillin acylases using nanoparticles. We indeed use various sophisticated techniques like TEM, UV-VIS spectroscopy in order to investigate the biosensing mechanism using gold nanoparticles. However, once this test is acceptable, in practice only colorimetric changes can be used to detect the presence of PGA.

2. EXPERIMENT

2.1. Reagents

Chloroauric acid trihydrate ($HAuCl_4.3H_2O$) and CTAB was obtained from Thomas Baker, India and Molychem, India respectively. Penicillin G (pen G) was obtained from Hindustan Antibiotics Limited, Pune, India. Enzyme penicillin G acylase (PGA) was purified from the gram-positive bacteria *Arthrobacter viscosus* (ATCC 15294). The enzyme was produced extracellularly in the culture broth. The cells were separated by centrifugation, and the clear broth was used for further purification by hydrophoric chromatography (octyl sepharose) followed by anion exchange chromatography (Q-sepharose). Purity of the enzyme was checked by native as well as SDS-PAGE (not shown for the brevity). The concentration of enzyme used was 0.7 mg/ml, so in 10 µl of solution, 7 µg of enzyme is present.

2.2. CTAB Capped Gold Nanoparticles

CTAB capped gold nanoparticles were synthesized by reducing aqueous solution of 5×10^{-4} M $HAuCl_4$ (10 ml) containing 0.2 M CTAB with 1×10^{-2} M ice cold $NaBH_4$ (0.6 ml). The solution was stirred for 3 hours and then kept at room temperature for 3 days. 10 µl of enzyme solution was added to 2 ml of gold nanoparticles solution followed by addition of 100 µl of substrate pen G (100 mg/ml). The solution was kept at 40 deg for 10 min. Absorption spectra were recorded after each step.

2.3. PGA Enzyme Assay

The enzyme activity of PGA was determined by measuring the amount of aminopenicillic acid (6-APA) produced in a reaction mixture containing 10 mg ml^{-1} penicillin G in 0.1 M phosphate buffer, pH 7.0, when incubated at 40˚C [36]. The 6-APA produced was estimated spectrophotometrically at 415 nm, after reaction with p-dimethylaminobenzaldehyde (PDAB), according to [7], modified by [37]. One unit of PGA activity is defined as the amount of enzyme required to produce 1 µmole of 6-APA per minute under the assay conditions (40˚C and pH 7.0)

2.4. Characterization

Absorption spectra of the samples were recorded in solution form on Perkin Elmer lambda 950 instruments in the range 200 to 800 nm. TEM images are acquired on Philips CM200 instrument with an accelerating voltage of 120 KV. For TEM analysis, samples were drop coated on copper grids and were allowed to dry for 45 minutes.

3. RESULTS AND DISCUSSION

CTAB capped nanoparticles have rarely been investigated for biosensing purposes due to the fact that CTAB bilayers are not easily displaced by biomolecules and hence are difficult to handle as far as bioconjugation is concerned. On the other hand, CTAB capped nanoparti-

cles are chemically more stable and would have a longer shelf life. In the present report we could observe the reaction between enzyme penicillin G acylase (PGA) and pen G in the solution of CTAB capped gold nanoparticles.

Plasmon resonance band of CTAB capped gold nanoparticles was observed at 527 nm. Gold nanoparticles synthesized here are covered with a bilayer of CTAB [38]. Inner layer is bound to the gold surface via the headgroup and is connected to the outer layer through the hydrophobic interactions while the headgroups of the outer layer are in the aqueous medium. Headgroup of the CTAB chain consists of an amine group. Hence, protonated amine group is present on the outermost surface of CTAB capped gold nanoparticles. No change in the absorption peak position of the gold was observed on addition of enzyme PGA (10 µl, 0.7 mg/ml). However, on addition of 100 µl of pen G (100 mg/ml), the plasmon band shifted from 527 nm to 545 nm (**Figure 1(a)**). After the addition, the solution was kept at 40˚C for 10 min to allow the reaction to occur completely. The experiment was also performed with different concentration of enzymes (**Figure 1(b)**). The red shift was found to gradually increase on increasing the concentration of enzyme from 0.007 mg/ml to 0.7 mg/ml. The concentration of pen G in this case was same as in **Figure 1(a)** *i.e* 100 mg/ml. The spectral shifts are thus sensitive for enzyme concentration as low as 0.007 mg/ml. **Figure 1(c)** shows gradual shifts in the plasmon band as the amount of pen G is increased from 10 to 100 µl (1 to 10 mg of pen G). The extinction spectrum started changing after an addition of 10 µl of pen G and on addition of 100 µl pen G it red shifted by 18 nm. The total red shift obtained after adding 100 µl of pen G varied in the range of 17 to 23 nm on repeating the experiment several times. Also, the spectrum was recorded four hours after the addition of pen G (**Figure 1(d)**). The plasmon band was found to be gradually shifted towards the longer wavelength (572 nm) and decreased in intensity. The gradual shift in the absorption band is attributed to slow removal of remaining CTAB layers from gold nanoparticles. After the complete displacement of CTAB,

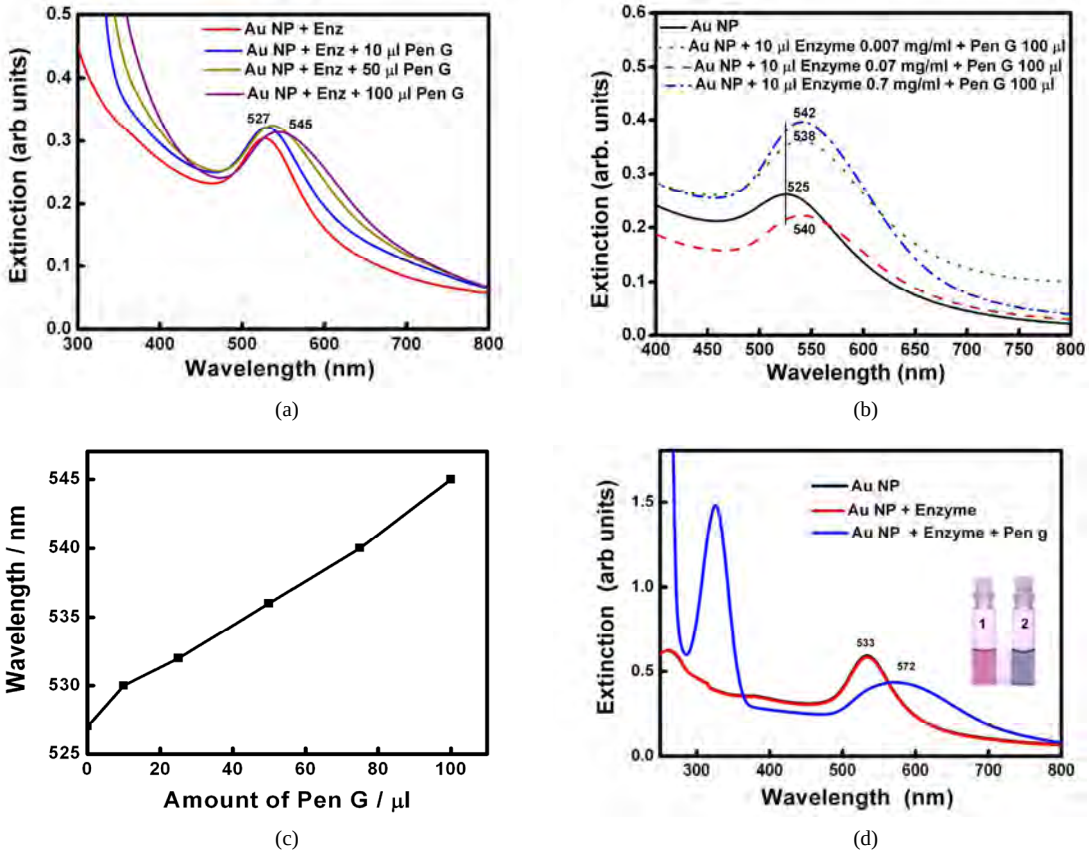

Figure 1. (a) changes in spectra on addition of different amounts of Pen G when the enzyme conc. is 0.69 mg/ml, (b) Changes in spectra after addition of different conc. of enzyme when the Pen G concentration is 100 mg/ml (c) Shift in extinction maximum of Au nanoparticles Vs. amount of Pen G (100 mg/ml) and (d) Spectra acquired after 4 hour of addition of Pen G. Inset shows change in the color of the Au nanoparticle solution (1) before and (2) after the enzyme-pen G addition.

the particles precipitate at the bottom of the bottle leaving clear supernatant. Peak at 322 nm is attributed to the absorption due to the penicillin G. Broadening of plasmon band along with decrease in the extinction intensity was also observed.

The spectral shifts in the surface plasmon band are accompanied by changes in the color of gold nanoparticle solution from red to blue (**Figure 1(d)** inset). Color of the solution started changing from red to dark pink after an addition of 10 µl of the pen G. However, on the addition of 25 µl Pen G, the color was purple. The purple color intensified on further addition of pen G. The figure shows the change in color after adding 100 µl of pen G.

The prominent shift in the plasmon band of gold nanoparticles can be attributed to the aggregation of nanoparticles. **Figure 2** shows TEM images of gold nanoparticles before and after the addition of the enzyme and the pen G. Size of gold nanoparticles was found to be ~15 nm. Particles are well dispersed before the addition of enzyme and pen G. On addition of the enzyme and pen G to gold nanoparticle solution, aggregation of particles is observed. TEM image, red shift in the plasmon band and the color change in the gold nanoparticle solution together indicate aggregation of gold nanoparticles.

Reaction occurring between the enzyme and the pen G is schematically shown in **Scheme 1**. PGA specifically catalyses the hydrolysis of the amide bonds in pen G. Cleavage of amide bond in pen G by PGA is accompanied by the formation of 6-aminopenicillanic acid (6-APA) and phenylacetic acid (PAA).

In order to confirm the mechanism of aggregation of gold nanoparticles due to enzyme-pen G reaction, we added just the products of this reaction to the solutions. 6-APA, PAA and mixture of 6-APA and PAA were added separately to the nanoparticle solutions in the absence of enzyme and pen G, and spectral changes were recorded (**Figure 3**). Interestingly, the color changes were obtained in the presence of 6-APA only. PAA (100 µl, 2.5mM) alone was not able to induce the color changes (**Figure 3(b)**). On addition of 6-APA (100 µl, 2.5 mM), no change in the spectral peak position was obtained

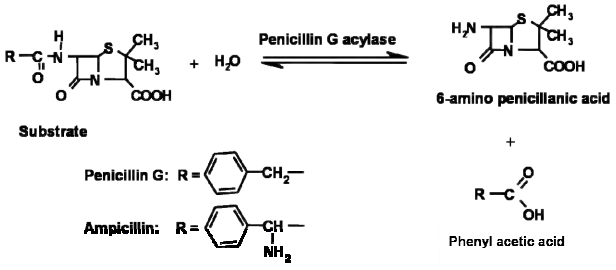

Scheme 1. Penicillin G Acylase catalysed hydrolysis of Penicillins.

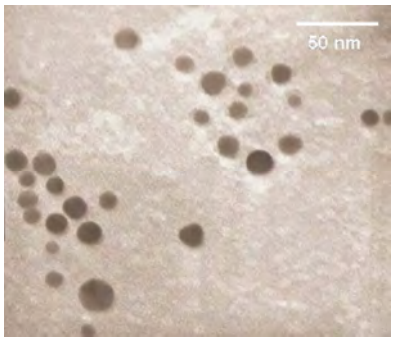

(a)

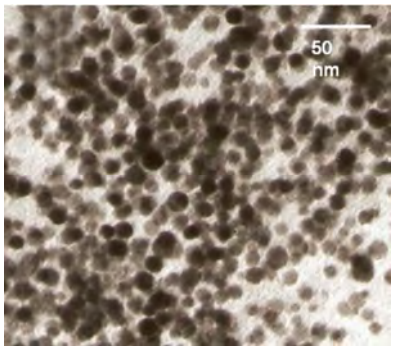

(b)

Figure 2. TEM images of (a) gold nanoparticles and (b) gold nanoparticles + enzyme + substrate.

immediately, however the plasmon band shifted from 527 to 565 nm after keeping the solution for two hours. Addition of mixture of 6-APA and PAA (same concentrations as mentioned above) to gold nanoparticle solution caused the plasmon band to shift from 527 to 545 nm immediately and to 600 nm finally after three hours. This was also accompanied by broadening of the plasmon band. This trend is very much similar to that obtained in the presence of enzyme and substrate pen G (see **Figure 1**). The spectral and colorimetric changes were obtained immediately when both acids were together added to the gold nanoparticle solution, which is also happening when the reaction is done in the presence of enzyme and the pen G. This indicates that the gold nanoparticles are sensing hydrolysis of the pen G. Hence, the combination of acids produced during the hydrolysis and the amount of 6-APA produced should be the key factor in determining the spectral and colorimetric changes produced in the nanoparticle solution due to the enzyme-substrate chemistry. This is further supported by the fact that the extent of red shift increases when we increase the concentration of enzyme PGA (**Figure 1(b)**). This is due to the increase in the amount of 6-APA produced.

The mechanism of sensing hydrolysis reaction can be

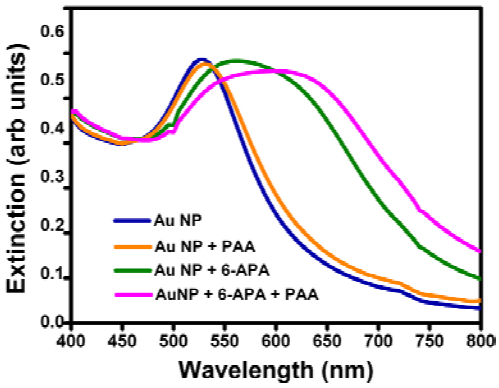

(a)

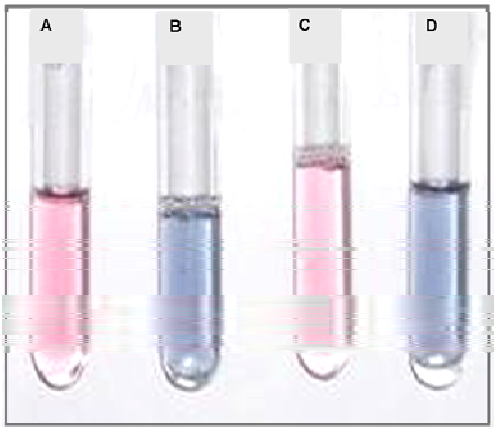

(b)

Figure 3. (a) UV-Vis spectra of gold nanoparticles, gold nanoparticles + PAA, gold nanoparticles + 6-APA and gold nanoparticles + 6-APA + PAA and (b) Photograph of (A) gold nanoparticles (B) gold nanoparticles + 6-APA (C) gold nanoparticles + PAA and (D) gold nanoparticles + 6-APA + PAA.

explained by **Scheme 2**. As mentioned earlier, a CTAB bilayer is present on the surface of gold nanoparticles such that N^+ group are present on both the ends. This bilayer is responsible for the stable dispersion of gold nanoparticles in the solution. When pen G is added to gold nanoparticle solution in presence of enzymes, specific interaction between enzyme and pen G occurs, leading to hydrolysis of pen G and formation of 6-APA and PAA. Since the colorimetric changes are obtained only after the addition of pen G, we propose that electrostatic interaction between CTAB and the products of hydrolysis (6-APA and PAA) cause partial removal of CTAB bilayer from gold nanoparticles leading to a decrease in their surface potential and hence aggregation. The dependence of the interparticle distance on the surface plasmon band of metal nanoparticles is well known [23,24]. Aggregated or assembled nanoparticles display red shift in the plasmon band when compared to the isolated gold nanoparticles. This phenomenon is attributed to the coupling between the dipole modes of plasmons of different particles. As the interparticle distance is decreased, more red shift in the plasmon band is observed due to an increase in the extent of coupling. A decrease in the interparticle distance after the completion of enzyme–pen G reaction is clearly observed in the TEM images (**Figure 2**). Along with the coupling of plasmon modes, contribution to the red shifting of plasmon band also comes from increased scattering of nanoparticle aggregates in the longer wavelength region [25].

Some of the previously reported work [1] have used thiol containing Cys functionalized gold nanoparticles and an assembly directing actuator to control the assembly of nanoparticles through pi-stacking interactions. Upon hydrolysis by enzymes, disassembly was observed due to increased repulsion between NH_3^+ groups and removal of the hydrophobic interactions between the actuator. This disassembly caused blue shift in the extinction spectrum of gold nanoparticles. It is noteworthy that we have not used any assembly directing ligand to control the assembly of gold nanoparticles. Also, in our case, the cleavage of pen G is actually leading to a red shift in the plasmon resonance band. This indicates that the products formed by the enzyme pen G reaction decrease the electrostatic repulsion between particles causing their aggregation.

In order to check the effect in the absence of enzyme PGA, UV-Vis spectrum of gold nanoparticles was acquired when the Pen G was added to the gold nanoparticle solution without enzyme PGA in it (**Figure 4**). 100 µl of pen G was added to 2 ml of gold nanoparticle solution and spectrum was recorded. On addition of penicillin G, spectral shift of only 2 nm was observed indicating that the aggregation is induced only by the product of enzyme–substrate reaction and not just by the presence of pen G. No change in the color of the solution was immediately observed in this case.

The activity of enzyme was also checked by estimating the amount of 6-aminopenicillanic acid (6-APA) in the reaction. The enzyme was found to be active after the reaction.

Same experiments were performed by changing the penicillin in the reaction (**Figure 5**). Instead of pen G, ampicillin was added to the gold nanoparticle-enzyme solution. Ampicillin differs from the Pen G in the sense that one extra amino group is present on α-carbon (**Scheme 1**). Enzyme penicillin acylase has less affinity towards ampicillin as compared to pen G. The reason for this lies in the action of the enzyme. The enzymes are folded in specific conformation with very unique active sites in which only particular penicillin can fit very

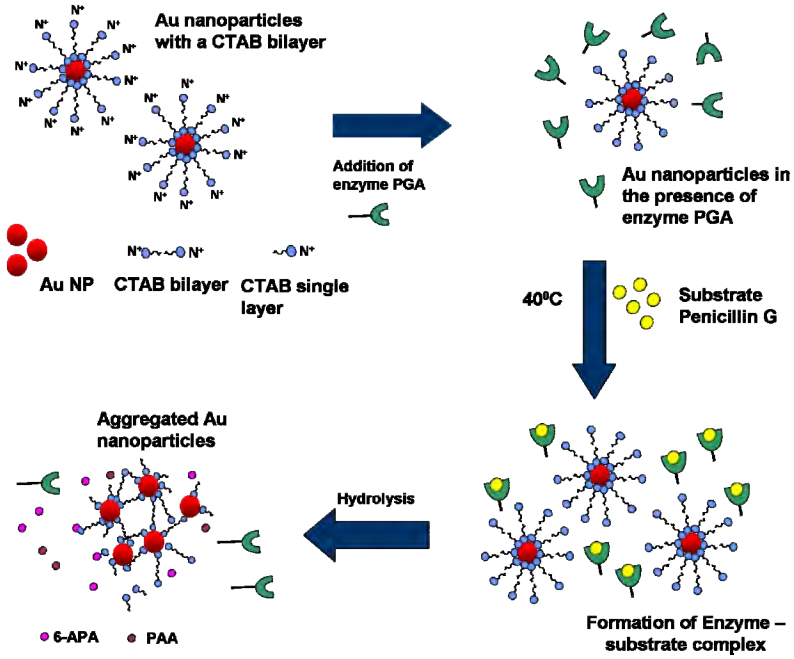

Scheme 2. Schematic showing the mechanism of detection of enzyme.

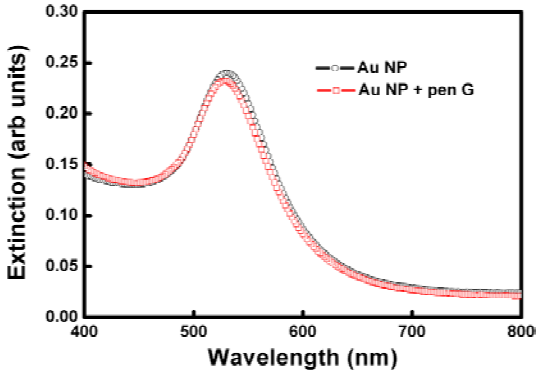

Figure 4. Absorption spectra of gold nanoparticles before and after addition of substrate Pen G in the absence of enzyme.

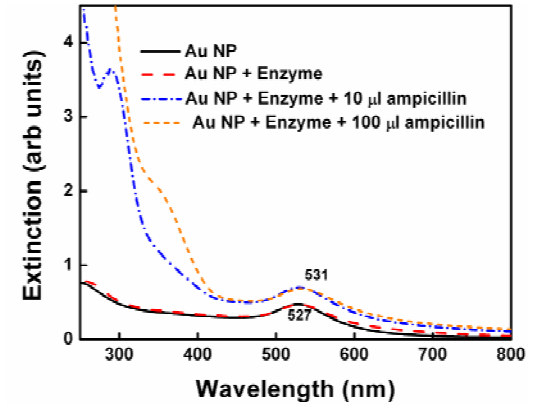

Figure 5. Spectral changes in gold nanoparticle-enzyme system on addition of ampicillin.

properly. Due to one extra amino group in ampicillin, the side chain becomes little bulkier compared to that in Pen G and cannot fit into the active site properly. Hence, PGA cannot react to the same extent on amide bond in ampicillin as it does with pen G and so it has less activity. Therefore, rate of enzyme penicillin complex formation is expected to decrease significantly. Indeed, in this case, the spectral shift obtained was only 5 nm and color changes were not obtained. Since, PGA catalyses the hydrolysis of pen G more efficiently than ampicillin, higher spectral shift was obtained in case of pen G.

4. CONCLUSIONS

In conclusion, we have reported here the colorimetric detection of Penicillin G acylase (PGA) without adding any chromogenic agent and eventually penicillin G (pen G) using CTAB capped gold nanoparticles. Gold nanoparticle aggregation is induced by interaction between PGA and pen G causing red to blue color shift of the gold nanoparticles. Aggregation of Au nanoparticles was confirmed by TEM. The aggregation was found to be caused by 6-aminopenicillic acid (6-APA), produced as a reaction product in the reaction. Also, the above effect was not observed in the absence of enzyme indicating that the aggregation of gold nanoparticles is caused by the enzyme- pen G reaction and not just by the presence of enzyme or pen G. To further confirm this, the experiment was also performed with another penicillin substrate (ampicillin) which is not a preferred substrate for PGA and it was observed that the spectral

changes are less and slower. Quantity of enzyme, which could be detected, was 0.007 mg/ml in gold nanoparticles solution. Hence using gold nanoparticles, simple, rapid and colorimetric detection of PGA at low concentrations could be achieved by making use of enzyme-substrate chemistry. Apart from this, the system could also identify the presence of different penicillins (pen G and ampicillin) by showing different degrees of spectral shifts for them. This method will be useful to detect other impurities in the penicillins by change in the SPR.

5. ACKNOWLEDGEMENTS

N R Tiwari would like to thank DST, India for financial support. S K Kulkarni would like to thank DST, India, UGC, India for constant support. This project has been supported by DST, India and Indo-US (AOARD-06-4045) project.

REFERENCES

[1] Laromaine A., Koh L., Murugesan M., Ulijn R.V. and Stevens, M.M. (2007), Protease triggered dispersion of nanoparticle assemblies. *Journal of the Amemirican Chemical Society*, **129(14)**, 4156-4157.

[2] Guarise, C., Pasquato, L., De Filippis, V. and Scrimin, P. (2006) Gold nanoparticles based protease assay. *Proceedings of the National Academy of Sciences*, **14**, 3978-3982.

[3] Zhang, X., Guo, Q. and Cui, D. (2009) Recent advances in Nanotechnology applied to biosensors. *Sensors*, **9(2)**, 1033-1053

[4] Li, Y., Schluesener, H.J. and Xu, S. (2010) Gold nanoparticles based biosensors. *Gold Bulletin*, **43 (1)**, 29.

[5] Liu, R., Teo, W., Tan, S., Feng, H., Padmanabhan, P. and Xing, B., (2010) Metallic nanoparticles bioassay for *Enterobacter cloacae* P99 β-lactamase activity and inhibitor screening. *Analyst*, **135(5)**, 1031.

[6] Batchelor, F.R., Chain, E.B., Hardy, T.L., Mansford, K.R.L. and Rolinson, G.N. (1961) 6-Aminopenicillanic acid. III. Isolation and purification. *Proceedings of Royal SocietyB*: *Biological science*, **154**, 498-508.

[7] Bomstein, J. and Evans, W.G. (1965). Automated colorimetric determination of 6-Aminopenicillanic Acid in fermentation media. *Analytical Chemistry*, **37**, 576-578.

[8] Sjoberg, G., Nathorst-Westfelt, L. and Ortengreen, B. (1967). Enzymatic hydrolysis of some penicillins and cephalosporins by *Escherichia coli* acylase. *Acta Chemica Scandinavica*, **21(2)**, 547-551.

[9] Baker, W.L. (1980). A note on the detection of penicillin acylase activity in *Escherichia coli* by the reaction of ampicillin with Buiret Reagent. *The Journal of Applied Bacteriology*, **49(2)**, 225-229.

[10] Mulvaney, P. (1996). Surface plasmon spectroscopy of nanosized metal particles. *Langmuir*, **12**, 788-800.

[11] Riboh, J.C., Haes, A.J., McFarland, A.D., Yonzon, C.R. and Van Duyne, R.P. (2003). A nanoscale optical biosensor: real-time immunoassay in physiological buffer enabled by improved nanoparticle adhesion. *The Journal of Physical Chemistry B.*, **107**, 1772-1780.

[12] Nusz, G., Marinakos, S., Curry, A., Dahlin, A., Hook, F., Wax, A. and Chilkoti, A. (2008) Label-Free plasmonic detection of biomolecular binding by a single gold nanorod. *Analytical Chemistry*, **80(4)**, 984-989.

[13] Storhoff, J.J., Mucic, R.C., Letsinger, R.L., Mirkin, C.A.. (1997). Selective colorimetric detection of polynucleotides based on the distance-dependent optical properties of gold nanoparticles. *Science*, **277(5329)**, 1078-1080.

[14] Kalele, S.A., Ashtaputre, S.S., Hebalkar, N.Y., Gosavi, S.W., Deobagkar, D.N., Deobagkar, D.D. and Kulkarni, S.K. (2005). Optical detection of antibody using silica-silver core-shell particles. *Chemical Physics Letters*, **404(1-3)**, 136-141.

[15] Kalele, S.A., Kundu, A.A., Gosavi, S.W., Deobagkar, D.N., Deobagkar, D.D. and Kulkarni, S.K. (2006). Rapid detection of escherichia coli by using antibody-conjugated silver nanoshells. *Small*, **2(3)**, 335-338.

[16] Jena, B. and Raj, C. (2008) Optical sensing of biomedically important polyionic drugs using nano-sized gold particles. *Biosensors and Bioelectronics*, **23(8)**, 1285-1290.

[17] Hossain, M., Huang, G., Kaneko, T. and Ozaki, Y. (2009) Characteristics of surface-enhanced Raman scattering and surface-enhanced fluorescence using a singleand a double layer gold nanostructure. *Physical Chemistry Chemical Physics*, **11(34)**, 7484.

[18] Kneipp, K., Kneipp, H., Itzkan, I., Dasari, R.R. and Feld, M.S. (1999). Ultrasensitive chemical analysis by raman spectroscopy. *Chemical Review*, **99(10)**, 2957-2975.

[19] Aslan, K., Lakowicz, J.R. and Geddes, C.D. (2005). Metal-enhanced fluorescence using anisotropic silver nanostructures: Critical progress to date. *Analytical and Bioanalytical Chemistry*, **382(4)**, 926-933.

[20] Liu, J. and Lu, Y. (2004). Adenosine-dependent assembly of aptazyme-functionalized gold nanoparticles and its application as a colorimetric biosensor. *Analytical Chemistry*, **76(6)**, 1627-1632.

[21] Ulijn, R.V. (2006). Enzyme-responsive materials: a new class of smart biomaterials. *Journal of Materials Chemistry*, **16**, 2217-2225.

[22] Fischer, N.O., McIntosh, C.M., Simard, J.M. and Rotello, V.M. (2002). Supramolecular chemistry and self-assembly special feature: inhibition of chymotrypsin through surface binding using nanoparticle-based receptors. *The Proceedings of the National Academy of Sciences*, **99(8)**, 5018-5023.

[23] Storhoff, J.J., Lazarides, A.A., Mucic, R.C., Mirkin, C.A., Letsinger, R.L. and Schatz, G.C. (2000). What controls the optical properties of DNA-linked gold nanoparticle assemblies? *Journal of American Chemical Society*, **122**, 4640.

[24] Brannigan, J.A., Dodson, G., Duggleby, H.J., Moody, P.C., Smith, J.L., Tomchick, D.R. and Murzin, A.G. (1995). A. protein catalytic framework with an N-terminal nucleophile is capable of self-activation. *Nature*, **378(6555)**, 416-419.

[25] Duggleby, H.J., Tolley, S.P., Hill, C.P., Dodson, E.J., Dodson, G.G. and Moody, P.C.E. (1995). Penicillin acylase has a single aminoacid catalytic center. *Nature*, **373**, 264-268.

[26] Arroyo, M., de la Mata, I., Acebal, C. and Pilar Castillôn,

M. (2003). Biotechnological application of penicillin acylases: State-of-the-art. *Applied Microbiology and Biotechnology*, **60(5)**, 507-514.

[27] Phadtare, S., Parekh, P., Gole, A., Patil, M., Pundle, A., Prabhune, A. and Sastry, M. (2002). Penicillin G acylase-fatty lipid biocomposite films show excellent catalytic activity and long term stability/reusability. *Biotechnology Progress*, **18(3)**, 483-488.

[28] Fadnavis, N.W., Sharfuddin, M. and Vadivel, S.K. (1999). Resolution of racemic 2-amino-1-butanol with immobilised penicillin G acylase. *Tetrahedron Asymmetry*, **10(23)**, 4495-4500.

[29] Van Langen, L.M., Oosthoek, N.P., Guranda, D.T., van Rantwijk, F., Svedas, V.K. and Sheldon, R.A. (2000). Penicillin acylase-catalyzed resolution of amines in aqueous organic solvents. *Tetrahedron Asymmetry*, **11(22)**, 4593.

[30] Shaikh, K., Talati, P.G. and Gang, D.M. (1973). Spectrophotometric method for the estimation of 6-aminopenicillanic acid. *Antimicrobial Agents and Chemotherapy*, **3**, 194.

[31] Daumy, G.O., McColl, A.S. and Apostolakos, D. (1982). Repression of penicillin G acylase of Proteus rettgeri by tricarboxylic acid cycle intermediates. *The Journal of Bacteriology*, **152(1)**, 104.

[32] Tewari, Y.B. and Goldeberg, R.N. (1988). Thermodynamics of the conversion of penicillin G to phenylacetic acid and 6-aminopenicillanic acid. *Biophysical Chemistry*, **29(3)**, 245-252.

[33] Szewczuk, A., Siewinski, M. and Slowinska, R. (1980). Colorimetric assay of penicillin amidase activity using phenylacetyl-aminobenzoic acid as substrate. *Analtical Biochemistry*, **103(1)**, 166-169.

[34] Chiang, D. and Bennet, R.E. (1967). Purification and properties of penicillin amidase from bacillus megaterium. *The Journal of Bacteriology*, **93**, 302-308

[35] Kutzbach, C. and Rauenbusch, E. (1974). Preparation and general properties of crystalline penicillin acylase from *Escherichia coli* ATCC 11105. *Hoppe-Seyler's Zeitschrift für physiologische Chemie*, **355**, 45-53.

[36] Balasingham, K., Warburton, D., Dunnill, P. and Lilly, M.D. (1972). The isolation and kinetics of penicillin amidase from *Escherichia coli*. *Biochimica et Biophysica Acta*, **276(1)**, 250-256.

[37] Shewale, G.J., Kumar, K.K. and Ambekar, G.R. (1987). Evaluation of determination of 6-aminopenicillanic acid by p-dimethyl aminobenzaldedyde. *Biotechnological Techniques*, **1**, 69-72.

[38] Nikoobakht, B. and El-Sayed, M.A. (2007). Evidence for bilayer assembly of cationic surfactants on the surface of gold nanorods. *Langmuir*, **17**, 6368-6374.

Advances in Bioscience and Biotechnology, 2010, 1, 330-337 **ABB**
doi:10.4236/abb.2010.14043 Published Online October 2010 (http://www.SciRP.org/journal/abb/).

Sponge-associated bacteria of Lakshadweep coral reefs, India: resource for extracellular hydrolytic enzymes

Annie Feby[1], Shanta Nair[2]

[1]Microbiology Laboratory, National Institute of Oceanography-Regional Centre, Kochi, India;
[2]Microbiology Laboratory, National Institute of Oceanography, Goa, India.
Email: shanta@nio.org

Received 8 July 2010; revised 19 July 2010; accepted 31 July 2010.

ABSTRACT

Sponges (Phylum: Porifera) is one of the major groups in the Lakshadweep coral reefs. These sponges harbor diverse bacteria with metabolic potentiality. From biodiversity to biotechnological prospecting, scientific investigations related to sponge associated microorganisms have expanded, but remain rather limited to few geographic locations. In this study, culturable bacteria associated with two demosponges viz *Dysidea granulosa, Sigmadocia fibulata* and the ambient water were screened for commercially important enzymes such as amylase, protease, gelatinase, lipase, deoxyribonucleic, phosphatase and urease. Amylase and phosphatase were the predominant enzymes produced by >80% of sponge-associated bacteria compared to the ambient water. Nearly 50% of the sponge-associated bacteria expressed multiple enzymatic activities (≥ 4) with variation in the percentage of expression of individual enzymes. More than 65% of the culturable heterotrophic bacteria associated with sponges were Gammaproteobacteria. The order Vibrionales was the main source for multiple enzyme production. Sponge associated bacteria formed more closely related clusters than the water isolates based upon their activity pattern. High recovery of sponge-associated bacteria with multiple enzymatic activities suggest that these versatile bacteria are yet unexploited potential for bioprospecting.

Keywords: Sponge-Associated Bacteria; Extracellular Hydrolytic Enzyme; Coral Reef; Lakshadweep

1. INTRODUCTION

Coral reefs are highly productive natural ecosystem and provide an excellent habitat for a vast array of marine organisms due to their structure, efficient biological recycling and high retention of nutrients [1]. Class Demospongiae comprises about 85% of the living sponges and is a major component of benthic community in the coral reef ecosystem [2]. Sponges filter 24,000 L of sea water kg^{-1} day^{-1}, resulting in colonization of large number of extracellular bacteria on the surface and internal mesohyl matrix. In addition, these unique ecological niches have copious amount of particulate organic matter [3,4]. A single sponge host can be inhabited by diverse bacteria. Bacteria which constitute 40% of the sponge volume [5] produce extracellular hydrolytic enzymes that facilitate the metabolism of complex organic matter thereby assisting the host in nutrition and various metabolic processes. Bacterial enzymes provide a greater diversity of catalytic activity and can be produced economically. Currently bacteria from terrestrial sources are employed for industrial production of enzymes. Sponges are considered as microbial fermenters that provide exciting new avenues in marine microbiology and biotechnology [6]. Although, the potentialities of hydrolytic enzymes from marine bacteria have been recognized, studies on enzymes from bacteria associated within the microhabitats of sponge for biotechnological application are rare [7]. We hypothesize that sponge associated bacteria are excellent source of not only enzymes but also multiple extracellular hydrolytic enzymes than seawater bacteria due their characteristic nutrient rich microhabitat provided by the host organism. The present study is the first of its kind which focuses on bioprospecting on various degrading enzymes from culturable heterotrophic marine bacteria associated with two sponges viz. *Dysidea granulosa* and *Sigmadocia fibulata* and ambient seawater in the Lakshadweep Islands. These bacteria can be effectively cultivated in culture media for production of enzymes.

2. MATERIALS AND METHODS

2.1. Sample Collection

In this study, we examined the bacterial composition of

two sponges, *Dysidea granulosa* Bergquist, 1965 and *Sigmadocia* (*Haliclona*) *fibulata* Schmidt, 1862 (here after mentioned in this article as *Sigmadocia fibulata*) belongs to Phylum: Porifera; class: Demospongiae; subclass: Ceractinomorpha. *D. granulosa* belongs to the order Dictyoceratida and *S. fibulata* belongs to the order Haplosclerida. Sponges and ambient seawater were collected from two locations, one outside the lagoon (10° 34' 25.64" N; 72° 38' 57.48" E) and the other inside the lagoon (10° 34' 44.51" N; 72° 38' 24.11" E) of Kavaratti Island, Lakshadweep, west coast of India (**Figure 1**) by SCUBA diving. These two species of sponges are very distinctive in gross morphology and microhabitat. Sponges were transferred immediately to Whirlpak sterile sampling bags (Nasco) and sealed underwater to prevent contact with air and possible oxidation and contamination. Ambient seawater was collected using 1.8L Niskin water sampler within 1m of the sponge colony and transferred to Whirlpak sterile sampling bags. Samples were processed within 2-3 hours of collection.

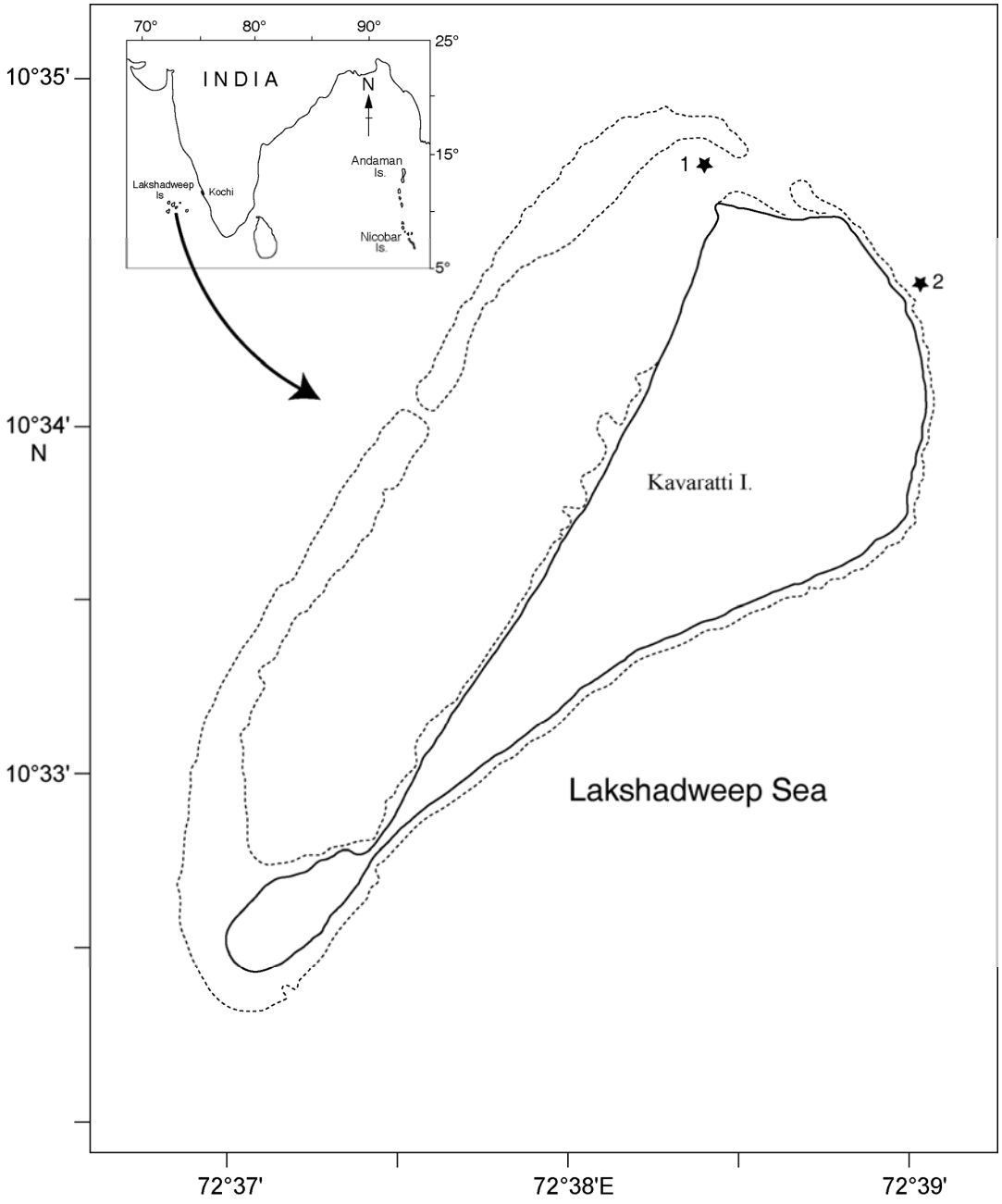

Figure 1. Map of Kavaratti Island, India showing sampling site 1 (inside the lagoon) and 2 (out side the lagoon).

2.2. Bacterial Isolation

Sponges were washed thoroughly with autoclaved; filter sterilized (0.22 µm-pore size filter) seawater until visibly free of debris and sediments. They were then homogenized using sterile mortar and pestle. Serially diluted sponge homogenate and direct sub samples of ambient water were spread plated onto various media differing in composition and concentration. Zobell marine agar was prepared in distilled water, nutrient broth of varying strength (100%, 50%, 25%, 10%) supplemented with 1.5% agar, OLIGO media (0.005% yeast extract, 0.05% tryptone, 0.01% sodium glycerophosphate, 1.2% Noble agar) prepared in seawater [8] were the different media employed for bacterial isolation. All plates were incubated at 28°C for 7 days. Random selection allowed a comprehensive collection of culturable heterotrophic bacteria found in this ecosystem. Pure cultures were cryopreserved in glycerol broth at –80°C. Bacterial isolates were identified using standard methods described [9,10].

2.3. Detection of Enzymatic Activity

Bacteria were screened for various hydrolytic enzymes such as amylase, protease, deoxyribonuclease, gelatinase, lipase, phosphatase and urease. Pure cultures were inoculated on plates supplemented with respective substrates and incubated at 28°C for 3 days and presence or absence of enzymatic activity were detected using the methods described below.

2.3.1. Amylase

Nutrient agar supplemented with 0.2% soluble starch were used to screen for amylase production. After incubation the plate was flooded with lugol's iodine solution. Presence of clear zone around the culture was taken as positive result and formation of blue color in the medium surrounding the colony was the negative reaction.

2.3.2. Protease

Skim milk (5%, final concentration) incorporated in nutrient agar was used as the screening medium. Clear zone around the bacterial colony after incubation indicated hydrolysis of casein, which is the positive reaction. No zone around the colony indicates negative reaction.

2.3.3. Deoxyribonuclease

DNase test agar base (Himedia, India) contains 0.2% DNA in final concentration (wt/wt). After incubation, DNase plate was flooded with 0.1% toluidine blue solution. Blue characteristic precipitate formed on bacterial colony is the positive reaction.

2.3.4. Gelatinase

Incorporated 0.4% gelatin (wt/wt) in nutrient agar and flooded with 15% mercuric chloride (wt/v) in concentrated hydrochloric acid (v/v) after incubation. Gelatinase positive isolates exhibits a clear zone around the colony.

2.3.5. Lipase

Nutrient agar was supplemented with 0.01% (w/v) of calcium chloride and 1% of Tween 80 (v/v) (polyoxyethylene sorbitan monooleate). After incubation presence of halo around the colony is regarded as positive reaction by the formation of calcium soaps with oleic acid. Absence of halo demarcates negative reaction.

2.3.6. Phosphatase

Phenolphthalein phosphate agar containing phenolphthalein diphosphate as phosphate source were inoculated and exposed to ammonia vapor after incubation period. Positive isolates turns into pink colored colonies after exposure.

2.3.7. Urease

Christensen agar base were supplemented with 40% (w/v) urea solution were inoculated and incubated. A change in the colour of the yellowish medium to a pink coloration around the bacterial colony is regarded as positive reaction.

2.3.8. API ZYM Micro Method

Selected candidate isolates with promising enzymatic activity were semi quantitatively determined with API ZYM (API bioMerieux Ltd) micro method [11]. The procedure was as per the manufactures instruction and expressed in nm of hydrolyzed substrates.

2.4. Statistical Analysis

Presence or absence data were square root transformed prior to analysis. Bray-Curtis similarities were used to produce a similarity matrix based on presence of enzyme (indicated by 1) or absence (indicated by 0). For the construction of a dendrogram demarcating the similarity of activity pattern of the bacterial isolates, group average linkage in the hierarchical clustering algorithm was performed using the PRIMER v6.1 program [12].

3. RESULTS

3.1. Identification of Heterotrophic Culturable Bacteria

Culturable bacteria associated with *S. fibulata* and *D. granulosa* mostly belonged to Gammaproteobacteria followed by Firmicutes, Actinobacteria and Betaproteobacteria. Ambient water isolates were dominated by Actinobacteria followed by Gammaproteobacteria, Firmicutes and Betaproteobacteria. Betaproteobacteria were absent in *D. granulosa* (**Table 1**). Although the two sponges vary considerably in ecological distribution and

Table 1. Percentage of culturable heterotrophic bacterial groups of *D. granulosa* and *S. fibulata* and ambient seawater.

Group	D.granulosa (%)	S.fibulata (%)	Water (%)
Actinobacteria	12.6	10.9	39.1
Firmicutes	19.6	21.7	19.6
Gammaproteobacteria	67.8	65.2	34.8
Betaproteobacteria	0	2.2	6.5

conditions, bacterial isolates reflected a striking similarity at the phylum level in their microbial communities. Majority of the sponge-associated Gammaproteobacteria belonged to the order Vibrionales.

3.2. Extra Cellular Enzymatic Activity

Bacterial isolates showed activity for at least one enzyme screened irrespective of their location and source. Amylase and phosphatase were the dominant enzymes in this system. Urease was the least expressed enzyme. Sponge associated bacteria exhibited higher percentage of hydrolytic enzymatic activity compared to the bacteria from ambient water (**Figure 2**). Though all the enzymes were expressed by both species, there was considerable variation in the percentage of positive isolates. Occurrence of hydrolytic enzymes such as amylase, lipase and protease was higher in. *D. granulosa* isolates than in *S. fibulata* (**Figure 3**). However, phosphatase and Deoxyribonuclease activity were higher in the case of *S. fibulata* (89.1% & 47.8%) than in *D. granulosa* (85% & 29.9%). Manifestation of multiple enzymatic activities was observed in bacteria associated with sponge (**Figure 4**). Nearly 50% of the sponge associated culturable bacteria expressed $\geq$ 4 hydrolytic enzymes, where as only 33% of the ambient water isolates could produce at least 2 enzymes. Selected candidate isolates showed promising enzymatic activity using API ZYM. The activity of the extra cellular hydrolytic enzymes of the bacteria is shown in **Figure 5**. All the isolates showed higher phosphatase activity. Ambient water isolates showed relatively lower lipase activity. The bacteria associated with the sponge *D.* granulosa showed the highest activity for all enzymes tested.

3.3. Statistical Analysis

Based upon the enzymatic activity pattern bacterial isolates were grouped into clusters using Bray–Curtis similarity matrix. Bacterial isolates from both sponges show a high similarity. They form 26 clusters (**Figure 6**) and the lowest similarity among the bacterial isolates from sponges were 40.3% whereas the water isolates formed

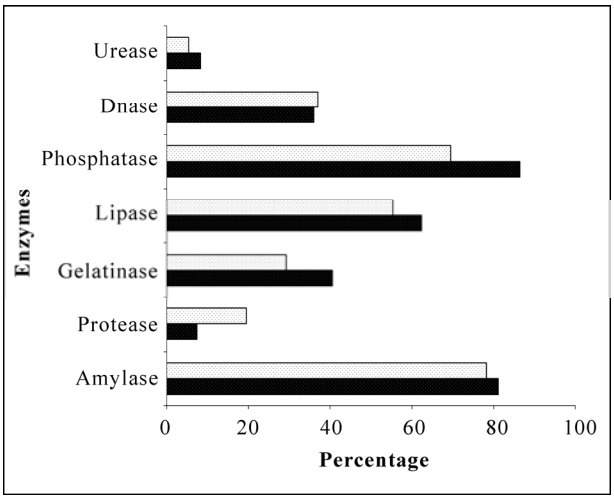

Figure 2. Comparison of percentages of heterotrophic bacterial isolates of ambient seawater and sponges with extracellular hydrolytic enzymes. Water; Sponge.

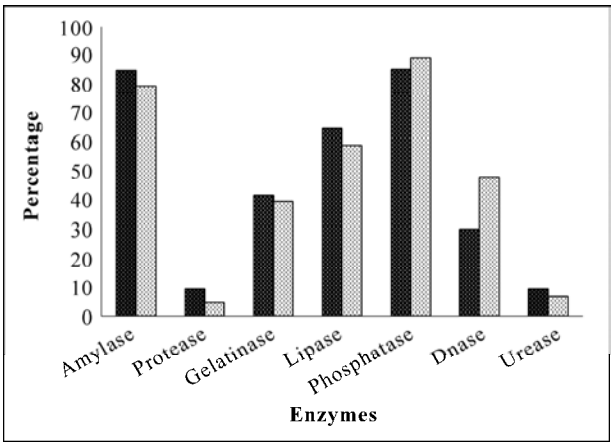

Figure 3. Comparison of percentage of culturable heterotrophic bacteria with extracellular hydrolytic enzymatic activity in *D. granulosa* and *S. fibulata*. *D. granulosa*; *S. fibulata*.

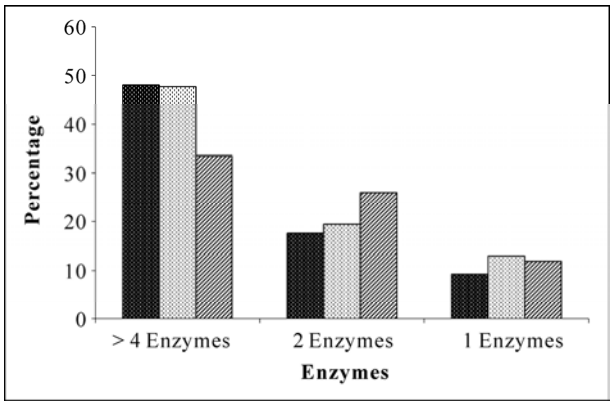

Figure 4. Frequency of incidence of multiple extracellular hydrolytic enzymes in bacteria associated with sponges and ambient seawater. *D. granulosa*; *S. fibulata*; Water.

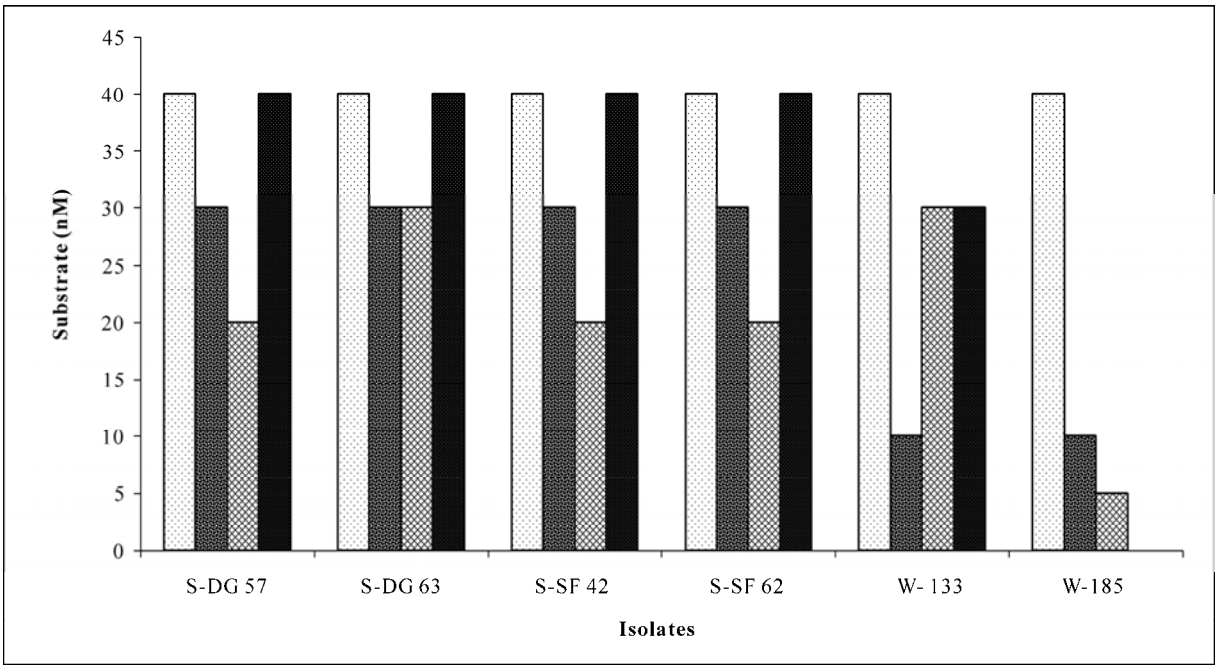

Figure 5. Semi quantification of potential isolates with multiple enzymatic activities from different sources using API ZYM. Phosphatase; Lipase; Protease; Gelatinase.

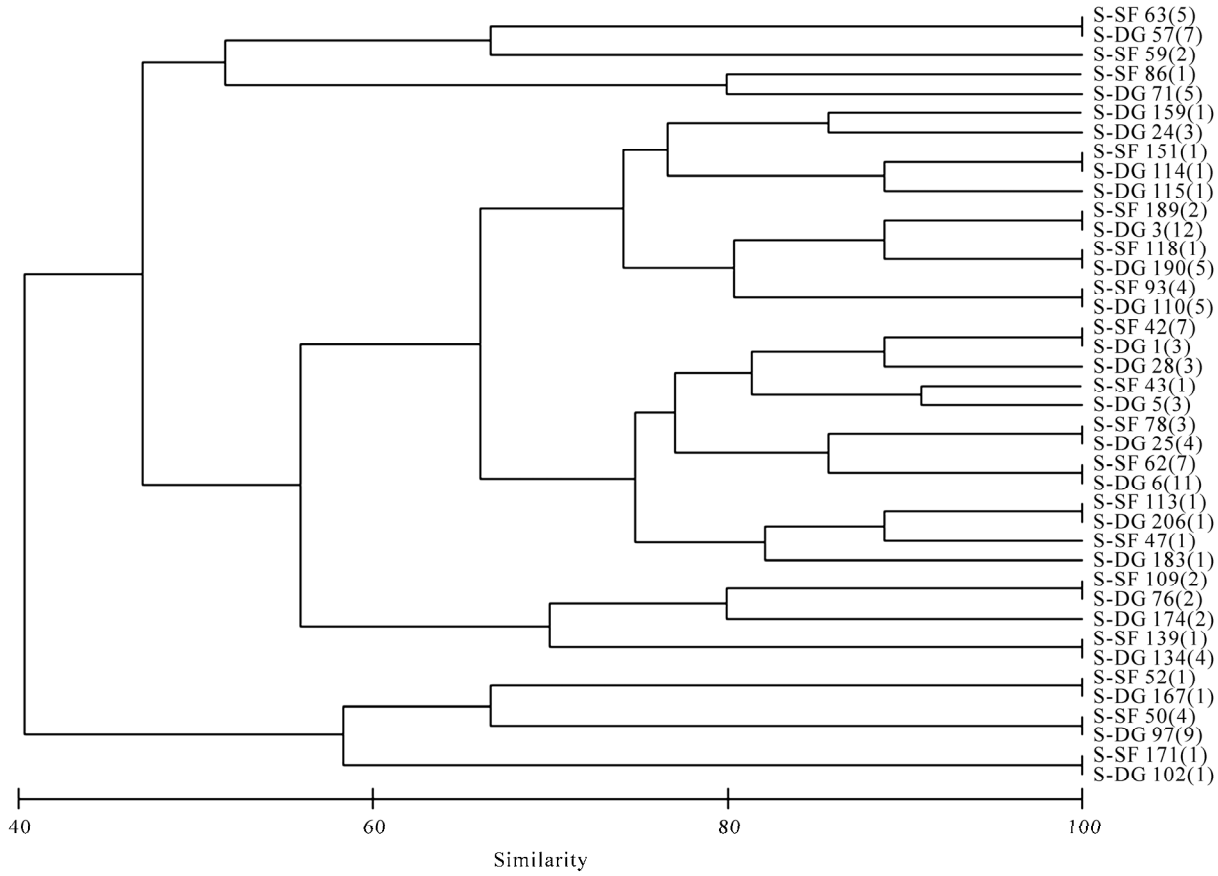

Figure 6. Cluster analysis showing the similarity (%) of activity pattern among sponge isolates. *Dysidea* granulosa indicated as S-DG and *Sigmadocia fibulata* as S-SF. Total isolates showing the same activity pattern is given in parentheses.

34 clusters and the lowest similarity of 16.5% was recorded among water isolates (**Figure 7**).

4. DISCUSSION

Microorganisms play a central role in sponge biology, as they are associated with many sponges either extracellularly, intracellularly or both. They also serve as food source for the host. Isolation is a mandatory approach to obtain novel microbes and also for evaluating their biochemical characteristics to understand the ecophysiological and environmental functions *vis a vis* their potential applications [13]. The discovery of enormous microbial diversity in marine sponges provides unprecedented research opportunities. Increased metabolic capabilities of sponge-associated bacteria were directly correlated with increased levels of potentially available nutrients in the sponge. Sponges filter seawater and accumulate copious amount of organic matter within the choanocytic chambers along with bacteria [8,14]. Transfer of photosynthate by the cyanobacterial symbionts to the sponge was proven [15], likewise the abundant bacterial population within the mesohyl, choanocytes and aquiferous chambers were also actively participating in the sponge nutrition by secreting extracellular enzymes and it acts upon the particulate organic matter accumulated within the sponge body. Although some dissolved inorganic and organic components of small size can be more or less directly absorbed by the organisms, many of the vital carbon- and/or nitrogen-containing compounds are in the form of macromolecular structures in the natural environment. To access these substrates, microorganisms must secrete enzymes capable of hydrolyzing these compounds [16]. In the presence of vast amount of substrates, bacteria are induced to produce extra cellular enzymes and release them into immediate surroundings leading to the degradation of various complex molecules accumulated. Consequently, the released nutrients can be taken up by the sponge [17,18]. Seawater isolates were limited in their ability to utilize different nutritional sources and appeared to be metabolically restricted due to the reduced concentration of nutrients in the water column [19]. Amylase was the most prominent enzyme in the study region. High amylase activity has also been reported from bacteria associated

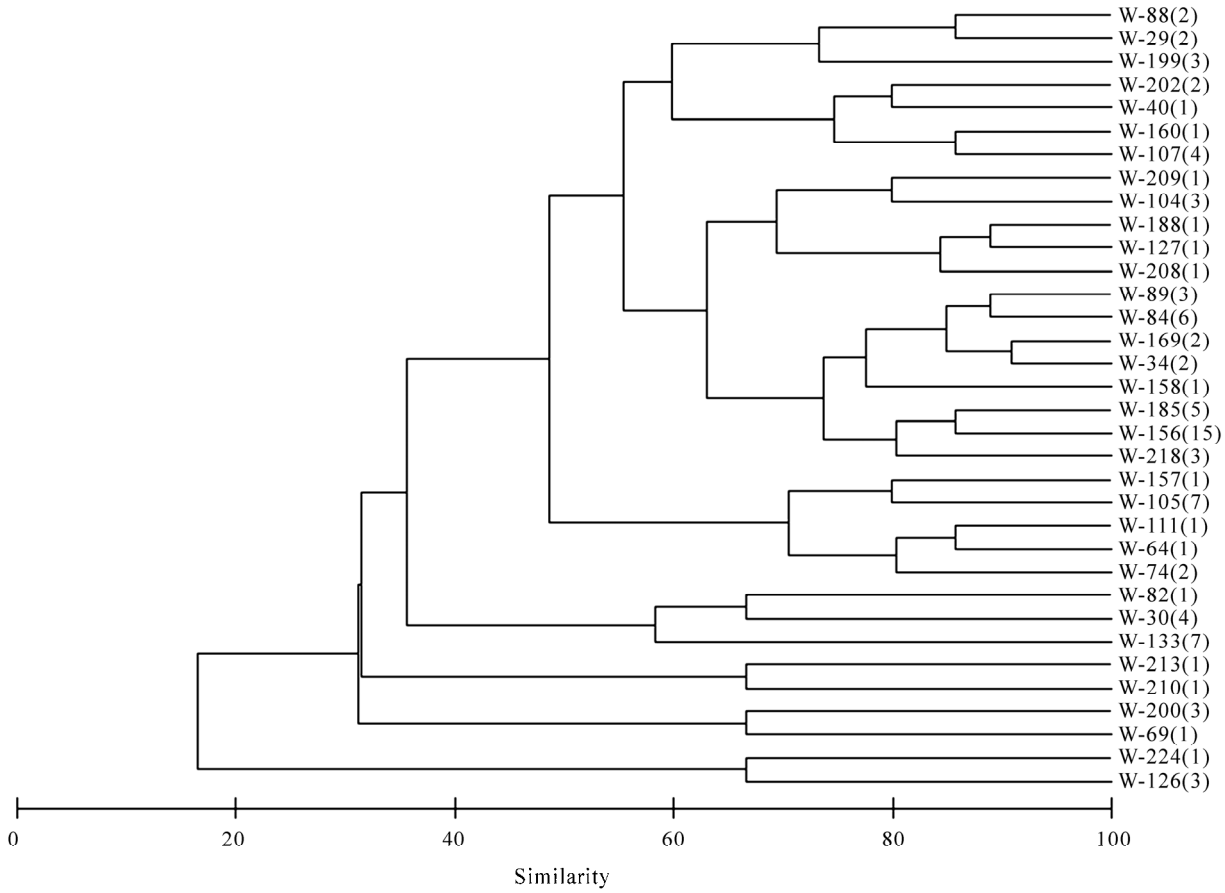

Figure 7. Cluster analysis showing the similarity (%) of activity pattern among water isolates. Total isolates showing the same activity pattern is given in parentheses.

with marine sponge *Fasciospongia cavernosa*, collected from the eastern peninsular coast of India [20]. Hydrolytic enzymes such as lipases still belong to the most important biocatalysts, because they accept a broad range of substrates, and are usually very stable in organic solvents [21]. The ability of sponge-associated bacteria to produce other hydrolytic enzymes such as phosphatase, lipase and gelatinase suggests that they play an important role in the degradation of organic matter and help in regeneration of nutrients. Most of the bacteria associated with the Caribbean demosponge *Ceratoporella nicholsoni* were able to utilize substrates like DNA, gelatin and a range of fatty acids like Tween 40 to Tween 80 [19]. Between the two species presently studied, differences were observed in the number of isolates and their enzyme activity. This could be due to the differences in their physiological requirement and the ambient variation in the quality and quantity of the organic matter. Associated bacteria of the marine sponge *Ircinia dendroides* from the Mediterranean Sea, multiple enzyme expression of gelatinase and lipase were observed [22].

In the present study the highest percentage (89%) of sponge-associated bacteria showed phosphatase activity. Hauksson [23] have described phosphatase producing marine *vibrio* sp. Bacteria associated with the marine sponge *Haliclona* sp have also been reported producing phosphatase enzyme [24]. Zaccone [25] opinioned that bacteria play a key role in the P cycle and that phosphatase was widespread in marine bacteria. Some bacteria associated with *D. granulosa* were found to produce urease enzyme in our study. Based on this study and earlier studies [19,20,24,26,27], it can be deduced that sponge-associated bacteria represent excellent sources for extracellular enzymes like amylase, protease, gelatinase, lipase, deoxyribonuclease and phosphatase. Enzymes from these bacteria can be obtained by mass fermentation followed by extraction and subsequent purification [20]. Further our results re-affirm that sponge-associated bacteria differ largely from the surrounding population of ambient seawater, both quantitatively and qualitatively.

Even though different media of varying compositions and concentrations have been used for isolation of heterotrophic bacteria, approximately 78% of the culturable bacteria associated with the sponge *C. nicholsoni* demonstrated phenotypic characteristics most closely related to species belonging to the orders Vibrionales and Aeromonadales [8]. From our study, Vibrionales emerged as the influential group inhabiting in both the sponges; they were abundant among the culturable bacteria as well as functionally dynamic with multiple enzymatic activities.

The present study has revealed the presence of high numbers of diverse culturable heterotrophic bacteria in association with sponges producing extracellular enzymes responsible for biopolymer degradation. *D. granulosa* is an excellent source of bacteria that can produce amylase, protease, lipase and urease, whereas *S. fibulata* associated bacteria produce phosphatase and deoxyribonuclease. The data obtained through the study reveals the crucial role played by culturable heterotrophic bacteria associated with sponge and seawater in the degradation of biopolymers. These kind of broad screening investigations indicate that the production of certain enzymes is not restricted to isolates belong to single source. It also improves our understanding of the functional role of bacteria in coral reef ecosystem. However, future studies with radio labeled and/or genetic probes are warranted to elucidate the action of bacterial enzymes in sponge nutrition. In particular, the development of new and innovative cultivation strategies holds great potential for accessing the microbial lineages that are so far under represented in culture. Mass fermentation of sponge–associated bacteria can provide a renewable resource of enzymes and harnessing these microbes for other metabolites as well as conserving the natural population of sponges.

5. ACKNOWLEDGEMENTS

The authors thank the Director, National Institute of Oceanography. AF thankfully acknowledges Council for Scientific and Industrial Research (CSIR) for the award of junior research fellowship. The laboratory facility was extended by MMRF of NIO, RC –Kochi funded by the Ministry of Earth Sciences, New Delhi. We thank taxonomist Dr. P. A. Thomas, Scientist Emeritus, CMFRI for identification of sponges. We also acknowledge Dr. C. T. Achuthankutty (visiting scientist, NCAOR, Goa) for critically reading the manuscript. This is NIO contribution number 4807.

REFERENCES

[1] Kleypas, J.A. (1997) Modeled estimates of global reef habitat and carbonate production since the last glacial maximum. *Paleoceanography*, **12(4)**, 533-545.

[2] Hooper, J.N.A. and van Soest, R.W.M. (2002). Phylum Porifera. *Class Demospongiae Sollas*, 1885 Kluwer Academic/ Plenum Publishers, New York.

[3] Vogel, S. (1977) Current-induced flow through living sponges in nature. *Proceedings of the National Academy of Sciences of the United States of America*, **74(5)**, 2069-2071.

[4] Wehrl, M., Steinert, M. and Hentschel, U. (2007) Bacterial uptake by the marine sponge. *Aplysina aerophoba*. *Microbial Ecology*, **53(2)**, 355-365.

[5] Wilkinson, C.R. (1978) Microbial associations in sponges. II. Numerical analysis of sponge and water bacterial populations. *Marine Biology*, **49(2)**, 169-176.

[6] Hentschel, U., Usher, K.M. and Taylor, M.W. (2006) Marine sponges as microbial fermenters. *FEMS Microbiology Ecology*, **55(2)**, 167-177.

[7] Wang, G.Y. (2006) Diversity and biotechnological potential of the sponge-associated microbial consortia. *Journal of Industrial Microbiology and Biotechnology*, **33(7)**, 545-551.

[8] Santavy, D.L., Willenz, P. and Colwell, R.R. (1990) Phenotypic study of bacteria associated with the Caribbean sclerosponge, *Ceratoporella nicholsoni*. *Applied and Environmental Microbiology*, **56(6)**, 1750-1762.

[9] Holt, J.G., Krieg, N.R., Sneath, P.H.A., Staley, J.T. and Williams, S.T. (2000). Bergey's manual of determinative bacteriology. Lippincott Williams & Wilkins Philadelphia, USA.

[10] Gerhardt, P., Murray, R.G.E., Costilov, R.N., Nester, E.W., Wood, W.A., Kreig, N.R. and Philip, G.B. (1981) Manual of methods for general bacteriology. In: Philips, G.B. Eds., American Society for Microbiology, Washington DC, 409-443.

[11] Zdanowski, M.K. and Figuerias, F.G. (1999) CFU bacterial fraction in the esturine upwelling ecosystem of Ria de Vigo, Spain: variability in abundance and their ecophysiological description. *Marine Ecology Progress Series*, **182**, 1-15.

[12] Clarke, K.R., Warwick, R.M., Somerfield, P.J. and Gorley, R.N. (2005) Methods manual: Changes in marine communities; PRIMER v6.1.10.

[13] Sfanos, K., Harmody, D., Dang, P., Ledger, A., Pomponi, S., McCarthy, P. and Lopez, J. (2005) A molecular systematic survey of cultured microbial associates of deep-water marine invertebrates. *Systematic and Applied Microbiology*, **28(3)**, 242-264.

[14] Wilkinson, C.R., Garrone, R. and Vacelet, J. (1984) Marine sponges discriminate between food bacteria and bacterial symbionts: Electron microscope radioautography and in situ evidence. *Proceedings of the Royal Society of London, Series B-Biological Sciences*, **220(1221)**, 519-528.

[15] Sara, M. (1971) Ultrastructural aspects of the symbiosis between two species of the genus *Aphanocapsa* (Cyanophyceae) and *Ircinia variabilis* (Demospongiae). *Marine Biology*, **11(3)**, 214- 221.

[16] Marx, J.C., Collins, T., D'Amico, S., Feller, G. and Gerday, C. (2007) Cold-adapted enzymes from marine antarctic microorganisms. *Marine Biotechnology*, **9(3)**, 293-304.

[17] Lee, Y.K., Lee, J.H. and Lee, H.K. (2001) Microbial symbiosis in marine sponges. *Journal of Microbiology*, **39(4)**, 254-264.

[18] Reiswig, H.M. (1981) Partial Carbon and energy budgets of the bacteriosponge *Verongia fistularis* (Porifera: Demospongiae) in Barbados. *Marine Ecology-an Evolutionary Perspective*, **2(4)**, 273-293.

[19] Santavy, D.L. and Colwell, R.R. (1990) Comparison of bacterial communities associated with the Caribbean Sclerosponge *Ceratoporella nicholsoni* and ambient seawater. *Marine Ecology-Progress Series*, **67**, 73-82.

[20] Shanmughapriya, S., Kiran, G.S., Selvin, J., Gandhimathi, R., Baskar, T.B., Manilal, A. and Sujith, S. (2009) Optimization, production, and partial characterization of an alkalophilic amylase produced by sponge associated marine bacterium *Halobacterium salinarum* MMD047. *Biotechnology and Bioprocess Engineering*, **14(1)**, 67-75.

[21] Karpushova, A., Brummer, F., Barth, S., Lange, S. and Schmid, R.D. (2005) Cloning, recombinant expression and biochemical characterization of novel esterases from *Bacillus* sp associated with the marine sponge *Aplysina aerophoba*. *Applied Microbiology and Biotechnology*, **67(1)**, 59-69.

[22] Lee, O.O., Lau, S.C.K., Tsoi, M.M.Y., Li, X.C., Plakhotnikova, I., Dobretsov, S., Wu, M.C.S., Wong, P.K., Weinbauer, M. and Qian, P.Y. (2006) *Shewanella irciniae* sp nov., a novel member of the family *Shewanellaceae*, isolated from the marine sponge *Ircinia dendroides* in the Bay of Villefranche, Mediterranean Sea. *International Journal of Systematic and Evolutionary Microbiology*, **56(12)**, 2871-2877.

[23] Hauksson, J.B., Andresson, O.S. and Asgeirsson, B. (2000) Heat-labile bacterial alkaline phosphatase from a marine *Vibrio* sp. *Enzyme and Microbial Technology*, **27(1-2)**, 66-73.

[24] Graeber, I., Kaesler, I., Borchert, M.S., Dieckmann, R., Pape, T., Lurz, R., Nielsen, P., von Dohren, H., Michaelis, W. and Szewzyk, U. (2008) *Spongiibacter marinus* gen. nov., sp nov., a halophilic marine bacterium isolated from the boreal sponge *Haliclona* sp 1. *International Journal of Systematic and Evolutionary Microbiology*, **58(3)**, 585-590.

[25] Zaccone, R., Caruso, G. and Cali, C. (2002) Heterotrophic bacteria in the northern Adriatic Sea: seasonal changes and ecoenzyme profile. *Marine Environmental Research*, **54(1)**, 1-19.

[26] Zhang, H., Zhang, F. and Li, Z. (2009) Gene analysis, optimized production and property of marine lipase from *Bacillus pumilus* B106 associated with South China Sea sponge *Halichodria rugosa*. *World Journal of Microbiology and Biotechnology*, **25(7)**, 1267-1274.

[27] Mohapatra, B.R., Bapuji, M. and Sree, A. (2003) Production of industrial enzymes (Amylase, carboxymethylcellulase and protease) by bacteria isolated from marine sedentary organisms. *Acta Biotechnologica*, **23(1)**, 75-84.

Advances in Bioscience and Biotechnology, 2010, 1, 338-347 **ABB**
doi:10.4236/abb.2010.14044 Published Online October 2010 (http://www.SciRP.org/journal/abb/).

Molecular genetic program (genome) contrasted against non-molecular invisible biosoftware in the light of the Quran and the Bible

Pallacken Abdul Wahid

Hira, J.T. Road, Thalassery, Kerala, India.
Email: pawahid@hotmail.com

Received 27 August 2010; revised 10 September 2010; accepted 15 September 2010.

ABSTRACT

The current perception of biological information as encoded by a chemical structure (genome) is critically examined. Many features assigned to the genome are violations of chemical fundamentals. Perhaps the most striking one is that a living cell and its dead counterpart are materially identical, *i.e.*, in both of them all the structures including genome are intact. But yet the dead cell does not show any sign of bioactivity. This clearly shows that the genome does not constitute the biological program of an organism (a biocomputer or a biorobot) and is hence not the cause of "life". The molecular gene and genome concepts are therefore wrong and scientifically untenable. On the other hand, the Scriptural revelation of the non-molecular biosoftware (the soul) explains the phenomenon of life in its entirety. The computer model of organism also helps understand the Biblical metaphor "Adam's rib" as chromosome, the biomemory of the cell. The Quran provides ample insight into the phenomenon of human biodiversification. It also reveals the source of biological information required for creating biodiversity in human population. The Scriptural revelation of the invisible non-molecular nature of biosoftware rules out the possibility of creating life from chemical molecules without involving a living cell (or organism) in the process. Claims of creation of "synthetic life" or "synthetic forms of life" employing living cell in the process cannot be accepted as creation of life from non-life as non-molecular biosoftware can be copied from the living cell to the prosthetic cell. Instead of chemically synthesizing a cell from scratch to prove life is a material phenomenon, biologists can as well resort to a more practical and convincing method by restoring life to a dead cell (which carries all the hardware structures including the genome but lacks the biosoftware) by chemical means. The failure of experiments to produce life through purely chemical means or to restore life to a dead cell would in fact invalidate the molecular biological program (genome) concept. More importantly, the failure would confirm the Scriptural revelation of non-particulate nature of the divine biosoftware and the existence of God.

Keywords: Genome; Divine Non-Molecular Biosoftware; Synthetic Life; Computer Model of Organism; The Quran; The Bible; Biosoftware Engineering; Human Biodiversification; Genome Anomalies

1. INTRODUCTION

Over the past six decades following elucidation of the chemical structure of DNA, the genetic research has been centred round the molecular gene and genome concepts. Genome is believed to constitute the genetic program or the 'blue print of life' that is responsible for the biological features and functions of an organism. In other words, "life" is treated as a material phenomenon. In contrast to this, a computer model of organism was proposed earlier in the light of the Quranic revelation of intangible (*ghayb* in Arabic) non-molecular biosoftware (*rooh* or *nafs* of man) to explain the phenomena of life and death, and biological functioning [1,2]. The model is consistent with the non-particulate gene originally proposed by Wilhelm Johannsen in 1909 that agrees well with the Scriptural revelations. This paper addresses the problems associated with the molecular genome bringing to light its inherent weaknesses and also inconsistencies with the fundamentals of chemistry. The relevance of the Quranic and the Biblical revelations about the phenomenon of life is also highlighted in the wake of failure of attempts to create life by chemical means without involving a living cell.

2. ANOMALIES OF THE GENOME CONCEPT

2.1. The Gene is Indefinable

The perception that DNA molecule encodes the biological program has run into serious problems. Although molecular biologists hoped that it would be possible to identify the genes for different attributes of an organism, the gene remained elusive. According to geneticist Peter Portin, "The gene is no longer a fixed point on the chromosome, producing a single messenger RNA. Rather, most eukaryotic genes consist of split DNA sequences, often producing more than one mRNA by means of complex promoters and/or alternative splicing. Furthermore, DNA sequences are movable in certain respects, and proteins produced by a single gene are processed into their constituent parts. Moreover, in certain cases the primary transcript is edited before translation, using information from different genetic units and thereby demolishing the one-to-one correspondence between gene and messenger RNA. Finally, the occurrence of nested genes invalidates the simpler and earlier idea of the linear arrangement of genes in the linkage group, and gene assembly similarly confutes the idea of a simple one-to-one correspondence between the gene as the unit of transmission and of genetic function...." [3]. Other leading scientists like Thomas Fogle and Michel Morange also concede that there is no longer a precise definition of what could count as a gene [4,5]. An important objective of genome projects is the identification of genes. Current estimates of human genes generated from genome sequencing range between 30,000 and 40,000 with occasional excursions to 100,000 or more. One reason for the continuing ambiguity is that genes are neither well defined nor easily recognizable [6]. Horace Freeland Judson writing in *Nature* notes: "The phrases current in genetics that most plainly do violence to understanding begin "*the gene for*": the gene for breast cancer, the gene for hypercholesterolaemia, the gene for schizophrenia, the gene for homosexuality, and so on. We know of course that there are no single genes for such things." [7].

The objective of genomic research is to ultimately understand the relationships between heritable units and their phenotypes. But it appears that genome concept would not deliver this information. The genome organization is extremely complex. Genes reside within one another, share some of their DNA sequences, are transcribed and spliced in complex patterns, and can overlap in function with other genes of the same sequence families. "Today, in the era of genomic sequencing and intense effort to identify sites of expression, the declared goal is to search for genes, entities assumed to have physical integrity. Ironically, the sharper resolving power of modern investigative tools make less clear what, exactly, is meant by a molecular gene, and therefore, how this goal will be realized and what it will mean", observes Fogle [4].

Instead of generating more evidence in support of the particulate nature of the gene, research in molecular biology is generating evidence to the contrary. Craig Holdrege observes: "The complexity at the molecular level reveals that the simple mechanisms one imagined in the 1960s simply do not exist in that form. It has become less and less clear what a gene actually is and does. And although the deterministic gene is still the gene that lives in the minds of many students, lay people, and - at least as a desire - in the minds of many biologists, the findings of late twentieth century genetics show one thing clearly: the simple deterministic gene, the foundational "atom" of biology is dead. There is no clear-cut hereditary mechanism-no definite sequence of nitrogenous bases in a segment of a DNA molecule that determines the make-up and structure of proteins, which in turn determine a definite feature of an organism." [8]. Evelyn Fox Keller makes the case for a radically new thinking about the nature of heredity in her book *The Century of the Gene*. In her articulate and insightful history of genetics and molecular biology, she suggests that most of our common assumptions about genes are either too simplistic or simply incorrect. It turns out, for example, that a single functioning gene may be split and found in several locations on a chromosome, and it is rare that a gene can be determined to have caused any particular trait, characteristic or behavior [9].

2.2. Phenomenon of Cell-Induced Mutations

Exposure of living organisms to natural radiation is supposed to be the major cause of DNA mutations, which ultimately paves way for evolution of new structures and new species. The annual dose of background radiation received by a human being is 2 to 3 mSv. Whether this too low a dose is sufficient to change a chemical structure is doubtful. Change in cell DNA is invariably attributed to background radiation ignoring the fact that cell itself has the mechanism to bring about that change. Even if the background radiation damages the DNA molecule, how can it make rearrangement of the bases and create new 'viable' DNA molecule is another question that has been overlooked by biologists. Thirdly there is also no explanation as to why no other cell structure is similarly affected by background radiation.

Stephen C. Meyer in an excellent comprehensive review of the evolutionary literature discusses the problems and difficulties in the evolution of novel genetic

information through random mutations [10]. According to Ohno (1996) even a mutation rate of 10^{-9} per base pair per year results in only a 1% change in the sequence of a given section of DNA in 10 million years. Thus, mutational divergence of preexisting genes cannot explain the origin of the Cambrian forms in that time [11].

In 1970 Miroslav Radman discovered that the phenomenon of mutation is cell-directed. He found that bacteria harboured information to make mutations [12]. In 1988 Cairns *et al*. confirmed that genetic mutations are induced from within the cell. They found cell-induced changes of various elements of the lac operon in *Escherichia coli* bacteria [13]. According to Chicural, "…depending on their environmental conditions, bacteria might be able to direct mutations to particular genes….Outraged, a number of evolutionary biologists quickly embarked on their own studies to test the notion" [12]. Clearly biologists do not look beyond the genome. Goodman described the studies conducted by Joshua Lederberg at the University of Wisconsin which showed that mutations for resistance to some antibiotics occurred spontaneously in cells that had never been exposed before to the antibiotics [14]. A recent report of resistance of bacteria to antibiotics further confirms cell-induced mutation [15,16]. Reviewing the works in this area, Pennisi remarked: "Genetic change, and hence the evolution of new species, is commonly thought to result from small, random mutations in individual genes, but a growing wealth of data emphasizes that the perception is wrong. Indeed the mutations leading to evolutionary change can involve the wholesale shuffling or duplication of the genetic material, changes that can affect the expression of genes or free up duplicated genes to evolve new functions. What's more, these changes may not be totally random….mainstream biologists need to consider genomes, and the kinds of evolutionary changes they undergo, in a much different light." [17]. As discussed elsewhere [1,2], there are a variety of natural biosoftware engineering mechanisms (e.g., crossing over between chromosome sectors, deletion, duplication of chromosomal sectors, etc.) that can bring about changes in chromosome composition. The discovery of built-in biosoftware engineering mechanisms dates back to Nobel laureate Barbara McClintock's pioneering cytogenetic studies on transposable elements during the late 1940s and early 1950s [18]. These mobile elements offer a versatile cut-and-splice tool in bringing about specific changes in the organization of chromosomes. These are biosoftware-dictated mechanisms to generate new information. Transposition plays an important role in chromosome rearrangements. Insertion, deletion and inversion occur either as a direct consequence of transposition or by general recombination. These elements are present in all prokaryotes and eukaryotes.

Surprisingly, biologists look at these mechanisms as 'errors' and 'mistakes'. These mechanisms are in fact programmed phenomena to produce radically different chromosome compositions and hence semantic (bioinformation) content. They are mechanisms operating in the cell in accordance with the biosoftware of the organism. They are not mistakes or errors. Strictly speaking, a computer cannot make mistakes; its hardware can only carry out instructions as dictated by the software. Same is the case with a cell also. The need to recognize natural biosoftware engineering processes as programmed phenomena is very much reflected in the discovery of cell-induced mutagenesis. All these phenomena are opposed to the particulate biological program concept but they strengthen the view that biosoftware exists in the cell as stored information in non-molecular form. It is because of the existence of biological program independently of any chemical structure, cell-induced DNA mutations occur in response to environmental stimuli. The reports of heritable changes occurring in the organisms including that caused by background radiation are to be viewed in this light.

Development of resistance to pesticides in certain microorganisms [14] and environmental stress-induced changes [13] are examples of environment-induced biomemetic responses. In all these cases the stimuli or signals received from the environment act as switches to trigger specific biomemes into operation. Not all organisms will respond similarly to a given stress or environmental stimulus. An organism reacts to an environmental stimulus in accordance with its biomemome. This would imply that every phenomic change that occurs in an organism is biomemome-directed phenomena from within the cell and not externally induced adaptations as is believed now. These are also instances of abioprogram-bioprogram interactions consistent with the divine control program. The availability of biomemes to respond to special or unusual environmental conditions is natural evidence of God's designing the organism. DNA mutations have to be seen as hardware changes required for the execution of the newly activated biosoftware package in the organism.

Results obtained in several other studies can also be explained the same way. For instance, the observations made by Grant and Grant of the changes in beak size of Darwin's finches (bird species) [19] can be explained as a case of cell-induced genetic change and not as evolution caused by random mutation by some external mutagen. They studied two predominant species namely, *Geospiza fortis* (medium ground finch) and *G. scandens* (cactus finch). The main food items of the birds were

seeds, flowers, etc. The former had a bigger beak and could crack larger and harder seeds whereas the latter had a smaller beak and hence was more efficient in handling smaller seeds. Their results indicated that mean body size and beak shape were significantly different in both species at the end of a thirty-year experimental period. The changes in beak size occurred depending on the kind of seeds available to them in a changing environment influenced by drought etc. The environmental changes acted as switches to bring specific biomemes into operation and as a result beak size altered to suit the new environment. The other examples often cited as "evolution in action" are also products of cell-directed mutations and not random mutations. These include changes in mouth sizes of mud snails of the genus *Hydrobia* that eat diatoms (diatoms are protected by a hard silicate shell and the size of the snail mouth determines what size diatoms it can eat), changes in wingspan in bird-eating hawks and eagles of the family Accipitridae to enable them to carry their prey, changes in mouth sizes of desert seed-eating rodents of the families Cricetidae and Heteromyiidae, and changes in mouthparts in Cichlid fishes [20]. The variations in morphological characters observed in these organisms cannot be considered as random phenomena but are cell-directed changes to counter specific environmental stress experienced by the organism concerned.

There are many kinds of DNA repairs. Rosenfeld gives a detailed account of the self-healing strategies of the master molecule. If a base is put in wrong place during replication, there are enzymes to correct the mistake. Purines, without any errors and without any damages drop out by the thousands every day presumably due to wear and tear of existence in the chromosomes only to be promptly replaced by insertases. A base can spontaneously undergo change. A cytosine, for example, will lose an amino group and become uracil. Uracil is perfectly at home in RNA but not in DNA. The enzymes called uracil glycosylases recognize the uracil, remove it and replace it with a new cytosine. Suppose that an error has occurred in one of the DNA strands say, a T has been put across from a G, where a C really belongs. This would give rise to two strands one with a G and the other with a T. The enzymatic apparatus 'knows' that cannot be correct, but how does it know whether to replace the C with a T on one strand, or the C with an A on the other? If the replacement takes place not on the right strand, the result would be either death of the cell or a mutation. How does it know which is the authentic original? Rosenfeld gives a couple of explanations for the existence of a protective recognition system in the chromosomes [21]. But still the question of how a chemical structure (DNA) is *aware of* the change in its composition or how the wrong one is corrected remains a mystery. DNA repair is a true reflection of the existence of the biological program independent of the DNA structure. All these documented evidences confirm that DNA mutation is not a random phenomenon but is biosoftware-directed hardware change.

2.3. Lack of Genome-Phenome Correspondence

Studies at the molecular level fail to demonstrate the expected correspondence between genome and phenotype. The most spectacular example of this is the morphological dissimilarity between human being and chimpanzee despite a 98.7% similarity in their DNA [22]. Although evolutionary biologists speak of genomes of chimp and man as being almost identical in support of their argument of human evolution from an animal, and for establishing chimpanzee as the closest animal ancestor of human being, they have not enumerated so far the identical phenotypic characters in human and chimp in terms of anatomy, physiology, development and other biological features. In fact there is none! A chimp is not even 0.1% human being nor a human being 0.1% chimp. A human being differs from chimp in every detail and at every point of the body. The only similarity between chimp and man is in the DNA. The differences in traits, characteristic behaviour, instincts and capabilities between human (*Homo sapiens*) and chimpanzee (*Pan* sp.) are far greater than the small degree of sequence divergence (1.3%) could account for.

The chimp-human comparison is a case of similar genomes but dissimilar phenotypes. The reverse case is also known. *Caenorhabditis elegans* and *C. briggsae* are physically very similar organisms. It takes an expert to distinguish them. The two have near-identical biology, even down to the minutiae of developmental processes. Surprisingly, however, their genomes are not so similar. *C. elegans* has more than 700 chemoreceptor genes when *C. briggsae* gets on by just 430. There are also many genes unique to each of them [23]. "Typically when people say that the human genome contains 27,000 genes or so, they are referring to genes that code for proteins," points out Michel Georges, a geneticist at the University of Liège in Belgium. But even though that number is still tentative – estimates range from 20,000 to 40,000 – it seems to confirm that there is no clear correspondence between the complexity of a species and the number of genes in its genome. "Fruit flies have fewer coding genes than roundworms, and rice plants have more than humans," notes Mattick [24].

Many insects exhibit alternative morphologies (polyphenisms) based on differential gene expression rather than genetic polymorphism (differences in genes themselves). One of the best understood insect polyphenisms

is the queen-worker dimorphism in honey bees. Both the queens and the workers are females but morphologically distinct forms. Besides, the queen is fertile whereas the worker is sterile. Studies conducted with the bee species *Apis mellifera* revealed that numerous genes appeared to be differentially expressed between the two castes [25]. The seven differentially expressed loci observed in the study belonged to at least five distinctly different functional groups. The queen and the worker castes in honey bee provide an unfailing proof of natural existence of similar genomes exhibiting dissimilar phenotypes. The absence of genome-phenome relationship is very much evident from these studies. It implies that genome does not constitute the biological program. All these cases indicate the independent existence of biosoftware as non-molecular information stored on the chromosome.

3. GENOME IS CHEMICALLY UNTENABLE

Several non-chemical features have been attributed to the material genome. Some of the obvious departures from the chemical fundamentals are given below.

3.1. Junk DNA

It has been observed that an overwhelming 95% of DNA consists of non-coding DNA in eukaryotes and about 5% is constituted by the coding-DNA (or the genes). The non-coding DNA (ncDNA) is referred to as "junk DNA". Though structurally comparable to coding DNA, surprisingly, the so-called junk DNA does not encode similar biological information (or vice versa).

3.2. Genome Can Change its Own Structure

Another surprising feature of the genome is that DNA is the only molecule in nature that can undergo self-alteration. How is it possible for a chemical structure to encode information for its own change? For example, in human being with the formation of the zygote, the biological program comes into operation. The zygote undergoes ontogenetic development; then the individual passes through adult stage and old age, and ultimately dies. It is a continuous process like the operation of an integrated computer program. During ontogenetic development, the genome produces not only tissues with diverse functions but also undergoes itself changes in its structure as is evident from the recent discovery of variations in the genomes of different tissues [26]. Prior to this discovery (in 2009) it was believed that the genomes of the body cells, irrespective of the tissues to which they belong, were all identical. That view is also a violation of chemical fundamentals as it implies that a given chemical structure can show different properties—in this case, differences in the information encoded by identical genomes in different tissues. The discovery of variable genomes in different tissues also brings up another issue as to how such differences arise in the daughter cells as a result of successive mitotic divisions of the same parent cell—the zygote.

3.3. Dead Cell Genome Does Not Encode Biological Information

A fundamental feature of chemical molecule is that it cannot but exhibit the properties assigned by its structure. The genome is an exception to this rule also. Going by the present concept of particulate genetic program, a cell carrying the genome should invariably show the life properties. However a dead cell with its genome remaining intact fails to exhibit "life" clearly indicating the genome does not encode the biological program. If not, how can a molecule lose the information encoded by its structure? All these issues are chemically inexplicable. The gene and genome concepts are therefore fundamentally wrong.

3.4. Other Odd Features

Although there are certain criteria to identify the genes, their application has not been straightforward. Besides, issues like overlap, alternative splicing, and pseudogenes are also involved. "Pseudogenes are similar in sequence to normal genes, but they usually contain obvious disablements such as frameshifts or stop codons in the middle of coding domains. This prevents them from producing a functional product or having a detectable effect on the organism's phenotype…. The boundary between living and dead genes is often not sharp. A pseudogene in one individual can be functional in a different isolate of the same species… and so technically is a gene only in one strain…. there are other pseudogenes that have entire coding regions without obvious disablements but do not appear to be expressed…. Ultimately, we believe that identification of genes based solely on the human genome sequence, while possible in principle, will not be practical in the foreseeable future." [27].

The variation observed in the use of triplet codes among organisms is another issue. Like the pseudogene this aspect is against chemical fundamentals and remains unexplained. The degenerate nature of the biological code implies several triplets coding per amino acid. Further, two amino acids have only one mRNA codon each; AUG for methionine and UGG for tryptophan. Hence 59 degenerate triplets code 18 amino acids; these 18 have two to six synonymous codons each. Choices between synonymous codons are not random; some codons in the set specific to an amino acid are used more than the others [28]. The 'genome hypothesis' which tries to explain the variation in codon use states that codon use is spe-

cies-specific, *i.e.*, each genome or type of genome shows a particular pattern of choices between synonymous codons. Thus overall codon usage differs between taxa; but codon bias is also influenced by other factors like gene length, gene expressivity (the amount of protein made per gene), environment and lifestyle of the organism [29]. The codon bias gives rise to the paradox whether protein evolution determined DNA sequence or DNA commanded protein evolution. Many such dilemmas remain in molecular evolution. The origin of bias in codon and anticodon frequencies continues to elude researchers [28].

4. DIVINE NON-MOLECULAR BIOSOFTWARE

The invisible (*ghayb* in Arabic) nature of human biosoftware was discussed in detail in an earlier paper [2]. "Breathing of *rooh*" into a clay model to create man (Adam) mentioned in the Quran (Q. 15:26-29) and "breathing of life" mentioned in the Bible (Genesis 2:7) refer to one and the same event – installation of divine non-molecular biosoftware in a clay model of man. Upon installation of the *rooh* (the term *nafs* is also used in the Quran) in that non-living clay model, it sprang to life much like a lifeless computer springs to "life" when software is installed. Thus the *rooh* or "breath of life", which is non-physical, is the divine biosoftware (bioprogram or the soul) of human species. Based on that, the phenomenon of life has been defined and explained as the manifestation of the execution of the divine biosoftware. The Quran further informs us that it is the removal (or in computer parlance, 'deletion') of the *nafs* (biosoftware of human being) that causes death (Q. 6:93). In other words, a dead body is like a computer without software [2].

As in the case of man-made computer program, the non-molecular biosoftware needs a physical medium for its storage. The storage device is the chromosome. This can be deduced from the Quranic and Biblical revelations. The Quran states that it was from the *nafs* (biosoftware) of Adam, woman (Eve) was created (Q. 7:189). The Bible further says that it is from Adam's rib, Eve was created. The "rib" mentioned in the Bible may be taken as metaphor to mean X chromosome of Adam for the obvious reason that chromosome was unknown to the people of Prophet Moses's time [30]. Ribs are the only part of human body that morphologically resemble the chromosome. As two arms of a chromosome are joined on either side of the centromere, two ribs are joined on either side of a vertebra (**Figure 1**). Of the two sex chromosomes (X and Y), Adam's rib must be referring to the X chromosome because XX combination determines femaleness. Further, the arms of the X chromosome are more nearly equal in length than those of the Y chromosome. This characteristic of X chromosome makes it more comparable with the ribs on either side of a vertebra. Since the Bible mentions only one rib, the biomeme for femaleness might be located on one of the arms of X chromosome. The analogy of rib used in the Bible for chromosome is revelation of the biosoftware storage medium. The Scriptural account of creation of Eve from Adam also reveals the karyotypes of Adam and Eve. If we designate karyotype of Adam as 22 $(\text{autosomes})_A + (XY)_A$, where subscript A denotes Adam, the karyotype of Eve will be 22 $(\text{autosomes})_A + (XX)_A$.

4.1. Human Biodiversification

4.1.1. Source of Bioinformation

Biodiversity is in reality phenotypic manifestation of diverse biosoftware. How new information arises in human beings for creating variability in the population is still not understood. The Quran is the only source which provides information on this subject. The Quran reveals that human species was created from a single biosoftware (*nafs*). "O mankind! Fear your Lord who created you from a single *nafs* and from that, He created its mate, and from them both, He (created and) spread plenty of men and women…." (Q. 4:1). The *nafs* (biosoftware) mentioned here is the *rooh* which created Adam (Q. 15:26-29) as discussed elsewhere [2]. The Quran further reveals: "O mankind! Indeed we created you from a male and a female and made you into divisions (civilizations, nations, cultures, etc.) and tribes that you may know each other…." (Q. 49:13). "And among His signs is the creation of the skies and the earth, and the variations in your languages and your colours. Verily in that are signs for those with knowledge." (Q. 30:22). These revelations imply Adam's *nafs* is the microbioprogram (*i.e.*, bioprogram at the species level) of the human species. It serves as the common biomeme pool to create phenotypic diversity in human species in time and space. The process of human biodiversification is therefore a

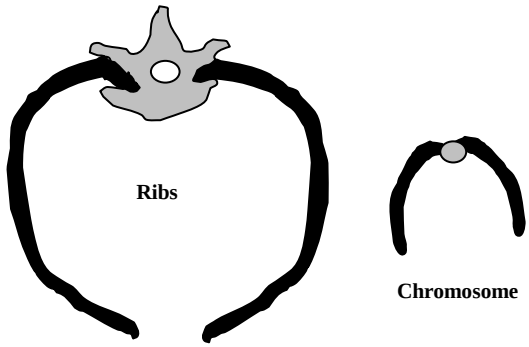

Figure 1. Morphological semblance between human ribs and chromosome.

programmed phenomenon through which God creates diverse individuals, communities with different colours, languages, etc., at different times and in different geographical regions.

Human biodiversity is manifested in biological attributes including mental prowess. Some of the readily observable variations include morphological (e.g., body shape and size, height, bone structure, obesity), gender, race, ethnicity, physical abilities, color (e.g., skin, eyes and hair), blood type, temperament, cultural differences, mental abilities (e.g., intelligence, aptitude, likes and dislikes, etc.), language, food preferences, etc. With wide-ranging characters, skills and talents, human biodiversity profile is unwieldy and overwhelming to say the least. No two individuals including the so-called monozygotic twins are identical. *Homo sapiens* is the only species whose members can be identified by face as well as by other phenotypic characters because of the variability. Each human being is unique, unprecedented and unrepeated in time and space. Such is the magnitude of variation existing in human race. And the source of biological information responsible for this scale of biodiversity is Adam's *nafs*, the divine microbioprogram of *Homo sapiens*. The Quran also informs us that longevity of a human individual is also biosoftware-controlled. "And Allah created you from dust (or clay); then from a sperm-drop; then He made you mates. And no female conceives or delivers without His knowledge. No man is granted extension of life nor is his lifespan shortened except in accordance with (what is given) in a record. All that is easy for Allah." (Q. 35:11).

4.1.2. Phenomenon of Human Biodiversification

As biosoftware is non-particulate and is stored on the chromosomes as biomemetic sectors [2], changes in biological information can be brought about via shuffling and mixing of the biomemetic sectors on the chromosomes. Appropriate natural biosoftware engineering mechanism comes into operation during gametogenesis (gamete formation through meiosis followed by mitosis) to produce gametes carrying biomemes as specified in the biosoftware. A particularly notable phenomenon in this context is the "crossing over" taking place during meiosis during which the segments of non-sister chromatids of a homologous pair of homologous dyads are exchanged. This swapping of portions leads to alteration of biomemetic content of the resulting chromosomes. Huge biomemetic differences observed between siblings are the result of this crossover. The exchange is not carried out in random fashion as is believed now; it is a programmed function executed in accordance with the biosoftware of the individual to prepare the next generation biomememomes (biosoftware of individuals). If it were a random process, most of the resulting gametes would have been infertile. This implies that the programmed "crossing over" produces diversity in human population along a specified timeline and based on specific distribution pattern. The origin of diverse ethnic groups, races, cultures, linguistic groups, etc. at different times of human history and their distribution in different geographic locations on the earth can be explained as consequence of this programmed biodiversification.

Besides crossing over, another mechanism that controls the human biodiversification may be the fertilization phenomenon as can be inferred from the Quranic verse 13:8: "Allah knows what every female (womb) bears, by how much the wombs fall short (in number) or exceed. Every thing is in accordance with a calculated measure (due proportion) with Him." It is very clear that the whole process of creation of human individuals involving gametogenesis, fertilization in the female womb, infertility and fecundity, and phenotype determination is according to God's program. In support of these revelations we find that the fertilization of female egg with male sperm is a highly controlled phenomenon. As a general rule, we find only one sperm out of the millions in the ejaculate fertilizes the egg. Scores of sperms are produced in the human semen perhaps to provide options for wide-ranging situations. According to biochemist Jerry Hedrick, "Sperms have the opportunity to interact with many other kinds of cells in the female. How egg and sperm recognize one another is a fundamental question in reproductive biology." [31]. It is also surprising how a sperm evades fusion with another sperm. Further once fertilized by a sperm, the zygote (fertilized egg) is inaccessible to another sperm. Evidently there is a mechanism to guide a particular sperm to fertilize a particular egg (**Figure 2**).

Spermatozoa normally encounter the egg at the fertilization site (in the Fallopian tube) within 24 hours after ovulation. A considerable fraction of the spermatozoa ejaculated into the female reproductive tract remains motionless in storage sites until ovulation, when the spermatozoa resume maximal motility and reach the fertilization site within minutes. Although the nature of the signal for sperm movement is not known, a study conducted by Ralt *et al.* suggests that attraction of spermatozoa to a factor(s) released from the egg may be a key event in the fertilization process and may give insight into the mechanism underlying early egg-sperm communication [32]. In other words, which sperm must fuse with which ovum is determined by the biodiversification software. This is what Allah says in the Quran: "It is He who shapes you in the womb as He likes. There is no God but Him—the Mighty, the Wise." (Q. 3:6). It is evident from these Quranic messages that it is God who decides the biosoftware and hence phenotype of every

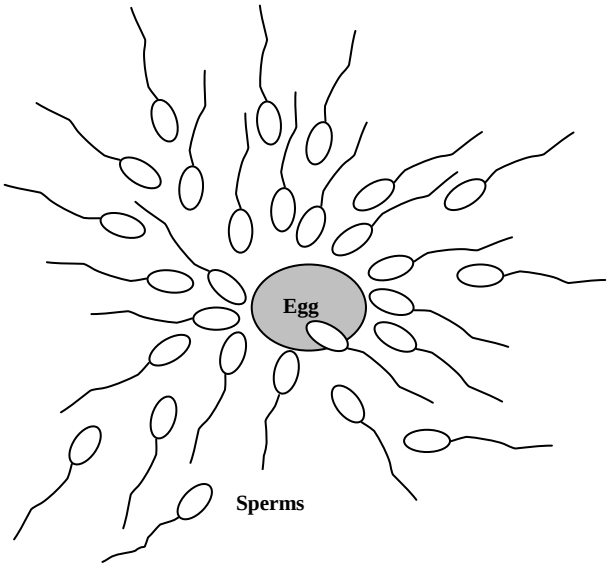

Figure 2. Fertilization of human female egg. Note: Diagram shows a swarm of sperms surrounding the egg. Only one sperm from among the millions present will be able to enter the egg and fuse with it.

individual.

It may also be deduced from these revelations that every one of us is carrying biomemes of hitherto unexpressed human potential for transmission to the next generation. It is one's biomemome that determines the biomemes to be expressed by the individual during his/her life and the biomemes to be generated in the gametes through biosoftware engineering processes for transmission to the next generation. The presence of unexpressed biomemes in one's biomemome makes him a 'biomemetic vector' (**Figure 3**) in the sense that he carries unexpressed biomemetic information for transmission to future generations [1].

The Quranic revelations are a clear indication of the programmed biodiversification process in human beings. Each human being represents a link in the biodiversification chain and carries a specific set of biomemetic instructions transmitted down to him through programmed diversification of the original *nafs* of Adam. The process preserves the continuity of a common bioinformation pool. It is not possible to say whether *Homo sapiens* has attained yet the maximum potentials physically and mentally. What we observe now is the scale of human biodiversity created so far. The biodiversification process will go on till the end of the world bringing about all the variability specified in the microbioprogram of human species (*i.e.*, Adam's *nafs*) at prescribed times and in prescribed geographic locations.

5. CREATION OF LIFE FROM NON-LIFE

From the foregoing, it is obvious that molecular biosoftware

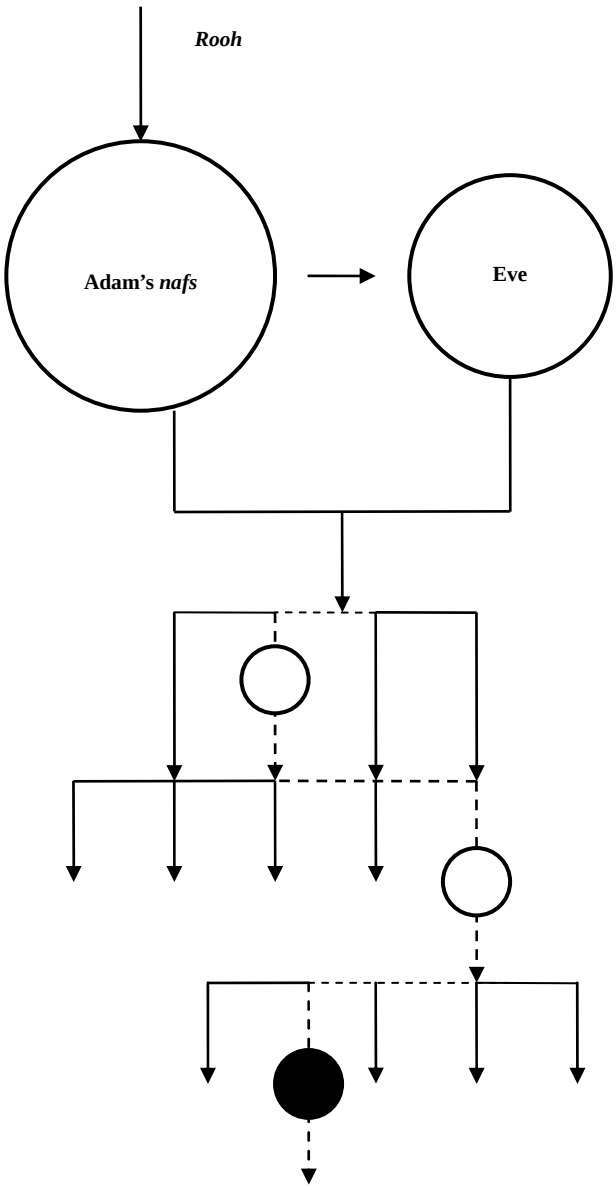

Figure 3. Illustration of programmed human biodiversification from a common biomeme pool (Adam's *nafs*). Note: A hypothetical biomemetic pathway of a biomeme is shown in the diagram by dashed line. Filled circle represents the individual in whom the biomeme is expressed. Unfilled circles represent vectors of the biomeme along the germ line. Downward arrows indicate diverse lineages. Racial, ethnic, linguistic, geographic, cultural and other types of phenomic diversity may be supposed to have been created in this way.

(genome) concept has several inexplicable anomalies and chemically untenable features. In contrast, Scriptural revelation of non-molecular biological information enables us to explain the phenomenon of life including human biodiversification comprehensively. Biologists are unable to explain "life" and "death" because the molecular gene and genome concepts adopted by them are

wrong. In other words, life is not a material phenomenon. Non-recognition of this truth leads biologists to try out synthesizing "life" from non-life. To create 'life", biologists start from scratch by synthesizing genome, chromosome, or a cell through artificial means using chemical molecules. Synthesis of these should in no way involve the use of living cell since it is likely that the non-molecular biosoftware of the living cell can be copied to the material or the cell being synthesized. The problem can be however approached from a totally different angle. Instead of creating synthetic cell without involving a living organism (which of course is impossible), a dead cell can be considered as equivalent to a prosthetic cell. It can be used as the starting material for the creation of life. The dead cell provides all the hardware configuration of a cell (genome, cytoplasm and other cell structures including cell wall) except life (biosoftware). That is to say, it is materially identical to a living cell. Biologists only have to restore life to it by chemical means without employing a living cell to prove that life is a material phenomenon and it originated from the combination of chemical molecules in the primitive environment. It may be noted in this context that the Scriptural revelation of non-material nature of bioinformation is a falsifiable proposition in the true scientific tradition. The failure to create a living cell through chemical synthesis without using a living cell or to restore life to a dead cell in fact invalidates the molecular biological program (genome) concept confirming instead the validity of the Scriptural revelation of the non-molecular invisible nature of the biosoftware and the existence of God.

REFERENCES

[1] Wahid, P.A. (2007) An introduction to islamic science. Adam Publishers and Distributors, New Delhi.

[2] Wahid, P.A. (2010) Memetics of the computer universe based on the Quran. *Journal of Software Engineering and Applications*, **3(7)**, 728-735.

[3] Portin, P. (1993) The concept of the gene: Short history and present status. *The Quarterly Review of Biology*, **68(2)**, 173-223.

[4] Fogle, T. (2000) The dissolution of protein coding genes in molecular biology. In: Beurton, P., Raphael, F. and Rheinberger, H.J. Eds., *The Concept of the Gene in Development and Evolution. Historical and Epistemological Perspectives*, Cambridge University Press, Cambridge, 3-25.

[5] Morange, M. (2000) The developmental gene concept: History and limits. In: Beurton, P., Raphael, F. and Rheinberger, H.J. Eds., *The Concept of the Gene in Development and Evolution. Historical and Epistemological Perspectives*, Cambridge University Press, Cambridge, 193-215.

[6] Eddy, S.R. (2001) Non-coding RNA genes and the modern RNA world. *Nature Reviews Genetics*, **2**, 919-929.

[7] Judson, H.F. (2001) Talking about the genome. *Nature*, **409**, 769, cited at: "Gene definitions", http://www.genomicglossaries.com/content/gene_def.asp

[8] Holdrege, C. (2005) The Gene: A Needed Revolution. *In Context*, **(14)**, 14-17, http://natureinstitute.org/pub/ic/ic14/gene.htm

[9] Keller, E.F. (2005) The Century of the Gene. Harvard University Press, http://www.scienceandreligionbookstore.org/book_details.asp?book_id=1231

[10] Meyer, S.C. (2004) The origin of biological information and the higher taxonomic categories. *Proceedings of the Biological Society of Washington*, **117**, 213-239.

[11] Ohno, S. (1998). The notion of the Cambrian pananimalia genome. *Proceedings of National Academy of Sciences*, **93**, 8475-8478.

[12] Chicurel, M. (2001) Can organisms speed their own evolution? *Science*, **292**, 1824-1827.

[13] Cairns, J., Overbaugh, J. and Miller, S. (1998) The origin of the mutants. *Nature*, **335**, 142-145.

[14] Goodman, B. (1992) Directed mutations: Heredity made to order. *Mosaic*, **23**, 24-33.

[15] Kohanski, M.A., DePristo, M.A. and Collins, J.J. (2010) Sublethal antibiotic treatment leads to multidrug resistance via radical-induced mutagenesis. *Molecular Cell*, **37**, 311-320.

[16] Enserink, M. (2010) ScienceNOW Daily News, **11**.

[17] Pennisi, E. (1998) How the genome readies itself for evolution. *Science*, **281**, 1131-1134.

[18] McClintock, B. (1987) The discovery and characterization of transposable elements. New York, Garland,

[19] Grant, P.R.andGrant, B.R. (2002) Unpredictable evolution in a 30-year study of Darwin's finches. *Science*, **296**, 707-711.

[20] Wahid, P.A. (2007) The Computer universe: A scientific rendering of the holy quran. Adam Publishers and Distributors, New Delhi.

[21] Rosenfeld, A. (1981) Master molecule heal thyself. *Mosaic*, **12(1)**.

[22] Wells, J. (2001) Homology in biology: A problem for naturalistic science. http://www.trueorigin.org/homology.asp

[23] Blaxter, M. (2003) Two worms are better than one. *Nature*, **426**, 395-396.

[24] Gibbs, W.W. (2003) The unseen genome: Gems among the junk. *Scientific American*, **289**, 46-53.

[25] Evans, J.D. and Wheeler, D.E. (1999) Differential gene expression between developing queens and workers in the honeybee, *Apis mellifera*. *Proceedings of National Academy of Sciences*, **96**, 5575-5580.

[26] Gottlieb *et al*., (2009) BAK1 gene variation and abdominal aortic aneurysms. *Human Mutation*, **30**, 1043.

[27] Snyder, M. and Gerstein, M. (2003) Genomics: Defining genes in the genomics era. *Science*, **300**, 258- 260.

[28] Grantham, R.L. (2001) Codon usage in molecular evolution. John Wiley & Sons, New York.

[29] Grantham, R. *et al*., (1981) Codon catalog usage is a genome strategy modulated for gene expressivity. *Nucleic Acids Research*, **9**, 43-47.

[30] Wahid, P.A. The Divine expert system. Centre for Studies on Science, Muslim Association for Advancement of Science, Aligarh, India.

[31] Guin, K. The facts of life. *UC Davis Magazine*, http://ucdmag.ucdavis.edu/su96/ magTOC.html
[32] Ralt *et al*. (1991) Sperm attraction to a follicular factor(s) correlates with human egg fertilizability. *Proceedings of the National Academy of Sciences*, **88(7)**, 2840-2844.

Advances in Bioscience and Biotechnology, 2010, 1, 348-352 **ABB**
doi:10.4236/abb.2010.14045 Published Online October 2010 (http://www.SciRP.org/journal/abb/).

N-methyl-D-aspartate (NMDA) mediates vascular relaxation via nitric oxide (NO) in rats but not in mice

Francesco Crespi

Biology Dept, Neurosciences CEDD GlaxoSmithKline, Medicines Research Centre, Verona, Italy.
Email: Francesco.M.crespi@GSK.com

Received 26 April 2010; revised 7 June 2010, accepted 28 June 2010.

ABSTRACT

Amperometric studies have indicated that substance P as well as NMDA stimulates release of NO in rat aortic rings. These data have been confirmed by functional observations of vaso-relaxant action of NMDA within noradrenaline pre-contracted aortic rings, supporting the presence of NMDA receptor in rat aortic rings. It is known that the enzyme endothelial NO synthase (eNOS) mediates vasodilatation not only in rats, but also in C57BL6 mice aortic ring, indicating that in this blood vessel NO is the endogenous endothelium-derived vasodilator. In this work, amperometry together with specifically nitrites insensitive micro-biosensors have been applied to examine the effect of NMDA and substance P upon NO release in rat and in two strains of mice aortic rings. The electrochemical data monitored demonstrate that NMDA mediates vascular relaxation via NO in rats but not in mice. These results are supported by functional data, therefore they suggest that NMDA receptors are "not responding" within these experimental conditions in mice aortic rings.

Keywords: Nitric Oxide; Amperometry; Carbon Fibre Micro-Electrodes; Mice; Rats; Aortic Rings; N-Methyl-D-Aspartate; Substance P

1. INTRODUCTION

In vivo studies have demonstrated the possibility to monitor NOx [mixture of nitrites and nitrates, *i.e.* metabolites of nitric oxide (NO)] by means of *in vivo* microdialysis in rat brain [1]. More recently, direct and selective measurement of NO has been performed by means of nitrites and nitrates insensitive carbon fibre micro-electrodes (mCFE) used as micro-biosensors in association with an electrochemical methodology such as amperometry [2-4].

In particular, these two *in vivo* electrochemical methodologies have shown that:

1) Infusion of N-methyl-D-aspartate (NMDA) via the microdialysis probe resulted in a dose-dependent increase in cerebellar NOx release. This increase was prevented by prior administration of an NMDA-receptor antagonist (*i.e.* AP5) or the NO synthase inhibitor N-G-nitroarginine. These results provided direct evidence for NOx release in response to NMDA receptor activation in the cerebellar cortex of adult rat [1].

2) Amperometric analyses performed in the striatum of anaesthetized adult rats, also showed that NMDA stimulates cerebral NO release *in vivo* and that treatment with NMDA receptor antagonists or NOS inhibitors prevented the NMDA-induced NO related signal. Furthermore, amperometric experiments performed together with selective NO detecting mCFE in rat aortic rings, did provide evidence that oxidation of NO can be directly and selectively measured within the lumen of such peripheral tissue [3,4]. In particular, addition of substance P [an amidated peptide which is a potent endothelium dependent vasodilator as it activates the enzyme nitrogen monoxide synthase in endothelial tissue (eNOS)] resulted in increased NO levels in rat aortic rings [3,4]. Accordingly, addition of NMDA to this peripheral tissue resulted in electrochemical activation, *i.e.* punctual increase of amperometric NO signal together with concomitant vascular relaxation (functional activity) [3,4]. These original data have then demonstrated that NMDA can stimulate NO release in rat aortic rings.

Previous works have shown that eNOS mediates vasodilatation also in C57BL6 mice aortic rings [5]. Indeed, in this tissue acetylcholine induced an endothelium-dependent relaxation that was inhibited by Nω-L-nitro-arginine, indicating that in this blood vessel NO is the sole endogenous endothelium-derived vasodilator [6]. Therefore, in mice, as well as in rats, NO has been implicated in the regulation of blood pressure [5].

In the present work, the feasibility of using amperometry and NO sensitive mCFE to analyze NO activ-

ity not only in rats but also in mice aortic rings has been tested.

2. METHODS

Naïve adult male CD rats (250-280 g) and two strains of mice: C57BL6 mice (20-22 g) and CD1 mice (20-22 g, Charles River) were supplied by Charles-River (Italy) and were kept in temperature- and humidity-controlled rooms (22°C, 50%) with lights on from 0700 to 1900 hours with water and food available *ad libitum*. All procedures were carried out in accordance with the Italian law (Legislative Decree no.116, 27 January 1992), which acknowledges the European Directive 86/609/EEC, and were fully compliant with GlaxoSmithKline policy on the care and use of laboratory animal and codes of practice. Furthermore, all efforts were made to minimize the number of animals used and their suffering.

Rat aortic rings (approximately 3 mm in length and 1.5 mm diameter) and mice aortic rings (approximately 3 mm in length and 0.5-1 mm diameter) have been prepared accordingly to the literature [7] and maintained in aerated Krebs with the addition of calcium and glucose. Then, each aortic ring was positioned within the voltammetric well and immersed in 200 µl of Krebs as described earlier [4].

The NO sensitive carbon fibre micro electrode (mCFE, 30 µm diameter, 3 mm length) was prepared as previously illustrated in order to avoid detection of nitrites, *i.e.* NO metabolites having an oxidation potential similar to that of NO: approximately + 700/+ 800 mV [8]. Briefly, the micro-biosensor was coated with Nafion, a sulphonated polymer that repels anions (such as nitrites) while allowing the specific oxidative detection of NO [9,10]. In addition, the mCFE was electropolymerised with ortho-phenylenediamine (oPD) as described previously [11] in order to improve selectivity by limiting access of large molecules (such as nitrites), to the surface of the biosensor. Then, the mCFE was positioned in direct contact with the endothelium inside the lumen of the vessel ring under light microscopy (**Figure 1**). In such way "endothelial" amperometric experiments could be performed as reported earlier at the oxidation potential of + 800 mV [3,4] by means of the voltammetric apparatus "MicroAutolab II" (EcoChemie, The Netherland) [10]. Then two different current values were examined:

1) Basal current level expressed in nanoAmperes (nA) due to the oxidation of basal endogenous NO;

2) NO stimulated release, obtained via local application of:

- A chemical known to have vascular dilating properties such as Substance P [12];
- NMDA that has been described able to stimulate NO release in rat aortic rings [3,4,13].

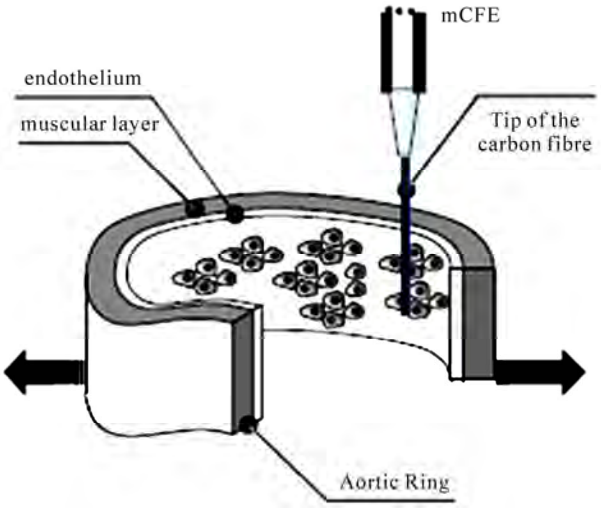

Figure 1. Functional and amperometric preparation for mice aortic rings immersed within 200 µl Krebs (test sample). The active tip (carbon fibre) of the Nafion-oPD CFE is parallel and in contact with the endothelium of the aortic ring. Arrows emulate the apparatus for functional studies as described previously [3,4].

3. RESULTS & DISCUSSION

It appeared that basal amperometric NO related current levels can be monitored in rats as well as in mice aortic rings. In particular, these amperometric NO basal current levels were similar within the two types of mice aortic rings: approximately 2.61 ± 0.52 nanoAmperes (nA) in C57BL6 and 3.49 ± 0.82 in CD1 mice while it was about 0.22 ± 0.03 nA in CD rats aortic rings.

Higher endothelial NO levels in mice than in rat aortic rings could be related to the smaller diameter of the lumen in the former specie in which therefore endothelial NO could more easily [and possibly more profusely] enter in contact with the mCFE. This will allow the mCFE to capture more NO within the reduced time-span [from fraction of second to few seconds] in which this highly reactive, short living molecule is present in the aortic lumen [14-16].

Successively, stimulation of the release of NO was performed as described earlier [3,4]. Briefly, it consisted in a single addition of 5 µl Substance P 1 mM or NMDA 0.1 mM (or 5 µl of the vehicle Krebs, control experiment) to each mouse or rat aortic ring immersed within 200 µl of Krebs in the voltammetric well. Thus, in the well, the final concentration of Substance P and NMDA was 25 µM and 2.5 µM, respectively. The addition was performed during the amperometric scan that was lasting 300seconds: precisely it was done at the 50th second of the amperometric measurement [3,4].

Data obtained indicated that substance P was able to significantly increase the basal NO related amperometric

current levels monitored in rats and in mice aortic rings, while NMDA did induce significant release of NO in rats aortic rings only. More precisely, addition of NMDA within mice aortic rings resulted in a signal similar to that obtained when vehicle (Krebs) was added to the same aortic rings (see **Figure 2** and corresponding **Table 1**).

For an easier comparison between rats and mice values in **Figure 2** data are expressed in percent of control (addition of Krebs) while in **Table 1** amperometric NO levels are expressed in real current values (nA).

Therefore, the present data demonstrate that: 1) Substance P stimulated NO release within aortic rings of both CD1and C57BL6 mice as well as in rats; 2) in contrast to data monitored in rat aortic rings, NMDA did not cause NO release in aortic rings from both type of mice (see **Figure 2** and **Table 1**). Precisely, NMDA addition in the mice test samples was followed by a reduced, transient increase of the amperometric current similar to that obtained when Krebs (vehicle) was added (see **Table 1**). This small increase could be a nonspecific signal related to mechanical stimuli given to the tissue while performing the local application of compounds. On the other hand, this action could be sufficient to activate synthesis and release of a reduced amount of NO.

Thus, these ex vivo data indicate that NMDA was unable to stimulate a significant NO release when added to mice aortic rings, suggesting lack of NMDA receptor functioning or lack of or sensitivity to the [large] dose of NMDA applied in this mice peripheral tissue.

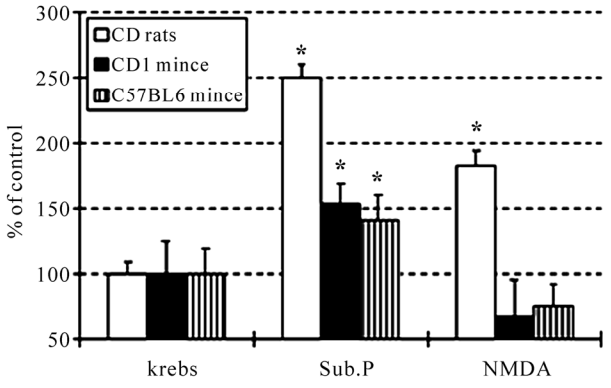

Figure 2. Mean of the size of the amperometric transient peaks monitored in CD rat, CD1 and C57BL6 mice aortic rings to which Krebs (vehicle, 5µl), Substance P (25 µM) or NMDA (2.5 µM) were added (n = 6 each compound). Data are expressed in % of control (addition of Krebs), mean ± S.D.; however, statistics were calculated from the raw data using ANOVA with STATISTICA software version 6.0. In the case of statistically significant differences between mean values produced by drug treatments versus controls (vehicle treatment) main factor Dunnet *post-hoc* test was applied. Statistical significance was set at $p < 0.05$ [*].

Table 1. Mean of the size (current level) of the transient amperometric NO related peaks resulting from addition of Krebs (vehicle, 5 µl), Substance P (25 µM) or NMDA (2.5 µM) to aortic rings of CD1 mice, C57BL6 mice or CD rats (n = 6 each). Data are expressed in nA, mean ± S.D. *p < 0.05 Dunnett's test.

COMPOUND	CD1 mice Current level nA	C57BL6 mice	CD rats
Substance P	**8.47** ± 1.01*	**5.18** ± 0.78*	**0.75** ± 0.08*
NMDA	**3.68** ± 0.47	**2.77** ± 0.34	**0.55** ± 0.06*
Krebs	**4.15** ± 0.79	**2.76** ± 0.52	**0.30** ± 0.03

Functional studies [17] have been undertaken in order to verify this hypothesis: in particular, the already proposed feasibility of combining amperometry with functional test [3] has been further verified. Briefly, aortic rings from both type of mice were maintained within Krebs in the voltammetric well and were contracted via addition of 1 µM noradrenaline (NA) (see **Figure 3(a)**: arrow a). Successively the active tip (3 mm length) of the NO sensitive mCFE was positioned parallel and in contact with the ring endothelium as described above (figure 1 top). Then nitrites 100 µM and NO 6.6 µM (**Figure 3(a)**: arrows b and c, respectively) were consecutively added to the well.

It appeared that in both strains of mice:

1) Addition of nitrites did not alter the contracted state of the aortic ring as well as the amperometric current monitored concomitantly (see **Figure 3(a)** and **(b)**, arrows b).

2) Successive addition of NO was followed by vaso-relaxation and concomitant significant increase of the amperometric signal (**Figure 3(a)** and **(b)**, arrow c).

These data confirm that NO is the compound responsible for vascular relaxation [6] and that its presence as well as its vaso-relaxing efficacy can be directly monitored by means of amperometric measurements associated with functional analysis.

In successive analysis, 1µM NA pre-contracted rats or mice aortic rings were prepared in Krebs at 37°C as described earlier [7,17]. Then acetylcholine (ACh, used as a reference compound [7] or NMDA at various concentrations (from 1 nM to100 µM) were added. This resulted in the expected ring relaxation in response to Ach in both rats and mice aortic rings tested. In contrast, no relaxation was monitored in mice aortic rings in response to any NMDA concentration, while rats aortic rings appeared to be responsive to the NMDA challenge (see **Figure 4**). This allows suggesting that NMDA addition to mice aortic rings does not stimulate NO release, therefore supporting the electrochemical data presented above.

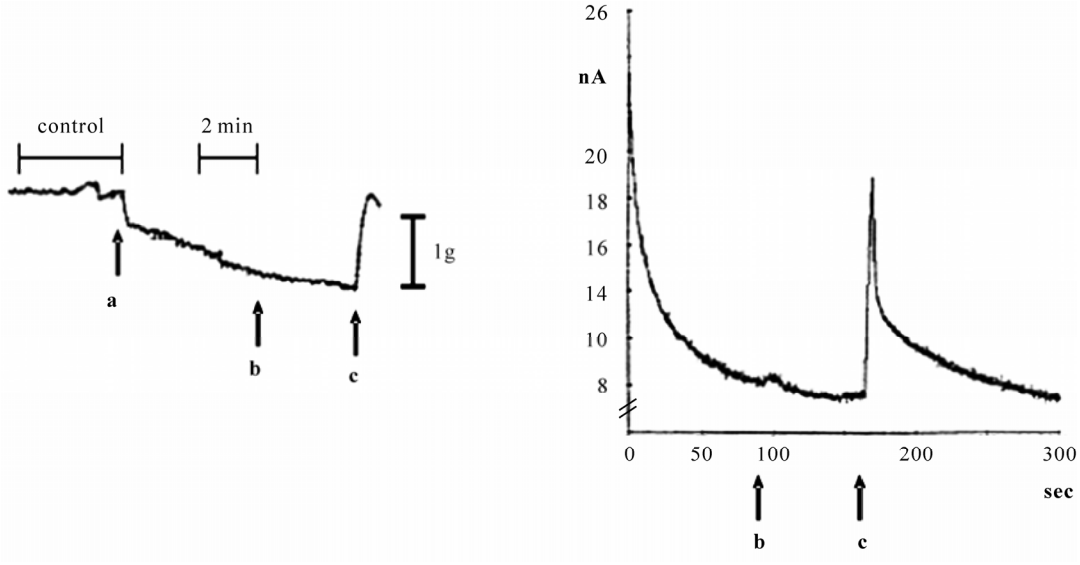

(a) (b)

Figure 3. (a) contracting effect of NA 1 µM (arrow a) upon an untreated (CONTROL) CD1 mouse aortic ring. Then nitrites 100 µM (arrow b) and NO 6.6 µM (arrow c), respectively were added to the aortic ring. Note that addition of NO but not addition of nitrites, relaxes the aortic ring. This figure is n = 1, very similar data have been obtained in aortic ring preparations from other 4 CD1 mice. Similar outcome was monitored in five C57BL6 mice and five rats; (b) concomitant amperometric measurements of the effect of addition of nitrites (arrow b) and NO (arrow c) upon basal current levels. Similar data have been obtained in five CD1, five C57BL6 mice and five rat aortic rings.

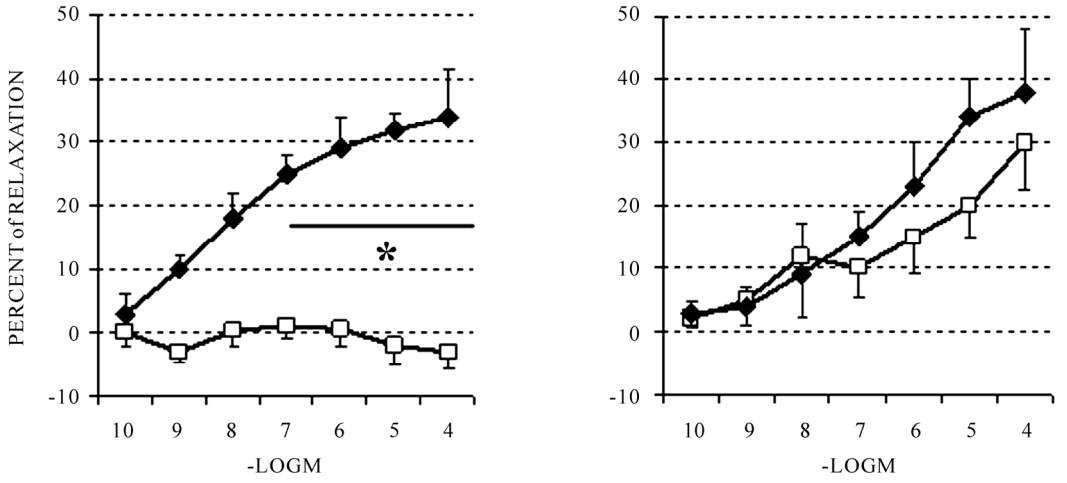

Figure 4. relaxation of mice [LEFT] or rats [RIGHT] aortic rings pre-contracted with NA 0.1 µM following treatment with ACh (◆) or NMDA (□) at various concentrations. Data are expressed in % of relaxation considering zero% as maximum contraction level of each aortic ring. Mean ± S.D., n = 5 aortic rings for each compound tested, *p < 0.05 [see above for statistic evaluation].

When the present data are compared with similar experiments performed earlier in rats [4] it appears that NA has to be more concentrated to obtain vascular contraction in mice than in rats *i.e.* 1 µM in mice versus 0.1 µM in rats [4]. On the other hand, vasodilatation has been obtained with lower ACh concentration in mice (approximately 15% or 28% relaxation with ACh 10 nM or 1 µM, respectively) than in rats (approximately 5% or 18% relaxation with ACh 10 nM or 1 µM, respectively [3]). These data indicate that higher concentration of NA or lower concentration of ACh are needed to obtain vascular contraction or vasodilatation in mice, respectively when compared to similar functional tests in rats. Thus, these data further support the hypothesis mentioned

above about a possible higher "reactivity" of endothelial NO system in mice than in rats. Finally, these data provide direct evidence that amperometry can monitor basal as well as stimulated NO activity within rodents aortic rings and that this electrochemical methodology can be associated with functional vascular studies. In addition, they propose that NMDA directly mediates vascular relaxation via NO in rats but not in mice, suggesting that NMDA receptor could be "functionally" absent in C57BL6 as well as CD1 mice aortic rings.

REFERENCES

[1] Luo, D., Knezevich, S. and Vincent, S. (1993) NMDA induced NO release: An *in vivo* microdialysis study. *Neuroscience*, **57**, 897-900.

[2] Crespi, F. (1990) *In vivo* voltammetry with microbiosensor for analysis of neurotransmitter release and metabolism. *Journal of Neuroscience Methods*, **34**, 53-658.

[3] Crespi, F., Lazzarini, C., Andreoli, M. and Vecchiato, E. (2000) Voltammetric and functional evidence that *N*-methyl-D-aspartate and substance P mediate rat vascular relaxation via nitrogen monoxide release. *Neuroscience Letters*, **287(3)**, 219-222.

[4] Crespi, F., Vecchiato, E., Lazzarini, C. and Gaviraghi, G. (2001) Electrochemical evidence that lacidipine stimulates release of nitrogen monoxide (NO) in rat aorta. *Neuroscience Letters*, **298(3)**, 171-174.

[5] Huang, P.L., Huang, Z., Mashimo, H., Bloch, K.D., Moskowitz, M.A. and Fishman, M.C. (1995) Hypertension in mice lacking the gene for endothelial nitric oxide synthase. *Nature*, **377(21)**, 239-242.

[6] Chataigneau, T., Feletou, M., Huang, P.L., Fishman, M.C., Duhault, J. and Vanhoutte, P.M. (1999) Acetylcholine-induced relaxation in blood vessels from endothelial nitric oxide synthase knockout mice. *British Journal of Pharmacology*, **126(1)**, 219-226.

[7] Furchgott, R.F. (1980) The obbligatory role of endothelial cells in the relaxation of arterial smooth muscle by Acetylcholine. *Nature*, **288**, 373-376.

[8] Privat, C., Lantoine, F., Bedioui, F., Millanvoye, van Brussel, E., Devynck, J. and Devynck, M.A. (1997) Nitric Oxide production by endothelial cells: comparison of three methods of quantification. *Life Sciences*, **61(12)**, 1193-1202.

[9] Crespi, F., Martin, K.F. and Marsden, C.A. (1988) Measurement of extracellular basal levels of serotonin *in vivo* using nafion coated carbon fibre microelectrodes combined with differential pulse voltammetry. *Neuroscience*, **27**, 885-898.

[10] Crespi, F. (2009) Anxiolytics antagonize Yohimbine-induced central noradrenergic activity: a concomitant *in vivo* voltammetry-electrophysiology model of anxiety. *Journal of Neuroscience Methods*, **180**, 97-105.

[11] Friedemann, M.N., Robinson, S.W. and Gerhardt, G.A. (1996) *o*-Phenylenediamine-Modified Carbon Fiber Electrodes for the Detection of Nitric Oxide. *Analitical Chemistry*, **68**, 2621-2628.

[12] Oldham, C.D., Li, C., Feng, D., Scott, R.O., Wang, W.Z., Moore, A.B., Girard, P.R., Huang, J., Caldwell, R.B., Caldwell, R.W. and May, S.W. (1997) Amidative peptide processing and vascular function. *American Journal of Physiology*, **273**, 1908-1914.

[13] Crespi, F. and Rossetti, Z. (2004) Pulse of Nitric Oxide Release in Response to Activation of N-Methyl-D-Aspartate Receptors in the Rat Striatum: Rapid Desensitisation, Inhibition by Receptor Antagonists and Potentiation by Glycine. *Journal of Pharmacology & Experimental Therapeutics*, **309(2)**, 462-468.

[14] Moncada, S., Palmer, R.M.J. and Higgs, E.A. (1989) Biosynthesis of nitric oxide from L-arginine. A pathway for regulation of cell function and communication. *Biochemical Pharmacology*, **38**, 1709-1715.

[15] Rossetti, Z.L. and Crespi, F. (2004) Inhibition of nitric oxide release *in vivo* by ethanol. *Alcoholism*: *Clinical Experimental Research*, **28**, 1746-1751.

[16] Wood, J. and Garthwaite, J. (1994) Models of the diffusional spread of nitric oxide: implications for neural NO signalling and its pharmacological properties. *Journal of Neuropharmacology*, **33(11)**, 1235-1244.

[17] Furchgott, R.F. (1984) The role of endothelium in the responses of vascular smooth muscle to drugs. *Annual Review of Pharmacology & Toxicology*, **24**, 175-197.

Advances in Bioscience and Biotechnology, 2010, 1, 353-361 **ABB**
doi:10.4236/abb.2010.14046 Published Online October 2010 (http://www.SciRP.org/journal/abb/).

Genetic variability of *Aspergillus terreus* from dried grapes using RAPD-PCR

Banu Narasimhan, Madhivathani Asokan

Assistant Professor, Vels University, Pallavaram, Chennai.
Email: banunkl@yahoo.com

Received 6 May 2010; revised 7 June 2010; accepted 18 June 2010.

ABSTRACT

RAPD was used to examine the genetic variability among five isolates of *Aspergillus terreus* spp.. Two random primers were selected for the RAPD assay PG01–5' CAGGTGTTGC 3' and PG02–5' CTGGACAGAC 3' (Progen Technologies). The characterization of *Aspergillus terreus* species have been mostly applied on the basis of morphology, phenotype and physiology. DNA Polymorphisms are based on differences in DNA sequences and have advantages over protein polymorphisms. But morphological characterization besides molecular tools will remain a basic and powerful key in the identification of *Aspergillus terreus* species. The objective of the present study was to isolate the fungal contaminants from dried grapes and compare the genomic profile of the *Aspergillus terreus* speices isolated from the dried grapes, through RAPD analysis. In the present study with primer PG 01 four different discriminations was there among the *A. terreus* isolates. There was a homology of genotype between the isolates 1 & 3. And with primer PG 02 four different discriminations were there and there was a homology between 1 & 3. The predominant type was type I in primer I & II. The other isolates belonged to 2, 3 and 4. No similarity was detected for isolates 3, 4 and 5 indicating great genomic diversity of *A. terreus*.

Keywords: *Aspergillus Terreus*, Dried Grapes, Genetic Variability, RAPD-PCR.

1. INTRODUCTION

Aspergillus terreus is a common soil saprophyte that has been recovered from desert soil, grasslands and compost heaps. *A. terreus* produces a variety of secondary metabolites that are economically significant, such as lovastatin, a antihypercholesteroleic drug [1]. Importantly, most members of this species have decreased susceptibility to the antifungal drug amphotericin B (AMB) *in vitro* and *in vivo* [2]. Accordingly, the ability to distinguish *A. terreus* from other species of *Aspergillus* can be important to the clinician for therapeutic decision making and prognosis.

In addition, *A. terreus* produces globose, heavy-walled hyaline cells laterally on the hyphae, which are called accessory conidia or are sometimes referred to as aleuroconidia. *A. terreus* is the only member of the genus *Aspergillus* that produces such structures [3].

The genus *Aspergillus* is divided into seven subgenera, which in turn are subdivided into several sections with each section comprised of a few to several closely related species. Using morphological methods as delineators, Raper and Fennell recognized *A. terreus* as the only known species within the section *Terrei*, subgenus *Nidulantes*, along with the rarely encountered varieties of *A. terreus var*. *aureus* and *A. terreus* var. *africanus* [3]. Both of these varieties of *A. terreus* differ significantly from *A. terreus* morphologically in that both grow as bright orange colonies and *A. terreus var. africanus* sometimes produces sclerotium-like bodies on laboratory media.

Several recent studies have clearly demonstrated that morphological methods are poor markers of species in the genus *Aspergillus*, and molecular methods may be useful in species identification [4,5]. Phylogenetic analyses of DNA sequences derived from ITS regions and showed the presence of three main clades, which included *A. terreus*, *A. carneus* and *A. niveus* within the section *Terrei* [1]. However, that study concluded the section *Terrei* warranted further detailed molecular analysis including more loci and isolates. It has been known for sometime that apart from *A. terreus*, numerous cryptic species may be present within the section *Terrei*. Phylogenetic analyses using sequence information from multiple protein coding regions may further clarify the taxonomy of these isolates within the section.

Previous phylogenetic studies in the section *Fumigati*,

genus *Aspergillus* have revealed the presence of numerous species which were not morphological methods alone. For example, *A. lentulus* as a novel, cryptic species within the section *Fumigati* by employing both the maximum likelyhood algorithms, as well as utilizing DNA sequence information from the ITS region, the mitochondrial cytochrome b region, and protein coding region for the β-tubulin gene, the rodlet A gene and the salt responsive gene [4]. Phylogenetic analyses revealed that *A. lentulus* isolates were present as a monophyletic clade in the majority of the single-locus genealogies, thus, fulfilling the phylogenetic species recognition concept, which requires both genealogical concordance and genealogical nondiscordance in the genealogies evaluated.

Invasive fungal infection due to *Aspergillus* species have become a major cause of morbidity and mortality among immunocompromised patients. *Aspergillus fumigatus* is most frequently isolated from clinical specimens, but other important species include *A. flavus*, *A. niger* and *A. terreus*. *A. terreus* appears to be emerging as a cause of opportunistic infections [5-7].

Aspergillus spp. moulds can cause various diseases, invasive aspergillosis (IA), aspergilloma, allergic bronchopulmonary aspergillosis, rhinocerebral aspergillosis and otomycosis being the most frequent forms. IA is the most life threatening one, which recently possess a threat not only to patients suffering from hematological malignancies [8]. It also occurs in a much broader patient population then the classical immunocompromised hosts and includes mechanically and ventilated intensive care unit patients and patients receiving coreicosteroids for treatment of chronic lung diseases [9].

RAPD-PCR typing has proven useful in many epidemiological investigations [2,10]. The polymerase chain reaction (PCR) has been adapted for fingerprinting microorganisms by using paired primers derived from previously characterized sequences for PCR amplification. This technique has been applied to bacteria, [11], viruses [12] and fungi .

Based on PCR amplifications, a new DNA polymorphism assay, random amplification of polymorphic DNA (RAPD), was developed [13,14]. Random sections of genomic DNA are amplified by using a single arbitrary nucleotide sequence to make polymorphic DNA patterns.

No prior sequence information is required for this method, which has been used to differentiate organisms with close relationships and particularly to differentiate isolates below the species level [15-19]. Furthermore, PCR makes it possible to analyze a small amount of genetic material and handle a large number of specimens in a short time. Furthermore, RAPD was applied to these strains to develop an accurate and simple method for differentiating *Aspergillus terreus*.

The method has been applied to two fungal plant pathogens, *Fusarium solani* and *Leptosphaeria maculans* [15,20]. The application of the random amplification of polymorphic DNA (RAPD) assay to the human pathogen *A. fumigatus* was described in the year 1993 [16].

Recently, the development of molecular biology has made it possible to study taxonomy by investigating genetic materials directly in addition to observing the expresses behavior of genetic materials. Several molecular characteristics, such as DNA base composition, DNA hybridization, and rRNA relatedness, etc., have been applied in fungal classification [21]. PCR was adapted to fingerprint microorganisms by using paired primers derived from previously characterized sequences for PCR amplification.

Besides, with RAPD, the appearance of new ligation sites only creates new annealing sites without impairing pre-existing ones, which would continue to be amplified. Consequently, RAPD allows an independence of characters, which is a clear advantage over techniques that directly or indirectly make use of restriction enzymes, such as restriction fragment length polymorphism (RFLP). Various phenotypic and genotypic methods have been used successfully in fingerprinting *A. fumigatus*. However, no comparable data are available for *A. terreus*. For those reasons, we aimed to compare the genomic profile of different strains of *A. terreus* isolated from five samples through RANDOM AMPLIFICATION OF POLYMORPHIC DNA (RAPD) analysis.

2 MATERIALS AND METHODS

2.1. Collection of Samples

Five different samples of dry grapes were collected for the isolation of *Aspergillus terreus*.

2.2. Morphological Studies

2.2.1. Isolation and Identification

Five different samples of dry grapes were collected for the isolation of *A. terreus*. Grapes were surface sterilized with 0.1% Mercuric chloride and placed on the CDA medium. The plates were then incubated at room temperature for about 3-4 days. Triplicates were maintained for each sample. The identification and nomenclature of *Aspergillus terreus* was done with standard manual [3].

2.2.2. Subculturing

Among the various colonies identified, only *Aspergillus terreus* colonies were subcultured onto the Czapek-Dox Agar plates amended with chloramphenicol under sterile conditions, to obtain the pure culture. These plates were

then incubated at room temperature (30°C) for about 3-4 days.

2.3. Molecular Genotyping

The Czapek-Dox Broth was prepared and 100 ml of the medium was dispersed equally into ten separate 250ml conical flasks. These were sterilized in an autoclave at 121°C for 15 minutes at 15 lbs pressure. The flasks were inoculated with the isolates of *Aspergillus terreus* under sterile conditions and were then subjected for incubation at room temperature for about 3-4 days.

The flasks were observed every day for the growth of the fungus. The mycelial mats should be harvested within 36-40 hours of incubation. The harvested mats were then stored at 4°C under sterile conditions for further use.

2.3.1. DNA Extraction and Isolation [22]

0.2-0.5 g (dry wt) of lyophilized pad was taken in a 50 ml disposable centrifuge tube, by brief shaking the pad was powdered with the help of a spatula or glass rod. 10 ml (for 0.5 g pad) of CTAB extraction buffer was added gently mixed to wet all the powdered pad. It was placed in 65°C water bath for 30 minutes. It was Cooled and equal volume chloroform: ethanol (24:1) was added and mixed. The tubes were centrifuged in table-top centrifuge for 10 minutes at full speed. The aqueous supernatant was transferred to a new tube. An equal volume of isopropanol was added and centrifuged at low speed for 5 minutes. The supernatant was poured out. The pellet containing DNA was rinsed with 70% ethanol. It was air dried and 1-5 ml of TE containing 20 µg/ml of Rnase A was added. The samples were placed in 65°C bath, or pellets were allowed to resuspend overnight at 4°C.

2.4. RAPD Analysis

The PCR Primer Used in this work was PG01–5' CAGGTGTTGC 3' and PG02–5' CTGGACAGAC 3' (Progen Technologies). The primer is 10 nucleotides in length, had G-C and A-T contents more or less equal in amounts and did not contain palindromic sequences.

Amplification was carried out with a 50 µL reaction mixture containing the following.

Primer (2 µM/µL)	-	8.0 µL
10X Buffer	-	5.0 µL
2 MmM dNTP Mix	-	5.0 µL
Taq DNA polymerase (U/µL)	-	0.5 µL
Template DNA (50 ng)	-	2.0 µL
Sterile Distilled Water	-	29.5 µL
Total	-	50.0 µL

2.4.1. PCR Amplification Condition

The Amplification was carried out with Eppendorf Mastercycler® ep thermal cycler. The program used to carry out the amplification process is an initial denaturation at 94°C for 5 min, with 34 cycles of denaturation at 94°C for 40 sec, annealing at 36°C for 30 sec, extension at 72°C for 90 sec and a final extension at 72°C for 10 mins. Both the primers were run under the same conditions.

A blank control with all the PCR reagents except DNA was always included. The resulting banding patterns were indexed by capital letters and even a single band mismatch led to a different letter code.

The amplified products were separated on a 0.8-1% agarose gel in 1X TBE at 75V for 3 h. The gel was stained with ethidium bromide and the amplified product was visualized under a UV transilluminator. Gel products were sized to a relative to a 1 kb ladder standard. A molecular weight marker was run in parallel. RAPD patterns were compared visually. An isolate was defined as different when a band with a density equal to or greater than that that of the 0.8 kb band of the marker occurred and no corresponding band (not even a trace) was detectable in the other isolates. To demonstrate reproducibility of the patterns, all isolates were investigated three times independently, with different subcultures.

2.5. Discrete Character Programme

Tree was constructed by using Phylip 3.69.

3 RESULTS

Altogether, five different fungi were isolated from the dried grapes. Among this *Aspergillus terreus* is the most prevalent organism (**Plate 1** & **2**).

3.1. Morphological Characteristics of Aspergillus Terreus

Aspergillus terreus belongs to the genus *Aspergillus*, sub-genus *Nidulantes* and it was identified in the laboratory by morphological methods. The *A. terreus* isolates did not differ in their macroscopic and microscopic morphology on Czapek-Dox agar, *A. terreus* showed rapid growth with very variable colony appearance ranging from heavily sporulating colonies to fluffy, poorly sporulating phenotypes. Microscopically, conidiophores are typically long, colourless (hyaline) and smooth giving rise to sub-spherical vesicles that are biseriate. Conidia range in size from 1.5-2.4 µm in diameter, are smooth walled, slightly elliptical and striate (**Plate 3** & **4**).

3.2. Molecular Characterization

3.2.1. Isolation of DNA

Genomic DNA was isolated from *Aspergillus terreus* obtained from five different dried grapes samples based

Plate 1. Plates showing fungal colonies on dried grapes.

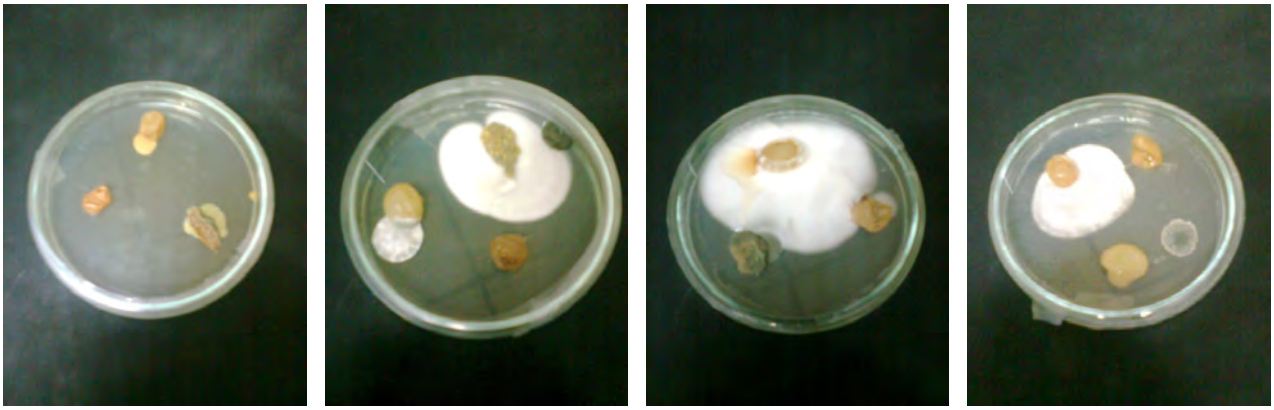

Plate 2. Plates showing fungal colonies on dried grapes.

on the protocol standardized. The isolated genomic DNA was checked on 0.8-1% agarose gel (**Plate 5**).

3.2.2. RAPD Analysis

3.2.3. Genotypic Typing

The isolated genomic DNA of *Aspergillus terreus* from dried grapes was amplified using the primers PG01–5' CAGGTGTTGC 3' and PG02–5' CTGGACAGAC 3' (Progen Technologies) and the amplification was carried out with EPPENDORF Mastercycler ep thermal cycler. The amplified DNA was checked in 0.8-1% agarose gel electrophoresis as shown in Plate VI & VII. The amplified DNA bands of *Aspergillus terreus* isolates were observed and compared to estimate the genetic diversity. Though there were many bands in the gel, only the brighter bands were selected for the analysis of genetic diversity.

The isolates 1 & 2 produced the bands at 1500 kb, 1750 kb and 2000 kb. The isolates 3 & 4 produced the bands at 1250 kb and 1500 kb. The isolates 4 & 5 produced the bands at 1200 kb. Only the isolate 4 produced a single band at 2750 kb. The isolate 1, 2, 3 and 4 produced the bands at 1500 kb (**Table 1**). The isolates 1, 3 and 5 produced the bands ay 1200 kb. The isolates 4 and 5 produced bands at 1500 kb. Only the isolate 2 produced a single band at 1250 kb. The isolate 5 produced a single band at 1750 kb and 2000 kb (**Table 2**). Two different primers were used for typing in RAPD- PCR. Both the primers discriminated four RAPD types within the five isolates of *Aspergillus terreus.* The predominant type was type I in primer I and primer II. The other isolates belonged to II, III and IV (**Table 3**).

3.2.4. Phylogenetic Tree

Phylogenetic tree based on random amplified polymorphic DNA Profiles (RAPD) showing the genetic relationships among the four isolates of Aspergillus terreus isolated from fresh grapes were generated with the primers PG01 and PG02.

4. DISCUSSION

The present study shows *A. terreus* to be common in the environmental as a contaminant of various food items and to be common as a cause of Aspergillosis in Immunocompromised patients.

The molecular genotyping of *Aspergillus* species has proven useful in many epidemiologic situations. One of the most widely used genotyping techniques is RAPD-PCR, a relatively technically simple and rapid procedure. Although RAPD-PCR has been criticized for a lack of

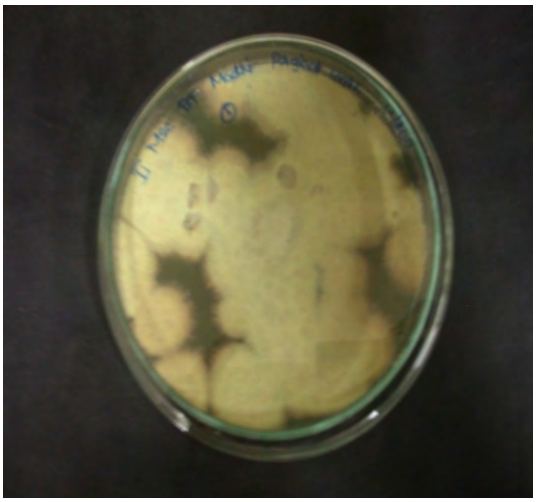

Aspergillus terreus isolate 1

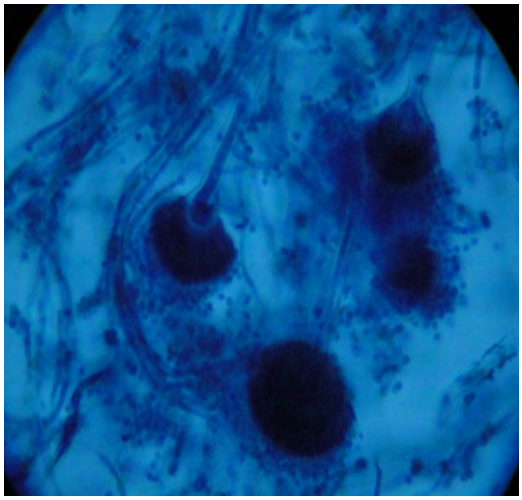

Microphotograph of *A. terreus* isolate 1

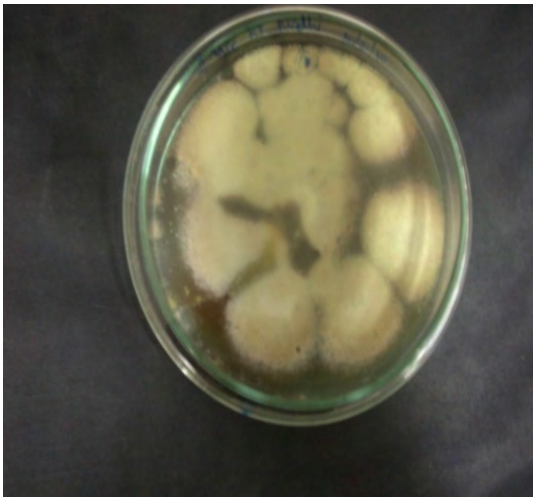

Aspergillus terreus isolate 2

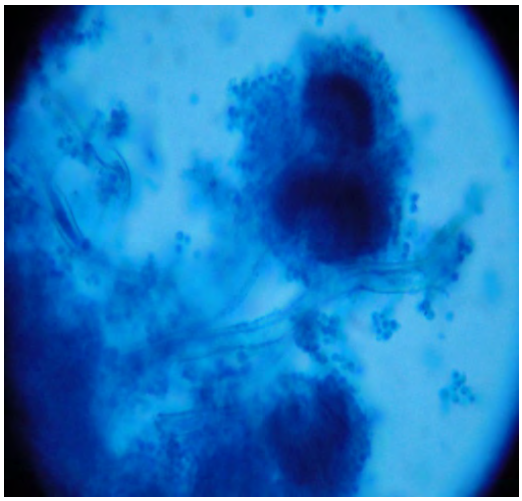

Microphotograph of *A. terreus* isolate 2

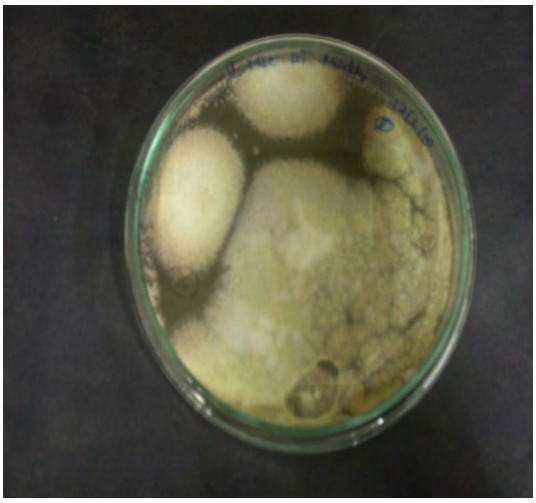

Aspergillus terreus isolate 3

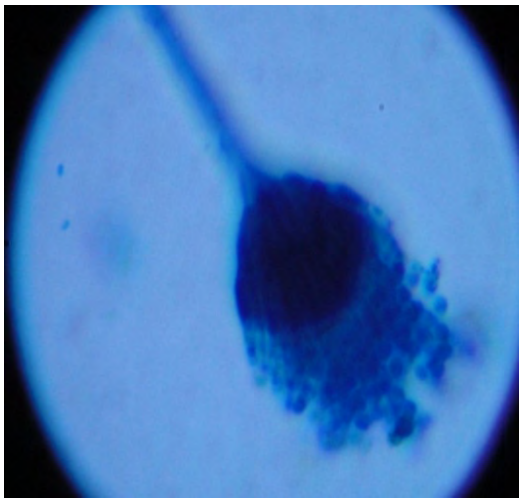

Microphotograph of *A. terreus* isolate 3

Plate 3. Plates with *Aspergillus terreus* isolates & its microphotographs.

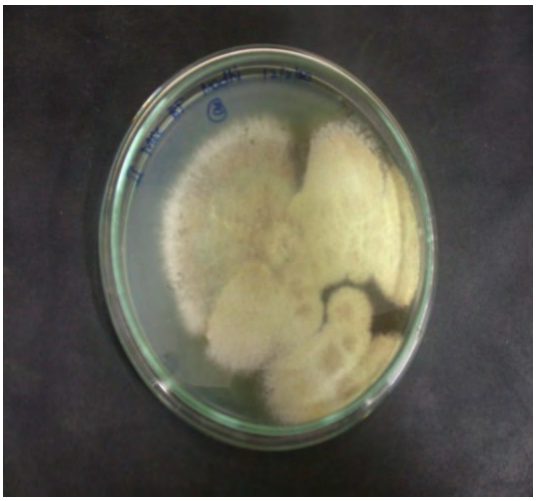

Aspergillus terreus isolate 4

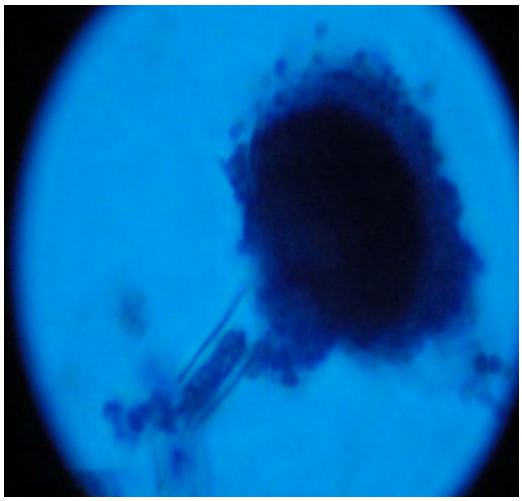

Microphotograph of *A. terreus* isolate 4

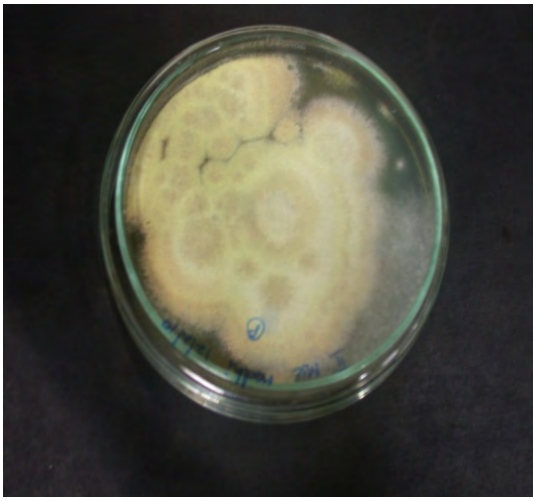

Aspergillus terreus isolate 5

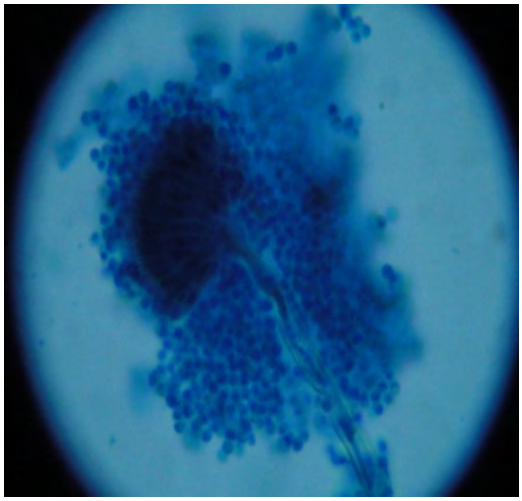

Microphotograph of *A. terreus* isolate 5

Plate 4. Plates with *Aspergillus terreus* isolates & its microphotographs.

reproducibility, this method has been used with the success for *A. terreus* isolates.

Five primers to test 14 isolates and found primers R108 and CII to be highly discriminatory [23]. Symoens and colleagues tested 43 isolates of environmental and clinical origins with the primers NS3 and NS7 [24]. Among epidemiologically unrelated species, the primers were highly discriminatory. In addition, they found RAPD-PCR to be useful tool in demonstrating the clonal origin of contamination of the environment in a hematology unit.

In the present study there are five different fungi were isolated (**Plate 1**, **2** and **3**). Among these *Aspergillus terreus* was given special emphasis for its genetic diversity. Five different isolates of *A. terreus* were isolated and they were subjected to morphological characterization. No difference was found in the macroscopic and microscopic morphology of the five different *A. terreus* isolates. Similar results were obtained by Rath [10]. The first report of different methods of strain differentiation for *A. terreus* was given by them. All isolates were produced aleuriospores, which are not only found in *A. terreus*, but also in *A. flavipens*, *A. niveus* and *A. carneus* [3] were found in the isolates under investigation. The RAPD analysis we performed was intended to assess the genetic diversity within the *A. terreus* species. RAPD fingerprints allow intraspecific genetic diversity studies but are not very good tools for such analysis at the interspecific level.

In the present study with primer PG 01 four different discriminations was there among the *A. terreus* isolates (**Table 1**; **Plate 6**). There is a homology of genotype between the isolates 1 & 3. And with primer PG 02 four different discriminations was there and there is a homology

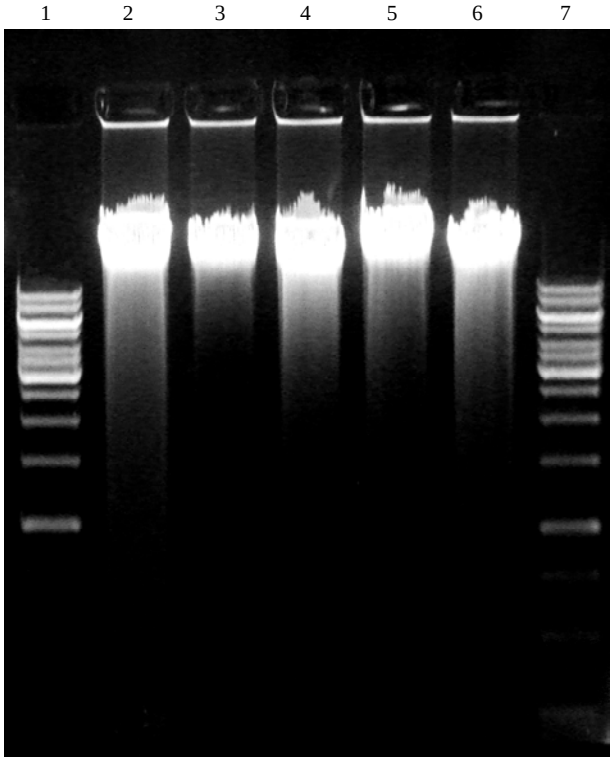

Lane 1-1 kb ladder; Lane 2-*Aspergillus terreus* isolate 1; Lane 3-*Aspergillus terreus* isolate 2; Lane 4-*Aspergillus terreus* isolate 3; Lane 5-*Aspergillus terreus* isolate 4; Lane 6-*Aspergillus terreus* isolate 5; Lane 7-1 kb ladder.

Plate 5. Genomic DNA of *Aspergillus terreus* isolates.

Table 1. RAPD Profile of *Aspergillus terreus* isolates from different samples with Primer PG01.

S. No	*Aspergillus terreus isolates*	Presence (+) or Absence (-) of Bands at the respective base pairs						
		1000	1200	1250	1500	1750	2000	2750
1	ISOLATE 1	-	-	-	+	+	+	-
2	ISOLATE 2	-	-	-	+	+	+	-
3	ISOLATE 3	+	-	+	+	-	-	-
4	ISOLATE 4	-	+	+	+	-	-	+
5	ISOLATE 5	-	+	-	-	-	-	-

Table 2. RAPD Profile of *Aspergillus terreus* isolates from different samples with Primer PG02.

S. No.	*Aspergillus terreus* isolates	Presence (+) or Absence (-) of Bands at the respective base pairs				
		1200	1250	1500	1750	1800
1	ISOLATE 1	+	-	-	-	-
2	ISOLATE 2	-	+	-	-	-
3	ISOLATE 3	+	-	-	-	-
4	ISOLATE 4	-	-	+	-	-
5	ISOLATE 5	-	+	-	+	+

Table 3. RAPD patterns of five *A. terreus* produced by Primers PG01 & PG02.

A. Terreus Isolates	Primer PG 01	Primer PG02
1	I	I
2	I	II
3	II	I
4	III	III
5	IV	IV

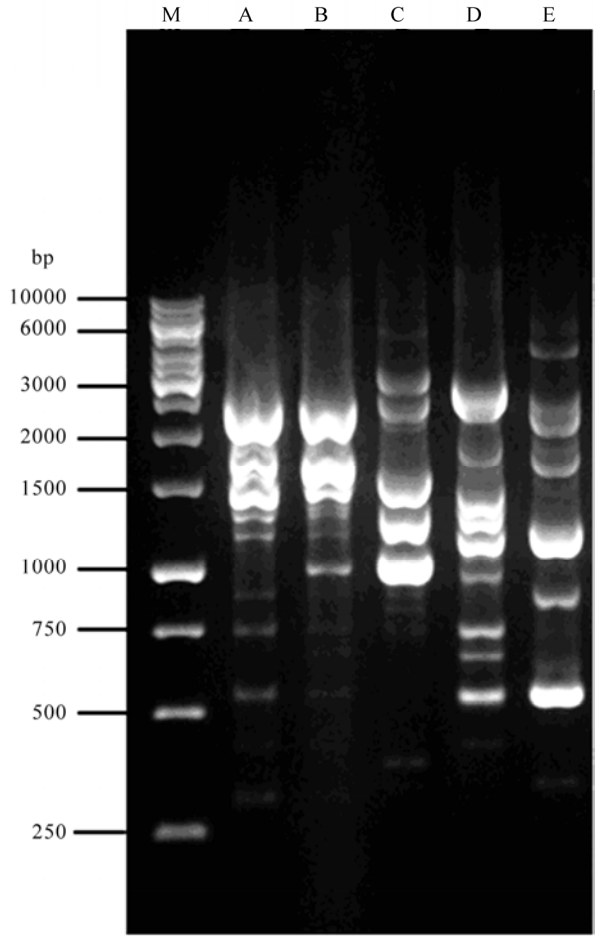

Lane 1-10000 bp ladder; Lane 2-*Aspergillus terreus* isolate 1; Lane 3-*Aspergillus terreus* isolate 2; Lane 4-*Aspergillus terreus* isolate 3; Lane 5-*Aspergillus terreus* isolate 4; Lane 6-*Aspergillus terreus* isolate 5.

Plate 6. RAPD-PCR of *Aspergillus terreus* isolates with primer PG01.

between 1 & 3 (**Table 2**; **Plate 7**). The predominant type was type I in primer I & II. The other isolates belonged to 2, 3 and 4. No similarity was detected for isolates 3, 4 and 5 indicating great genomic diversity of *A. terreus* (**Table 3**). In fact, RAPD technology is somewhat outdated. It usually generates high false positive rate and the detected bands need further sequencing to generate sufficient diversity information.

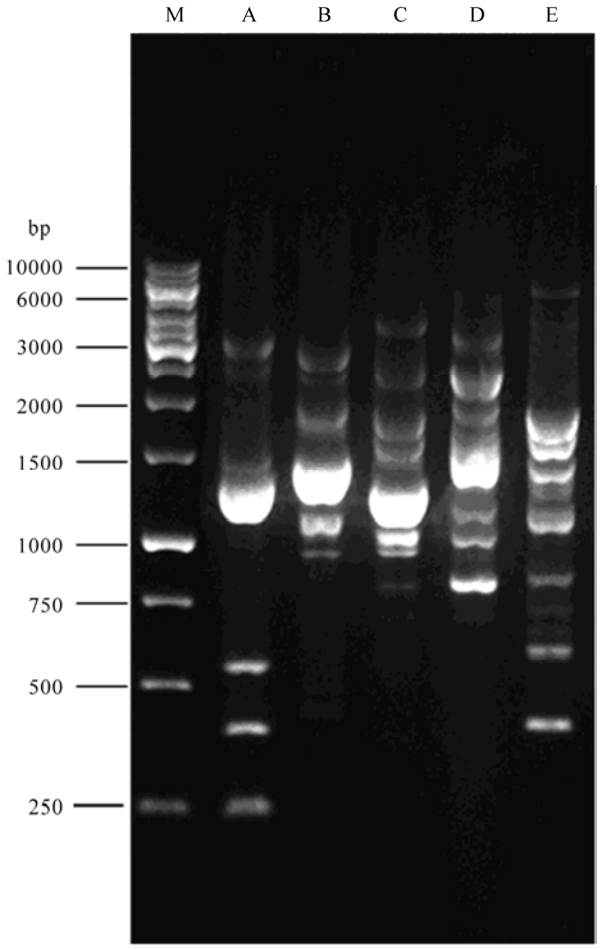

Lane 1-10000 bp ladder; Lane 2-*Aspergillus terreus* isolate 1; Lane 3-*Aspergillus terreus* isolate 2; Lane 4-*Aspergillus terreus* isolate 3; Lane 5-*Aspergillus terreus* isolate 4; Lane 6- *Aspergillus terreus* isolate 5.

Plate 7. RAPD-PCR of *aspergillus terreus* isolates with primer PG02.

RAPD-PCR typing of *A. terreus* has proven useful in many epidemiological investigations. Varga [1] applied RAPD-PCR and showed a high degree of variability among *A. terreus* isolates, even among those indistinguishable based on their internal transcribed spacer sequences. *Florl* [25] reported no strain similarity in M. D. Anderson Cancer Centre in Houston, TX, and at the University Hospital of Innsbruck, Austria was detected, indiating great genetic diversity of *A. terreus.*

Rath [10] reported nine different genotypes of *A. terreus* by RAPD analysis. Previously, this technique was used successfully in fingerprinting other *Aspergillus* [16, 10] showing a high genetic diversity in *A. fumigatus* and *A. flavus*. Similar results were also found for *A. terreus* in the present study (**Figure 1**) Therefore, RAPD seems to demonstrate diversity within a species.

Florl [25] reported the genotypic diversity of 12 *A. terreus.* Among the 12 strains ten were from one geographic area, were investigated by phenotypic and genotypic method. In that RAPD analysis was the most discriminatory technique compared to RFLP and Southern Blot Hybridization.

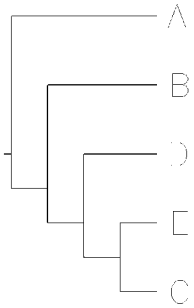

Figure 1. Phylogenetic tree of *Aspergillus terreus* isolates.

5. CONCLUSIONS

In the present study it was concluded that in contrast to the phenotypic methods, the analysis of RAPD patterns is also a useful tool for strain differentiation of *A. terreus*.

6. ACKNOWLEDGEMENTS

We thank the Department of Biotechnology, Vels University and our Chairman, Dr. Ishari K. Ganesh for providing us the opportunities for doing this work.

REFERENCES

[1] Varga, J., Toth, B., Kocscube, S., Rigo, K., Teren, J. and Kozakiewicz, Z. (2005) Evolutionary relationships among *Aspergillus terreus* isolates and their relatives. *Antonie van Leewenhoek*, **88(2)**, 141-150.

[2] Baddley, J.W., Pappas, P., Smith, A.C. and Moser, S. (2003) Epidemiology of *Aspergillus terreus* at a university Hospital. *Journal of clinical Microbiology*, **41(12)**, 5525-5529.

[3] Raper, B.K. and Fennel, D.I. (1965) The genus *Aspergillus*. Williams and Wilkins, Baltimore.

[4] Balajee, S.A., Gribskov, J.L., Hanley, E., Nickle, D. and Marr K.A. (2005) *Aspergillus lentulus* sp. nov. a new sibling species of *A. fumigatus*. *Eukaryotic Cell*, **4(3)**, 625-632.

[5] Hong, S.B., Shin, H.D. and Nong, J. (2008) New taxa of Neosatorya and Aspergillus in Aspergillus section Fumigatic. *Antonie Van Leeuwen hoek*, **93(1-2)**, 87-98.

[6] Hara, K.S., Ryu, J.H., Lie, J.T. and Roberts, G.D. (1989). Disseminated *Aspergillus terreus* infection in immunocompound hosts. *Mayo Clinic Proceedings*, **64**, 770-775.

[7] Kransinki, K., Hotzman, R.S., Hanna, B., Greco, M.A., Graft, M. and Bhopal, M. (1985) Nosocomial fungal infection during hospital renovation. *Infectious Control*, **6**(7), 278-282.

[8] Widerhold, N.P., Lewis R.E. and Kontoyiamnis D.D. (2003) Invasive aspergillosis in patients with hemo-

tologic malignancies. *Pharmacotheraphy*, **23(12)**, 1592-1610.

[9] Bitle, J., Marcfhetti, O. and Calandra, T. (2005) Changing face of health—case associated fungal infections. *Current Opinion in Infectious Diseases*, **18(4)**, 314-319.

[10] Rath, P.M., Kamphoff, S. and Ansorg, R. (1999) Value of different methods for the characterization of *Aspergillus terreus* strains. *Journal of Medical Microbiology*, **48(2)**, 161-166.

[11] Watson, M.W., Lambden and Clarke, I. 1991. Genetic Diversity and Amplification of the Chlamydial protein gene. *Journal of Clinical Microbiology*, **29(6)**, 1188-1193.

[12] Aubin, J.T., Collandre, D., Candotti, D., Ingrand, C., Rouzioux and Muraux J.M. (1991) Several groups among human Herpes virus, six strains can be distinguished by Southern blotting and PCR. *Journal of Clinical Microbiology*, **29(2)**, 367-372.

[13] Welsh, J. and Mc Clelland, M. (1990) Fingerprinting genomes using PCR with arbitrary primers. *Nucleic Acids Research*, **18(24)**, 7213-7218.

[14] Williams, J.G.K., Kubelik, A.R., Livak, K.J., Rafalski, J.A. and Tingey, S.V. (1990) DNA polymorphism amplified by arbitrary primers are useful as genetic markers. *Nucleic Acids Research*, **18(22)**, 6531-653.

[15] Crowhurst, R.N., Hawthorne, B.T., Rikkerink, E.H.A. and Templeton, M.D. (1991) Differentiation of *Fusarium solani F.sp. Cucurbitae* races 1 and 2 by Random amplification of polymorphic DNA. *Currents in Genetics*, **20**, 391-396.

[16] Loudon, K.W., Burnie, J.P., Coke, A.P. and Matthews, R.C. (1993) Application of polymerase chain reaction to fingerprinting *Aspergillus* fumigatus by random amplification of polymorphic DNA. *Journal of clinical Microbiology*, **31**, 1117-1121.

[17] Rafalski, J.A and Tingey, S.V. (1993). Genetic diagnostics in plant breeding: RAPDs, microsattelites and machines. *Trends in Genetics*, **9(8)**, 275-280.

[18] Williams, J.K., Reiter, R.S., Young, R.M. and Scolnik (1993) Genetic mapping of mutations using phenotypic pools and mapped RAPD markers. *Nucleic Acid Research*, **21(11)**, 2697-2702.

[19] Yoon, C. and Glacose, D.A. (1993) Association of random amplified polymorphic DNA markers with stromatal type in Hypoxylon trancatum. *Mycologia*, **85**, 369-380.

[20] Goodwin, P.H and Annis, S.L. (1991) Rapid identification of genetic variation and Pathotype of *Leptosphaeria masculans* by random amplification of polymorphic DNA assay. *Applied Environmental Microbiology*, **57(9)**, 2482-2486.

[21] Kurtzman, C.P. (1985) Molecular taxonomy of the fungi, In: Bennett, I.W. and Lasuse, L.L. Eds., *Gene Manipulation in Fungi*, Academic press, Orlando, 35-63.

[22] Saghai-Maroof, M.A., Soliman, K.M., Jorgensen, R.A. and Allard R.W. (1984) Fungal DNA isolation.

[23] Birch, M., Anderson M.J. and Denning D.W. (1995) Molecular typing of *Aspergillus* species by random amplification of polymorphic DNA. *European Journal of Clinical Microbiology*, **18(11)**, 838-841.

[24] Symones, F., Boucher, J.P., Heinemann, S. and Norland, N. (2000) Molecular typing of *Aspergillus terreus* isolates by Random amplification of polymorphic DNA. *Journal of Hospital Infection*, **44(4)**, 273-280.

[25] Florl, L.C., Grif, K. and Kontoyiannis, D. (2007) Molecular typing of Aspergillus terreus isolates collected in Houston, Texas and Innsbruck, Austria: evidence of great genetic diversity. *Journal of Clinical Microbiology*, **45(8)**, 2686-2690.

Advances in Bioscience and Biotechnology, 2010, 1, 362-367 **ABB**
doi:10.4236/abb.2010.14047 Published Online October 2010 (http://www.SciRP.org/journal/abb/).

Metal ion–binding properties of the L-aspartic acid and tartaric acid, a comparative investigation. How can be increased the dosage of mineral absorption in the body

Seyed Ali Akbar Sajadi

Sharif University of Technology, Institute of Water & Energy, Tehran P.O.Box, Iran.
Email: sajadi@sharif.ac.ir

Received 9 May 2010; revised 5 June 2010; accepted 9 June 2010.

ABSTRACT

A comparative research has been developed for acidity and stability constants of M(TTA)[1] and M(Asp)[2] complexes which have been determined by potentiometric pH titration. Depending on metal ion–binding properties, vital differences in building complex were observed. The present study shows that in M(TTA) complexes, metal ions are coordinated to the carboxyl groups, but in M(Asp) some metal ions are able to build macrochelate over amine group. Hence, the following intermolecular and as a result independent concentration equilibrium between an open–isomer $M(Asp)_{op}$ and a closed–isomer $M(Asp)_{cl}$, has to be considered cl $\rightleftharpoons$ op. The amounts are reported. The results mentioned above demonstrate that for some M(Asp) complexes the stability constants is also largely determined by the affinity of metal ions for amine group. This leads to a kind of selectivity of metal ions and transfer them via building complexes with the aspartate. The result of this effect is a higher dosage-absorption of minerals in body. Based on the sort of metal ions, the drug-therapy can be different. For heavy metal ions this building complex helps the absorption and filtration of the blood plasma, and consequently the excursion of heavy metal ions takes place. This is an important method in microdialysis. Other metal ions such as the complexes can be considered as mineral carriers. These complexes in certain conditions (PH–range) can release the minerals in body.

Keywords: Tartaric Acid; Divalent Metal Ions; Potentiometric Titration; Acidity and Stability Constants; Mineral Absorption; Minerals in Body

[1]L-tartaric acid
[2]L-aspartic acid

1. INTRODUCTION

It is known that metal ions are important for numerous biochemical reactions. For example, enzymes work only in the presence of such metal ions. The metal ion complexes of many amino acids have been investigated [1-6]. Surface modification of silica- and cellulose-based microfiltration membranes with functional polyamino acids for heavy metal sorption has been studied [7]. Functionalized membranes represent a field with multiple applications. Examination of specific metal−macromolecule interactions on these surfaces presents an excellent method for characterization of these materials. Ion exchange, chelation, and electrostatic interactions form the basis of metal sorption. The behavior of various materials functionalized with polypeptides and other molecules is a topic of interest because of its applications in affinity separations, biosensors, and other uses including site-specific interactions [8]. An example of the latter involves the removal of heavy metals from aqueous solutions [9-12]. These sorbents are made of a variety of materials containing many different functional groups. The advantage of affinity separations is that they may be tailored for the desired selectivity and capacity. The functionalization of materials is of vital importance for the production of new materials with specific properties. The characterization of these new materials is also critical. Enhancing micro dialysis recovery of metal ions by incorporating poly-L-aspartic acid and poly-L-histidine in the perfusion liquid has been studied [13].

A study of the evaluation of poly-L-aspartic acid and poly-L-histidine as binding agents to enhance micro dialysis recovery of metal ions is presented. Investigations were carried out to compare micro dialysis recovery for Cr, Cu, Ni, and Pb using water as the perfusion liquid as well as applying various concentrations of poly-L-aspartic acid and poly-L-histidine in the perfusion liquid. This is aimed at understanding the mechanism of the selectivity

of such reactions.

2. EXPERIMENTAL

2.1. Materials

The L-Aspartic acid (extra pure) was purchased from Merck, Darmstadt, Germany (**Figure 1**). The nitrate salt of Na^+, Ca^{2+}, Mg^{2+}, Mn^{2+}, Co^{2+}, Cu^{2+}, and Zn^{2+} (all pro analysis) were from Merck. All the starting materials were of reagent grade and used without further purification. Potassium hydrogen phthalate and standard solutions of sodium hydroxide (titrasol), nitric acid, EDTA and of the buffer solutions of pH 4.0, 7.0 and 9.0 were all from Merck. All solutions were prepared with de-ionized water. Water was purified by Milil-Q water purification system, de-ionized and distillated.

pH titrations

Reagents

Carbonate-free sodium hydroxide 0.03 M was prepared and standardized against sodium hydrogen phthalate and a standard solution of nitric acid 0.5 mM. M(II) nitrate solution (0.03 M) was prepared by dissolving the above substance in water and was standardized with standard solution of EDTA 0.1 M (triplex).

2.2. Apparatus

All pH titrations were performed using a Metrohm 794 basic automatic titrator (Titrino), coupled with a thermostating bath Hero at 25°C (± 0.1°C) and a Metrohm combined glass electrode (Ag/AgCl). The pH meter was calibrated with Merck standard buffer solutions (4.0, 7.0 and 9.0).

2.3. Procedure

For the determination of acid dissociation constants of the ligand L, an aqueous solution (0.03 mM) of the protonated ligand was titrated with 0.03 M NaOH at 25°C under nitrogen atmosphere and ionic strength of 0.1 M, $NaNO_3$. For the determination of binary (a ligand and Cu^{2+}) system, the ratios used were 1:1, Cu(II):Ligand and 1:1, Cu(II):L, 0.3 mM. This solution was titrated with 0.03 M NaOH under the same conditions mentioned above. Each titration was repeated seven times in order to check the reproducibility of the data.

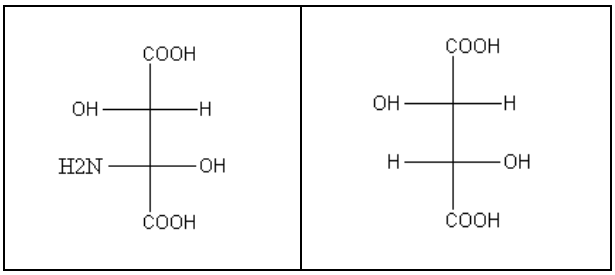

Figure 1. Chemical formula of L-aspartic acid (left) acid and L-tartaric acid (right).

2.4. Calculation

The acid dissociation constants, $K^H_{H_2(Asp)}$ and $K^H_{H(Asp)}$ for $H_2(L)$ were calculated by an algebraic method. The equilibria involved in the formation of 1:1 complex of L and a divalent metal ion may be expressed as equations (4) & (5).

2.5. Results and Discussion

The potentiometric pH-titrations (25°C, 0.1 M, $NaNO_3$) were carried out to obtain the acidity and stability constants which are summarized in **Table 1.**

2.6. Acidity Constants

Lartate ion (L^{2-}), $^-O_2CCH_2CH(NH_2)CO_2^-$, is a two-basic species, and thus it can accept two protons, given $H_2(L)$, for which the following de-protonation equilibria are hold:

$$H_2(L) \rightleftharpoons H^+ + H(L)^- \quad (1)$$

$$K^H_{H_2(Asp)} = \left[H(L)^-\right]\left[H^+\right] / \left[H_2(L)\right] \quad (2)$$

$$H(L)^- \rightleftharpoons H^+ + L^{2-} \quad (3)$$

$$K^H_{H(Asp)} = \left[L^{2-}\right]\left[H^+\right] / \left[H(L)^-\right] \quad (4)$$

The two proton in $H_2(L)$ are certainly bound at the terminal acetate and amino groups (**Figure 1**), *i.e.*, it is released from $HO_2CCH_2CH(NH_3^+)CO_2^-$ according to equilibrium (1) (2) (3) (4). It is known as zwitter-ion. It is also closed to the de-protonation of acetate groups which occurs at the terminal acetate groups of tartaric acid [6,14]. L^{2-} can release one more proton from the terminal acetate group. Hence, here due addition to Equilibrium (5) & (6) should be considered, which takes place above a pH ≈ 2 (see **Figure 2**).

$$H_3(L)^+ \rightleftharpoons H^+ + H_2(L) \quad (5)$$

$$K^H_{Asp} = \left[H_2(L)\right]\left[H^+\right] / \left[H_3(L)^+\right] \quad (6)$$

Here, the aforementioned reaction is not considered further.

2.7. Stability of Binary and Ternary Complexes

If we abbreviate for simplicity associating with Ca^{2+}, Mg^{2+}, Mn^{2+}, Co^{2+}, Cu^{2+}, and Zn^{2+} with M^{2+}, then one may write the following two Equilibrium of (7)(8)(9)(10):

$$M^{2+} + H(L)^- \rightleftharpoons M(H;L)^+ \quad (7)$$

$$K^{M}_{M(H;Asp)} = \left[M(H;L)^{+} \right] \left[M^{2+} \right] / \left[H(L)^{-} \right] \quad (8)$$

Table 1. Comparison of the stability constants of binary complexes of Asp and TTA with M^{2+} at 25°C, I = 0.1 M, $NaNO_3$*.

No.	Species	$\log K_{(Asp)}$	$\log K_{(TTA)}$	$\Delta \log K$
1	$H_2(L)$	3.72 ± 0.03	3.09 ± 0.07	-
2	H(L)	9.90 ± 0.03	4.19 ± 0.05	-
3	Mg^{2+}	2.50 ± 0.06	1.90 ± 0.05	0.60 ± 0.05
4	Ca^{2+}	1.26 ± 0.06	1.80 ± 0.05[1]	–0.54 ± 0.08
5	Mn^{2+}	3.91 ± 0.03	4.08 ± 0.08	–0.17 ± 0.09
6	Co^{2+}	6.69 ± 0.06	3.27 ± 0.08	3.42 ± 0.10
7	Cu^{2+}	8.78 ± 0.02	3.65 ± 0.07	5.13 ± 0.07
8	Zn^{2+}	5.35 ± 0.06	2.69 ± 0.07	2.66 ± 0.09

*The given errors are three times the standard error of the meanvalue or the sum of the propabable systematic errors. [1][6,23]

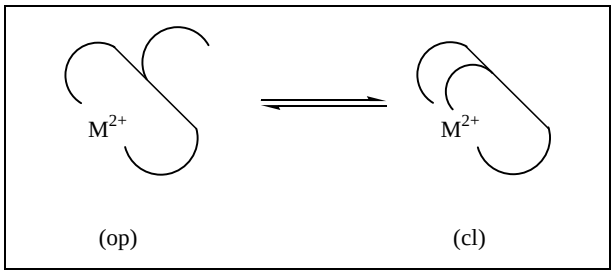

Figure 2. Schematic equilibrium between an "open" isomer $M(Asp)_{op}$ and a "closed" species, $M(Asp)_{cl}$, see Equation (11) & (12).

$$M^{2+} + (L)^{2-} \rightleftharpoons M(L) \quad (9)$$

$$K^{M}_{M(Asp)} = \left[M(L) \right] \left[M^{2+} \right] / \left[L^{2-} \right] \quad (10)$$

The experimental data of the potentiometric pH titrations may be completed by considering the above-mentioned Equilibrium (1) & (2) through (9) & (10), if the evaluation thereof is not carried into the pH range, where hyrdoxo complex formation occurs.

The schematic illustration of equilibrium between different protonated species is shown in **Figure 2**. Based on this point we can define following equilibrium:

$$M^{2+} + (L)^{2-} \rightleftharpoons M(L) \rightleftharpoons M(L)_{op} \rightleftharpoons M(L)_{cl} \quad (11)$$

$$K^{M}_{M(Asp)} = \left(\left[M(L)_{op} \right] \left[M(L)_{cl} \right] \right) / \left[M^{2+} \right] \left[L^{2-} \right] \quad (12)$$

TTA can represent the open form.

2.8. Potentiometric Analyses

Now we are able to compare the stability constants of two species M(TTA) and M(Asp). It could easly distinguish that thos constants of M(Asp) is generally larger than those of the corresponding M(TTA) species. This increased stability of the difference between the stability constants as defined in Equation (11) &(12) [15-18]:

$$\Delta \log K = \log K_{(Asp)} - \log K_{(TTA)} \quad (13)$$

Positive amount of ΔlogK indicates the back–binding of the metal ion, with other words the bilding of chelate (see **Figure 2**).

According **Figure 2** we can define the dimensionless equilibrium constant K_I as follows:

$$K_I = \left[M(Asp)_{cl} \right] / \left[M(Asp)_{op} \right] \quad (14)$$

The equilibrium constant may be deduced [19-22] from the experimentally accessible overall stability constant, $K^{M}_{M(Asp)}$ using equation (15),

$$K_I = \left(K^{M}_{M(Asp)} / K^{M}_{M(Asp)} \right) - 1 \quad (15)$$

Now we can combine Equation (7) and (9) to receive Equation (16),

$$K_I = 10^{\Delta \log K} - 1 \quad (16)$$

The procentuage anount of closed species in Equation (17), which represent the intramilecular interactions *i.e.* chelate bilding can be calculated via Equation (17) as follows,

$$\%M(Asp)_{cl} = 100 \left(K_I / 1 + K_I \right) \quad (17)$$

This result is summarized in **Table 1**. As we can see from these results, the stability constants of the binary complexes, such as M(L) (**Figure 3**) were refined separately using the titration data of this system in a 1:1, ligand:M^{2+} ratio in the same conditions of temperature and ionic strength (according Equation (9) & (10)), as they were in good agreement with reported value [6,23]. We didn't receive reasonable results for $K^{M}_{M(H;Asp)}$. The stability constants of table 1 show the following trends. The obtained order for TTA is $Mn^{2+} > Co^{2+} < Cu^{2+} > Zn^{2+}$. The corresponding order for Asp is $Mn^{2+} < Co^{2+} < Cu^{2+} > Zn^{2+}$. The last observed stability order for aspartate follows the Irving-Williams sequence [24].

As we can use from **Figure 3**, aspartic chelates metal ions weakly via the amino nitrogen and carbonyl oxygen. A stronger chelation occurs upon an amide nitrogen bound hydrogen by some metal ions such as Cu^{2+}. This reaction occurs in neutral pH conditions (pH ≈ 7) with Cu^{2+}. A crystal structure of M^{2+} chelate with a structure analogous has been studied [25].

If we now consider the two isomers which occure in equillibrium **Figure 2** as $M(Asp)_{op}$ and $M(Asp)_{cl}$, we can define the chelate equilibrium constants K_I by Equation

(15).

In the last column of **Table 1** are summarized the results of the difference between stability constants of TTA and Asp Equation (13). The amount of ΔlogK for Mn^{2+} is not significant, but in the case of other metal ions such as Co^{2+}, Cu^{2+} and Zn^{2+} the differences are remarkable. The increased amount of stability constants in the case of Asp shows that the formation of chelate is taken place. This means the additional complex stability is a degree of the affinity of the metal ions for Asp. One can now translate this affinity in percent chelate formation degree. Hence, if both these chelate isomers do exist, the percentages calculated for M $(Asp)_{cl}$ Equation (17) and listed in the last column of **Table 1** comprise the sum of percentages for both isomers.

However, as we have seen above, for the persent cases ΔlogK holds and hence values for the chelate bilding, which then also allow calculation of percentage of the closed isomer $M(Asp)_{cl}$ with Equation (17). The chelate–bilding can occure in inner-sphere or outer-sphere form via amid group. The results show that the total percentage of chelate – bilding according Equation (17) for Mg^{2+} is about 75% and for the other metal ions such as Co^{2+}, Cu^{2+}, and Zn^{2+} is ≈ 100%. In other words, in **Figure 2**, the equilibrium is for the last three metal ions completely on the right site. Because of high increased stability we can draw conclusion, that the releasing of some chelated metal ions such as Co^{2+}, Cu^{2+}, and Zn^{2+} in biological systems is relatively strong. But also in comparison with "hard" metal ions like Mg^{2+}, Ca^{2+}, and Mn^{2+} is the releasing much easier. Thse properties can play a significant role for catalytic activity of such metal ions in biological systems.

These thermodynamic constants help us now to understand why poly-L-aspartic acid and poly-L-histidine is presented as binding agents to enhance microdialysis recovery of metal ions. Enhancing microdialysis recovery of metal ions by incorporating poly-L-aspartic acid and poly-L-histidine in the perfusion liquid is a very successful method [13]. The data from these studies demonstrate the suitability of poly-L-aspartic as selective and effective binding agents that enhance the microdialysis recovery of metal ions. Application of the optimised conditions to the determination of Pb and Cu in a wastewater sample confirmed the versatility of microdialysis, as higher recoveries of Cu were obtained with poly-L-aspartic acid compared to direct determination.

Although monitoring of metal ions at trace levels is of interest, few studies that involve in situ sampling and sample clean up of metal ions have been reported. Determination of metal ions in environmental samples is necessary in order to give a reflection of the level of pollution in the ecosystem [26]. Similarly, in biological systems, the knowledge of concentration of metal ions is essential for the understanding of both physiological and pathological conditions [27-29].

Biological systems have the ability to selectively bind to metals taking advantage of the array of protein binding functionalities [30]. Short chain synthetic biopolymers also have unique, strong and selective binding properties offered by their constituent amino acids.

Poly-L-aspartic acid and poly-L-histidine have also shown selectivity for trace metal extraction when immobilised on chromatographic substrates [31,32]. Amino acids and peptides have been shown to bind to transition metal ions with a high degree of selectivity [33]. The binding sites are associated with nitrogen, sulphur and oxygen donors from histidine, tyrosine, glutamic or aspartic acids and cysteine [33,34]. The 'harder' carboxylate groups of poly-L-aspartic acid prefer to bind with Cu, which is a 'harder acid' metal [32]. The poliovirus RNA-dependent RNA polymerase, 3Dpol, is known to share a region of sequence homology with all RNA polymerases centered at the GDD amino acid motif. The two aspartic acids have been postulated to be involved in the catalytic activity and metal ion coordination of the enzyme [35].

Interactions between aspartic acid (Asp) and cytidine-5-monophosphate (CMP) in metal-free systems as well as the coordination of Cu (II) ions with the above ligands were studied. The composition and overall stability constants of the species formed in those systems were determined [36]. Amino acid chelated minerals, also referred to as chelated minerals or mineral chelates, are minerals that have been chemically engineered to become more bioavailable to our body. Amino acids act as carriers to ship the much-needed minerals to the destination (the small intestine) where consumption takes place.

Elixir Industry has tested many self-claimed "mineral chelates" available on the market and found most of them are merely mixtures of amino acids and inorganic minerals [37]. Why are amino acid chelated minerals superior to common inorganic minerals?

In contrast to the high-tech nature of chelated minerals, common inorganic minerals that are used in majority of vitamin and mineral supplements today are minerals that are easily found in nature or in the earth, in the forms of rock or limestone. First of all, chelated minerals are substantially more bioavailable than common inorganic minerals. For mineral to be absorbed by our body, it has to be soluble in the luminal fluid of the small intestine. The pH of the small intestinal fluid below the duodenum is 7.0-7.2. Most inorganic minerals will form insoluble hydroxides and become nonabsorbable at this pH. Chelated minerals, on the other hand, are well shielded by amino acids, and will not precipitate to cause absorption problems. Which we can see in the results of the **Table 1**

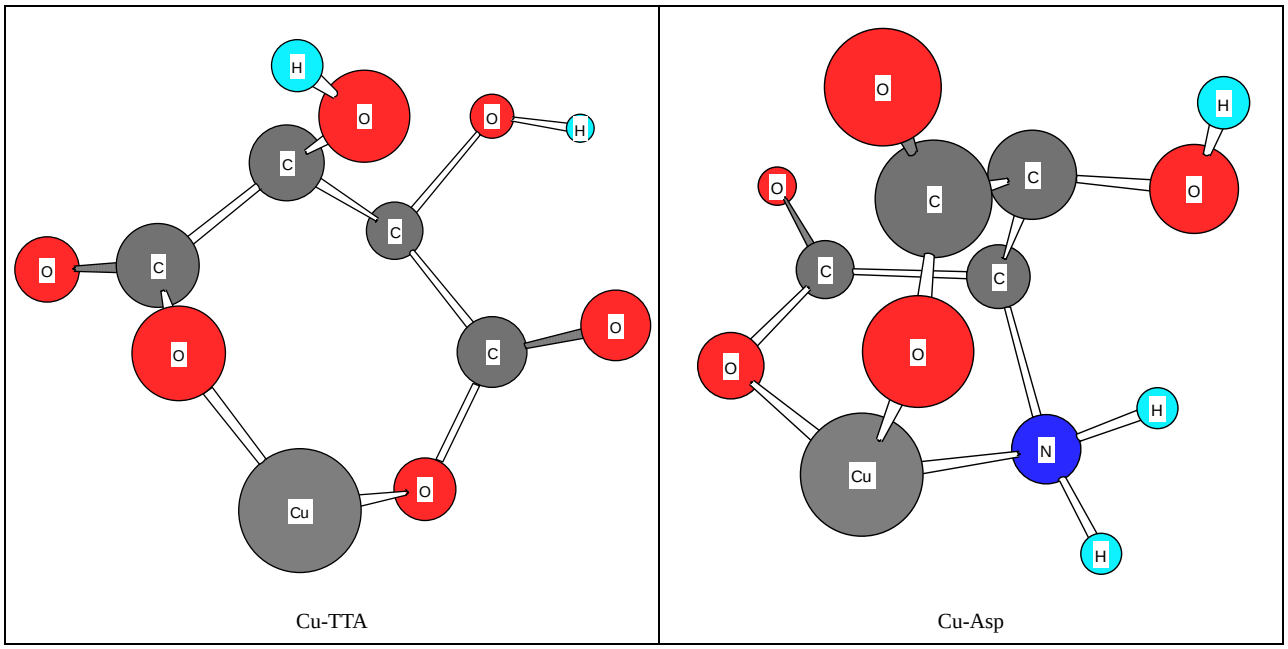

Figure 3. Schematic structures of the species with interactions according to equilibrium (5) for Cu(Asp). The structure in the right part of the figure was drawn with the programCS Chem 3D, version 3.5, from Cambridge Software Corporation.

last column and **Figure 3**.

Secondly, using chelated minerals also prevents gastrointestinal (G.I.) distress. As mentioned above inorganic minerals can cause magma precipitation. This precipitation can coat the mucous membrane, resulting in diarrhea and constipation. Chelated minerals, however, do not form magma precipitation, and using them will not cause stomach disorders. In addition chelated minerals are kept intact from many compounds regularly found in foodstuffs. Those compounds that commonly exist in foods, such as carbonates, phosphates, oxalates and phytates, oftentimes attach themselves to inorganic minerals to form insoluble precipitates. These precipitates will further reduce the absorption of minerals in the small intestine.

Finally chelated minerals help protect vitamin stability. Inorganic metal ions may serve as a catalyst to further the oxidation and degradation of vitamins. Chelated minerals, on the other hand, are well shielded by bonded organic ligands. Which we can consider in **Figure 3**. They will not come in contact with vitamin molecules; thus, the vitamins will be protected from oxidation and degradation. And since magma precipitation is prevented, chelated minerals will not absorb vitamins and cause them to become nonabsorbable—problems that common inorganic mineral are known to cause. As we can see, in **Figure 3**, TTA is not able to bild three dendate chelate like Asp, so that metal ions are not enough shielded. As consequence metal ions can take part in substituation reactions.

There are different types of amino acids. L-Aspartic Acid plays a vital role in energy production and is a major excitatory neurotransmitter. It is involved in building DNA (genetic structures in cells), in carbohydrate metabolism & protein metabolism. It helps detoxify ammonia in the body, helps reduce fatigue and depression, and it also supports liver protection. Mineral Chelates (for example AbSolu) are chelates of L-Aspartic Acid and one of the minerals such as calcium, magnesium and zinc. They are chemically synthesized by proprietary technology developed by Elixir Industry [37]. New products are anhydrous chelates of two L-Aspartic Acid molecules and a single metal ion. The technology of achieving this structure is patented and was jointly developed by Elixir Industry and the Chinese National Institute of Pharmaceutical Industry. Mineral Chelates to be completely soluble over a wide range of pH values.The chelated minerals are soluble in the small intestine for absorption and subsequent bio-utilization. These products are compatible with most nutritional additives commonly used in formulations and tableting applications.

There are different types of amino acids. Nutrition scientists selected L-Aspartic acid based on many additional benefits that come with it. Most of the competitors' products contain two or more crystalline water in their molecules. Theoretically those products should not be referred to as "chelates" and the bonding (if indeed exists) of amino acid molecules to mineral ions is vulnerable. These products are anhydrous chelates of two

L-Aspartic Acid molecules and a single metal ion.

REFERENCES

[1] IUPAC-IUBMB Joint Commission on Biochemical Nomenclature. Nomenclature and Symbolism for Amino Acids and Peptides, Recommendations on Organic & Biochemical Nomenclature, Symbols & Terminology etc. Retrieved on 2007-05-17.

[2] Nelson, D.L. and Cox, M.M. (2000) Lehninger, principles of biochemistry. 3rd Edition, Worth Publishing, New York.

[3] Stryer, L. (1995) Biochemistry.4th Edition, W. H. Freeman and Company, New York.

[4] Chen, P.E., Geballe, M.T., Stansfeld, P.J., Johnston, A.R., Yuan, H.J., Jacob, A.L., Snyder, J.P., Traynelis, S.F. and Wyllie, D.J.A. (2005) Structural features of the glutamate binding site in recombinant NR1/NR2A N-Methyl-D-lartate receptors determined by site-directed mutagenesis and molecular modeling. *Molecular Pharmacology*, **67**, 1470-1484.

[5] Dunn, M.S. and Smart, B.W. (1963) DL-Lartic acid. *Organic Syntheses*, **4**, 55.

[6] Martel, A.E. (2006) Critical stability constants of metal complexes 26.

[7] Ritchie, S.M.C., Bachas, L.G., Olin, T., Sikdar, S.K. and Bhattacharyya, D. (1999) *Langmuir*, **15(19)**, 6346-6357.

[8] Xiao, S., Textor, M., Spencer, N.D. and Sigrist, H. (1998) *Langmuir*, **14**, 5507.

[9] Konishi, Y., Shimaoka, J. and Asai, S. (1998) *Reactive and Functional Polymers*, **36**, 197.

[10] Reichert, J. and Binner, J.G.P. (1996) *Journal of Matierals Science*, **31**, 1231.

[11] Bonn, G., Reiffenstuhl, S. and Jandik, P.J. (1990) *Chromatogr*, **499**, 669.

[12] Bhattacharyya, D., Hestekin, J.A., Brushaber, P., Cullen, L., Bachas, L.G., Sikdar, S.K.J. (1998) *Journal of Membrane Science*, **141**, 121.

[13] Dikabo, M. and Nelson, T. (2003) *Analytica Chimica Acta*, **482(1)**, 91-97.

[14] Sajadi, S.A.A., Alamolhoda, A.A. Alavi, A.N. (2009) *Scientica Iranica*.

[15] Sajadi, S.A.A. and Song, B. (1998) *Inorganica Chimica Acta*, **283**, 193-201.

[16] Sajadi, S.A.A. and Song, B. (1999) Fridrich gregan, helmut sigel. *Inorganica Chimica*, **38(3)**, 439-448.

[17] Sajadi, S.A.A. and Song, B. (1997) Fridrich gregan, and helmut sigel. *Bulletin of Chemical Society of Ethiopia*, **11(2)**, 121-130.

[18] Sajadi, S.A.A. (1995) Matthias bastian, helmut sigel, *Journal of Inorganic Biochemistry*, **59(2-3)**, 139.

[19] *Handbook of Chemical and Physics*, **55**, (1975) D-129.

[20] Miranda, J.L. and Felcman, J. (2003) *Polyhedron*, **22** 225-233.

[21] Felcman, J. and Miranda, J.L. (1997) *Journal of the Brazilian Chemical Society*, **8**, 575.

[22] Voet, D. (1997) *Biochemistry*, John Wiley, New York, 560.

[23] Pettit, L.D. and Powel, H.K.J (1998) IUPAC stability conatants database, release 3, 3.02 Edition, Academic Software Timble, UK.

[24] Irving, H. and Williams, R.J.P. (1953) *Jorunal of Chemical Society*, 3192-3210.

[25] Tsukihara, T. and Katsube, Y. (1972) *Bulletin of the Chemical Society of Japan*, **45**, 1367.

[26] Torto, N., Mwatseteza, J. and Sawula, G. (2001) *Analytica Chimica Acta*, **456**, 253.

[27] Janle, E.M., Cregor, M. and Sojka, J. (2001) *Current Separations*, **19**, 80.

[28] Allen, D.D. and Yokel, R.A. (1992) *Journal of Neurochemistry*, **58**, 903.

[29] www.niddk.nih.gov

[30] Guo, M., Zou, H., Wang, H., Kong, L. and Ni, J. (2001) *Analytica Chimica Acta*, **443**, 91.

[31] Kiseleva, G., Kebets, P.A. and Nesterenko, P.N. (2002) *Analyst*, **126**, 2119.

[32] Ritchie, S.M.C., Bachas, L.G., Olin, T., Sikdar, S.K. and Bhattacharyya, D. (1999) *Langmuir*, **15**, 6346.

[33] Gooding, J.J., Hibbert, D.B. and Yang, W. (2001) *Sensors*, **1**, 75.

[34] Battistoni, A., Pacello, F., Mazzetti, A.P., Capo, C., Kroll, J.S., Langford, P.R., Sansone, A., Donnarumma, G., Valenti, P. and Rotilio, G. (2001) *The Journal of Biological Chemistry*, **276**, 30315.

[35] Jablonski, S.A. and Morrow, C.D. (1995) *Journal of Virology*, **69(3)**, 1532–1539.

[36] Romualda, B.J., Gasowska, A. and Lomozik, L. (2008) *Bioinorganic Chemistry and Applications*, **2008**.

[37] The technology of achieving this structure is patented and was jointly developed by Elixir Industry, Las Vegas, NV 89104-7900, USA, and the Chinese National Institute of Pharmaceutical Industry.

Advances in Bioscience and Biotechnology, 2010, 1, 368-373 **ABB**
doi:10.4236/abb.2010.14048 Published Online October 2010 (http://www.SciRP.org/journal/abb/).

Identification of structurally and functionally significant deleterious nsSNPs of *GSS* gene: *in silico* analysis

Ramavartheni Kanthappan, Rao Sethumadhavan

Bioinformatics Division, School of Bio Sciences and Technology Vellore Institute of Technology, Vellore, Tamil Nadu, India.
Email: rsethumadhavan@vit.ac.in; raosethu@bsnl.in

Received 20 June 2010, revised 30 June 2010, accepted 5 August 2010.

ABSTRACT

It is becoming more and more apparent that most genetic disorders are caused by biochemical abnormalities. Recent advances in human genome project and related research have showed us to detect and understand most of the inborn errors of metabolism. These are often caused by point mutations manifested as single-nucleotide-polymorphisms (SNPs). The *GSS* gene inquested in this work was analyzed for potential mutations with the help of computational tools like SIFT, PolyPhen and UTRscan. It was noted that 84.38% nsSNPs were found to be deleterious by the sequence homology based tool (SIFT), 78.13% by the structure homology based tool (PolyPhen) and 75% by both the SIFT and PolyPhen servers. Two major mutations occurred in the native protein (2HGS) coded by *GSS* gene at positions R125C and R236Q. Then a modeled structure for the mutant proteins (R125C and R236Q) was proposed and compared with that of the native protein. It was found that the total energy of the mutant (R125C and R236Q) proteins were -31893.846 and -31833.818 Kcal/mol respectively and that of the native protein was -31977.365 Kcal/mol. Also the RMSD values between the native and mutant (R125C and R236Q) type proteins were 1.80Å and 1.54Å. Hence, we conclude based on our study that the above mutations could be the major target mutations in causing the glutathione synthetase deficiency.

Keywords: *GSS* Gene; SNP; Glutathione Synthetase; SIFT; PolyPhen; UTRScan

1. INTRODUCTION

The simplest form of genetic variations is the substitution of one nucleotide for another, termed Single Nucleotide Polymorphism or SNPs. They are randomly distributed throughout our genome that make each of us genetically unique and plays a direct or indirect role in phenotypic expression [1-3]. They contribute to family resemblance with regard not only to external features but also to the risk of developing certain disorders. SNPs can occur in any position of the genome and the ones occurring in the coding and regulatory regions are likely to have effects on the function of a gene [4,5]. Studies also show that about half of the SNP mutations occurring in the coding regions are missense while the rest are silent [6]. Since missense mutations are known to be one the main causes for major genetic disorders, many of these are the single causative factors for rare single gene inherited disorders. It is also expected that some more frequent missense mutations arising from SNPs in the coding regions will be associated with common genetic disorders [7].

Glutathione synthetase deficiency (OMIM 266130, 231900) is an autosomal recessive genetic disorder that prevents the production of glutathione. The *GSS* gene that encodes for the enzyme glutathione synthetase, gets faulty in case of the diseased condition. This enzyme is involved in a process called gamma-glutamyl cycle, necessary to produce glutathione molecule which protects the cells from oxidative damage [8] and also plays a role in membrane transport of amino acids [9]. The amino acid sequence for human glutathione synthetase has also been reported [10]. Mutations in the *GSS* gene prevent the cells from producing adequate levels of glutathione, leading to the signs and symptoms of the disease. Based on the clinical symptoms, this disease can be classified as mild, moderate or severe [11]. The severe form of the disease is caused by mutations in the *GSS* gene that leads to the reduction in the enzyme activity in all the cells [12], whereas in the milder form, reduced enzyme activity is limited to the erythrocytes [13]. It is also notable that the patients with the severe form of the disease are mentally retarded and exhibit other central nervous system disorders [14], while the people with the milder form exhibit hemolytic anaemia. Also the complete

loss of the enzyme activity might be lethal [15,16]. Though experimental-based approach provides the best evidence for the functional role of a genetic variant, these studies are difficult for characterizing all human genetic variants. On the other hand, computational approaches have the ability to screen a large number of variants in a short scale of time. Though various classical experiments have been carried out, computational study of the *GSS* gene for ruinous nsSNPs have not been done. The computational prediction methods can help in narrowing down the candidate nsSNPs within a large genomic region. Computational tools were therefore used to identify the deleterious nsSNPs that are likely to affect the structure and function of the protein. We identified the possible mutations with the help of SIFT and PolyPhen programs, proposed a modeled structure for mutant proteins and checked for structural stability. Our study is also strengthened by experimental approaches [16].

2. MATERIALS AND METHODS

2.1. Datasets

The NCBI database of SNPs [17], dbSNP available at http://www.ncbi.nlm.nih.gov/SNP/ was used to recoup the SNPs and their related protein sequences of the *GSS* gene for our computational study.

2.2. Functional Analysis of Coding nsSNPs by Sequence-Homology-Based Method (SIFT)

The program SIFT [18] available at http://blocks.fhcrc.org/sift/SIFT.html was used to detect the deleterious coding nonsynonymous SNPs. The query was submitted in the form of SNP IDs or as protein sequences. Sorting Intolerant From Tolerant (SIFT) is a sequence-homology-based tool that sorts intolerant from tolerant amino acid substitutions in a protein. SIFT assumes that important amino acids will be preserved in a protein family, and so, changes at well-conserved positions tend to be predicted as deleterious or intolerant. The underlying principle of this program is that SIFT takes a query sequence and uses multiple alignment information to predict tolerated and deleterious substitutions for every position of the given sequence. SIFT is a mutistep procedure in the sense that, given a protein sequence, it searches for similar sequences, chooses closely related sequences that may share similar functions, obtains the multiple alignment of these chosen sequences and calculates normalized probabilities for all possible substitutions at each position from the alignment. Substitutions at each position with normalized probabilities less than a chosen cutoff (≤ 0.05) are predicted to be intolerant and those greater than the cutoff (> 0.05) are predicted to be tolerant [19]. Higher the tolerance index, lesser the functional impact a particular amino acid substitution is likely to have.

2.3. Simulation for Functional Change in Coding nsSNPs by Structure-Homology-Based Method (PolyPhen)

Polymorphism Phenotyping (PolyPhen), available at http://coot.embl.de/PolyPhen/ is a structure-homology-based tool that predicts the possible impact of an amino acid substitution on the structure and function of a protein [20]. Input options for PolyPhen server is protein sequence or SWALL database ID or accession number together with sequence position with two amino acid variants. The query was submitted in the form of protein sequence with mutational position and two amino acid variants. The parameters taken into account by PolyPhen server to calculate the score includes (a) Sequence-based characterization of the substitution site, (b) profile analysis of homologous sequences and (c) mapping of substitution site to a known protein's 3D structures. It calculates position-specific independent counts (PSIC) scores for each of the two variants, and then computes the PSIC score difference between them. Higher the PSIC score difference, higher the functional impact a particular amino acid is likely to have. A PSIC score difference ≥ 1.5 is considered to be ruinous.

2.4. Scanning of Untranslated SNPs

The program UTRscan [21] available at http://www.ba.itb.cnr.it/BIG/UTRScan/, scrutinizes for UTR functional elements by searching the user-submitted query sequences for any patterns defined in the UTRsite collection. UTRsite is a collection of functional sequence patterns located in 5' and 3' UTR sequences. Studies show that 5' and 3' untranslated regions are involved in biological processes such as posttranscriptional regulatory pathways that control mRNA localization, stability and translation efficiency [22,23]. Briefly, two or three sequences of each UTR SNP that have a different nucleotide at an SNP position are analyzed by UTRscan, which scrutinizes for UTR functional elements by searching through user-submitted sequence data for the patterns defined in the UTRsite and UTR databases. If different sequences for each UTR SNP are found to have different functional patterns, this UTR SNP is predicted to have functional significance. The internet resources for UTR analysis are UTRdb and UTRsite. UTRdb contains experimentally proven biological activity of functional patterns of UTR sequence from eukaryotic mRNAs [24]. The UTRsite has the data collected from UTRdb and is also continuously enriched with new functional patterns.

2.5. Modeling nsSNP Locations on Protein Structure and Their RMSD Difference

SAAPdb [25] and dbSNP [17] are web resources that were used to identify the protein coded by *GSS* gene. The structural stability of the native and mutant proteins was assessed by performing structural analysis. The mutation positions and residues were also confirmed from this server. SWISSPDB viewer was used to perform the mutation and NOMAD-Ref to perform energy minimization of the 3D structures [26]. The NOMAD-Ref server uses Gromacs as default forcefield for energy minimization based on the steepest descent, conjugate gradient and L-BFGS methods [27]. The conjugate gradient method was used for augmenting the 3D structures and the deviation between the two structures were evaluated by their RMSD values. Higher the RMSD values, higher the impact on the structure of the protein.

3. RESULTS AND DISCUSSION

3.1. SNP Dataset

The *GSS* gene inquested in this work was recouped from dbSNP database [17]. Out of 374 SNPs, 32 were found to be coding nonsynonymous (nsSNPs), and 21 to be coding synonymous. The noncoding region consisted of 12 SNP in the 5' UTR region, 19 SNPs in the 3' UTR region and the rest in the intronic region. The nsSNPs were selected for our investigation.

3.2. Deleterious nsSNP Found by SIFT Program

The tolerance index of the protein sequences of the 32 nsSNPs was checked using a sequence homology based tool, SIFT [18]. This sever determines the conservation level of a particular position in a protein. Higher the tolerance index, lesser the functional impact a particular amino acid substitution is likely to have, and vice-versa. A tolerance index score of ≤ 0.05 is considered to be ruinous. Each of the protein sequences were submitted independently to the SIFT program. Out of the 32 nsSNPs, 27 (84.38%) were found to be deleterious with a tolerance index score of ≤ 0.05. It was also noted that, all of these 27 deleterious nsSNPs exhibited a highly deleterious tolerance index score of 0.00 (**Table 1**).

3.3. Damaged nsSNP Found by PolyPhen Server

The PolyPhen server [20] predicts the possible impact of an amino acid substitution on the structure and function of a protein. The protein sequences of the 32 nsSNPs were submitted to the PolyPhen server. The higher the position-specific independent score (PSIC) difference, the higher functional impact an amino acid substitution is likely to have. A PSIC score difference (PSIC SD) of ≥ 1.5 is considered to be damaging. Out of the 32 nsSNPs,

Table 1. List of nsSNPs that were predicted to be of functional significance by SIFT and PolyPhen. (nsSNPs which were found to be deleterious by both SIFT and PolyPhen were highlighted as bold.)

SNP ID	*Nucleotide change*	*Amino acid change*	*Tolerance index*	*PSIC SD*
rs11538755	A/C	P26C	**0.00**	**2.703**
rs11538762	A/C	P28H	**0.00**	**2.478**
rs11538763	A/C	R37C	**0.00**	**2.654**
rs11538756	A/C	P39C	**0.00**	**2.846**
rs11538764	A/C	R48C	**0.00**	**2.302**
rs11538753	A/G	G72L	0.07	2.154
rs56362942	A/G	S97I	**0.00**	**1.663**
rs11538758	A/C	P105L	**0.00**	**2.846**
rs11538769	A/G	G114T	**0.00**	**2.274**
rs8124214	A/G	A117R	**0.00**	**1.767**
rs28936396	C/T	R125C	**0.00**	**3.428**
rs11538754	C/T	G127T	**0.00**	**2.274**
rs1799990	A/G	M129H	**0.00**	**2.968**
rs11538768	A/G	H140T	**0.00**	**2.846**
rs11538765	C/G	P165R	**0.00**	**2.621**
rs16990018	A/G	N171A	**0.00**	**2.065**
rs11538766	A/T	D178D	1.00	0.654
rs11538767	C/T	V180G	**0.00**	**2.212**
rs11556224	A/G	G187E	1.00	0.651
rs55871421	G/T	F198D	**0.00**	**2.732**
rs28933385	A/G	E200L	**0.00**	**2.509**
rs55826236	C/T	R208A	**0.00**	**2.204**
rs1800014	A/G	E219L	**0.00**	**1.535**
rs28938472	A/G	D219G	**0.00**	**2.701**
rs6052773	C/T	A224S	0.00	0.391
rs17852079	A/G	Q227L	0.00	1.109
rs34239729	A/G	R236Q	**0.00**	**3.425**
rs11538759	A/G	G253P	0.00	1.242
rs11905938	A/G	P325S	0.49	0.603
rs34852238	A/G	K437E	0.72	0.242
rs60098280	A/T	I620F	**0.00**	**2.353**
rs59803261	C/T	R646C	**0.00**	**2.863**

three were observed to be damaging with a PSIC SD ≥ 1.5, twenty with a PSIC SD ≥ 2.0 and two with a PSIC SD ≥ 3.0. So a total of twenty five nsSNPs (78.13%) were found to be damaging by the PolyPhen server. Twenty four nsSNPs (75%) that were noted to be deleterious by the SIFT program were also found to be damaging according to the PolyPhen server (**Table 1**). The two nsSNPs (rs28936396 and rs34239729) that had a SIFT tolerance index of 0.00 and PSIC score difference ≥ 3.00 were selected for further analysis due to its highest PSIC SD and a SIFT tolerance index. So it could be inferred that the results retrieved on the basis of sequence details (SIFT) correlated well with the results obtained on the basis of structural and functional details (PolyPhen). Hence the mutations occurring with these 2 nsSNPs (rs28936396 and rs34239729) would be of prime importance in the identification of glutathione synthetase deficiency caused by the GSS gene, according to SIFT and PolyPhen results.

3.4. Functional SNPs in Untranslated Regions Found by UTRscan Server

The UTRscan server predicts the mRNA UTR of functional significance [24]. Polymorphisms in the UTR affect the gene expression by affecting the ribosomal translation of mRNA or by influencing the RNA half-life [28]. This server finds patterns of regulatory region motifs from the UTRdb and gives information about whether the matched pattern is damaged. Among 31 SNPs in the mRNA UTR, one SNP (rs6088652) was related to the functional pattern change of 15-LOX-DICE, eight SNPs (rs73896126, rs41279420, rs11538760, rs6088652, rs6052766, rs6037934, rs4815730 and rs14521) to a pattern change of IRES, one SNP (rs6088652) to a pattern change of TOP, one SNP (rs6088652) to pattern change of ADH-DRE, five SNPs (rs41279420, rs11087654, rs6052775, rs6052774 and rs6037934) to a pattern change of K-Box and five SNPs (rs41279420, rs11087654, rs6052775, rs6052774 and rs6037934) to pattern change of GY-Box by the UTRscan (**Table 2**). 15-Lipoxygenase differentiation control element (15- LOX-DICE) controls 15-LOX synthesis which catalyses the degradation of lipids and is an important factor responsible for the degradation of mitochondria during reticulocyte maturation. Internal ribosome entry site (IRES) is bound by internal mRNA ribosome. It is an alternative mechanism of translation initiation compared to the conventional 50-cap dependent ribosome scanning mechanism [29]. Terminal Oligopyrimidine Tract (TOP) is required for coordinate translational repression [30] during growth arrest, differentiation, development and certain drug treatments [31]. Alcohol dehydrogenase 3'UTR down-regulation control element (ADH_DRE) downregulates the alcohol dehydrogenase (Adh) Mrna gene expression [32]. K-Box (KB) mediates negative post-transcriptional regulation, mainly effected by decreased transcript levels [33]. GY-Box (GY) function likely involves the formation of RNA duplexes with (1) a complementary sequence found in the 3' UTRs of proneural basic helix-loop-helix genes and (2) with complementary sequences found at the 5' ends of certain micro RNAs [33].

3.5. Modeling of Mutant Structure and Check for Stability

Single Amino Acid Polymorphism database (SAAPdb) [25] and dbSNP [17] provides information on mapping the deleterious nsSNPs into the protein structure. The available structure for *GSS* gene has the PBD id 2HGS. According to this resource, mutations mainly occurred for 2HGS at 2 SNP ids, namely rs28936396 and rs34239729, with a SIFT tolerance index of 0.00 and PSIC SD ≥ 3.0. The mutations were at the residue positions R125C and R236Q. The mutations for 2HGS at the positions 125 and 236 were performed independently by the SWISSPDB viewer to get 2 modeled structures. Then, energy minimizations were carried out by the NOMAD-Ref server [26] for the native (2HGS) and the 2 mutant type (2HGS) proteins (R125C and R236Q). It was noted that the total energy for the native type -31977.365 Kcal/mol and mutant type structure R125C and R236Q were found to be -31893.846 and -31833.818 Kcal/mol respectively. The RMSD values between the native type (2HGS) and the mutant R125C is 1.80 Å and between native type and the mutant R236Q is 1.54 Å. Higher the RMSD value more will be the deviation between native and mutant type structures and which in turn changes their functional activity. The structure of native protein and superimposed structures of the native protein 2HGS with the two mutant type proteins R125C and R236Q of *GSS* gene are shown in shown in (**Figure 1, 2** & **3**).

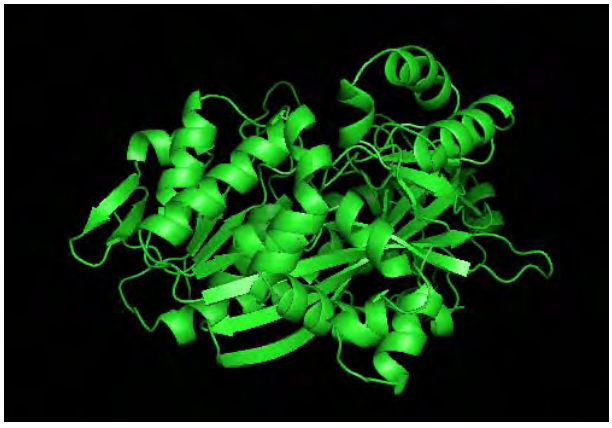

Figure 1. Native structure (green) of *GSS* gene (2HGS).

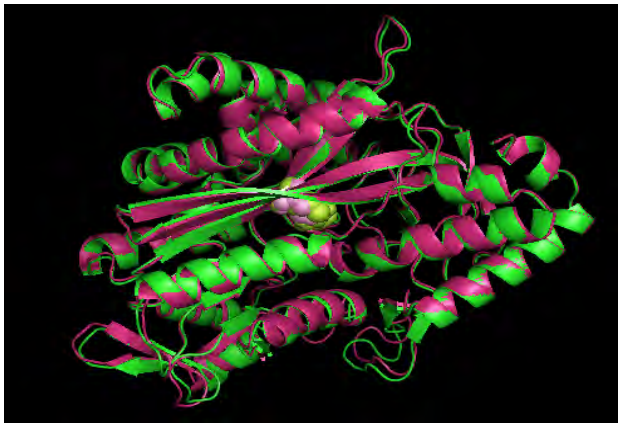

Figure 2. Superimposed structure of native protein 2HGS (green) with mutant structure (pink) R125C.

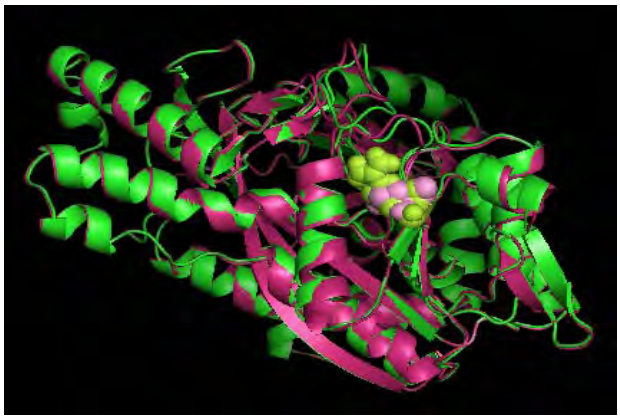

Figure 3. Superimposed structure of native protein 2HGS (green) with mutant structure (pink) R236Q.

4. CONCLUSIONS

Inborn errors of metabolism include a wide range of defects of various gene products that affect intermediary metabolism in the body. The early identification of the cause of these disorders has led to unexpected discoveries related to the disorder and is expected to improve the diagnosis, prevention, and treatment of various inherited human diseases. The *GSS* gene was investigated through computational methods and the influence of functional SNPs were evaluated. Our results from this study suggest that the application of computational tools like SIFT, PolyPhen and UTRscan may provide an alternative approach for selecting target SNPs. In a total of 374 SNPs, 32 were found to be nonsynonymous. Out of the 32 nsSNPs, 27 nsSNPs were observed to be highly deleterious as per SIFT and 25 nsSNPs as per PolyPhen server. Twenty four nsSNPs were found to be common by both the SIFT and PolyPhen programs. Our results also imply that the major mutations in the native protein of *GSS* gene were from R125C and R236Q. Hence, we conclude based on our study that the above mutations could be the major target mutations in causing the glutathione synthetase deficiency and might help to improve the diagnosis and treatment of the disease.

5. ACKNOWLEDGEMENTS

The authors thank the management of Vellore Institute of Technology University for providing the facilities to carry out this work.

REFERENCES

[1] Krawezak, M., Reiss, J. and Cooper, D.N. (1992) The mutational spectrum of single base-pair substitutions in mRNA splice junctions of human genes: causes and consequences. *Human Genetics*, **90(1-2)**, 41-54.

[2] Pitarque, M., vonRichter, O., Oke, B., Berkkan, H., Oscarson, M. and Ingelman-Sundberg, M. (2001) Identification of a single nucleotide polymorphism in the TATA box of the *CYP2A6* gene: impairment of its promoter activity. *Biochemical Biophysical Research Communications*, **284(2)**, 455-460.

[3] LeVan, T.D., Bloom, J.W., Bailey, T.J., Karp, C.L., Halonen, M., Martinez, F.D. and Vercelli, D. (2001) A common single nucleotide polymorphism in the CD14 promoter decreases the affinity of Sp protein binding and enhances transcriptional activity. *The Journal of Immunology*, **167(10)**, 5838-5844.

[4] Collins, F.S., Guyer, M.S. and Charkravarti, A. (1997) Variations on a theme: cataloging human DNA sequence variation. *Science*, **278(5343)**, 1580-1581.

[5] Syvanen, A.C., Landegren, U., Isaksson, A., Gyllensten, U. and Brookes, A.J. (1999) Enthusiasm mixed with skepticism about singlenucleotide polymorphism markers for dissecting complex disorders. *The European Journal of Human Genetics*, 7, 98-101.

[6] Halushka, M.K., Fan, J.B., Bentley, K., Hsie, L. and Shen, N. (1999) Patterns of single-nucleotide polymorphisms in candidate genes for blood-pressure homeostasis. *Nature Genetics*, **22(3)**, 239-247.

[7] Brookes, A.J. (1999) The essence of SNPs. *Gene*, **234(2)**, 177-186.

[8] Larsson, A. and Anderson, M. (2001) Glutathione synthetase deficiency and other disorders of the gamma-glutamyl cycle. 8th Edition, Mc Graw Hill, New York.

[9] Taniguchi, N., Higashi, T., Sakamoto, Y. and Meister, A. (1989) Gluthatione cennential: Molecular perspectives and clinical implications. Academic Press, New York.

[10] Gali, R.R and Board, P.G. (1995) Sequencing and expression of a cDNA for human glutathione synthetase. *Biochemical journal*, **310(pt1)**, 353-358.

[11] Ristoff, E., Mayatepek, E.and Larsson, A. (2001) Long-term clinical outcome in patients with glutathione synthetase deficiency. *The Journal of Pediatrics*, **139(1)**, 79-84.

[12] Shi, Z.Z., Habib, G.M., Rhead, W.J. Gahl, W.A., He, X., Sazer, S. and Lieberman, M.W. (1996) Mutations in the glutathione synthetase gene cause 5-oxoprolinuria. *Nature Genetics*, **14(3)**, 361-365.

[13] Ristoff, E. and Larsson, A. (1998) Patients with genetics

defects in the g-glutamyl cycle. *Chemico Biological Interactions*, **111-112(24)**, 113-121.

[14] Meister, A.and Larsson, A. (1995) Metabolic and molecular bases of inherited disease. In: Scriver, C.F., Beaudet, A.L., Sly, W.S. and Valle, D. Eds., 7th Edition, McGraw Hill, New York, 1461-1477.

[15] Dahl, N., Pigg, M., Ristoff, E., Gali, R., Carlsson, B., Mannervik, B., Larsson, A. and Board, P. (1997) Missense mutations in the human glutathione synthetase gene result in severe metabolic acidosis, 5-oxoprolinuria, hemolytic anemia and neurological dysfunction. *Human Molecular Genetics*, **6(7)**, 1147-1152.

[16] Runa, N., Katarina, C., Birgit, O., Birgit, C., Lel, W., Galina, P., Michael, W.P., Svante, N., Bengt, M., Philip, G.B. and Agne, L. (2000) Kinetic properties of missense mutations in patients with glutathione synthetase deficiency. *Biochemical Journal*, **349(pt1)**, 275-279.

[17] Sherry, S.T., Ward, M.H., Kholodov, M., Baker, J., Phan, L., Smigielski, E.M. and Sirotkin, K. (2001) dbSNP: the NCBI database of genetic variation. *Nucleic Acids Research*, **29(1),** 308-311.

[18] Pauline, N.C. and Henikoff, S. (2003) SIFT: Predicting amino acid changes that affect protein function. 2003, *Nucleic Acids Research*, **31(13)**, 3812-3814.

[19] Pauline, N.C. and Henikoff, S. (2001) Predicting deleterious amino acid substitutions. *Genome Research*, **11(5)**, 863-874.

[20] Ramensky, V., Pork, P. and Sunyaev, S. (2002) Human non-synonymous SNPs: server and survey. *Nucleic Acids Research*, **30(17)**, 3894-3900.

[21] Pesole, G. and Liuni, S. (1999) Internet resources for the functional analysis of 5' and 3' untranslated regions of eukaryotic mRNAs. *Trends in Genetics*, **15(9)**, 378.

[22] Sonenberg, N. (1994) mRNA translation: influence of the 5' and 3' untranslated regions. *Current Opinion in Genetics*, **4(2)**, 310-315.

[23] Nowak, R. (1994) Mining treasures from 'junk DNA'. *Science*, **263(5147)**, 608-610.

[24] Pesole, G., Liuni, S., Grillo, G., Licciulli, F., Mignone, F., Gissi, C. and Saccone, C. (2002) UTRdb and UTRsite: specialized databases of sequences and functional elements of 5' and 3' untranslated regions of eukaryotic mRNAs. *Nucleic Acids Research*, **30**, 335-340.

[25] Cavallo, A. and Martin, A.C. (2005) Mapping SNPs to protein sequence and structure data. *Bioinformatics*, **21(8)**, 1443-1450.

[26] Lindahl, E., Azuara, C., Koehl, P. and Delarue, M. (2006) NOMAD-Ref: Visualization, deformation and refinement of macromolecular structures based on all-atom normal mode analysis. *Nucleic Acids Research*, **34(suppl 2)**, W52-W56.

[27] Delarue, M. and Dumas, P. (2004) On the use of low-frequency normal modes to enforce collective movements in refining macromolecular structural models. *Proceedings of the National Academy of Sciences*, **101(18)**, 6957-6962.

[28] Van, D.S. (2000) Cytokine and cytokine receptor polymorphisms in infectious disease. *Intensive Care Medicine*, **26(suppl 1)**, S98-S102.

[29] Becky, M.P. and Anne, E.W. (2005) The implications of structured 5' untranslated regions on translation and disease. *Cell and Developmental Biology*, **16(1)**, 39-47.

[30] Kaspar, R.L., Kakegawa, T., Cranston, H., Morris, D.R. and White, M.W. (1992) A regulatory cis element and a specific binding factor involved in the mitogenic control of murine ribosomal protein L32 translation. *Journal of Biological Chemistry*, **267(1)**, 508-514.

[31] Kaspar, R.L., Morris, D.R. and White, M.W. (1993) Control of ribosomal protein synthesis in eukaryotic cells. In: Ilan, J. Ed., *Translational Regulation of Gene Expression* 2, Plenum Press, New York, 335-348.

[32] Parsch, J., Russell, J.A., Beerman, I., Hartl, D.L. and Stephan, W. (2000) Deletion of a conserved regulatory element in the Drosophila Adh gene leads to increased alcohol dehydrogenase activity but also delays development. *Genetics*, **156(1)**, 219-227.

[33] Lai, E.C., Burks, C. and Posakony, J.W. (1998) The K box, a conserved 3' UTR sequence motif, negatively regulates accumulation of enhancer of split complex transcripts. *Development*, **125(20)**, 4077-40 88.

